INHIBITION OF TELOMERASE ACTIVITY AND CELL GROWTH BY NATURAL PLANT PRODUCTS IN HUMAN BRAIN CANCER CELLS

KHAW AIK KIA

M.Sc (Molecular Biology)

Universiti Putra Malaysia

Malaysia

ACKNOWLEDGEMENTS

LIST OF PUBLICATIONS

1. **Khaw AK**, Yong WY, Hande MP. 2009. Genistein induces growth arrest and decreases telomerase activity in brain cancer cell lines. (**In preparation**).

2. Gurung RL, Soon FFJ, Shenoy K, **Khaw AK**, Baskar R, Hande MP. 2009. Thymoquinone inhibits cell proliferation, telomerase activity and shortens telomere length in brain cancer cells (**submitted**).

3. Banerjee B, Hande P, **Khaw AK**, Hande MP. 2009. Inhibiting telomerase in cancer therapy: Prospects and Challenges. In: **Genomic Instability and Cancer**. Ed(s): Hande MP and Hande VK, Research Signpost, Trivandrum, India (**In press**).

4. **Khaw AK**, Silasudjana M, Banerjee B, Suzuki M, Baskar R, Hande MP. 2007. Inhibition of telomerase activity and human telomerase reverse transcriptase gene expression by histone deacetylase inhibitor in human brain cancer cells. **Mutation Research.** 625(1-2):134-44.

5. Poonepalli A, Balakrishnan L, **Khaw AK**, Low GK, Jayapal M, Bhattacharjee RN, Akira S, Balajee AS, Hande MP. 2005. Lack of Poly (ADP-Ribose) Polymerase-1 gene product enhances cellular sensitivity to arsenite. **Cancer Research.** 65(23):10977-83.

6. Abraham J, Lemmers B, Hande MP, Moynahan ME, Chahwan C, Ciccia A, Essers J, Hanada K, Chahwan R, **Khaw AK**, McPherson P, Shehabeldin A, Laister R, Arrowsmith C, Kanaar R, West SC, Jasin M, Hakem R. 2003. Eme1 is involved in DNA damage processing and maintenance of genomic stability in mammalian cells. **The EMBO Journal.** 22(22):6137-47.

7. Melendez AJ, **Khaw AK**. 2002. Dichotomy of Ca2+ signals triggered by different phospholipid pathways in antigen stimulation of human mast cells. **Journal of Biological Chemistry.** 277(19):17255-62.

LIST OF CONFERENCES

1. **<u>Khaw AK</u>**, Yong WY, Hande MP. Genistein Induces Growth Arrest and Decreases Telomerase Activity in Glioblastoma Multiforme and Medulloblastoma Cell Lines Independent of DNA Damage. Keystone Symposia on Telomere Biology and DNA Repair. Australia. October 9th to 14th, 2009.

2. **<u>Khaw AK</u>**, Hande MP. Agilent Asia Pacific Cytogenetics User Summit 2009. Singapore. May 7th and 8th, 2009.

3. **<u>Khaw AK</u>**, Hande MP. Curcumin Inhibits Telomerase Activity and Triggers Apoptosis in Human Brain Cancer Cells. The 9th International Congress on Cell Biology (ICCB). Korea. October 7th to 10th, 2008.

4. **<u>Khaw AK</u>**, Hande MP, Yong WY, Hande MP. Growth inhibition and cell death by natural plant products in glioblastoma and medulloblastoma cells. Keystone Symposia on Stem Cells, Cancer and Aging. Singapore. September 29th to October 4th, 2008.

5. **<u>Khaw AK</u>**, Yong WY, Hande MP, Hande MP. Growth inhibition and cell death by natural plant products in glioblastoma and medulloblastoma cells. AACR Centennial Conference on Translational Cancer Medicine. Singapore. November 4th to 8th, 2007.

6. **<u>Khaw AK</u>**, Silasudjana M, Banerjee B, Suzuki M, Baskar R, Hande MP. Inhibition of telomerase activity and human telomerase reverse transcriptase gene expression by histone deacetylase inhibitor in human brain cancer cells. AACR Centennial Conference on Translational Cancer Medicine. Singapore. November 4th to 8th, 2007.

7. Newman J, Banerjee B, Balakrishnan L, Jayapal M, **<u>Khaw AK</u>**, Poonepalli A, Bhattacharjee R, Baskar R, Lee HW, Melendez A, Hande MP. Telomere dysfunction and DNA repair deficiency: Markers of sensitivity to mutagens and carcinogens? San Francisco Radiation Oncology Conference. USA. July 7th to 12th, 2007.

8. **<u>Khaw AK</u>**, Hande MP. Inhibition of telomerase activity and cell growth by curcumin in human brain tumour cells. AACR Centennial Conference on Cancer Research. USA. April 14th to 18th, 2007.

9. Poonepalli A, McPherson P, Banerjee B, **<u>Khaw AK</u>**, Putti T, Hakem R, Hande MP. Telomere-mediated genomic instability in breast tumour cells and in cells from mice lacking breast cancer genes. 11th International Congress of Human Genetics. Australia. August 6th to 10th, 2006.

10. Hande MP, Balakrishnan L, Poonepalli A, Low KM, Newman J, Kashimshetty R, **<u>Khaw AK</u>**, Bhattacharjee R, Akira S, Jayapal M, Balajee A. Oxidative damage-induced telomere attrition and genomic instability in DNA repair deficient mammalian cells. 2005. The 48th Annual Meeting of

Japan Radiation Research Society. Japan. May 25th, 2006.

11. Yong WY, Ch'ng HY, **Khaw AK**, Hande MP. Effects of genistein on telomere-chromosome integrity in glioblastoma cell lines. Inaugural International Congress on Complementary and Alternative Medicine (ICCAM). Singapore. February 26th to 28th, 2005.

12. **Khaw AK**, Hande MP. Effects of plumbagin on cell proliferation and death in human glioblastoma cell lines. Inaugural International Congress on Complementary and Alternative Medicine (ICCAM). Singapore. February 26th to 28th, 2005.

13. Melendez AJ, **Khaw AK**. Differential regulation of calcium signals triggered by different phospholipid intracellular signaling pathways in antigen stimulation of human mast cells. 6th NUS-NUH Annual Scientific Meeting. Singapore. August 16th to 17th, 2002.

TABLE OF CONTENTS

LIST OF FIGURES

ABBREVIATIONS

ADM-2	Aberration detection method 2
ADP	Adenosine diphosphate
ALT	Alternative Lengthening of Telomere
ANOVA	Analysis of variance
Array-CGH	Array-based comparative genomic hybridization
ATM	Ataxia telangiectasia mutated
BBB	Blood-brain barrier
BCL2	B-cell CLL/lymphoma 2
BCL2L1	BCL2-like 1
BIRC5	Baculoviral IAP repeat-containing 5
bp	Base-pair
CAM	Complementary and alternative medicine
Caspase	Cysteine-aspartic proteases
CCND1	Cyclin D1
CDK	Cyclin dependent kinase
CDKI	Cdk inhibitor
CDKN1B	Cyclin-dependent kinase inhibitor 1B
CDKN2A	Cyclin-dependent kinase inhibitor 2A
cDNA	Complementary DNA
cGy	Centigray
CHAPS	3[(3-Cholamidopropyl)dimethylammonio]-propanesulfonic acid
CNV	Copy number variations
CO_2	Carbon dioxide

cRNA	Complementary RNA
CT	Computed Tomography
Cy3.5	Cyanine dye 3.5
Cy5	Cyanine dye 5
D-loop	Displacement loop
DAPI	4',6-Diamidino-2-phenylindole
DAVID	Database for annotation, visualization and integrated discovery
DEAC	Diethylaminocoumarin
dH_2O	Distilled water
DIG	Digoxigenin
DMEM	Dulbecco's modified eagle medium
DMSO	Dimethyl sulfoxide
DNA	Deoxyribonucleic acid
dUTP	Deoxyuridine-triphosphate
EDTA	Ethylenediaminetetraacetic acid
EEG	Electroencephalogram
EGFR/Neu	Epidermal growth factor receptor-neu receptor
ETS2	v-ets erythroblastosis virus E26 oncogene homolog 2
FACS	Fluorescent-activated cell sorting
FBS	Foetal bovine serum
FITC	Fluorescein isothiocyanate
g	Gram
gDNA	Genomic DNA
Gy	Gray

H_2O_2	Hydrogen peroxide
HBSS	Hank's balance salt solution
HCl	Hydrochroric acid
hr	Hour
hr/PD	Hours per doubling
HRP	Horse redish peroxidase
HTATIP2	HIV-1 tat interactive protein 2
IAP	Inhibitor of apoptosis
IC_{50}	Inhibitory concentration at 50 % cell viability
IUPAC	International union of pure and applied chemistry nomenclature
kb	Kilobase-pair
kDa	Kilodalton
Ku86	86 kDa subunit of Ku antigen
L	Litre
M1	Mortality stage 1
M2	Mortality stage 2
MDM2	Murine double minute 2
MEM	Minimum essential medium
mFISH	Multicolour fluorescence *in situ* hybridisation
$MgCl_2$	Magnesium chloride
min	Minute
ml	Microlitre
mM	Milimolar
MRE11	Meiotic recombination 11 homolog A (S. cerevisiae)

MRI	Magnetic resonance imaging
mRNA	Messenger RNA
MRS	Magnetic resonance spectroscopy
mtDNA	Mitochondrial DNA
NAA	Nacetyl aspartate
NaCl	Sodium chloride
NaOH	Sodium hydroxide
NBS1	Nijmegen breakage syndrome 1
NCCAM	National centre for complementary and alternative medicine
NFκB	Nuclear factor-kappa B
OD	Optical density
Oligo	Oligonucleotide
PARP1	Poly (ADP-ribose) polymerase 1
PBGD	Porphobilinogen deaminase
PBS	Phosphate buffered saline
PCR	Polymerase chain reaction
PD	Population doubling
PET	Positron emission tomography
PI	Propidium iodide
PI3K	Phosphatidylinositol 3-kinase
POT1	Protection of telomeres 1 homolog (S. pombe)
RAD50	RAD50 homolog (S. cerevisiae)
Rb	Retinoblastoma
RLU	Relative luminescence units
RNA	Ribonucleic acid

rpm	Revolutions per minute
ROS	Reactive oxygen species
RT	Room temperature
RT-PCR	Reverse transcription polymerase chain reaction
SDS	Sodium dodecyl sulfate
sec	Second
SPECT	Single-photon emission computed tomography
SSC	Saline sodium citrate
SSCT	Saline sodium citrate with Tween-20
t-loop	Telomere loop
TANK	TRAF family member-associated NFκB activator
TBST	Tris-Buffered Saline with tween-20
TEMED	Tetramethylethylenediamine
TERC	Telomerase RNA component
TERT	Telomerase reverse transcriptase
TIN2	TRF1-interacting protein 2
TNFRSF1A	Tumor necrosis factor receptor superfamily, member 1a
TNFRSF10B	Tumor necrosis factor receptor superfamily, member 10b
Topo II	Topoisomerase II
TR	Telomerase RNA component
TRAF	Tumor necrosis factor receptor-associated factor
TRAIL	Tumour necrosis factor (TNF)-related apoptosis inducing ligand
TRF1	Telomere repeat-binding factor 1
TRF2	Telomere repeat-binding factor 2

TRITC	Tetramethyl rhodamine iso-thiocyanate
UV	Ultra violet
V	Volt
VDAC	Outer mitochondrial membrane channel
VIS	Visible
WHO	World health organization
°C	Degree celcius
λmax	Absorbance maximum
µg	Microgram
µl	Microlitre
µM	Micromolar
µm	Micrometer
%	Percentage

SUMMARY

According to Global Cancer Statistics 2002, brain cancer, one of the most challenging cancers to treat, with its high mortality rate, accounted for 189,000 new cases and 142,000 deaths worldwide annually. Cancer Statistics 2005 reported 18,500 new cases and 12,760 deaths in the United States. Current therapies for brain cancer treatment include chemotherapy, radiotherapy and surgical removal. However, such treatments were reported to have limitations and complications that result in poor prognosis; difficulty in surgical removal, low long-term survival rate and side effects from chemotherapy and radiotherapy confound the efficacy of brain cancer therapy.

Growing evidences point to the potential of phytochemicals such as plumbagin, genistein and curcumin as anti-cancer agents. However, the molecular mechanism(s) of action of these phytochemicals remain to be elucidated. Thus, by utilizing a variety of molecular and cytogenetic techniques, this study aims to investigate the potential of these phytochemicals with special attention paid to its possible role in the inhibition of telomerase and other oncogenic pathways in brain cancer cells.

In the present study, we show dose-dependent decrease in cell viability following plumbagin and curcumin treatments accompanied by increased DNA damage which correlates to cell cycle arrest and cell death. Furthermore, treatment of cancer cells with these phytochemicals were shown to result in differential expression of genes and proteins related to cell cycle and cell death such as *PTEN*, *E2F1*, *CCNE1*, *CDK2*, Bcl2 and Survivin. Interestingly, genistein induced cell cycle arrest at G2/M phase without causing DNA damage and cell death. This cytostatic characteristic is a proposition for the

use of genistein in combinatorial treatment to arrest or sensitize cancer cells to secondary cytotoxic drugs. We also found that radiosensitive cells have a higher tendency to undergo cell cycle arrest and cell death whereas radioresistant cells showed otherwise. In addition, all three drugs were shown to inhibit telomerase activity in brain cancer cells, resulting in shortening of telomere length following long-term treatment. To date, this property of plumbagin is the first to be reported in our study.

The understanding of the molecular and genetic mechanisms involved in cancer resistance will be helpful in the development and validation of novel therapeutic agents in the treatment of human malignancies. As telomerase is expressed in 90 % of human tumours, telomerase inhibition is an attractive target for anticancer therapy. We propose that the above drugs may elicit anticancer effects via gene regulation and telomerase inhibition.

Chapter 1   INTRODUCTION

1.1   Brain anatomy and brain tumours

The central nervous system includes three major parts of the brain (cerebrum, cerebellum and brainstem) and the spinal cord. The cerebrum is the largest area of the brain that is largely made up of neurons and glial cells (astrocytes, oligodendrocytes and ependymal cells). It consists of the left and right cerebral hemispheres; the hemispheres are further subdivided into frontal lobes, temporal lobes, parietal lobes and occipital lobes. The function of frontal lobes is to manage emotion, thought, reasoning, behaviour and memory; Parietal lobes govern sensory and motor information; Temporal lobes process sounds and spoken languages; Occipital lobes interpret images and written words.

The second largest part of the brain, the cerebellum, located at the lower back of the cerebrum, coordinates motor functions and controls balance. The brain stem, located in front of cerebellum and under the cerebrum, controls the unconscious activities such as breathing, heart rate, swallowing, wakefulness and sleep (Figure 1.1) (Black, 2006).
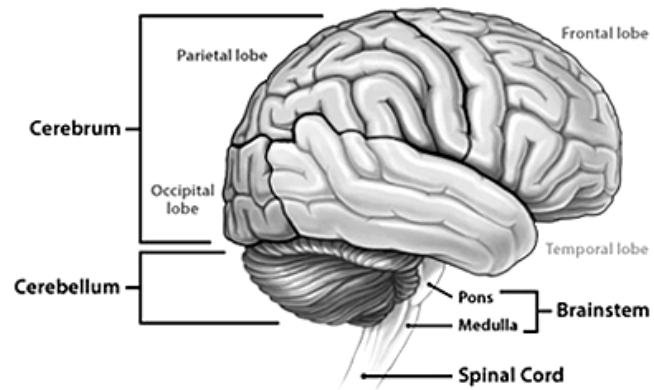
Figure 1.1. Anatomy of human brain. Human brain consists of cerebrum, cerebellum, brainstem and spinal cord. Cerebrum is further divided into frontal lobe, parietal lobe, occipital lobe and temporal lobe. (Picture taken from http://www.ohsu.edu)

1.1.1 Brain tumour incidence and mortality rate

According to Global Cancer Statistics 2002 (Parkin *et al.,* 2005), brain cancer accounted for 189,000 new cases and 142,000 deaths worldwide annually. This phenomenon is especially prominent in developed countries such as the United States, Canada and Japan. Cancer Statistics 2005 also reported that there were 18,500 new cases and 12,760 deaths in the United States (Jemal *et al.,* 2005). New cases and deaths in 2008 in United States were estimated in a recent report in SEER Cancer Statistics Review 1975 - 2005 to be 21,810 and 13,070 respectively (Ries LAG *et al.,* 2009). The reasons of such a high mortality rate are mainly attributed to poor prognosis, difficulty in surgical removal and low long-term survival rate. Advances in neuroimaging technologies contribute to the increasing trend of new cases.

Unlike tumour types that reside in other parts of the body, both benign and malignant brain tumours are fatal. A growing tumour in the brain places pressure on and compresses the neighbouring normal tissue against the skull, leading to brain tissue damage and dysfunction that can result in severe disability and even death. The tumour may also obstruct blood flow or spinal fluid from circulating around the brain. In malignant cases, the tumour may metastasize into the spinal fluid and spread into other parts of the brain and spinal cord.

1.1.2 Types and grades of brain tumours

There are many different types of tumours in the brain, spinal cord and meninges. Different names are given to these tumours depending on the location where they reside; Primary brain tumours are categorized into benign

and malignant tumours. Benign tumours consist of meningiomas, pituitary adenomas, vestibular schwannomas and carniopharyngiomas; they are slow growing and rarely spread. Histologically, these tumours have distinct borders. Common types of malignant tumours derived from glial cells include astrocytomas, glioblastomas, oligodendrogliomas, ependymomas and gangliogliomas. Other common types of malignant brain tumours include medulloblastomas and pineocytomas. Malignant tumours are more life-threatening due to their uncontrollable growth and invasiveness.

Given that a large portion of the brain is made up of glial cells, gliomas are the most common type of brain tumour in both children and adults. However, a higher proportion of malignant tumours tend to be found in adults, whereas the slower-growing gliomas are more often seen in children. Adult gliomas such as glioblastoma multiforme are commonly found in cerebral hemispheres, while children have a higher tendency of getting medulloblastoma which generally occur in the cerebellum and brain stem.

The different types of gliomas are further graded based on their pathologic evaluation, that is, their morphology in comparison to normal brain tissue observed under microscope. According to World Health Organization (WHO), astrocytomas are categorized into 4 different grades. For example, grade I gliomas are well-differentiated and usually have only a few fast proliferating cells. This tumour grade is usually considered safe and generally classified under benign tumours, it can be easily identified and removed and has a low possibility of recurrence. An example of grade I glioma is the pilocytic astrocytoma. Grade IV brain tumours such as glioblastoma multiforme and medulloblastoma however are less differentiated with more

uncontrolled proliferating cells and usually appear disorganised; blood vessels and necrotic cells can often be found in biopsy samples. This tumour grade is commonly known as malignant tumour. Grade II and III brain tumours are the intermediate-grade tumours that are categorised by their aggressiveness in between Grade I and IV (Black, 2006).

1.1.3 Symptoms of brain tumours

Depending on the location where brain tumours reside, body and physiological functions controlled by that brain region may be affected. Tumours that reside in the cerebrum often cause seizures and neurological dysfunctions. Tumours in the frontal lobes may affect personality, behaviour, intellectual dysfunction, hemiparensis, aphasia and focal motor seizures. Patients suffering from hemisensory impairment, visual disturbances and focal sensory seizures may have damages or tumours in parietal lobes. Tumours in temporal lobes cause visual disturbances, olfactory or gustatory hallucinations and psychomotor seizures. Tumours in occipital lobes may lead to visual disturbances, aura flashes of light and seizures. In the case of tumours in the cerebellum, patients can suffer from ataxia, nystagmus, dysmetria and unsteady gait. Other common symptoms of brain tumours include nausea and vomiting, visual impairments, weakness, confusion, imbalance, depression and fatigue. Spinal cord gliomas may cause pain, weakness or numbness in the extremities (Figure 1.2) (Virginia and Dubay, 2003).
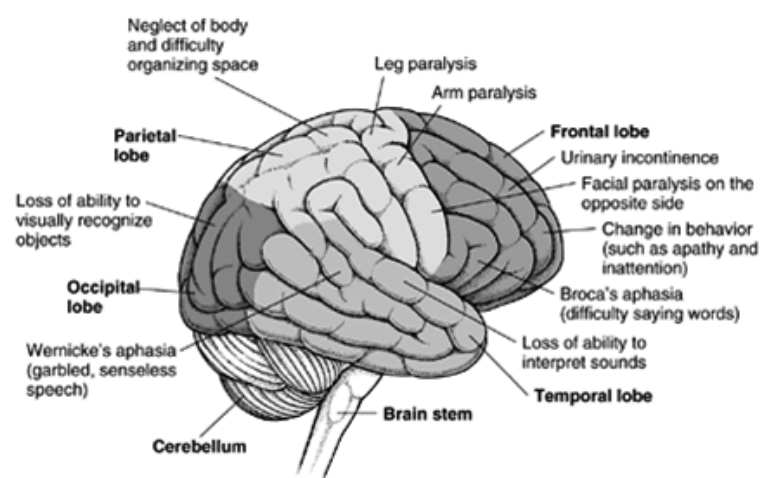
Figure 1.2. Common symptoms and disabilities in different parts of the brain of patients suffer from brain injuries and brain tumours (Picture taken from http://www.ohsu.edu).

1.1.4 Diagnosis, conventional treatments and limitations

Computed Tomography (CT), Magnetic Resonance Imaging (MRI), Positron Emission Tomography (PET) and Magnetic Resonance Spectroscopy (MRS) are widely used in the detection of brain tumours. CT scans show the axial image of the brain and provide important information to allow for anatomical comparisons between the left and right hemispheres to be made so as to identify distortions on either of the cerebral hemispheres. MRI detects the differences in magnetic properties of brain tissues, blood vessels and spinal fluid. PET scans detect the physiological differences in the brain tissue. Although PET images do not show fine details as in an MRI scan, it reveals the differences in metabolism of the brain cells, distinguishing malignant from benign tumour cells. MRS is a technique where brain water is suppressed. It detects ions and compounds like choline, creatine and N-acetyl aspartate (NAA) without the use of radioisotopes as in PET scan. MRS not only shows the presence of a tumour but also provides information on the grade of tumour and whether necrosis is present. Other methods use to diagnose brain tumours include single-photon emission computed tomography (SPECT) scan, electroencephalogram (EEG) and evoked responses (Virginia and Dubay, 2003).

The conventional treatments for brain tumours that are widely used are neurosurgery, chemotherapy and radiotherapy. In neurosurgery, neurosurgeons first perform a biopsy by craniotomy, a surgical opening of the skull, to extract a piece of the tumour to be examined by pathologist so as to confirm the diagnosis and to determine the appropriate treatment. Once the tissue has been confirmed as a tumour, further neurosurgery may be

7

performed to resect the tumour. However, neurosurgery has its own complications. The procedure greatly depends on the size and location of the tumour; tumours that reside in deep structures of the brain such as the brain stem and spinal cord are usually impossible to be extricated surgically compared to tumours found in meninges (outer layer of the brain). The presence of blood vessels around the tumours also further complicates the surgical procedures due to possibility of internal bleeding and infection. In many cases, neurological functions such as motor strength or coordination may become impaired immediately following surgery; patients may have to go through physical therapy, speech therapy and occupational therapy for rehabilitation (Virginia and Dubay, 2003).

Chemotherapy refers to the use of medication to treat cancer by inhibiting cancer cell growth and proliferation. Chemotherapy is given in cycles, which are daily medication for 3 to 8 weeks, to ensure that there is enough time for the bone marrow to recover and other toxicity of normal tissue to resolve besides killing cancer cells. Common drugs that are given orally include CCNU (lomustine), temozolomide (temodar®), procarbazine (matulane®) and etoposide (VP-16), while common intravenous drugs include BCNU (carmustine), carboplatin (paraplatin), cyclophosphamine (cytoxan), cisplatin, CPT-11 (camptosar®), etoposide (VP-16) and vincristine (Oncovin®). A fundamental problem in chemotherapy using synthetic drugs is the side effects that follow treatments, such as hair loss, anaemia (low red blood cells count), neutropenia (low white blood cells count), thrombocytopenia (low platelet count), weight loss, stomach ulceration, pulmonary fibrosis (lung scarring), kidney damage, peripheral neuropathy (numbness), severe nausea

and impotence. Also, complications such as bioavailability and blood-brain barrier (BBB) permeation often appear as a main concern in designing new drugs for brain cancer treatment. Bioavailability is the absorption of drug through the gastrointestinal tract when a drug is taken orally. BBB refers to the protective mechanism imposes restriction on drugs and other substances from crossing the capillary walls into brain tissues (Virginia and Dubay, 2003).

Radiotherapy is a treatment that is given in fractions (daily exposure of low dose in centiGray, cGy) of ionising radiation to target and induce DNA breaks in the cells. Normal cells and cancer cells are both exposed to the same risk of DNA damage. However, cancer cells generally have lower DNA repair efficiency. Over a treatment period of a few days, damaged DNA in cancer cells cannot be repaired and this eventually leads to cell death. There are various types of radiotherapies. Stereotactic radiosurgery and Gamma Knife are highly focused radiation therapy that focus a single high dose of radiation (15 ~ 30 Gray, Gy) to a small precise area of tumour. Brachytherapy is another technique whereby a radioactive material (pellet, seed or balloon catheter) is implanted inside of the tumour that emits the radiation energy from the inside of the tumour. The major side effects of partial or whole brain radiotherapy are fatigue, short term memory loss, cognitive changes, radiation necrosis, brain haemorrhages, hair loss, visual disturbances and loss of body coordination. The presence of radioresistant brain cancer cells further complicates the treatment and decreases the effectiveness of radiotherapy (Virginia and Dubay, 2003).

There are difficulties in surgical removal and treatments in brain tumours as compared to any other solid tumour types. Any damages to the

brain cells may also deteriorate normal body functions. Therefore, inevitably, we have chosen brain cancer cell lines in this study. Thus, two common grade IV brain tumours in adults and children i.e. glioblastoma multiforme and medulloblastoma are investigated.

1.2   Telomere and telomerase

1.2.1   Telomere biology

Telomeres were first identified by Hermann Muller and Barbara McClintock (Müller, 1938; McClintock, 1938; McClintock, 1941). Telomeres are the terminal ends of a chromosome and they have a series of repeats of the hexameric sequence 5'-TTAGGG-3' (in mammals) ranging from 5 to 20 kb that forms a 3'-end overhang structure. The overhang structure is protected by a self-forming loop that caps the DNA ends and prevents it from being recognized as a broken DNA strand. The loop is constructed by folding the telomere sequences to form a telomere loop (t-loop), the overhang strand invades and base-pairs with an upstream double-stranded region of the DNA, serving to stabilize the t-loop structure. The displaced strand thus forms the D-loop (displacement loop) (Greider, 1990; Blackburn, 1991; Greider, 1991; Griffith *et al.,* 1999). Studies have reported that DNA sensing and repair proteins and other telomere binding proteins such as TRF1, TRF2, ATM, Ku86, POT1, TIN2, TANK, MRE11, NBS1 and RAD50 were found in TRF1 and TRF2 complexes in this telomere loop (Figure 1.3) (http://www. genomeknowledge.org)

At every round of DNA replication during S phase of the cell cycle, the DNA strand unwinds and the telomere sequence is exposed. According to the

'end replication problem' model proposed by Olovnikov and Watson (Figure 1.4) (Watson, 1972; Olovnikov, 1973), terminal DNA sequences progressively shorten due to an unfilled gap left by replication primers at the 5'-end of leading strand. Loss of DNA residues ranging from 50 to 150 base pairs due to the end-replication problem have been reported (Harley *et al.,* 1990; Hastie *et al.,* 1990; Levy *et al.,* 1992; Lansdorp, 2000). The loss of coding functional DNA sequences are believed to be protected from nuclease attack and aberrant recombination by the presence of non-coding telomeric DNA at the end of every chromosome (de Lange, 2002; Artandi and Attardi, 2005).

As depicted in Figure 1.5, progressive telomere loss due to the end-replication problem eventually results in replicative senescence where cells stop proliferation but remain metabolically active at the G_0 quiescent phase; this stage was later termed as 'Hayflick limit' or Mortality stage 1 (M1) (Wright and Shay, 1992). However, some cells may inactivate tumour suppressor proteins such as p53 and Rb (retinoblastoma) (Dyson *et al.,* 1989; Werness *et al.,* 1990), thereby bypassing replicative senescence. These cells are able to proliferate for an additional 20 to 30 doublings until the telomeres are critically short, resulting in dysfunctional telomeres and genomic instability. At this stage, cell death is triggered to prevent accumulation of genetic aberrations. This stage is known as 'Crisis' or Mortality stage 2 (M2) (Wright and Shay, 1992). In very rare events, one in ten million cells bypass Crisis by triggering telomere maintenance mechanisms via activation of a reverse transcriptase enzyme called telomerase (Shay and Wright, 2005a); some cells also rescue short telomeres by initiating a homologous recombination mechanism called Alternative Lengthening of Telomere (ALT) (Wright and Shay, 1992; Bryan *et*

al., 1995; Bryan *et al*., 1997; Reddel *et al*., 2001). Cells that bypass Crisis acquire infinite replicative potential and become immortalised (Wright and Shay, 1992). The infinite replicative potential has been recognised as one of the hallmarks of cancer development (Hanahan and Weinberg, 2000).
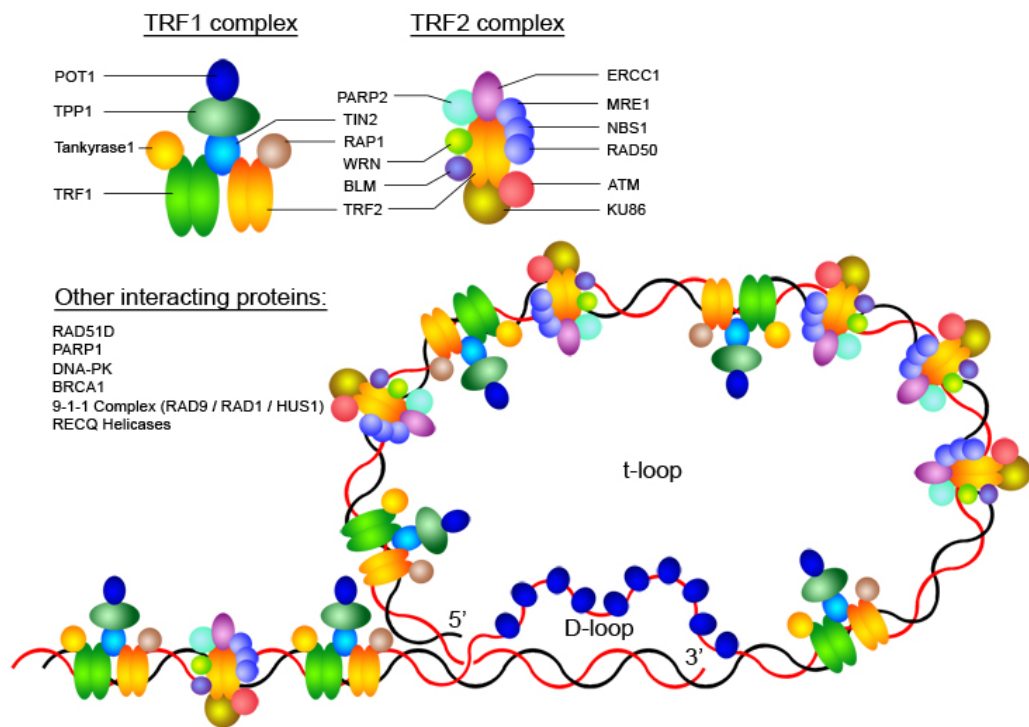
Figure 1.3. Telomere interacting proteins that bind onto t-loop and D-loop of telomere structure. (Modified from http://www.genomeknowledge.org)
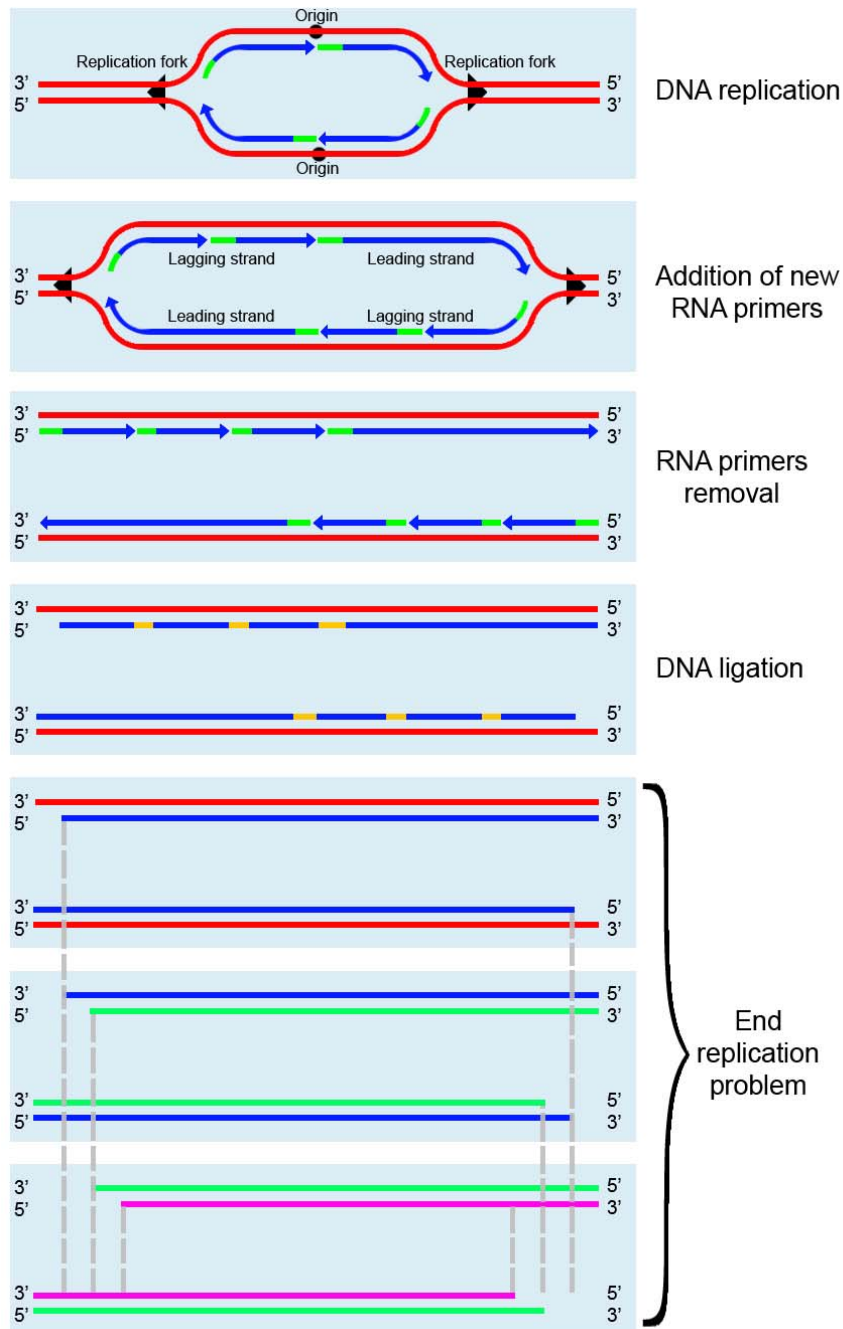
Figure 1.4. End replication problem. Telomeres at the end of DNA strand shorten progressively with every round of DNA replication due to the unfilled gap left by primers at the 5'-end of lagging strand (Modified from Shay and Wright, 2000).
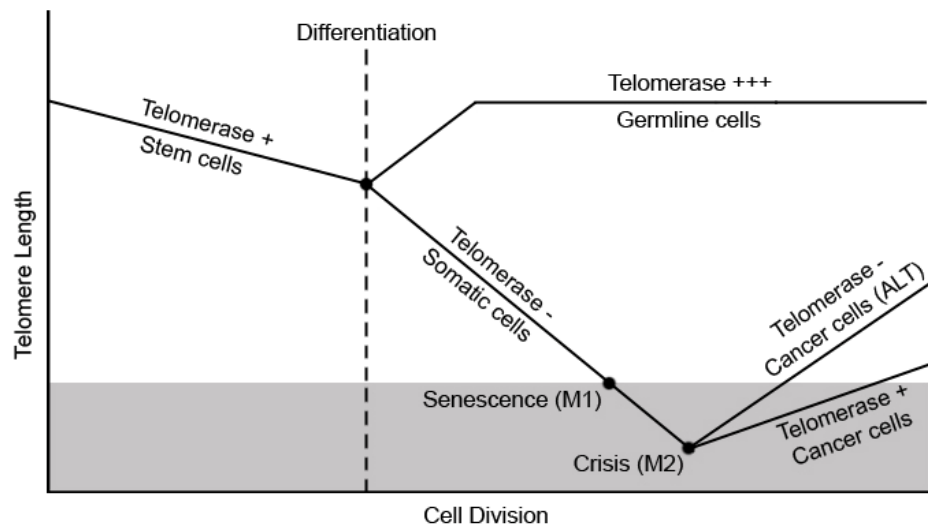
Figure 1.5. Telomere hypothesis of ageing. Progressive loss of telomeres in somatic cells resulting in replicative senescence (M1) and crisis (M2). Activation of telomerase enzyme or initiation of ALT mechanism rescue short telomeres but initiate carcinogenesis.

1.2.2 Telomerase enzyme

Telomerase is a ribonucleoprotein discovered by Carol W. Greider and Elizabeth Blackburn (Greider and Blackburn, 1985). It consists of an RNA component (TR) (Greider and Blackburn, 1987; Feng *et al.,* 1995), a catalytic subunit of reverse transcriptase (TERT) (Nakamura *et al.,* 1997) and dyskerin protein complex (Mitchell *et al.,* 1999; Vulliamy *et al.,* 2001). The RNA component consists of a nucleotide template with an 11 nucleotide sequence complementary to telomeric repeats (Greider and Blackburn, 1989). Telomerase synthesises new TTAGGG sequence by annealing its RNA template to the 3' overhang DNA of telomeres and using its reverse transcriptase to transcribe and extend the hexameric repeats (Greider and Blackburn, 1989; Shippen-Lentz and Blackburn, 1990; Yu *et al.*, 1990), thus replacing the sequences lost during DNA replication.

Telomerase is only detected in embryonic cells, germline cells, hematopoietic stem cells, activated lymphocytes, basal cells of the epidermis, intestinal crypt cells and most cancer cells (Hiyama *et al.*, 1995; Taylor *et al.*, 1996; Wright *et al.*, 1996; Harle-Bachor and Boukamp, 1996; Tahara *et al.*, 1999). In most human somatic cells, telomerase activity is absent (Kim *et al.*, 1994; Shay and Bacchetti, 1997; Shay and Wright, 2002; Shay and Wright, 2005b); It has been reported that 85 to 90 % of cancer cells express active telomerase and acquire the ability to proliferate infinitely, thereby achieving immortalisation (Kim *et al.*, 1994; Bryan and Cech, 1999).

1.2.3 Telomerase inhibition therapy for cancer treatment

Activation of telomerase enzyme is one of the characteristics of cancer cells. In addition, it has been reported that inhibition of telomerase can limit the growth of cancer cells (Shay and Bacchetti, 1997; Keith *et al.*, 2004). Hence, telomerase has become an attractive target for inhibition of cancer.

In the recent years, several strategies for the treatment of cancer have been proposed to develop potent catalytic inhibitors against the action of the telomerase enzyme either by denying the access of telomerase to the telomere *in situ* or perturbing the telomere structure (Parkinson and Minty, 2007). Key targets include *hTERT* and *hTR* genes and proteins, telomerase complex and telomere structure (Figure 1.6). Antisense oligonucleotides, RNA interference, ribozymes, dominant-negative mutant expression and telomerase oncolytic virus are categorized under immunotherapy, oligonucleotides-based therapy and gene therapy, these are the strategies proposed in cancer therapeutics (Cunningham *et al.,* 2006; Shay and Wright, 2006).

In the strategy of telomerase inhibition as shown in Figure 1.7, all cell types with telomerase activity will be affected at different extents. Telomere lengths will decrease during the treatment but as long as the telomere length is still considerable, these cells will not be very much affected. However, as cancer cells develop from somatic cells with critically short telomeres, these cells may be more sensitive to telomere deregulation from telomerase inhibition, eventually leading to cell death (Chen *et al.,* 2009). Another aspect to look at in cancer therapy is the uncontrolled division of cancer cells, which usually have shorter doubling times and defective contact inhibition properties

compared to non-cancerous cell types. As cancer cells proliferate faster and have critically short telomeres, they are believed to be more vulnerable to apoptosis by telomerase inhibition (Shay and Wright, 2002; Chen *et al.*, 2009).
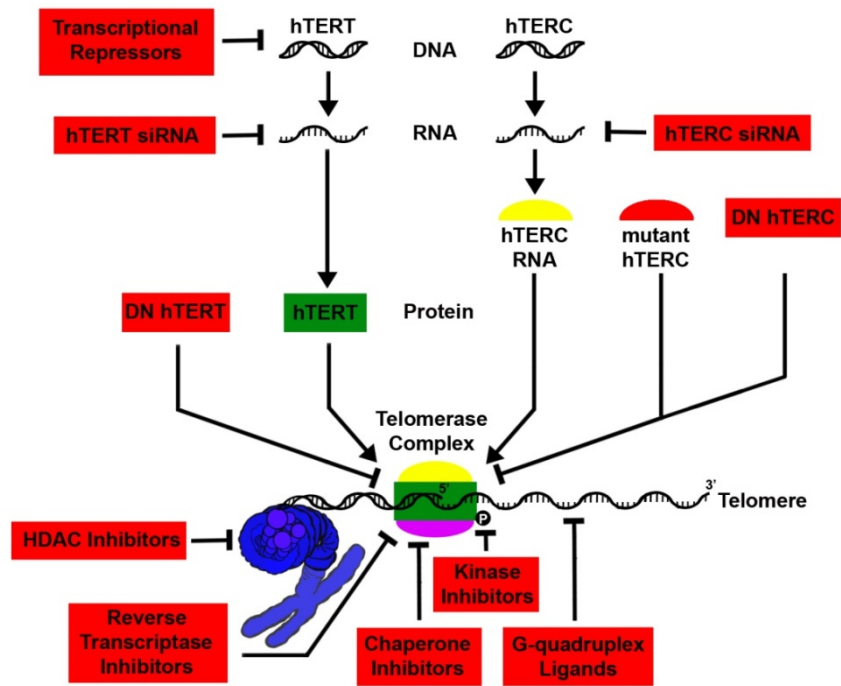
Figure 1.6. Strategy of targeting telomerase enzyme, disrupting telomerase access to telomere and manipulating telomere structure.
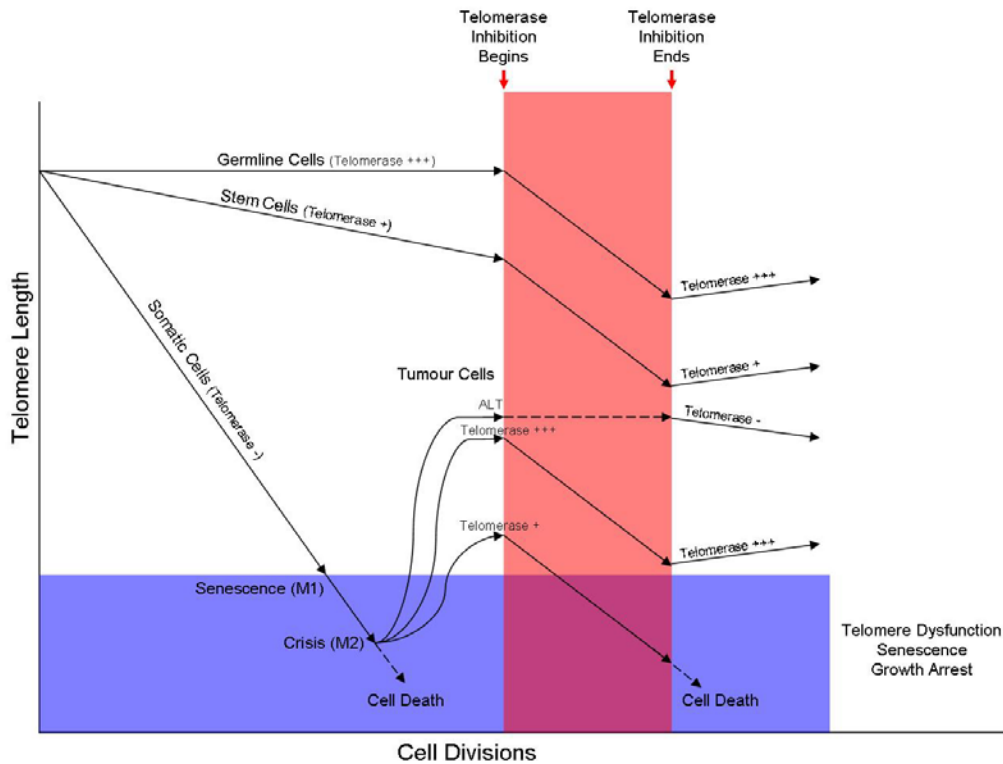
Figure 1.7. Telomerase inhibition of different cell types and cancer cells with different levels of telomerase activity may lead to different responses (Modified from Herbert *et al.,* 2001).

1.3   Complementary and Alternative Medicine

Complementary and Alternative Medicine (CAM) is a group of diverse medical and health care systems, practices and products that are not generally considered part of conventional medicine (Barnes *et al.,* 2008). CAM has emerged as an option to complement or provide a substitute to the conventional medicinal methods. According to National Centre for Complementary and Alternative Medicine (NCCAM), CAM treatments are categorized into 5 major categories: whole major systems, mind-body medicines, biologically-based practices, manipulative and body-based practices and energy medicines.

Many studies have been reported to use CAM treatments such as the use of natural plant products (Newman and Cragg, 2007; Mukherjee *et al.,* 2007), diet and nutrition (Divisi *et al.,* 2006), acupuncture (Lee *et al.,* 2005; Lu *et al.,* 2008), yoga and meditation (Bower *et al.,* 2005; DiStasio, 2008) and Qigong (Chen and Yeung, 2002; Lee *et al.,* 2007) to complement traditional cancer treatments.

CAM treatments based on natural plant products have been reported to have much potential in palliative therapy and in supportive strategies in the current cancer modalities (Munshi *et al.,* 2008). In the present study, we sought to investigate the effects of three phytochemicals on brain cancer cells.

1.4   Phytochemicals

Phytochemicals are biologically active non-nutrient secondary metabolites in fruits, vegetables, spices, grains and other plants that protect the plants against external threats such as pathogens, parasites, predators,

viruses and bacterial infections; Phytochemicals have the function of producing colour pigments that display vibrant colours to attract insects. Phytochemical extracts have been used throughout the world for centuries as traditional therapies and as homeopathic remedies to reduce the risk of major chronic diseases such as hypertension, cancer development, cardiovascular disease and diabetes (Boyer and Liu, 2004; Dhawan and Jain, 2005; Duthie *et al.*, 2006; Seymour *et al.*, 2008).

Studies have shown that phytochemicals are able to modulate DNA repair mechanisms, inhibit cell cycle progression, invasion and metastasis, and trigger apoptosis (Srinivas *et al.*, 2004; Dhawan and Jain, 2005; Ouchi *et al.*, 2005; Lanzilli *et al.*, 2006). Phytochemicals can be categorized into carotenoids, phenolics, alkaloids, nitrogen-containing compounds, organosulfur compounds and quinones as shown in Figure 1.8. Phenolic compounds are one of the major groups of phytochemicals that are being extensively explored for their potential in cancer prevention (Liu, 2004).

In this study, special interest is focused on cellular and molecular responses triggered by three phytochemicals, plumbagin (napthtoquinone), genistein (isoflavones) and curcumin (phenolic acids). Genistein and curcumin are active ingredients found in Asian diets such as that of Chinese, Indian, and Japanese, whereas plumbagin is a well-established anti-bacterial and anti-fungal drug that has recently gained attention in the field of cancer treatment research.

Phytochemicals

- Quinones
  - **Plumbagin**
    Mitomycin
    Thymoquinone
    Juglone
- Terpenes (Isoprenoids)
- Phenolic compounds
  - Phenolic acids
    - Hydroxy-benzoic acids
      Gallic
      Protocatechins
      Vannilic
      Syringic
    - Hydroxy-cinnamic acids
      Curcumin
      Caffeic
      Ferulic
      Sinapic
  - Monophenols
    Carnosol
    Rosemarinol
  - Polyphenol (Flavonoids)
    - Flavonols
      Quercetin
      Myricetin
      Galangin
      Fisetin
    - Flavones
      Apigenin
      Chrysin
      Luteolin
    - Flavanols (Catechins)
      Catechin
      Epicatechin
      Epigallocatechin
    - Flavanones
      Eriodictyol
      Hesperitin
      Naringenin
    - Anthocyanidins
      Cyanidin
      Pelargonidin
      Delphinidin
      Peonidin
    - Isoflavonoids (Phytoestrogens)
      Genistein
      Daidzein
      Glycitein
      Formononetin
  - Stilbenoids
    Resveratrol
    Pterostilbene
    Piceatannol
  - Coumarins
  - Tannins
    Gallotannins
    Ellagitannins
    Complex tannins
    Condensed tannins
  - Lignans (Phytoestrogens)
- Alkaloids
- Nitrogen-containing compounds
- Organosulfur compounds

Figure 1.8. Classification of major phytochemicals (Modified from Liu, 2004).

1.4.1 Plumbagin

Plumbagin (5-hydroxy-2-methyl-1,4-naphthoquinone) (Figure 1.9A) is a bicyclic napthoquinone present in members of the *Plumbagineae* and *Droseraceae* (Sundew) families. Common plants that contain plumbagin include sea lavender, Venus' flytrap, leadwort and sundew. *Plumbagineae* are found in Africa, Asia and Europe. *Droseraceae* are found in many temperate and tropical regions of the world, notably in Australia, New Zealand and South Africa. Impure extracts of plumbagin have been widely used in folk medicine for the treatment of rheumatoid arthritis, dysmenorrhoea and toothache (Mitchell and Rook, 1984; Mitchell and Rook, 2004).

Anti-microbial and anti-fungal properties of plumbagin have been well documented for the past 40 years (Durga *et al.,* 1990; de Paiva *et al.,* 2003; Chen *et al.,* 2006). However, only in the recent years have the anticancer properties of plumbagin started to attract the attention of scientists, making plumbagin a candidate chemotherapeutic agent for human tumours (Kuo *et al.,* 2006; Thasni *et al.,* 2008a; Nair *et al.,* 2008; Wang *et al.,* 2008; Powolny and Singh, 2008).

Plumbagin has been shown to downregulate the expression of epidermal growth factor receptor-neu receptor (*EGFR/Neu*) (Gomathinayagam *et al.,* 2008) and its downstream signalling targets such as phosphatidylinositol 3-kinase/AKT (*PI3K/AKT*) and transcription factor Nuclear Factor-kappa B (*NF$_K$B*) (Kuo *et al.,* 2006; Sandur *et al.,* 2006; Gomathinayagam *et al.,* 2008). Inhibition of *NF$_K$B* activation further decreases the expression of anti-apoptotic and proliferation genes such as Inhibitor of Apoptosis (*IAP), BCL2, BIRC5* and *CCND1* (Sandur *et al.,* 2006). Plumbagin

has also been shown to induce cell cycle arrest at G2/M phase, upregulate *p21/WAF1* and downregulate *CCNB1* (Kuo *et al.*, 2006; Hsu *et al.*, 2006; Wang *et al.*, 2008). An earlier report showed that plumbagin treatment resulted in the loss of mitochondrial membrane potential, which subsequently led to the release of *cytochrome c* and production of reactive oxygen species (ROS) (Srinivas *et al.*, 2004). Generation of ROS induces the inhibition of topoisomerase II by stabilising Topo II-DNA cleavable complex, leading to DNA cleavage and subsequently apoptosis (Kawiak *et al.,* 2007). To date, there is no study reporting on the telomerase inhibitory properties of plumbagin.

1.4.2 Genistein

Genistein (5,7-dihydroxy-3-(4-hydroxyphenyl)chromen-4-one) is an isoflavone under the polyphenolic compound group (Figure 1.9B). Genistein is produced exclusively by the *Leguminosae* family. A common member of *Leguminosae* family is the soybean that is commonly found in the Asian diet especially in the Chinese and Japanese population. Soybean is generally consumed in the form of soy sauce, soymilk, *tofu* (bean curd) and *miso* (fermented bean paste) soup.

Genistein is a well-known phytoestrogen, it is structurally similar to estradiol that could help to cure or reduce the risk of hormonal related cancers such as breast cancer, colon carcinoma, endometrial cancer and prostate cancer (Chen *et al.,* 2003; Kim *et al.,* 2005; Luo *et al.,* 2008; Jian, 2008; Sha and Lin, 2008). Conflicting reports have shown that genistein can trigger

estrogenic or anti-estrogenic effects (Bouker and Hilakivi-Clarke, 2000; Lamartiniere, 2000; Faqi *et al.,* 2004; Jefferson *et al.,* 2007).

Many studies have reported that genistein induces cell cycle arrest at the G2/M phase (Schmidt *et al.,* 2008; Li *et al.,* 2008). Genistein has been shown to have a role in matrix metalloproteinase inhibition and urokinase plasminogen activation, both of which can trigger the degradation of extracellular matrix proteins and thus prevent cancer cell invasion and metastasis (Farina *et al.,* 2006; Puli *et al.,* 2006). Genistein has also displayed the ability to downregulates *c-Myc* expression leading to decreased expression and transcriptional activity of *hTERT*, the catalytic component of telomerase (Ouchi *et al.,* 2005; Jagadeesh *et al.,* 2006).

The cytostatic and telomerase inhibition properties of genistein hint at its great potential to be developed as an effective anticancer drug. However, telomere shortening which happens during DNA replication cannot be initiated in an arrested cell. Hence, it is reasonable that genistein exerts its telomerase inhibition effect as a secondary anticancer strategy on cells that have escaped cell cycle arrest and continued to proliferate, thus selectively targeting tumour cells and exerting its growth inhibitory mechanism. In order to understand the mechanisms, it is essential to study gene expression patterns in cancer cells after exposure to genistein treatment to identify the key players in the growth inhibitory and telomerase inhibition mechanisms.

1.4.3 Curcumin

Curcumin ((1E,6E)-1,7-bis(4-hydroxy-3-methoxyphenyl)-1,6-hepta-diene-3,5-dione) is a polyphenolic compound isolated from turmeric (*Curcuma*

longa) (Figure 1.9C), it is also known as *kunyit* in some Asian countries. Turmeric is commonly found in Indian spices especially in curry powder; it has also been used as a colouring additive for mustard, yogurts, canned beverages and baked products. In some traditional medication in India, it is used as an antiseptic for cuts and wounds.

Curcumin has been shown to sensitize TRAIL-induced cell death in various cancer cells (Gao *et al.,* 2005; Jung *et al.,* 2005; Deeb *et al.,* 2005; Jung *et al.,* 2006; Shankar *et al.,* 2007; Wahl *et al.,* 2007). Expression of pro-apoptotic *BAX* and suppression of anti-apoptotic *BCL2* were also reported in cells treated with curcumin (Chakraborty *et al.*, 2006; Mukherjee Nee *et al.*, 2007). Curcumin has also been shown to induce mitochondrial hyperpolarization that results in the damage of mitochondrial DNA (mtDNA) and nuclear DNA (nDNA) (Cao *et al.,* 2006; Cao *et al.,* 2007). Inhibition of telomerase activity by curcumin has been reported in some cancer models (Ramachandran *et al.*, 2002; Chakraborty *et al.*, 2006; Cui *et al.*, 2006; Mukherjee Nee *et al.*, 2007). In addition, curcumin has been shown to inhibit telomerase by suppressing the translocation of *hTERT* to the nucleus in a *hTR-* or *c-Myc*-independent manner (Ramachandran *et al.*, 2002; Chakraborty *et al.*, 2006).

The biological effects of curcumin are multifactorial and telomerase inhibition may merely be one of the aspects of its overall growth inhibitory mechanisms that affect tumour cell growth (Ramachandran *et al.*, 2002). While the telomerase inhibition effects of curcumin have only been reported on a few cancer cell types such as breast cancer (Ramachandran *et al.*, 2002), leukemia (Chakraborty *et al.*, 2006; Mukherjee Nee *et al.*, 2007) and

pancreatic cancer (Teng and Fahey, III, 2002), no such study has yet been carried out on brain cancer cells. In addition, the relationship between telomerase inhibition and apoptosis has not been fully understood.

It is hypothesized that curcumin may selectively target cells that express telomerase enzyme; by inhibiting the telomerase enzyme, cells may become more sensitive to the cytotoxic effects of curcumin. Although many studies have been carried out to investigate the mechanisms of curcumin, more work must be done in order to understand the correlation between cell death, growth inhibition and telomerase inhibition.

A)

B)

C)
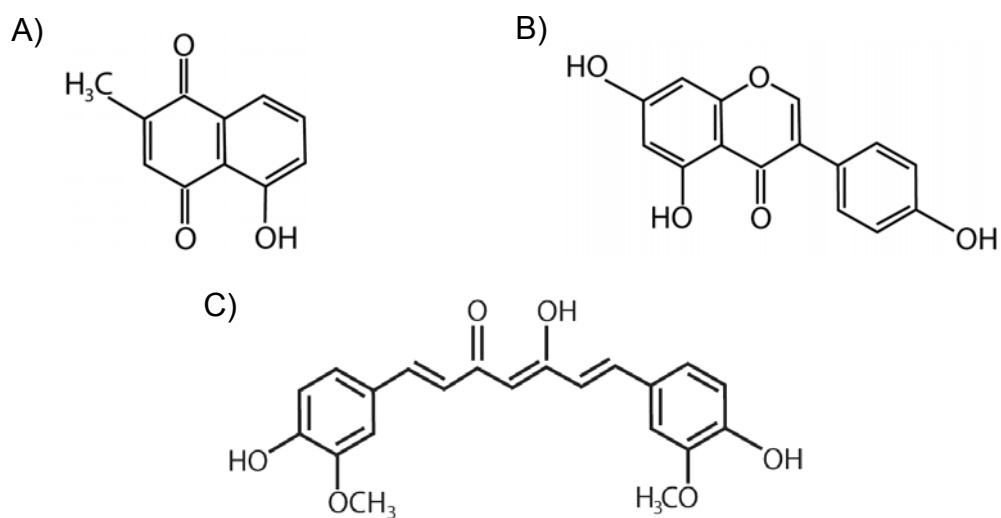
	Name	IUPAC* name	Molecular weight
A	Plumbagin	5-hydroxy-2-methyl-1,4-naphthoquinone	188.18
B	Genistein	5,7-dihydroxy-3-(4-hydroxyphenyl)chromen-4-one	270.24
C	Curcumin	(1E,6E)-1,7-bis(4-hydroxy-3-methoxyphenyl) - 1,6-heptadiene-3,5-dione	368.38

Figure 1.9. Chemical structures and molecular weights of phytochemicals used in this study. A) Plumbagin (napthtoquinone). B) Genistein (isoflavones). C) Curcumin (polyphenolic compound).

* International Union of Pure and Applied Chemistry Nomenclature

1.5   Hypothesis

Majority of the previous studies using phytochemicals were mainly focused on signalling pathways. To date, there is still little known about the telomerase inhibitory effects of plumbagin, genistein and curcumin. Telomerase inhibition is recognized as a newly discovered strategy for cancer treatment as telomerase is a unique enzyme that is detected in more than 90 percent of human cancer cells. As suggested by Ramachandran *et al.* (2002), any chemopreventive agent that could inhibit telomerase activity will be more important compared to those that could not.

However, as in any kind of therapy, the effectiveness of treatments is not solely based on the pathways that are triggered upon drug treatment, but also dependent on the characteristics of tumour cell types. These include the pathways that are defective specifically in target cells and the aberrations these cells carry that may affect the sensitivity of the cells toward the treatment. Hence in this study, we sought to investigate the mechanisms of actions of these phytochemicals based upon the understanding of the basal cell characteristics.

In this study, we hypothesize that the phytochemicals, plumbagin, genistein and curcumin, have great potential in telomerase inhibition apart from triggering multiple signalling cascades and immune responses.

1.6   Objectives

Cancer chemopreventive agents that inhibit telomerase activity are of great importance to cancer therapy as they are non-invasive yet specific. Hence, we set out to investigate the potential of natural plant products as

anticancer drugs. Three natural plant products of our interest are plumbagin, genistein and curcumin. In our study, investigations on the effects of the above phytochemicals were initiated based on the on the following objectives:

1) To determine the basal characteristics of the glioblastoma and medulloblastoma cell lines used in this study.
2) To investigate the growth inhibitory mechanisms of plant products on glioblastoma and medulloblastoma cell lines.
3) To study the inhibitory potential of plant products on telomerase activity and on telomere length in glioblastoma and medulloblastoma cell lines.

1.7   Significance

The findings from this study would provide a better understanding of the telomerase inhibitory properties of plumbagin, genistein and curcumin that may enable them to be later developed as effective complementary anticancer drugs. In addition, this study may contribute to a deeper understanding of the mechanisms of these compounds that affect the suppression of tumour cell growth. This study will also generate information on the gene and protein expression profiles regulated by plumbagin, genistein and curcumin, especially those involved in cell cycle control, DNA damage and repair, apoptosis, senescence, signal transduction and transcription.

Using the current understanding of various established mechanisms to explain the processes triggered by each drug, we will compare and determine the efficiency of each phytochemical and their potential in brain cancer treatment.

This study is focused on the cellular and molecular interactions in brain cancer cell models. Investigations on the bioavailability of these drugs and permeability into the BBB in an animal model will not be addressed in this study. However, we speculate that the phytochemicals used in this study would overcome the barrier as the sizes of each drug molecule are very much smaller compared to commercially available synthetic brain tumour drugs such as Temozolomide and Procarbazine which can cross the BBB. Some malignant brain tumours have been reported to have loose capillaries that cause the BBB to be more porous and less intact. In some chemotherapy, osmotic opening using concentrated sugar solution is used to temporarily disrupt the BBB in order to enhance targeted drug delivery (Kroll and Neuwelt, 1998).

Since these plant products have been well incorporated into the diet of some populations, we believe that these and many other phytochemicals can well tolerate the gastro-intestinal tract; hence they should not pose any complications in the bioavailability. Previous studies have also reported the use of these phytochemicals in animal models and clinical trials via oral administration (Munday and Munday, 2000; Parodi *et al.,* 2006; Zhou *et al.,* 2008; Pop *et al.,* 2008; Dhillon *et al.,* 2008; Kurd *et al.,* 2008).

Our intention of this study is not to discover the magic bullet for cancer therapy. Instead, we hope to provide alternatives that may enhance the efficiency of treatment and improve the life quality of cancer patients with the help of natural plant products. In addition, we expect to provide additional insights into the regular consumption or incorporation of natural products that contain these active ingredients into our diet as a prophylaxis for cancer.

In the next chapter, the rationale of experimental design and the details of various techniques will be addressed in order to provide an overview of the experimental flow and the rationale in selecting each technique.

Chapter 2   MATERIALS AND METHODS

2.1   Experiment design

This study is divided into three main sections. The first of which is the analysis of the properties of the phytochemicals. This section was performed to gain basic understanding on the stability of the phytochemicals under different conditions and the emission of fluorescence signals.

The second section focuses on the characteristics of brain tumour cells without drug treatment. We investigated the population doubling rate, radio-responses, endogenous chromosomal aberration, basal gene expressions and copy number variations at genome level.

In the third section, functional and molecular responses of cells upon phytochemicals treatment were investigated. Experiments were performed to determine the mode of trafficking of the phytochemicals, cell viability, cell cycle profile, DNA damage, colony formation, cell death, caspase activities, genes and proteins expression, telomerase activity and measurement of telomere length.

I Drugs Properties

UV-VIS spectroscopy (Drugs stability)
Spectrofluorometry (Fluorescence signal)

II Cells Characteristics

Population doubling (Growth rate)
Gamma irradiation (Radioresponse)
mFISH (Chromosomal aberration)
Microarray (Gene expression)
Array-CGH (Copy number variation)

III Cells Responses

Microscopy (Cell morphology)
Crystal violet assay (Cell density)
Flowcytometry (Cell cycle profile)
Comet assay (DNA damage)
Colony formation assay (Cell proliferation)
Annexin-V staining (Cell death)
Caspase assay (Caspase activity)
Real-time RT-PCR (mRNA expression)
Oligo GEArray (Gene expression)
Western blot (Protein expresssion)
TRAP (Telomerase activity)
TRF (Telomere length)

Figure 2.1. Experiment design of this study. This study is divided into 3 major sections. 1 - the understanding of properties of the drugs. 2 - the investigation of the cell characteristics. 3 - the examination of cell responses upon drug treatments.

2.2 Phytochemicals preparation and treatment

Rationale: Phytochemicals were dissolved in a universal solvent, dimethyl sulfoxide (DMSO) (Sigma-Aldrich, Missouri, USA). Drugs in different ranges of concentrations were prepared for dose-response studies and to identify the growth inhibitory doses. For experimental control, final concentration of DMSO at 0.1 % [v/v] was used.

Phytochemicals used in this study were plumbagin (Sigma-Aldrich), genistein (Sigma-Aldrich) and curcumin (Sigma-Aldrich). These phytochemicals were dissolved in 100 % DMSO to prepare 100 mM stock solution. Working concentrations were prepared by further diluting in DMSO.

For plumbagin, 1 µl of the final concentrations in 0.0, 1.0, 2.0, 3.0, 4.0, 5.0, 6.0 and 7.0 mM were added in the cell culture to achieve 0.0, 1.0, 2.0, 3.0, 4.0, 5.0, 6.0 and 7.0 µM respectively. For genistein, 1 µl of the final concentrations in 0.0, 5.0, 15.0, 25.0, 35.0 and 50.0 mM were added in the cell culture to achieve 0.0, 5.0, 15.0, 25.0, 35.0 and 50.0 µM respectively. For curcumin, 1 µl of the final concentrations in 0.0, 20.0, 40.0, 60.0, 80.0 and 100.0 mM were added in the cell culture to achieve same value of concentrations in micro molar (µM).

2.3 Cell lines and cell culture

Rationale: Treatment of brain cancer cell lines is the main focus in this study. Normal human lung fibroblasts (Normal1) were used as a control in initial functional study such as dose-response study, cell cycle profiles and DNA damage study. Telomerase-immortalised human foreskin fibroblasts (hTERT-BJ1) was used as another control cell line as it is a non-cancerous cell line

that mimics telomerase-positive cancer cells by expressing telomerase enzyme and does not senesce. Normal human lung fibroblasts (Normal1) and telomerase-immortalised human foreskin fibroblasts (hTERT-BJ1) were used as experimental controls instead of primary brain cells due to limited availability of primary brain cells. The experimental controls in this study are DMSO-treated cancer cell lines.

Human glioblastoma multiforme cell lines A172 (Japanese Collection of Research Bioresources, JCRB0228), KNS60 (Institute for Fermentation, IF050357), U251MG(KO) (Institute for Fermentation, IF050285) and medulloblastoma ONS76 (Institute for Fermentation, IF050355) were obtained from Dr. Masao Suzuki, National Institute of Radiological Sciences, Chiba, Japan. They were cultured in DMEM (Sigma-Aldrich) supplemented with 100 U/ml penicillin/streptomycin (Thermo Fisher Scientific, New York, USA) and 10 % foetal bovine serum (FBS). Normal human fibroblast cell line (GM03651) was obtained from Coriell Cell Repositories, New Jersey, USA. Early passage Normal1 cells were grown in minimum essential medium with Earle's salt (MEM) (Invitrogen, California, USA) supplemented with MEM amino acids (Invitrogen), 10 mM MEM non-essential amino acids (Invitrogen), MEM vitamin solution (Invitrogen), 10 % FBS and 100 U/ml penicillin/streptomycin (Thermo Fisher Scientific, New York, USA). Telomerase-immortalised human foreskin fibroblasts, hTERT-BJ1 (Clontech Laboratories, Inc., California, USA) was grown in DMEM and medium 199 (Sigma-Aldrich) in 4:1 ratio and enriched with 10 % FBS, 200 mM L-glutamine, 100 mM sodium pyruvate and 100 U/ml penicillin/streptomycin (Thermo Fisher Scientific). All cells were

maintained at 37°C in a 5 % humidified CO_2 incubator, cell density was kept below 80 % confluence and culture medium was changed every two days.

2.4 Phytochemical properties

2.4.1 Stability study using UV-visible spectroscopy

Rationale: Absorbance measurement is an essential step in assessing stability of a drug. Horizontal shift in absorbance peaks indicate changes in drug stability. Blue-shift (a shift towards left) is an indicator of compound degradation; whereas red-shift (a shift towards right) is an indicator of compound aggregation or polymerisation.

The experiments were performed by scanning 10 to 50 μg of plumbagin and curcumin prepared from 2 different stock solutions that are stored at different conditions i.e. frozen with light-protected box and non light-protected box at room temperature. Absorbance maximum (λ_{max}) was recorded for both stock solutions at 0, 7 and 14 days interval using UV-VIS scanning spectrophotometer (Shimadzu, Kyoto, Japan).

2.4.2 Emission wavelength analysis using fluorescence spectroscopy

Rationale: By utilising the fluorescence signals emitted by the phytochemicals, the trafficking of drugs into the treated cells can be viewed using fluorescence microscopy.

The wavelength of fluorescent emission of plumbagin and curcumin were studied using fluorescence spectrometer (Shimadzu). The excitation wavelengths (λ_{max}) of phytochemicals obtained from UV-VIS spectroscopy

were used to excite the two phytochemicals and fluorescence emission wavelength generated was recorded.

2.5 Cell lines characteristics

2.5.1 Population doubling

Rationale: Proliferation rate of the cell types were studied by monitoring the population doubling (PD). This was done to estimate the ideal treatment time which cells complete at least one round of cell cycle.

Population doubling study on cancer cell lines was carried out by using crystal violet staining and absorbance reading. Approximately 0.2×10^6 cells were plated on 6-well plate, crystal violet assay (detail in section 2.6.3) and absorbance readings were performed at 24, 48 and 72 hours. The formula used in the calculation is based on exponential regression where $y = a.e^{bx}$. Parameters of the formula are:

a = amplitude

b = exponent

Doubling time is calculated from the equation $ln(2)/b$ and the value unit is in hours per doubling (hr/PD).

2.5.2 Radioresponses

Rationale: To examine whether the cells are sensitive or resistant to radiation-induced DNA damage and cell death, cells were exposed to ionising radiation.

Cells cultured in T25 flasks were irradiated with 2 Gy using Gammacell® 40 Extractor (Best Theratronics Ltd., Ontario, Canada) with a

dose rate of 1.16 Gy/min. After irradiation, cells were allowed to rest for 2 hours before carrying out cell viability study, cell cycle analysis, and comet assay. Colony formation was performed by seeding 2×10^3 cells and allowed to form colonies for 10 days. Details of the each assay will be mentioned in section 2.6 in this chapter.

2.5.3 Multicolour Fluorescence *in situ* Hybridisation (mFISH)

Rationale: mFISH (Speicher *et al.*, 1996; Hande *et al.*, 2005) was performed to investigate genomic instability and chromosomal aberrations. By studying the aberrations and comparing across the cell lines of the same cell type, consistent aberrations may be identified.

- **Metaphase preparation**

Cells at density of 70 % confluence were arrested at mitosis by treatment with 0.1 µg/ml of KaryoMAX® Colcemid (Invitrogen) overnight. The cells were then harvested and incubated with a hypotonic solution of 0.075 M potassium chloride at 37°C for 12 minutes followed by fixation in Carnoy's fixative (75 % Methanol: 25 % Acetic Acid). Chromosomes at metaphase were dropped onto slide and allowed to air-dry.

- ***In situ* hybridisation**

The procedure was performed according to the manual of Metasystems Multicolour Probe Kits. Briefly, after pepsin treatment (1 g/50 ml) for about 2 minutes at 37°C, the chromosomes were post-fixed in 1 % formaldehyde in 1 X PBS with 50 mM $MgCl_2$ for 10 minutes at room temperature. The chromosomes are stabilised in 1 X SSC prior to the denaturation and were subsequently denatured with a basal solution (0.07 N

NaOH). Afterwards, the chromosomes were rinsed in 1 X SSC buffer again to stop the denaturation process and to stabilize their structure. The Metasystems 24XCyte Human mFISH probe cocktail (Metasystems, Altlussheim, Germany) was denatured 75°C for 5 minutes. The probe was allowed to hybridise for half an hour at 37°C to reduce unspecific binding of short or repetitive DNA pieces. The denatured and prehybridised probe cocktail was applied onto the denatured chromosome preparation, overlaid with a coverslip and sealed with rubber cement. The slides were then incubated at 37 °C in a humidified chamber for 72 hours. Post-hybridisation washing was done in 1 X SSC at 75°C for 5 minutes after removing the coverslips. Slides were incubated in 4 X SSCT for 5 minutes and blocked with blocking reagent at 37°C for 10 minutes. Subsequently, slides were incubated with detection 1+3 reagent to detect Cy5 which is indirectly labelled. Slides were then counterstained with VECTASHIELD® Mounting Medium with DAPI (Vector Laboratories, Inc., California, USA).

- **Image acquisition and analysis**

    Microscopic analysis was performed using Axioplan 2 Imaging fluorescence microscope (Carl Zeiss, Oberkochen, Germany) with filter sets for FITC, Cy3.5, Texas Red, Cy5, Aqua and DAPI. Fifty metaphases were captured and analysed using ISIS mFISH imaging system software (Metasystems). In the mFISH technique, all 24 chromosomes (1-22 and X and Y) are painted in different colours using combinatorial labelling by five varicoloured fluorochromes (DEAC, FITC, Spectrum Orange™, Texas Red®, Cy™5), so that any interchromosomal translocations are observed as colour junctions on individual chromosomes.

2.5.4 Microarray gene expression analysis

Rationale: cDNA expression profiling of each cell line was done by using microarray analysis in order to determine the signal transduction pathways status in these cells.

- **Ribonucleic acid (RNA) extraction and cDNA synthesis**

    RNA from non-treated brain cancer cells was extracted using RNA extraction kit (Qiagen, California, USA). Lymphocyte RNA extracted from a healthy individual was used as an experimental control. Double-stranded cDNA was synthesised from 5 Ag of total RNA using Superscript^{TM} II Reverse Transcriptase (Invitrogen) primed with T7-(dT)-24 primer. For biotin-labelled cRNA synthesis, *in vitro* transcription reaction was done in the presence of T7 RNA polymerase and biotinylated ribonucleotides (Enzo Diagnostics, Ney York, USA).

- **RNA hybridisation**

    The cRNA product was purified (Qiagen), fragmented, and hybridised to Affymetrix GeneChip® Human Genome Focus Array (Affymetrix, California, USA) in a Gene chip hybridisation oven 640 as per the Gene Chip Expression Analysis manual. After 16 hours of hybridisation, the gene chips were washed and stained using the Affymetrix Fluidic station and scanned by GeneArray® 2500 Scanner (Agilent Technologies Inc., Santa Clara, California, USA).

- **Image analysis**

    Image data were normalised and statistically analysed using GeneSpring 7.2 (Agilent Technologies Inc.). Subsequent data analysis involved agglomerative average-linkage hierarchical clustering for finding different patterns and levels of gene expression.

2.5.5 Array-based Comparative Genomic Hybridisation (Array-CGH)

Rationale: Array-CGH provides information on the copy number variations (CNV) of genes at high resolution in order to identify recurrent chromosome aberrations such as microdeletions and amplifications.

- **Genomic DNA extraction and amplification**

Array-CGH was performed using 14693 Human Genome CGH Microarray 244A (Agilent Technologies Inc.). All steps were done according to the manufacturer's instructions. Briefly, genomic DNA (gDNA) from cell culture was extracted and quantitated using NanoDrop (Thermo Fisher Scientific). Then amplification of gDNA was done using Qiagen REPLI-g mini kit (Qiagen).

- **Restriction digestion and purification of amplified gDNA**

Alu I (Promega, Wisconsin, USA) and *Rsa I* (Promega) were used to digest the amplified gDNA at 37°C for 2 hours. After digestion, the gDNA was purified using QIAprep Spin Miniprep Kit (Qiagen) and further quantitated using the NanoDrop (Thermo Fisher Scientific).

- **Fluorescent labelling of purified gDNA**

Purified gDNA was labelled with cyanine 3-dUTP (test) and cyanine 5-dUTP (reference) separately at 37°C for 2 hours. Excess unbound cyanine 3-dUTP and cyanine 5-dUTP were cleaned up from gDNA using Microcon YM-30 filters (Millipore, Massachusetts, USA). Then equal amount of differently labelled gDNA of test and reference were combined together and mixed well.

- **Microarray hybridisation**

The Cy3-labelled (test) and Cy5-labelled (reference) gDNA mixture was mixed with human Cot-1 DNA (Invitrogen) before hybridisation to a

gasket slide and incubation in a hybridisation oven at 65°C for 40 hours with rotation at 20 rpm.

- **Image acquisition and analysis**

After hybridisation, the slides were scanned immediately to minimize the impact of environmental oxidants on signal intensities using Agilent scanner (Agilent Technologies Inc.) and analysed using CGH Analytics software (Agilent Technologies Inc.).

2.6 Responses of cells after drug treatments

2.6.1 Cytotoxicity assay for DMSO

Rationale: This study was performed to ensure that the final concentration of DMSO in all controls and treated samples does not exert cytostatic or cytotoxic effects.

Cells were plated in 6-well plate at density of 0.2 X 10^6 per well. Twenty-four hours later, DMSO at final concentrations of 0.0, 0.1, 0.5, 1.0, 1.5 and 2.0 % were added to the cell culture. Crystal violet assay (detail in section 2.6.3) was performed at 48 hours after drug treatment to determine whether DMSO affects cell density either by inducing growth arrest or cell death.

2.6.2 Phase-contrast observation of cell morphology and fluorescence microscopy observations of drugs trafficking

Rationale: After drug treatments, cells were observed under normal light microscope to examine the morphology of arrested or apoptotic cells. By utilizing the fluorescent signals emitted by the phytochemicals and the help of

acridine orange counter-stain, the trafficking of drugs into the treated cells can be viewed using fluorescence microscopy.

For morphological observation using normal light microscope after 48-hour of phytochemicals treatment, images of cell morphology were captured at 100 X and 200 X magnifications.

Drug trafficking experiment was designed based on the emission signals of plant products upon UV light excitation. Cells were cultured on sterile coverslips that were placed in 6-well plates and treated with DMSO and drugs for different time-points at 2.0, 6.0, 8.0, 12.0, 24.0 and 48.0 hours. Based on the observation that plumbagin emits blue fluorescent signal that may interfere with auto-fluorescent of cells, when harvesting plumbagin-treated cells, coverslips were placed onto microscope slides with acridine orange (30 µg/ml) to differentially stain the cytoplasm and nucleus. As for curcumin-treated cells, no counter-stain was used. Fluorescent emission of plumbagin and curcumin together with counter stains were observed using Axioplan 2 Imaging fluorescence microscope (Carl-Zeiss) with filter sets for FITC, TRITC and DAPI to monitor the drug trafficking processes.

2.6.3 Crystal violet cell density assay

Rationale: This experiment was carried out to determine the half-maximal concentration (IC_{50}) of each drug that affects cell density either by inhibiting cell growth and/or inducing cell death.

For plumbagin treatment, cells were treated with plumbagin to reach final concentrations of 0.0, 1.0, 2.0, 3.0, 4.0, 5.0, 6.0 and 7.0 µM. For genistein treatment, cells were treated with genistein to reach final

concentrations of 0.0, 5.0, 15.0, 25.0, 35.0 and 50.0 µM. For curcumin treatment, cells were treated with curcumin to reach final concentrations of 0, 20.0, 40.0, 60.0, 80.0 and 100.0 µM. Following 48 hours treatment, cell culture medium was aspirated and cells were gently washed with 1 X PBS. After aspirated the 1 X PBS, 750 µl of crystal violet staining solution (Sigma-Aldrich) (0.75 % crystal violet in 50 % ethanol: dH_2O with 1.75 % Formaldehyde and 0.25 % NaCl) was added to each well of the 6-well plate and incubated in room temperature for 15 minutes. After which, the crystal violet dye was aspirated gently and the 6-well plate was washed with 1 X PBS for few times to remove excess stain. Thereafter, 1.5 ml of 1 % SDS was added to each well and mixed evenly on a rotator. When the stain was completely dissolved, absorbance reading at 595 nm was measured using TECAN SpectraFluor Plus microplate reader. The absorbance readings were later translated into percentage of viable cells in the treatments in order to calculate the inhibitory concentration at 50 % cell viability (IC_{50}). All steps were performed by gently adding or aspirating the solution without disturbing the layer of cell culture.

In subsequent experiments, different IC_{50} as detected by crystal violet assay were used for each cell line. Twenty-four hours after seeding, cells were then treated with plumbagin, genistein or curcumin for 48 hours for short-term experiments and 15 days for long-term experiments. Final concentration of DMSO was 0.1 % [v/v] for all samples.

2.6.4 Flow cytometry cell cycle analysis

Rationale: After identification of the IC_{50}, cell cycle analysis was done to investigate at which cell cycle phase the cells are arrested at the end of the treatments using fluorescence-activated cell sorting (FACS) analysis; this study also provide information on presence of DNA fragmentation i.e. apoptotic cell death.

The control and phytochemical-treated cells were washed with 1 X PBS and fixed overnight in 70 % ethanol. The fixed cells were later stained and with propidium iodide/Triton X-100 staining solution with RNase A and incubated at 37°C for 30 minutes. Samples were then analysed by flow cytometry at 488 nm excitation λ and 610 nm emission λ. Samples were then analysed using a FACSCalibur^{TM} flow cytometer (Becton Dickinson, New Jersey, USA). Approximately 10,000 events per sample were collected and the data was analysed using Cytometry Software WINMDI.

2.6.5 Colony formation assay

Rationale: In the event of growth inhibition detected in cell cycle analysis, colony formation assay is performed to validate the observation by showing that the drug-treated culture is compromised in colony formation.

Cells were harvested after 48 hours of phytochemicals treatment. Cell counting was performed using trypan blue staining on haemocytometer. Two thousand cells were plated on 100 mm Falcon^{TM} culture dish (BD Biosciences, New Jersey, USA) and kept under standard culture conditions for 10 days. Culture medium was changed every 3 days. On day-10, cell culture medium was aspirated and culture dish was washed with 1 X PBS. Thereafter, 2 ml of

1 % crystal violet solution was added for 15 minutes. Crystal violet solution was then aspirated and the culture dish was air-dried before performing colony counting. Confirmation was done by dissolving the crystal violet with 1 % SDS and the resultant absorbance are read at OD 595 nm.

2.6.6 Single cell gel electrophoresis assay (Comet assay)

Rationale: Comet assay was carried out to determine whether the growth arrest observed in cell cycle analysis was induced by DNA damage due to drug treatment.

The control and phytochemical-treated cells were harvested by trypsinisation, washed in ice-cold 1 X PBS and resuspended in HBSS with 10 % DMSO with EDTA. The cells were then suspended in molten 0.7 % low melting point agarose and immediately transferred onto the comet slide (Trevigen, Maryland, USA). After the gel has solidified in 4 °C, the slides were immersed in lysis solution at 4°C for 1 hour to remove cellular proteins. Slides were then placed in an electrophoresis tank containing 300 mM NaOH and 1 mM EDTA for 40 minutes to denature the DNA strands before electrophoresis at 25 V, 300 mA for 20 minutes at room temperature in the same alkaline electrophoresis buffer. Following electrophoresis, slides were washed with neutralization buffer (500 mM Tris-HCL, pH 7.5) for 5 minutes and dehydrated by dipping in 70 % ethanol for 5 minutes. After the slides have air-dried, they were stained with SYBR[®] green and covered with coverslips. Fifty comets per sample were analysed and the mean tail moment (the product of the tail length and the fraction of total DNA in the tail) of the comets was quantified using CometImager software (Metasystems).

2.6.7 Annexin V-FITC staining

Rationale: Apart from sub-G1 population detected in cell cycle analysis, apoptotic cell death is confirmed by performing annexin V staining to detect the population of live cells, apoptotic cells and necrotic cells using fluorescence-activated cell sorting (FACS) analysis.

This experiment was done using Annexin V-fluorescein isothiocyanate (FITC) labelled staining kit (Sigma-Aldrich). In this experiment, three control treatments were used: unstained control, propidium iodide (PI)-stained hydrogen peroxide (H_2O_2)-treated cells (necrotic control) and FITC-stained staurosporine-treated cells (apoptotic control). Apoptosis was induced by adding 1 μg/ml staurosporine for 24 hours prior to harvest. Necrosis was induced by adding H_2O_2 for 2 hours prior to harvest. The 48-hour DMSO and phytochemical-treated cells were harvested and washed with 1 X PBS before mixing with 1 ml of 1 X binding buffer. Thereafter, 5 μl of annexin V-FITC and 10 μl PI were added to each cell suspension and incubated for 10 minutes in 37 °C incubator and protected from light. Samples were then analysed using a FACSCalibur^TM flow cytometer (Becton Dickinson). Approximately 10,000 events per sample were collected and the data was analysed using WINMDI.

2.6.8 Caspase-3/7 activity

Rationale: To determine if the cell death induced by drug treatment is due to caspase-dependent cell death pathway, activity of caspase-3/7 upon drug treatment was investigated.

Activity of caspase-3/7 was performed using Caspase-Glo® Assay Kits (Promega). Cell density at 3 X 10^3 cells/well were cultured and treated with

phytochemicals in white-walled 96-well luminometer plate (Thermo Fisher Scientific) and harvested at 2, 4, 6, 12, 24 and 48 hours according to the manufacturer's instructions. After 1-hour incubation at 30 ºC with equal volume of pre-mixed Caspase-Glo® Substrate and Caspase-Glo® Buffer, luminescent signal was read using TECAN SpectraFluor Plus microplate reader. Controls in this experiment were DMSO-treated samples and cell-free medium with phytochemicals.

2.6.9 Oligo GEArray gene expression analysis

Rationale: To validate the observations in functional studies, Oligo GEArray was carried out to study gene expression profiles of phytochemical-treated cells.

- **RNA extraction, cDNA and cRNA synthesis**

    Gene expression profile was performed using Cancer PathwayFinder Oligo GEArray in HybTube Format (SABiosciences, Maryland, USA). Briefly, total RNA was extracted using RNA extraction kit (Qiagen), cDNA was reverse transcribed from the extracted RNA and the resultant cDNA was used to synthesise cRNA labelled with Biotin-16-UTP (Roche Molecular Systems, USA).

- **Hybridisation, washing, and blocking of array membrane**

    Purified biotin-labelled cRNA was hybridised to the array membrane overnight at 60°C with agitation. Subsequent washing steps were performed using 2 X SSC with 1 % SDS followed by 0.1 X SSC with 0.5 % SDS at 60°C. Array membrane was blocked for 40 minutes at room temperature with gentle agitation.

- **Alkaline phosphatase-conjugated streptavidin binding and CDP-star chemiluminescent substrate hybridisation**

Alkaline phosphatase-conjugated streptavidin was added to the array membrane and CDP-Star chemiluminescent substrate was added to produce chemiluminescent signals.

- **Image detection and acquisition**

Signal detection was performed by exposing array membrane to CL-XPosure Film (Thermo Fisher Scientific) and developed using Kodak Medical X-ray Processor 102 (Kodak, New York, USA).

- **Data analysis**

Analysis was performed using GEArray Expression Analysis Suite 2.0 software (http://geasuite.sabiosciences.com).

2.6.10 Western blotting

Rationale: To further confirm the gene expression patterns, protein expression was analysed to validate the observations in functional studies.

- **Protein extraction**

Total proteins from control and treated cells were isolated using 100 µl of ice-cold RIPA (radio-immunoprecipitation assay) buffer (1 % nonidet P-40, 1 % sodium deoxycholate, 0.1 % SDS, 0.15 M NaCl, 0.01 M sodium phosphate, 2 mM EDTA, 50 mM sodium fluoride, 0.2 mM sodium vanadate and 100 U/ml aprotinin, pH 7.2) with complete protease inhibitor cocktail tablet (Roche Molecular Systems). Samples were gently mixed for 45 minutes at 4 °C, then centrifuged at 14,000 rpm for 30 minutes at 4 °C to collect supernatant into fresh tubes.

- **Protein quantification**

    Protein concentration was estimated by the Bradford assay, using protein assay dye reagent (Bio-Rad, California, USA) and serial diluted bovine serum albumin (0.5 μg, 0.25 μg, 0.125 μg, 0.0625 μg and 0.03125 μg) to establish the standard curve. Concentrated protein assay dye reagent was diluted using distilled water at the ratio of 1:4. 1 ml of diluted reagent was mixed with 18 μl of distilled water and 2 μl of protein sample in cuvette. Before reading the absorbance at 595 nm using UV-VIS scanning spectrophotometer, UV-1601 (Shimadzu), machine was normalised using RIPA control as blank, after which, samples were measured.

- **Polyacrylamide gel preparation**

    Resolving polyacrylamide gel at 7.5, 10.0, and 12.0 % were prepared using distilled water, Tris buffer (pH 8.8), 40 % Acrylamide/Bis Solution (Bio-Rad), 10 % SDS, TEMED (Bio-Rad) and 10 % Ammonium Persulfate (Bio-Rad).

- **Sample preparation**

    Twenty-one microlitre of protein samples containing 45 μg each were mixed with 4 μl of 6 X sample buffer and boiled at 99 °C for 10 minutes. Samples were then quick spun and immediately loaded into 1 mm thick polyacrylamide gel. Precision Plus Protein Standard (Bio-Rad) was used as marker in each gel.

- **Sodium dodecyl sulfate polyacrylamide gel electrophoresis (SDS-PAGE)**

    SDS-PAGE was performed at 100 V constant voltages until the dye-front of loading dye reached the bottom of the gel. Proteins on the gel were

then transferred onto a 0.45 μm nitrocellulose membrane (Whatman, Springfield Mill, UK) at 100 V constant voltage at 4 °C in pre-cooled transfer buffer (3.03 g Tris, 14.4 g Glycine, 10 ml of 10 % SDS, 200 ml absolute ethanol, top-up to 1 L with distilled water). Thereafter, nitrocellulose membrane was stained with Ponceau S (Sigma-Aldrich) to ensure proper transfer. Ponceau S stain was removed by shaking in Tris-Buffered Saline Tween-20 (TBST). Membrane was then blocked for 1 hour in 5 % non-fat milk in TBST.

- **Immunoblotting (Western blotting)**

    Membranes were probed with primary antibodies against Bax, Bcl2, Survivin, p21, p53, MDM2, Cyclin B, Cyclin D, Cdk1, Caspase-8, Caspase-9, PARP1 and β-actin (Santa Cruz Biotechnology, USA) at 4 °C for overnight or 37 °C for 1 hour. Secondary antibodies of horse radish peroxidase (HRP)-bound anti-mouse or anti-rabbit were used after washing off excess primary antibodies with TBST.

- **Immuno-detection**

    Immuno-detection was performed by using SuperSignal West Pico Substrate (Thermo Fisher Scientific) and SuperSignal West Femto Maximum Sensitivity Substrate (Thermo Fisher Scientific). Chemiluminescent signal was exposed to CL-XPosure Film (Thermo Fisher Scientific) and developed using Kodak Medical X-ray Processor 102 (Kodak).

- **Data analysis**

    Densitometry measurement was carried out using Molecular Imaging Systems software (Kodak).

2.6.11 Real Time Reverse Transcription Polymerase Chain Reaction (RT-PCR) of *hTR* and *hTERT* mRNA expressions

Rationale: Real time RT-PCR was performed to investigate the expression of *hTR* and *hTERT* mRNA in drug-treated samples. Changes in *hTR* and *hTERT* mRNA expressions may implicate alteration of telomerase activity and telomere length.

Quantitative detections of *hTR* and *hTERT* mRNA was performed with the commercially available LightCycler *TeloTAGGG hTERT* Quantification Kit (Roche Molecular Systems, USA) and LightCycler *TeloTAGGG hTR* Quantification Kit (Roche Molecular Systems) using LightCycler® instrument (Roche Molecular Systems). All subsequent quantification steps were done according to the manufacturer's instructions. Briefly, total RNA was extracted using RNeasy kit (Qiagen) according to the manufacturer's instructions. RNA yield and purity was assessed by Nanodrop (Thermo Fisher Scientific). Total RNA of 200 ng was used to perform real-time RT-PCR for *hTR*, *hTERT* and porphobilinogen deaminase (PBGD) in separate reactions. Expression of *hTR* and *hTERT* was calculated on a standard curve constructed from the standards supplied in the kit. For quantification, *hTR* and *hTERT* values were normalized to those of PBGD and expressed as the ratio of *hTR* and *hTERT* mRNA copy numbers to PBGD mRNA copy number.

2.6.12 Telomerase activity detection using Telomeric Repeat Amplification Protocol (TRAP)

Rationale: TRAP assay was carried out to investigate the changes in telomerase activity of drug-treated sample compared to its DMSO-treated

control. Decrease in telomerase activity can be interpreted either as interruption of the function of telomerase enzyme and/or down-regulation of the expression of telomerase enzyme.

- **Total protein extraction and quantification**

Telomerase activity detection was performed with the commercially available TRAPeze® XL Telomerase Detection Kit (Millipore). Total protein was extracted by incubating cell pellet in the CHAPS lysis buffer provided for 30 minutes on ice. Samples were spun at maximum speed at 4 °C for 20 minutes to collect supernatant. Protein quantification was carried out using Bradford method (section 2.6.10) and 1.5 µg proteins was treated with 1 µl/ml RNasin ribonuclease inhibitor (Promega) to eliminate RNA before performing the next step.

- **Polymerase chain reaction (PCR) setup**

In the PCR reaction, 50 µl of reaction mix containing 10 µl of the 5 X TRAPeze XL® Reaction Mix, 0.4 µl of 2 U Taq Polymerase (Promega), 37.6 µl of sterile polymerase chain reaction (PCR) water, and 2 µl of the sample cell extract was prepared. This mixture was then incubated at 30 °C for 30 minutes to allow the telomerase enzyme to synthesise telomeric repeats. PCR amplification of the telomeric repeats was performed on a thermocycler using a three-step PCR at 94 °C for 30 seconds, 59 °C for 30 seconds and 72 °C for 1 minute for 35 cycles, followed by a 55 °C at 25 minutes for extension step. Controls for this experiment are telomerase-positive cell lysate from human carcinoma cells. Standard curve was generated from TSR8 with serial dilutions. Negative controls in this experiment were Taq-negative control,

CHAPS-only negative control, heat treated sample and sulforhodamine house-keeping control.

- **Fluorescence signal detection**

Fluorescence signals of PCR products were measured according to fluorescein (Ex: 485 nm; Em: 535 nm) and sulforhodamine (Ex: 585 nm; Em: 620 nm) using SpectraFluor Plus fluorescence plate reader (TECAN, Männedorf, Switzerland).

- **Data analysis**

The telomerase activity of each sample was determined by calculating the ratio of the increase in fluorescein absorbance (produced by the amplification of telomeric repeats) to the increase in sulforhodamine absorbance.

2.6.13 Telomere length measurements using Terminal Restriction Fragment (TRF)

Rationale: Telomere length analysis was performed to correlate telomere shortening to telomerase activity in long-term treatment studies. This assay also used to study massive telomere attrition and alternative lengthening of telomere (ALT).

- **Isolation and digestion of genomic DNA**

Telomere length analysis was performed with the commercially available *TeloTAGGG* Telomere Length Assay kit (Roche Molecular Systems). Genomic DNA was extracted from 15-day drug-treated samples using DNA extraction kit (Qiagen). DNA was digested using *Hinf I* and *Rsa I* restriction

enzymes at 37°C for 2 hours to generate the telomere restriction enzyme fragments.

- **DNA electrophoresis**

  One microgram of digested DNA was then run on 0.8 % agarose gel at 60 V. The gel was first submerged in acid solution to depurinate DNA strands then alkaline solution to denature DNA into single strand and finally neutralisation solution before it was set up for southern blot transfer.

- **Southern blot transfer**

  Southern blot was setup by placing agarose gel on top of a wet sponge with 20 X SSC with a nylon membrane put above the agarose gel. Pressure was applied evenly using paper towels and weights to create capillary action. The transfer was allowed to carry out overnight.

- **Hybridisation with DIG-labelled probe and anti-DIG alkaline phosphatase**

  After southern blotting, the membrane was cross-linked using UV and washed with 2 X SSC salt solutions. Hybridisation was performed by incubating membrane with DIG-labelled probe for 3 hours. After washing off excess probe, anti-DIG alkaline phosphatase was incubated with the bound hybridisation probe on the membrane. Detection buffer and substrate were then added to the membrane for signal detection.

- **Analysis of telomere length**

  Telomere signals were developed onto x-ray film, and the mean telomere lengths were estimated using Molecular Imaging Systems software (Kodak).

2.7 Statistical analysis

Statistical comparisons between and among the groups were made using two-way ANOVA, Student's t-test (two-tailed) and contingency tables analysis (*chi-square* test and Fisher's exact test) using Microsoft Excel 2003 (Microsoft Corporation, Washington, USA) and GraphPad Prism version 4.00 for Windows (GraphPad Software, USA). The statistically significant differences are represented as follows: ∗ indicates $p < 0.05$, ∗∗ indicates $p < 0.01$, ∗∗∗ indicates $p < 0.001$.

Chapter 3   RESULTS AND DISCUSSION

3.1   Properties of phytochemicals.

The effectiveness of a treatment is determined by the efficacy of the interaction and synergy between the exogenous and endogenous factors of a therapy. Exogenous factors include the duration of treatment, treatment cycles and drug properties. The endogenous factors are based on the characteristics of all cells without treatment. In this section, properties of the phytochemicals such as compound stability and emission of fluorescence signals are investigated.

3.1.1. Plumbagin, genistein and curcumin are stable at room temperature and to the exposure to light.

The stability of phytochemicals remains to be an important issue in determining the duration of treatment. To explore these phytochemicals as potential cancer therapeutics, studies on the stability of phytochemicals are first carried out using the spectrophotometer. All phytochemicals used in this study were dissolved in dimethyl sulfoxide (DMSO) to get a final concentration of 0.1 %. The stability of plumbagin, genistein and curcumin was investigated by comparing the UV-VIS spectra of these phytochemicals under two different conditions: exposed to light and stored at room temperature versus protected from light and at stored at -20°C. Chemical compound degradation is indicated by a λ_{max} wavelength shift towards lower wavelength (left-shift), whereas aggregation of chemical compound is shown by a λ_{max} wavelength shift towards higher wavelength (right-shift). Figures 3.1A, 3.1B and 3.1C show that over a period of 7 and 14 days, plumbagin, genistein and curcumin

stored at two different conditions did not exhibit any shift in the λ_{max}. The amplitude of the absorbance curve did not change drastically indicating that the concentration remained the same as that on day 0. This experiment shows that plumbagin, genistein and curcumin can be stored at room temperature and exposed to light without detectable deterioration by light absorbance. In addition, freezing and thawing of the phytochemicals did not result in any shift in the peaks of the wavelength. However, as a precaution, these phytochemicals are kept in the dark and at -20°C to avoid changes in concentration that might occur due to decreases in drug volume over time. Freeze-thaw processes were avoided by aliquoting the phytochemicals.
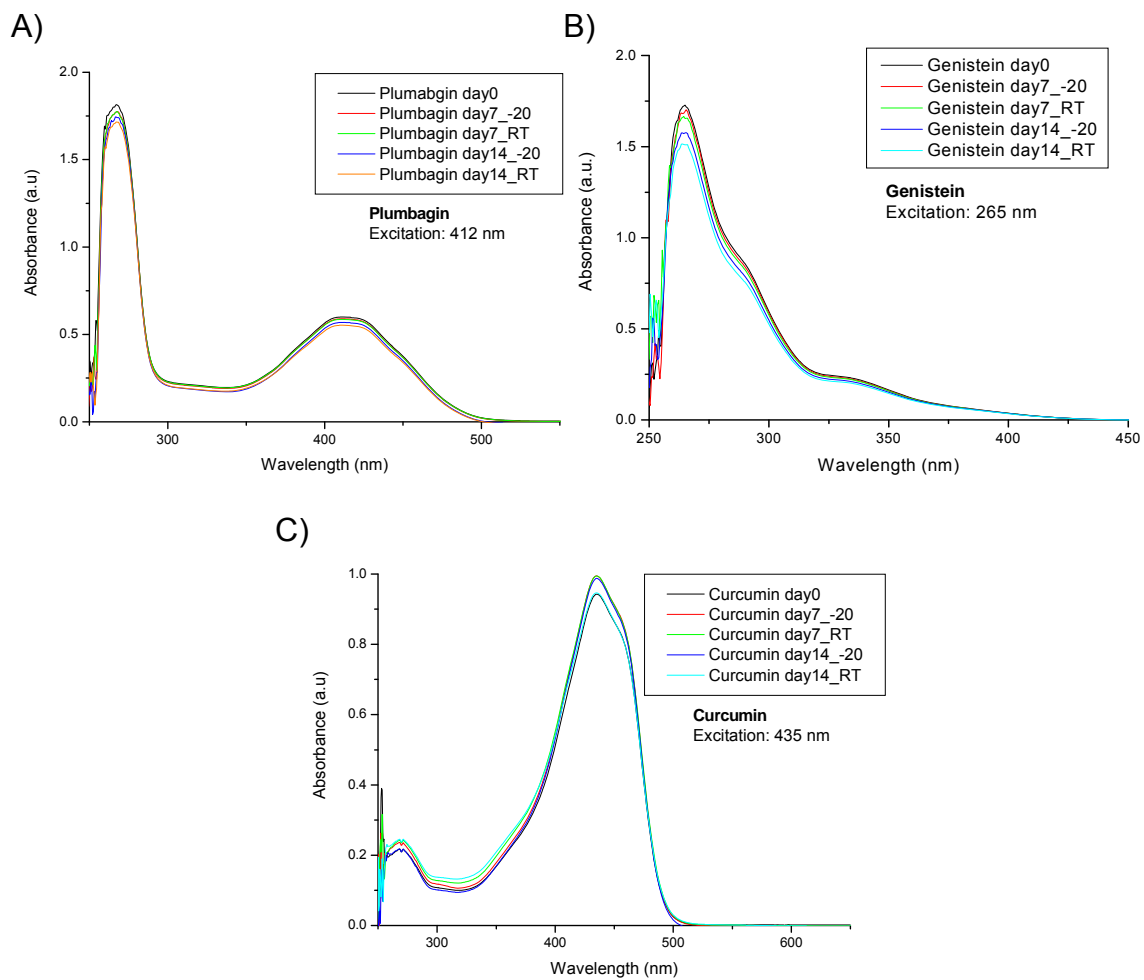
Figure 3.1. Absorbance values of A) plumbagin B) genistein and C) curcumin stored at -20°C protected from light and room temperature (RT) exposed to light measured at day 0, 7 and 14.

3.1.2. Plumbagin and curcumin but not genistein emit fluorescence signals upon excitation by ultra-violet light.

The absorbance values of the compounds not only serve as an indicator of compound aggregation or degradation but are also used to determine the excitation wavelength for measuring fluorescence of the phytochemicals. The fluorescence spectra of plumbagin showed distinct peaks with maximal emission wavelength at 414 and 472 nm when excited at 412 nm (Figure 3.2A and 3.2B). As the emission wavelength at 414 nm is in close proximity to the excitation wavelength used and therefore might interfere with the emission reading, emission wavelength at 472 nm (blue fluorescence) was selected. Also, the use of excitation wavelength at 267 nm as indicated in Figure 3.2A did not emit fluorescence signals. Genistein showed a maximal excitation peak at 265 nm when analysed using UV-VIS spectrophotometer. However no fluorescence signal was detected when genistein was excited at the wavelength of 265 nm. As for curcumin, the maximal excitation wavelength at 435 nm was used to generate a maximal emission signal at 531 nm, corresponding to the green region in the UV-VIS spectra (Figure 3.2C and 3.2D). In these experiments, the emission wavelengths of each phytochemical were determined and used in drug localization studies during treatments with phytochemicals. The drug trafficking observation will be further discussed in section 3.3.2.1 for plumbagin and 3.3.4.1 for curcumin.

Overall, the absorbance analyses show that phytochemicals used in this study are stable in normal storage conditions. Of the three phytochemicals used, only plumbagin and curcumin emit fluorescence that is useful in tracking the route of drug in the cell during treatment.
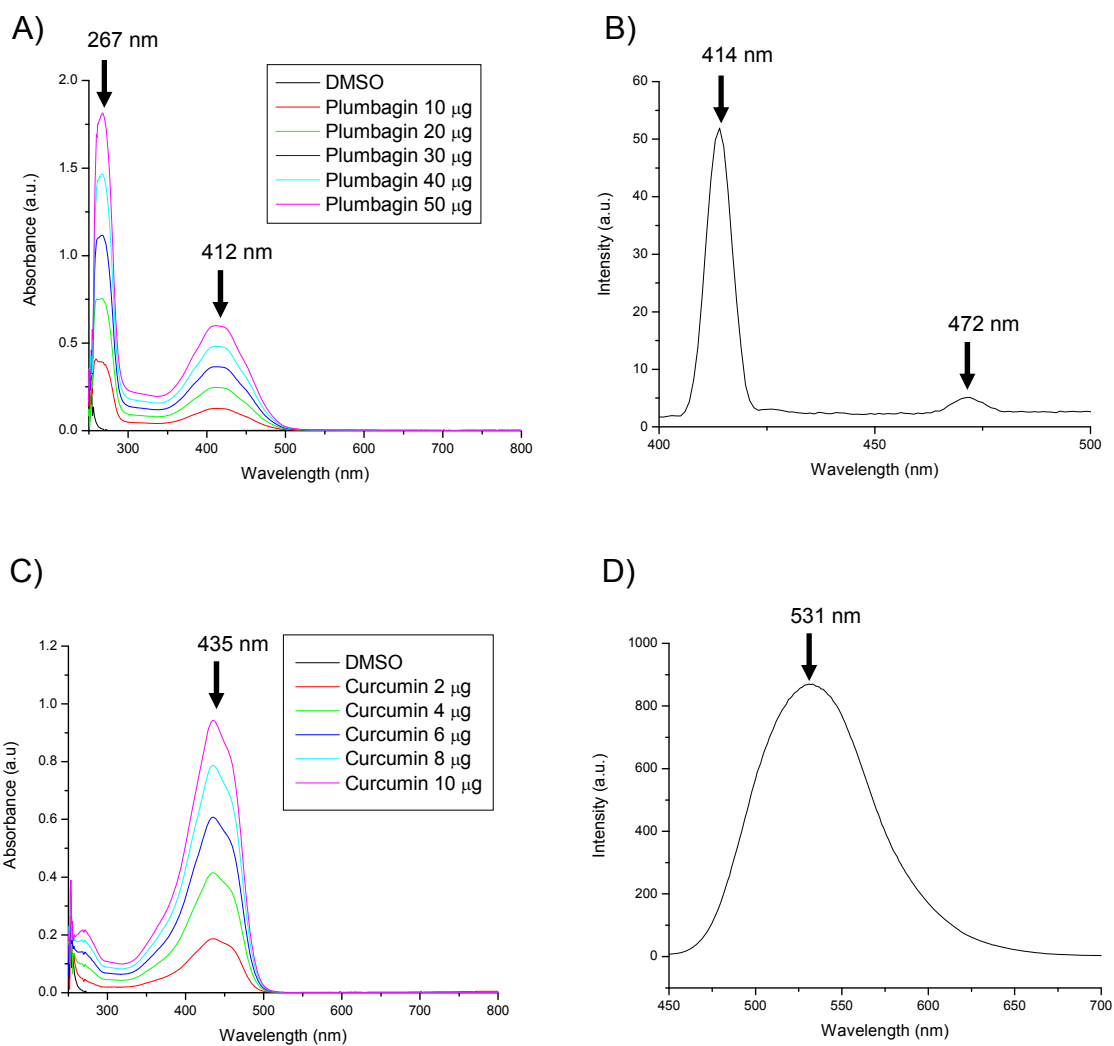
Figure 3.2. Detection of the excitation and emission wavelengths of plumbagin and curcumin. A) Plumbagin excites at 267 nm and 412 nm. B) Plumbagin emits fluorescence at 414 nm and 472 nm. C) Curcumin excites at 435 nm. D) Curcumin emits fluorescence at 531 nm.

3.2. Characteristics of brain cancer cells

Besides understanding the properties of the phytochemicals, it is equally important to look at the characteristics of the brain cancer cells used in this study. Understanding the basal properties of cells will help to explain the differential responses to different drugs. The flow of the investigation of this study will start with the basal population doubling rate. Thereafter, the relationship of p53 mutations and responses to irradiation will be addressed. Lastly, integrative genomic analysis using chromosomal aberrations, gene expression and oligonucleotide array-based comparative genomic hybridisation (array-CGH) studies will be discussed.

3.2.1. Population doubling rates in different cancer cell lines

To measure the basal growth rate of the brain cancer cells, the optical density (OD) values of cells cultured for 3 consecutive days were measured after staining with crystal violet. As shown in Figure 3.3, all brain cancer cell lines exhibited different population doubling rates. The medulloblastoma cell line, ONS76, displayed the fastest doubling rate at 22.62 hours/generation. Among the glioblastoma cell lines, the A172 cell line showed the slowest growth rate at 40.67 hours/generation. All cell lines underwent exponential growth that resulted in higher cell density at day 3. The population doubling rates obtained will greatly facilitate our understanding of cell responses related to growth rate and also justify the use of 48 hours as treatment duration.
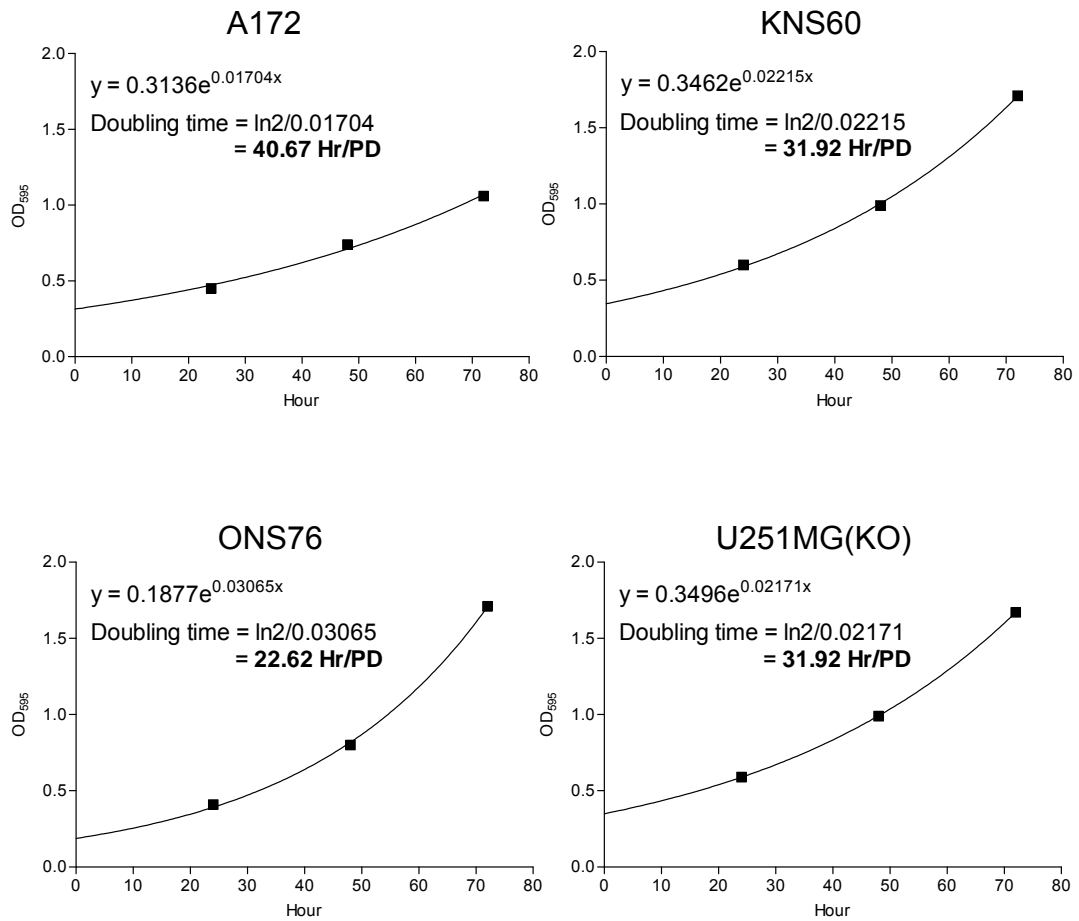
Figure 3.3. Population doubling rates of brain cancer cell lines. ONS76 grew faster at a doubling time of 22.62 hours while A172 displayed the slowest doubling rate at 40.67 hours/generation.

3.2.2. Brain cancer cell lines used in this study carry endogenous *TP53* mutations and exhibit different responses to radiotherapy

In this section, we sought to categorize the brain cancer cell lines as radioresistant or radiosensitive by testing the sensitivities of the brain cancer cell lines towards gamma irradiation. The responses of the brain cancer cells to radiotherapy were correlated to their status of the endogenous p53 proteins. The four brain cancer cell lines used in this study carry different mutations in the p53 tumour suppressor gene (Ishikawa *et al.,* 2006). A172 and ONS76 cell lines harbour a mutation at codon 72 in the proline-rich domain which alters the ability of p53 to induce apoptosis and diminish its DNA repair capacity (Hu *et al.,* 2005; Siddique and Sabapathy, 2006). The KNS60 cell line carries a mutation at codon 193 while U251MG(KO) has a mutation at codon 273, both of which are within the DNA binding domain. Mutation in this domain can cause major conformational change of the folding of core-binding domain in p53 protein, thus affecting the DNA binding ability and stability of p53 (Lu *et al.*, 2007; Ma *et al.*, 2005).

To study the radioresponse, cell cycle profile, colony formation and DNA damage response were analysed upon irradiation of the brain cancer cells with a dose of 2 Gy. Cell cycle analysis was carried out to examine cell death and cell arrest upon irradiation. As shown in Figure 3.4, irradiated cells show different degrees of cell death and arrest. The cell cycle profiles show that most cell lines exhibited a similar trend of cell cycle arrest at the S and G2/M phase with a significant decrease in the G1 population. However, KNS60 did not exhibit any significant changes in the S and G2/M populations. In summary, the cell cycle analysis shows that A172, ONS76 and

U251MG(KO) cells responded to the damage induced upon radiation via cell cycle arrest at the S and G2/M phase. In addition, U251MG(KO) exhibited increased cell death as depicted by the increased in the sub-G1 region.

With the observation that some cells were arrested upon radiation treatment, colony formation assay was performed to further investigate the clonogenicity of cells. In the colony formation assay (Figure 3.5), all irradiated cells showed a reduction in the colony numbers after 10 days of culture compared to control cell lines. A172, ONS76 and U251MG(KO) cell lines exhibited a greater decrease in colony numbers compared to the KNS60 cell line. This finding suggests that A172, ONS76 and U251MG(KO) cells are sensitive to irradiation.

The amount of damaged DNA induced by radiation was also investigated. The comet assay, also known as single cell gel electrophoresis assay, was carried out to investigate the sensitivity of cell lines towards radiation-induced DNA damage. As shown in Figure 3.6, all cell lines exhibited an increase in the mean tail moment, a representation of DNA damage. The A172 and ONS76 cell lines exhibited significantly more damage compared to their untreated controls. KNS60 did not exhibit any significant increase in damages upon irradiation. U251MG(KO) cell showed high levels of DNA damage in both untreated and irradiated samples, indicating that the cells might have harboured higher level of DNA damage even without any treatment. The comet results suggest that the A172 and ONS76 cell lines are more susceptible to the damages induced by irradiation than KNS60 and U251MG(KO).

Taken together, it is plausible that A172 and ONS76 cell lines are more sensitive to radiation-induced damage compared to KNS60 and U251MG(KO) cell lines. The higher population of cells detected in the sub-G1 region and the reduction in colony numbers in irradiated U251MG(KO) may not be seen as an effect of radiation treatment, instead, it is more likely to be attributed to higher endogenous DNA damage where the radiation treatment synergistically enhance the effects resulting in the induction of cell death and reduction of clonogenicity. Hence, it can be postulated that cells harbouring a mutation at codon 72 in the proline-rich domain of p53 may be more susceptible to radiation-induced damage, while cells that have mutations in other regions of p53 are relatively resistant to radiation-induced damage. Observation of the radioresponses closely correlates with an earlier report by Ishikawa *et al.* (2006). Genes that may be involved in the radioresponses will be discussed in section 3.2.3.
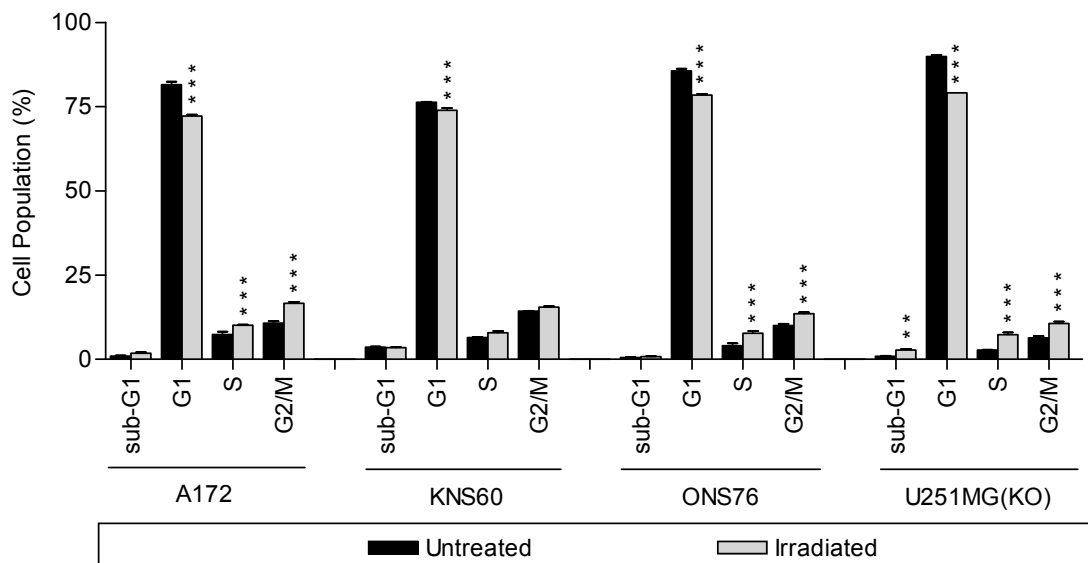
Figure 3.4. Cell cycle analysis of irradiated brain cancer cell lines using propidium iodide staining and flow cytometry detection. All cell lines exhibited a significant decrease in G1 phase population, and most cell lines have a higher population of cells in S and G2/M phase after irradiation at 2 Gy without significant cell death. ** indicates p < 0.01, *** indicates p < 0.001.
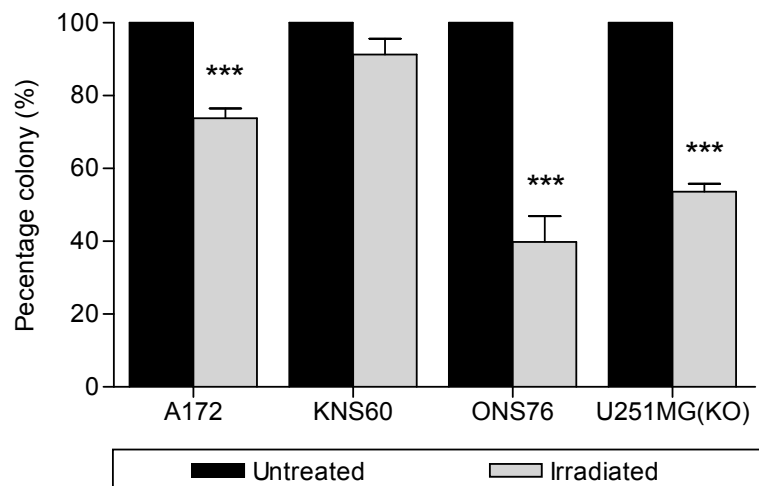
Figure 3.5. Colony formation assay of irradiated brain cancer cell lines. All cell lines showed a decrease in colony numbers after irradiation. Significant reduction was observed in A172, ONS76, and U251MG(KO) cell lines. *** indicates p < 0.001.
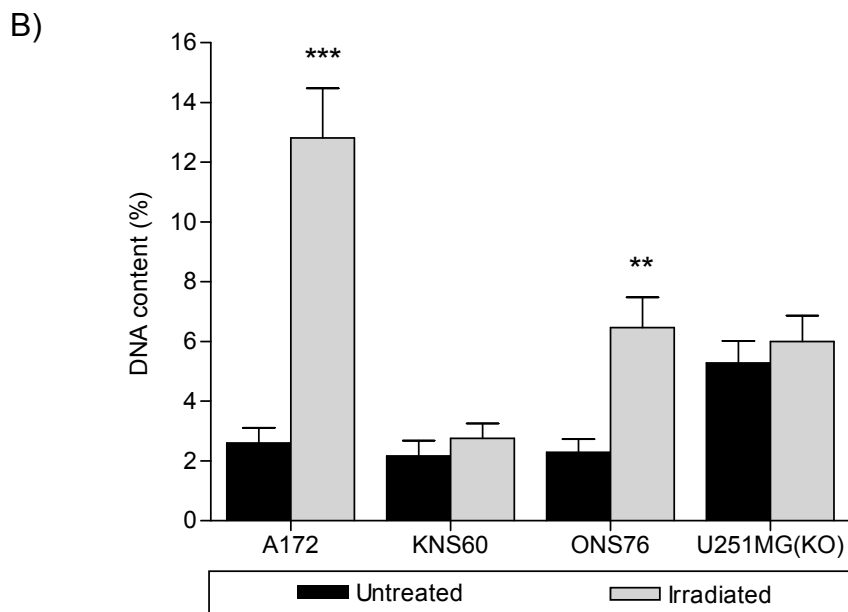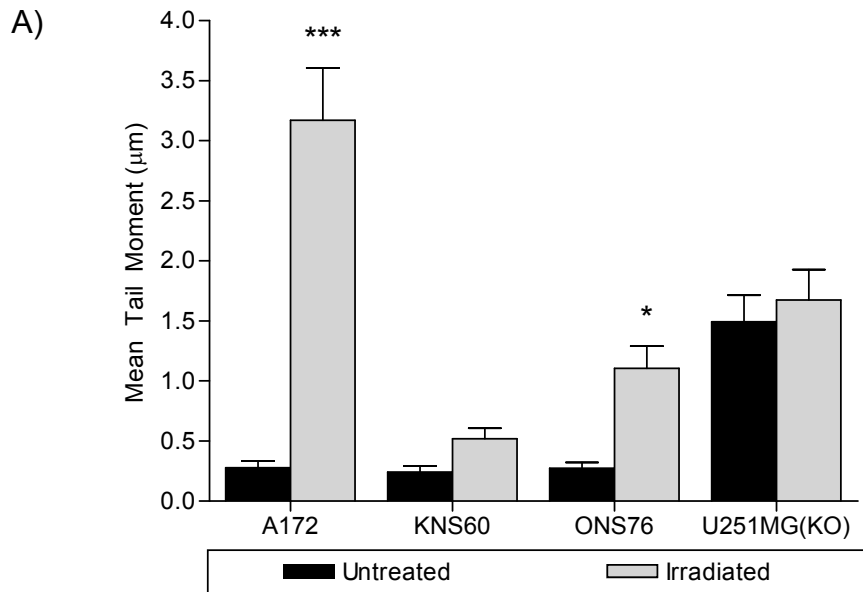
Figure 3.6. DNA damage analysis of brain cancer cell lines performed using single cell gel electrophoresis assay. A) A172 and ONS76 cell lines harbour more damages after irradiation compared to KNS60 and U251MG(KO) cell lines. B) Representation of DNA content in comet tails in percentage. * indicates p < 0.05, ** indicates p < 0.01, *** indicates p < 0.001.

3.2.3. Integrative genomic analysis of chromosomal aberration analysis, microarray gene expressions and array-CGH

To further analyse the characteristics of brain cancer cells, integrative genomic analysis was performed by analysing the data generated from multicolour Fluorescence *in situ* Hybridisation (mFISH), microarray gene expression and array-CGH. Chromosomal aberration analysis was carried out using the mFISH technique. As shown in Figure 3.7, all cell lines exhibited aneuploidy, a phenotype typical of cancer cells. Complex and simple chromosomal translocations were observed in all cell lines. The A172 cell line showed incidences of translocation between chromosomes 1–11–17, 2–14–5, 3–21–9 and 6–16–7 (Figure 3.7A). The KNS60 cell line exhibited consistent translocations in chromosomes 3–6, 8–21–5, 16–14 and 9–20–7 (Figure 3.7B). Translocations in the ONS76 cell line were present in chromosomes 4–7, 6–8, 16–20 and 3–9 (Figure 3.7C). In the U251MG(KO) cell line, complex translocations were found in chromosomes 2–19–8, 11–10–15 and 13–7 (Figure 3.7D). Global deletion of chromosome 19 was observed in all karyograms and chromosome 7 was found to have undergone multiple translocations in all brain cancer cell lines. However, there were no noticeable chromosomal aberrations that differentiated between the glioblastoma and medulloblastoma cell lines, and between radiosensitive and radioresistant cell lines, probably because the aberrations that determine the radioresponses and brain cancer types are not present at the chromosomal levels but at the gene levels, thus the resolution of mFISH is insufficient for identifying those aberrations. It is important to note that translocation of alleles do not necessarily represent dysfunction of genes present in the translocated allele.

Nonetheless, the mFISH data has corroborated the fact that cancer cells have extremely complex genomic aberrations with multiple chromosomal translocations.

Further investigation using microarray gene expressions analysis was carried out using Affymetrix GeneChip® Human Genome Focus Array to identify differentially regulated genes in all brain cancer cell lines as compared to normal human lymphocyte cells. Figure 3.8 shows the hierarchical cluster analysis of four brain cancer cell lines in a heat-map format. From 3435 genes analysed using the Affymetrix platform, selected groups of differentially regulated genes were clustered using the online DAVID Functional Annotation Tool. The gene clusters include genes involved in apoptosis and cell death regulation, cell cycle regulation, DNA damage and repair regulation, signal transductions, angiogenesis, migration and invasion, and telomere regulation. These clusters of differentially regulated genes are presented in Figure 3.9. In A172 cells, 744 genes in the mentioned groups were upregulated and 1141 genes were downregulated. For KNS60 cells, 596 genes were overexpressed, whereas 1030 gene expressions were suppressed. ONS76 cells showed upregulation of 677 genes and downregulation of 1189 genes. Finally, in U251MG(KO) cells, enhanced expression of 719 genes and decreased expression of 1169 genes was identified. Most of the differentially regulated genes in all cell lines were involved in cell cycle and cell death gene clusters. Among the clusters, the KNS60 cell line exhibited a relatively different profile compared to the other three brain cancer cell lines.

From the data presented in the gene clusters, selected gene expression profiles from the microarray analysis were further classified under

different molecular events such as cell cycle, apoptosis and signal transduction molecules. As shown in Figure 3.10, the same trends with different degrees of gene expressions were identified in all cell lines. Cell cycle regulatory genes such as *CDK2*, *CDKN1B* and *CDKN2A* were all downregulated in the brain cancer cells. Among these genes, *CDKN2A* showed the greatest decrease in gene expression. Incidentally, *CDKN2A* encodes for p16, a *CDK4* inhibitor, which is frequently mutated or deleted in a wide variety of tumours suggesting the fact that cell cycle inhibition in these cells are not efficient. Apoptosis regulatory genes, *BCL2L1*, *TERT*, *TNFRSF10B* and *TNFRSF1A* were overexpressed in all cell lines, whereas *BIRC5*, *CASP9* and *HTATIP2* were suppressed. *BCL2L1* that exhibits anti-apoptotic activity is the most highly expressed gene. Pro-apoptotic genes such as *CASP9* and *HTATIP2* were downregulated, indicating that these brain cancer cell lines may be resistant to cell death. In the signal transduction molecules cluster, most of the selected genes showed expressions below the threshold values of detection. Figure 3.11A shows that medulloblastoma cells specifically express certain genes differentially from glioblastoma cells. Among these genes, there were great differences in the expression of *MDM2* and *ETS2* in medulloblastoma and glioblastoma cells. When comparing the gene expressions between the radiosensitive and radioresistant cells, three genes as shown in Figure 3.11B were identified. Interestingly, while all cell types showed decreased expression of *S100A4*, the radioresistant cell lines expressed a larger magnitude of decreases. The other two genes were at the marginal levels of the threshold of detection. This evaluation suggests that these three genes may be potential target genes for further investigation for

the identification of genetic markers of different brain cancer types or different radioresponses. It should be noted that this data is preliminary; by studying a larger number of brain cancer cell lines, a larger and more accurate database can be acquired for better characterisation of brain cancer cells.

In another attempt to characterize brain cancer cells, array-CGH was carried out to study the copy number variation (CNV) and common aberrations. Figure 3.12 shows the CNV profiles of A172, KNS60, ONS76 and U251MG(KO) cell lines respectively in comparison with commercially available genomic DNA control. These CNV profiles were subsequently compared and converted into data that represent common aberrations to show amplified and deleted genes. In Figure 3.13A, the common aberration analysis of all brain cancer cell lines are presented. All cell lines exhibited heterozygous and homozygous aberrations in chromosome 4, 3p, 6q, 11q, 13 and 18q while heterozygous and homozygous amplifications were found in chromosome 1q, 5, 7, 9, 16, 17, 19 and 20. Due to the limitation of having only one medulloblastoma cell line available in this study, the common aberration analysis for medulloblastoma was not performed. Following the removal of the medulloblastoma profile, the common aberration analysis of glioblastoma cells was generated as indicated in Figure 3.13B. Apart from the aberration analysis for brain cancer cells and glioblastoma cells, common aberration analyses of radiosensitive cell lines (A172 and ONS76) and radioresistant cell lines (KNS60 and U251MG(KO)) were also shown. Common aberration analyses of radiosensitive cells and radioresistant cells were presented in Figure 3.13C and 3.13D respectively. Radiosensitive cells displayed greater aberrations in chromosome 1q, 6q, 12, 17, 19 and Xq

whereas radioresistant cells exhibited distinct aberrations in chromosome 4q and 7p. These results have elucidated certain locations and regions of chromosomes that may contain potential aberrations for the identification of brain cancer and glioblastoma cells. Alleles that may be involved in radioresponses are also shown here. However, in order to conclusively determine the distinct aberrations that potentially serve as genetic markers of glioblastoma cells, more samples should be cross-compared.

Interestingly, chromosome 19 is detected using this technique while it was not detected in all the brain cancer cell lines as presented by mFISH. In Figure 3.14, most of the cell lines showed regions in pink, indicating heterozygous amplification of chromosome 19. The ONS76 cell line exhibits homozygous amplification as represented by red regions while KNS60 shows some regions in green indicating deletion. These results suggest that chromosome 19 might have undergone multiple translocations that are beyond the detection resolution of mFISH.

As discussed in the microarray analysis (Figure 3.10), the *BCL2L1* gene was upregulated while the *CDKN2A* gene was downregulated. The differential regulations of these two genes are the most striking among the genes studied. Hence, the CNV profiles of the *BCL2L1* and *CDKN2A* genes were investigated using array-CGH (Figure 3.15A and 3.15B). As expected, the copy number variation of *BCL2L1* gene in chromosome 20 showed 0.5 to 2.0 copies increase in expression, indicating both heterozygous and homozygous amplifications. On the other hand, the copy number variation of *CDKN2A* gene showed 1.0 to 4.0 folds suppression, suggesting homozygous deletion. These results correlate with the findings in the microarray analysis

and confirm that the differential regulation of these two genes was influenced by copy number difference.

It is important to note that this data is preliminary and hence not entirely conclusive for determining genetic markers for brain cancer until the study involving larger sample numbers and comparisons with other cancer cell types is carried out.
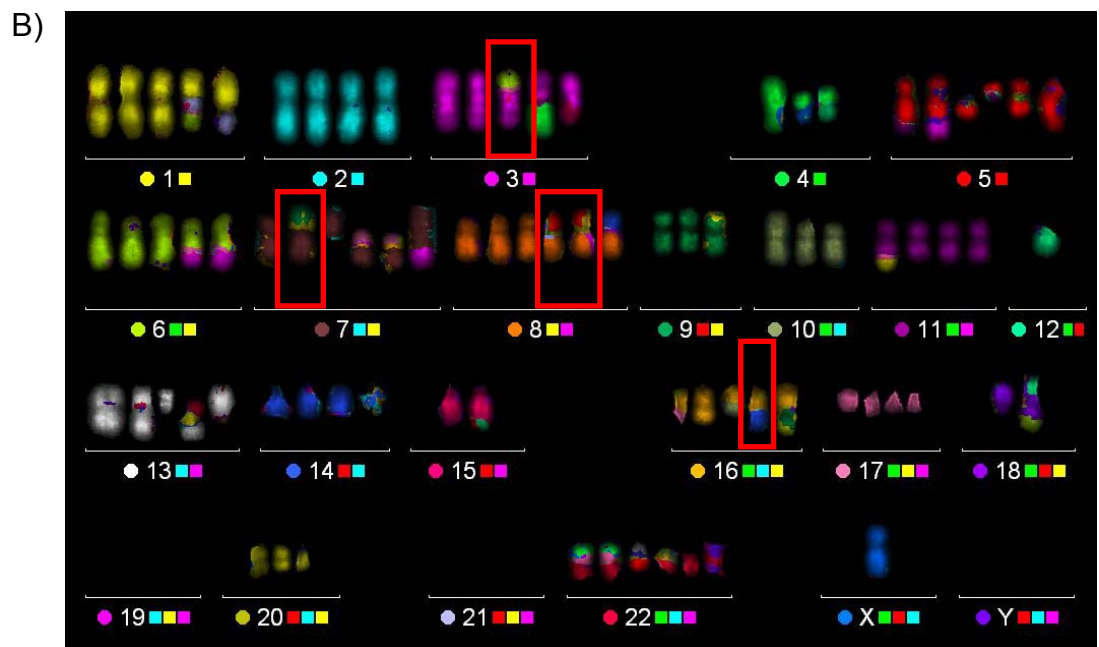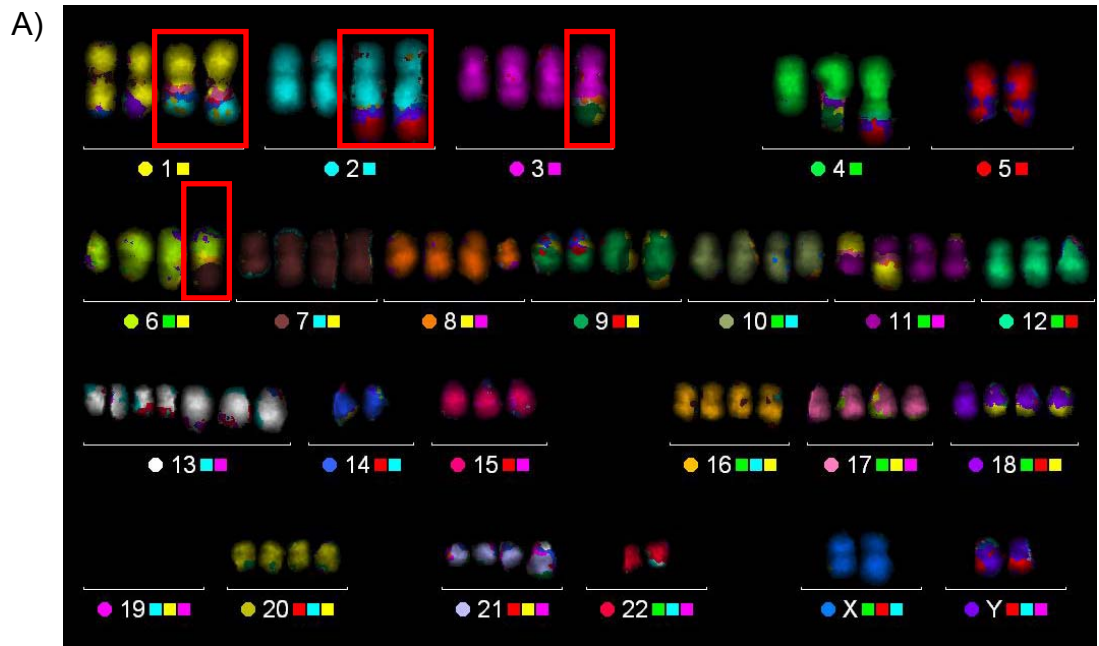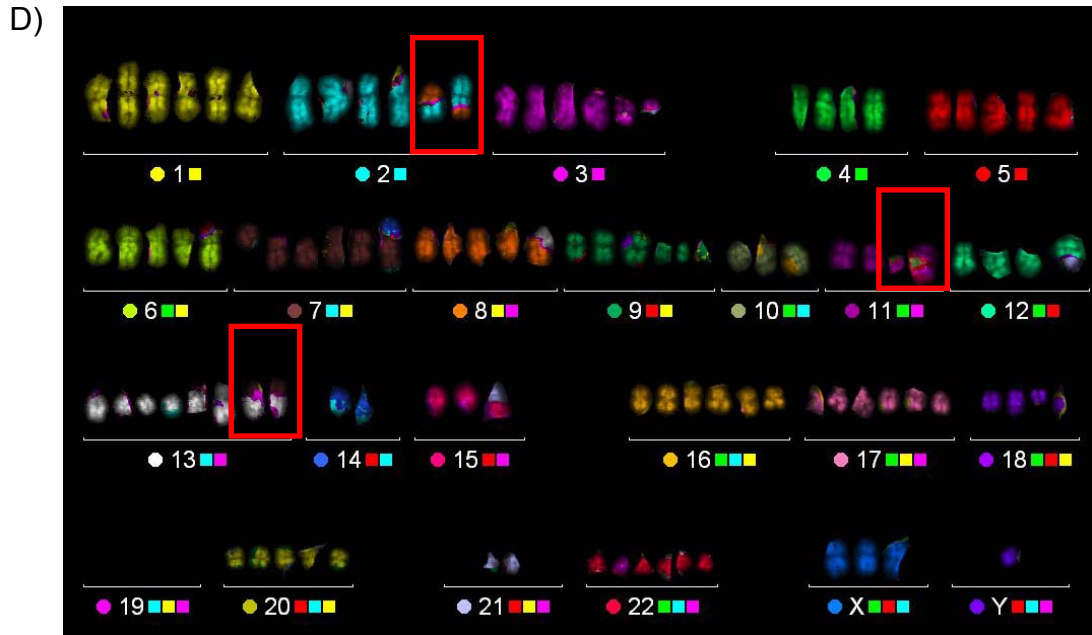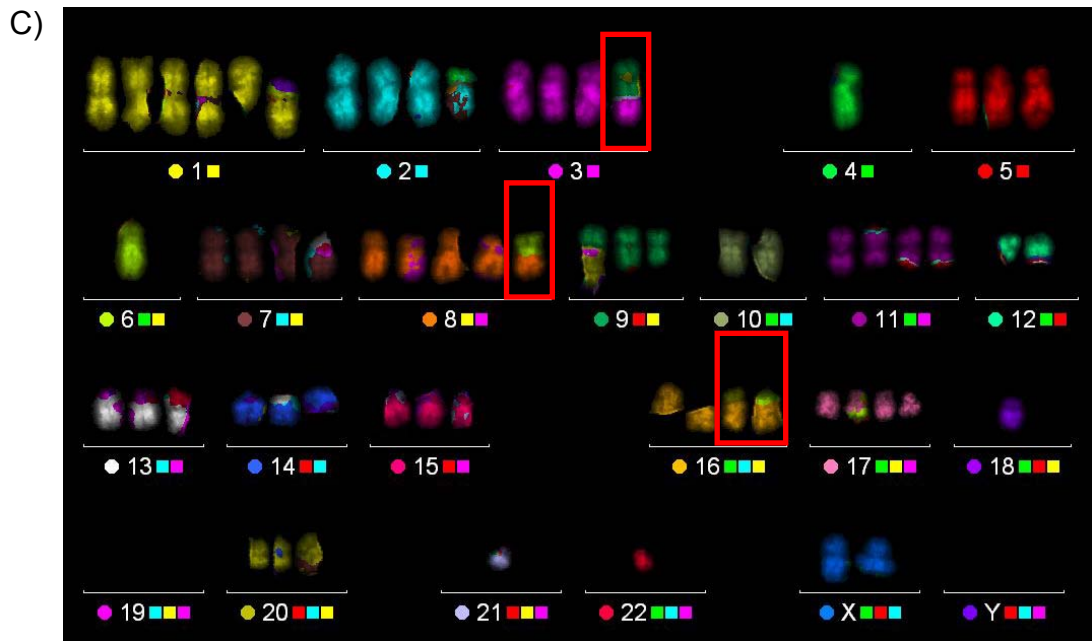
Figure 3.7. Karyograms of A) A172, B) KNS60, C) ONS76 and D) U251MG(KO) cell lines showing complex chromosomal aberrations. Red boxes indicate common aberrations present in 50 metaphases.
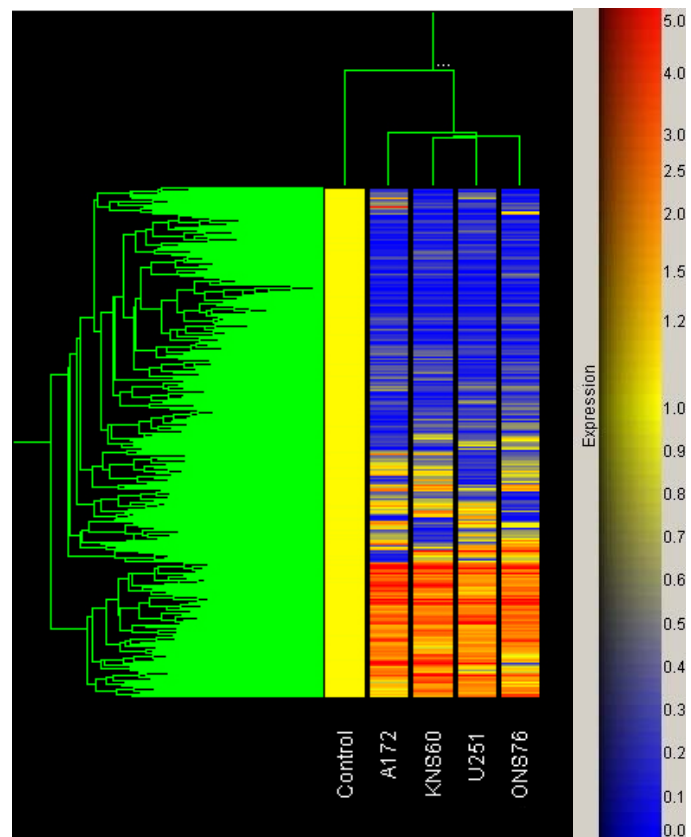
Figure 3.8. Two-way condition tree and expression scale of microarray analysis performed on four brain cancer cell lines.

A)

B)
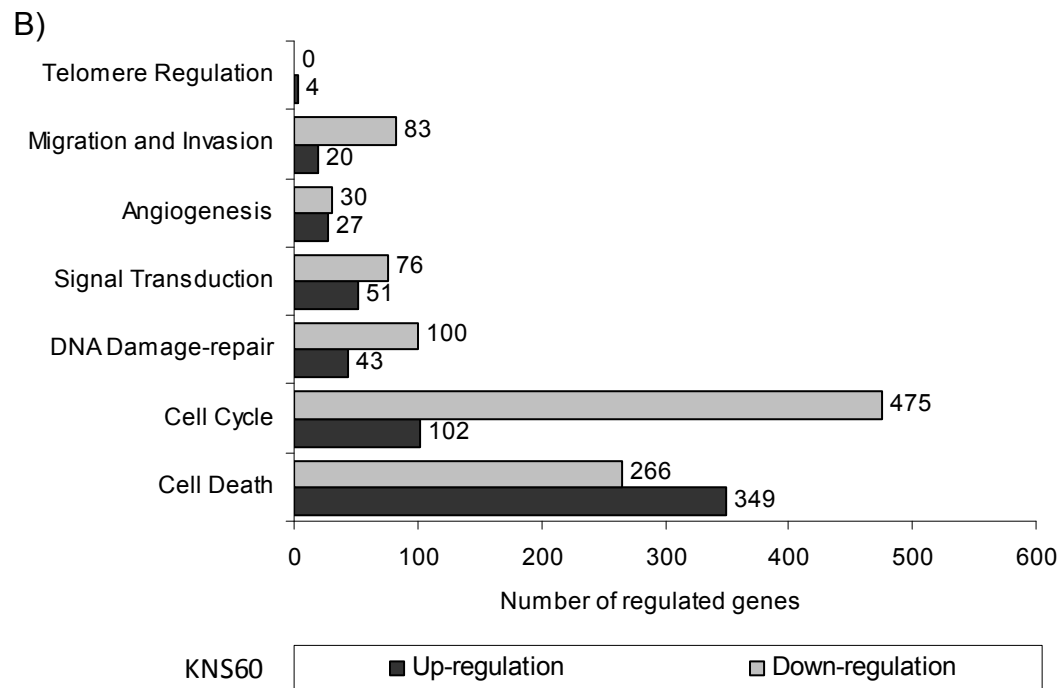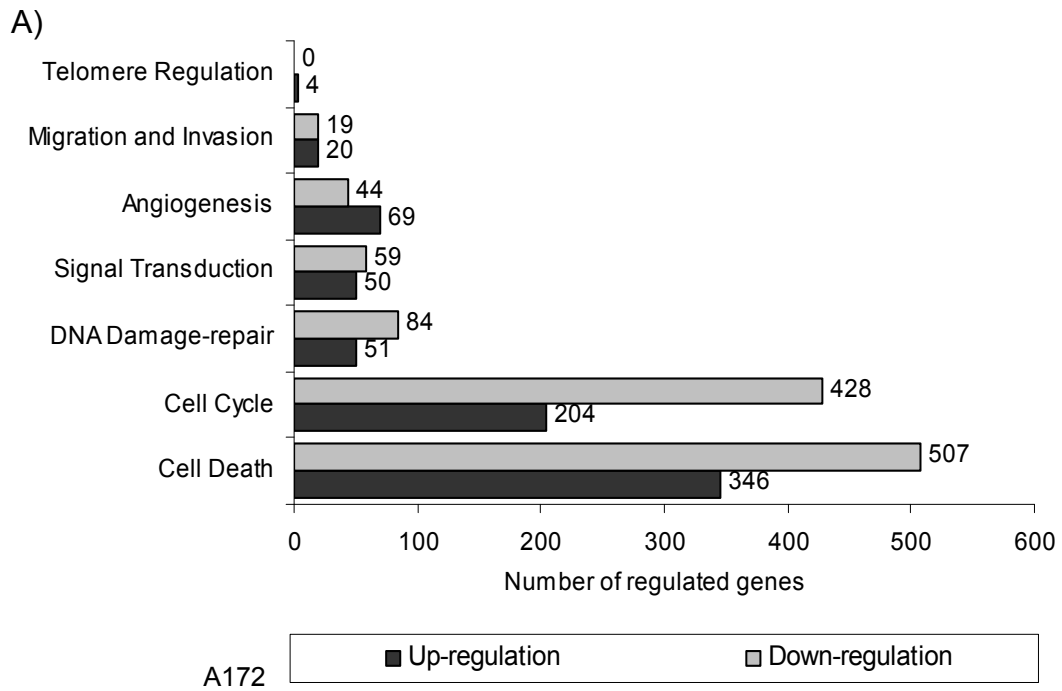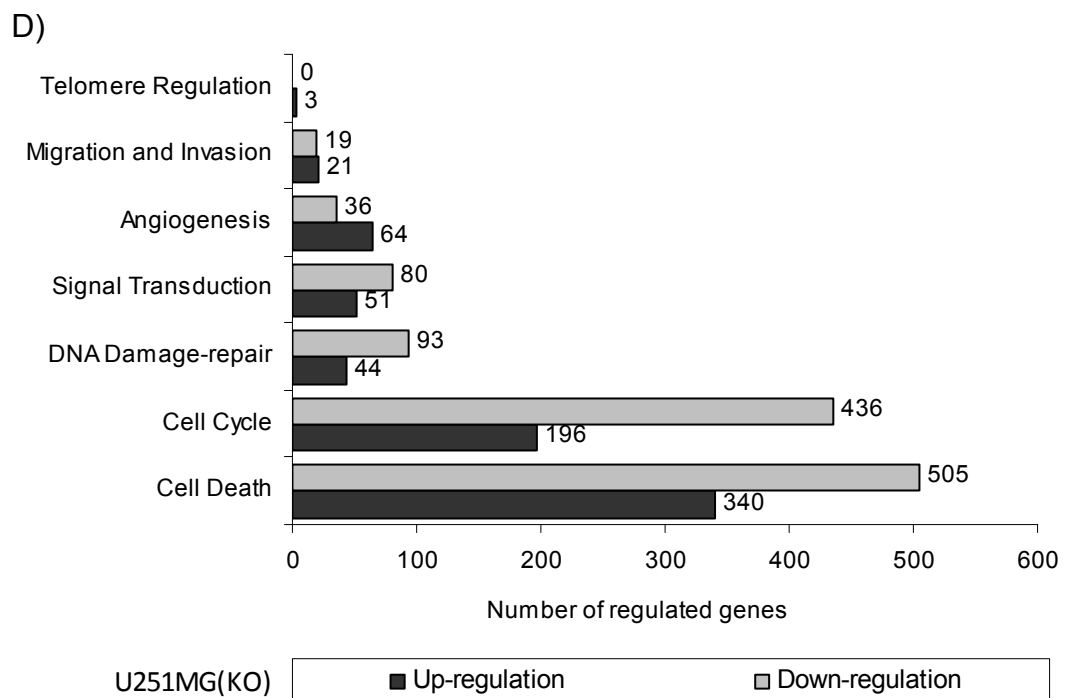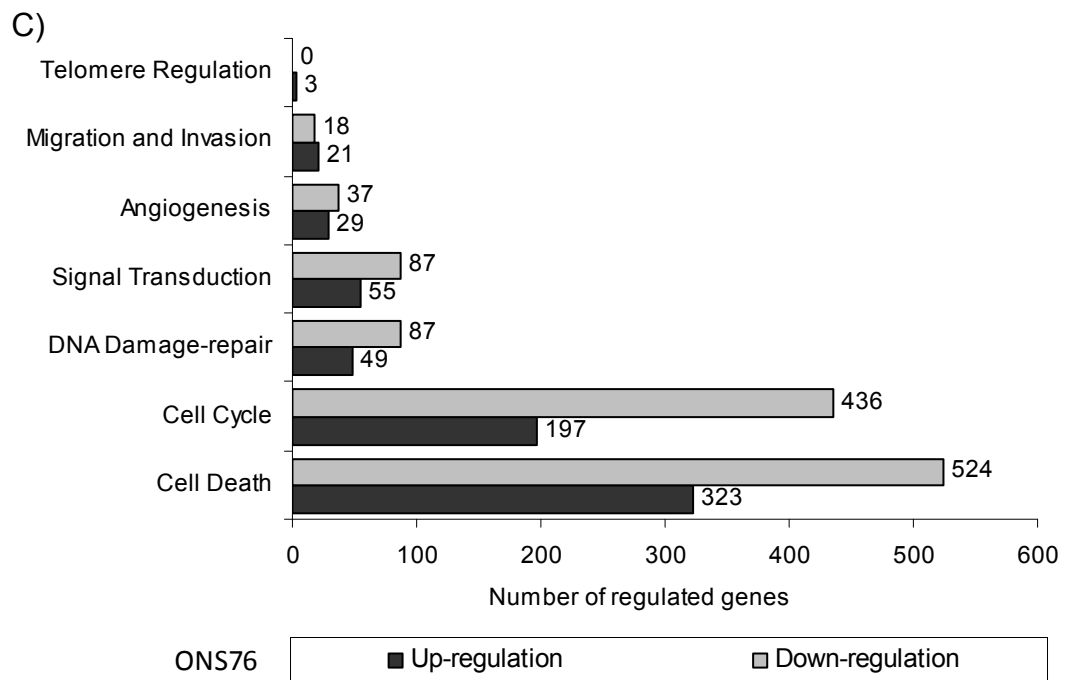
Figure 3.9. Gene clustering charts showing differentially regulated genes of selected gene groups in A) A172, B) KNS60, C) ONS76 and D) U251MG(KO) cell lines.
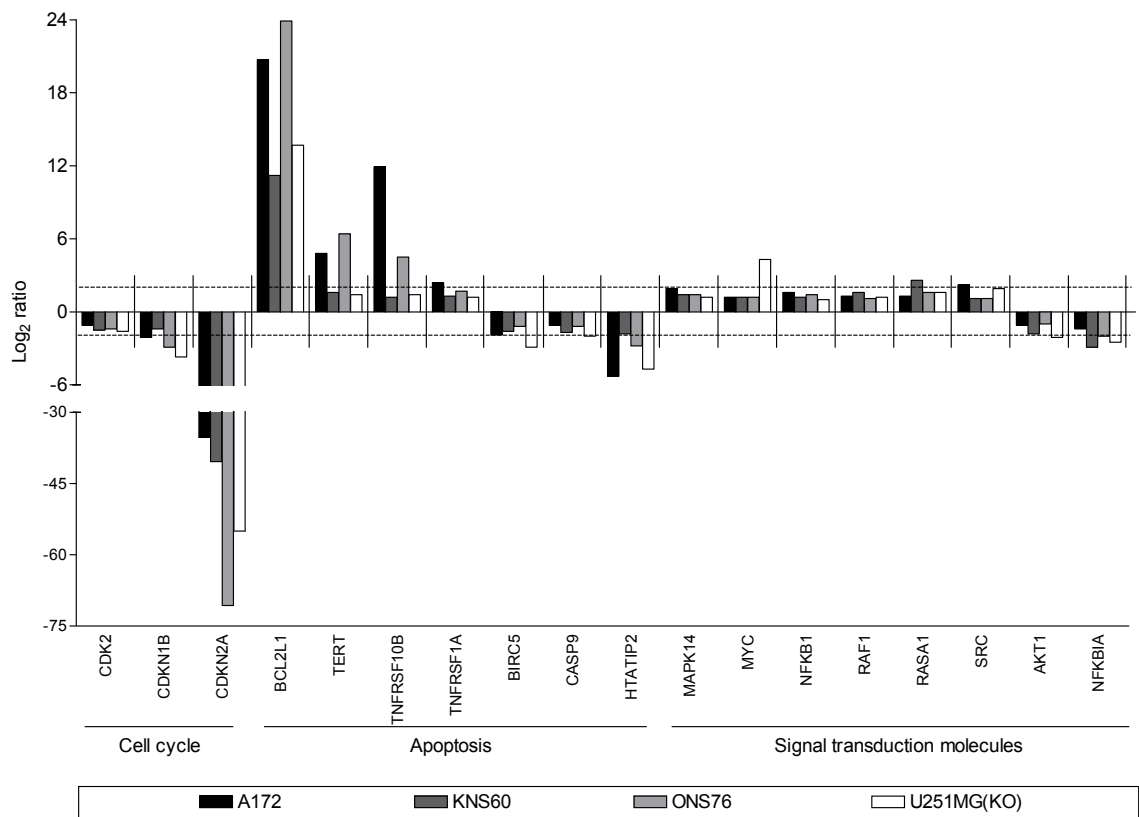
Figure 3.10. Microarray gene expression profiles of genes in selected cellular pathways in brain cancer cells. Dotted lines indicate threshold level at ±0.2.
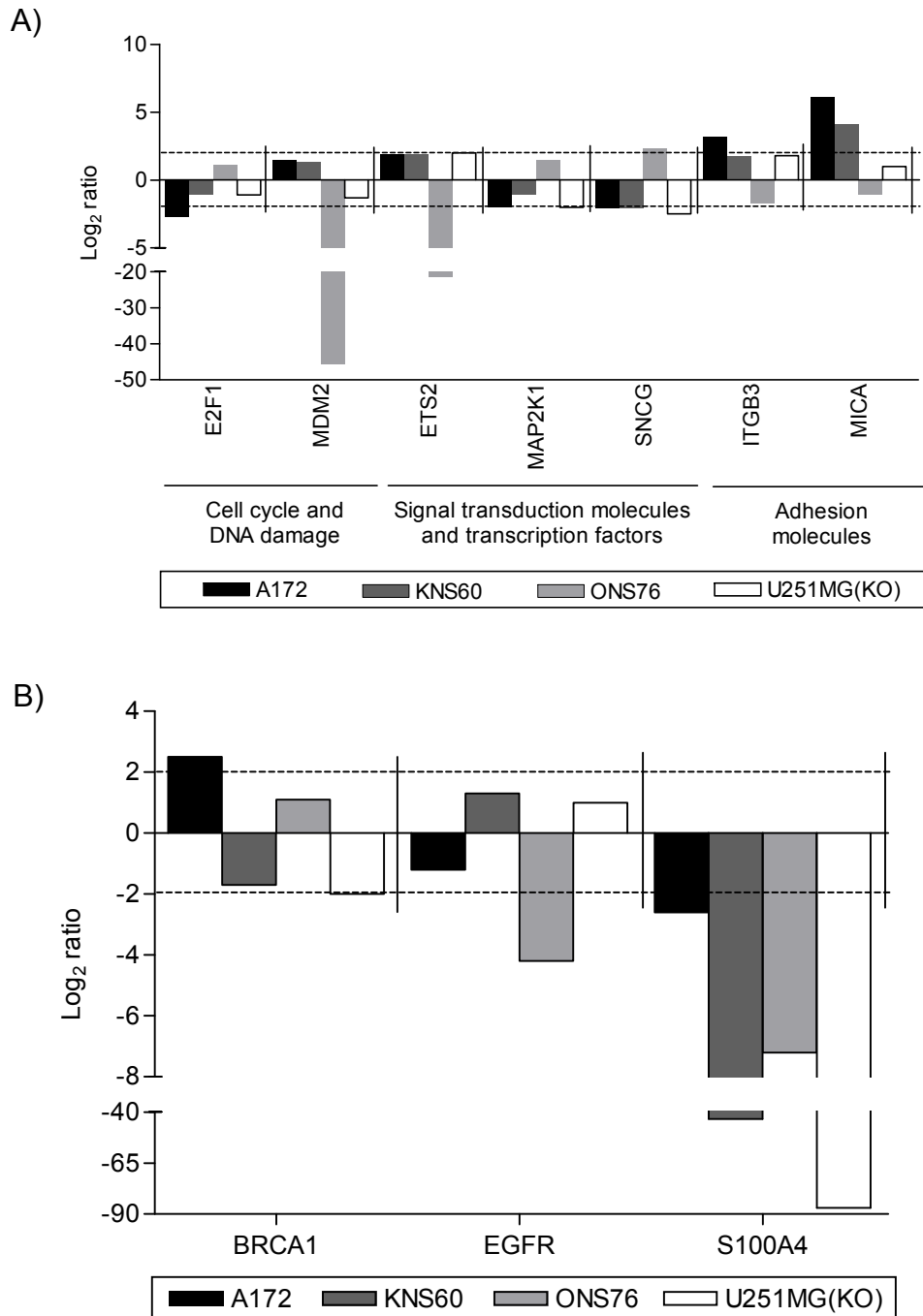
Figure 3.11. Differentially regulated genes in A) medulloblastoma versus glioblastoma B) radiosensitive versus radioresistant cell lines. ONS76 is the medulloblastoma cells whereas A172, KNS60 and U251MG(KO) are the glioblastoma multiforme cell lines. A172 and ONS76 cells are radiosensitive whereas KNS60 and U251MG(KO) cell lines are radioresistant. Dotted lines indicate threshold level at ±0.2.

A)
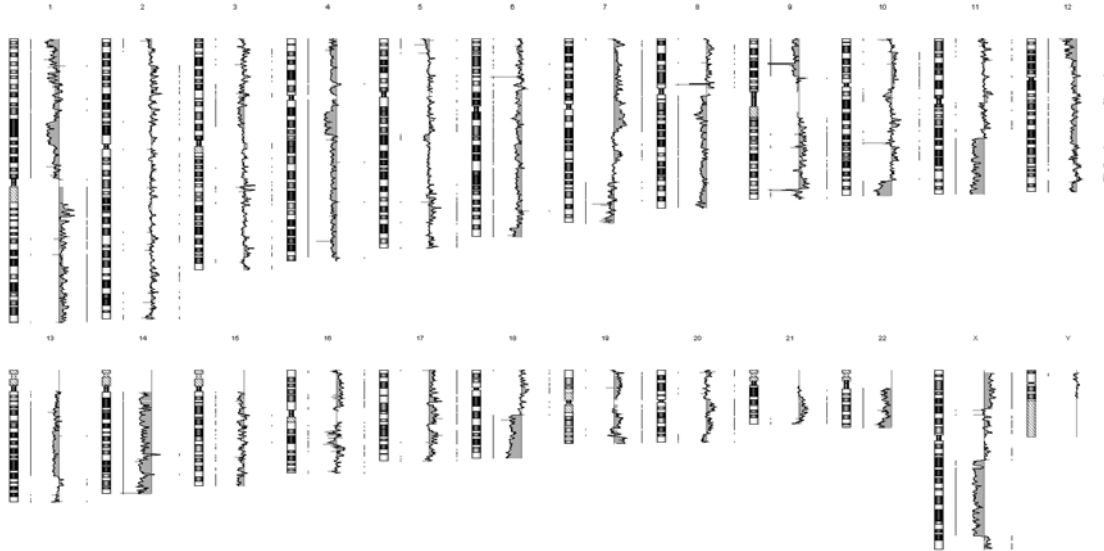
B)
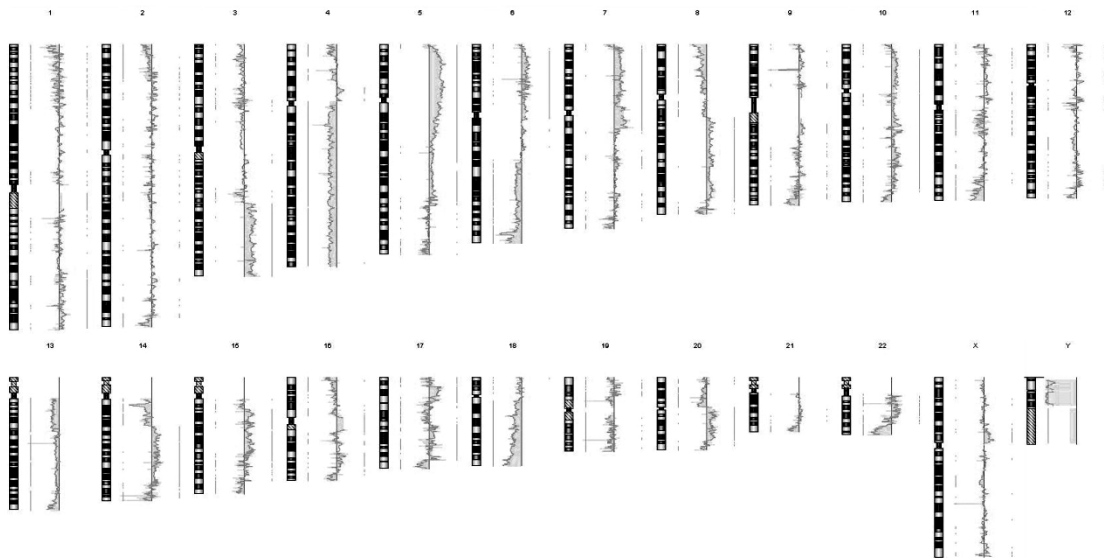
C)

D)
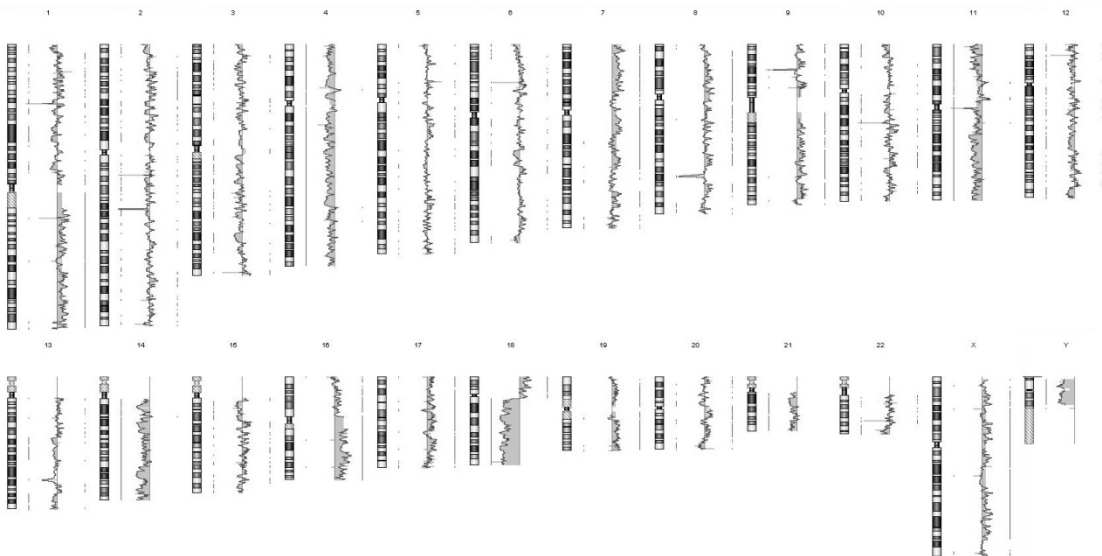
Figure 3.12. Copy number variation profile of A) A172, B) KNS60, C) ONS76 and D) U251MG(KO) cell lines. The analysis was carried out using the ADM-2 statistical algorithm in CGH Analytics software.

A)
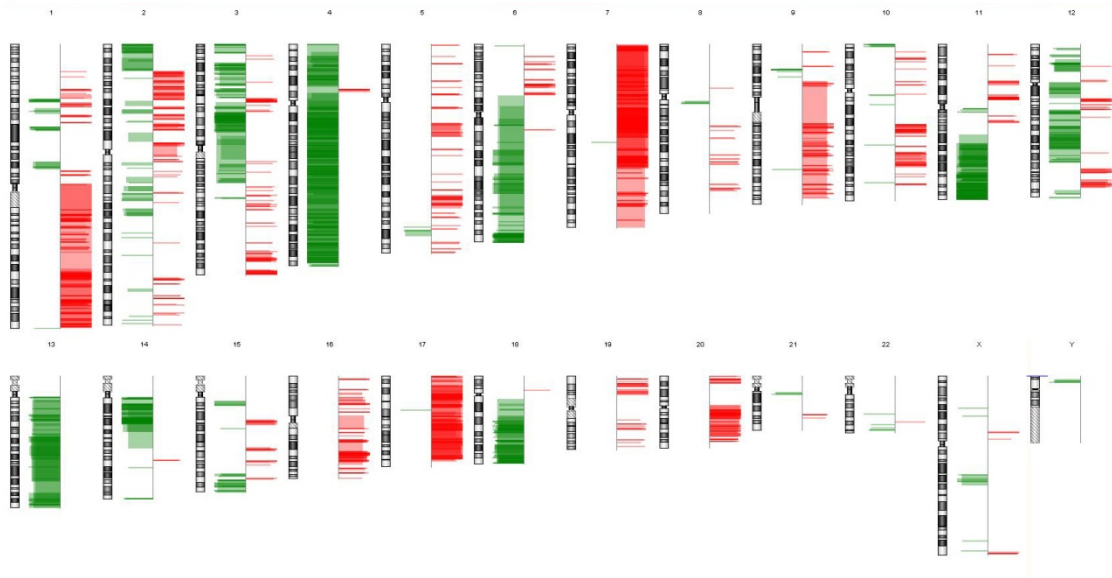
B)
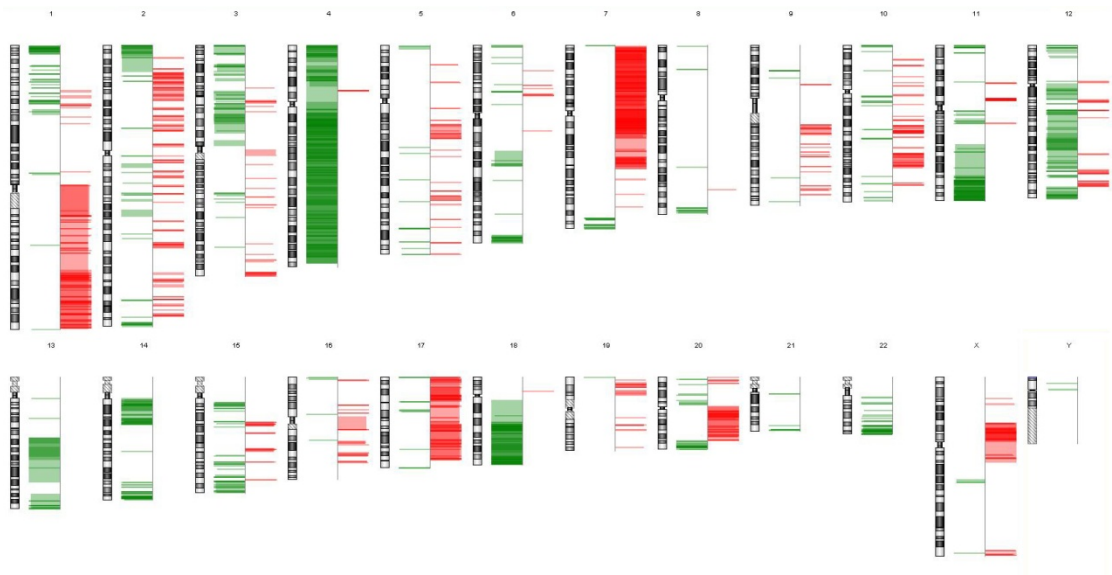
C)
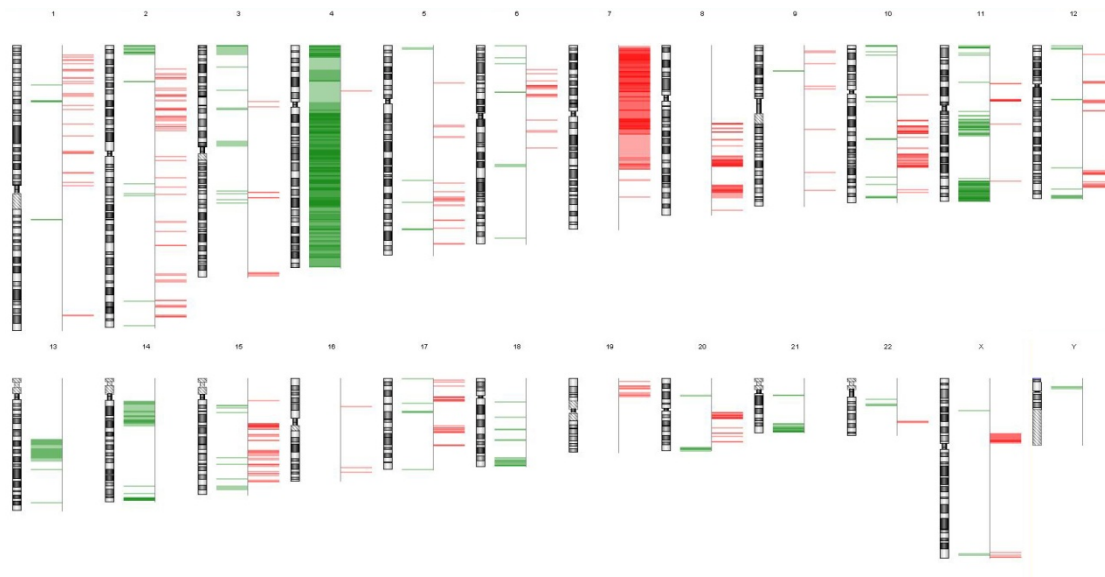
D)
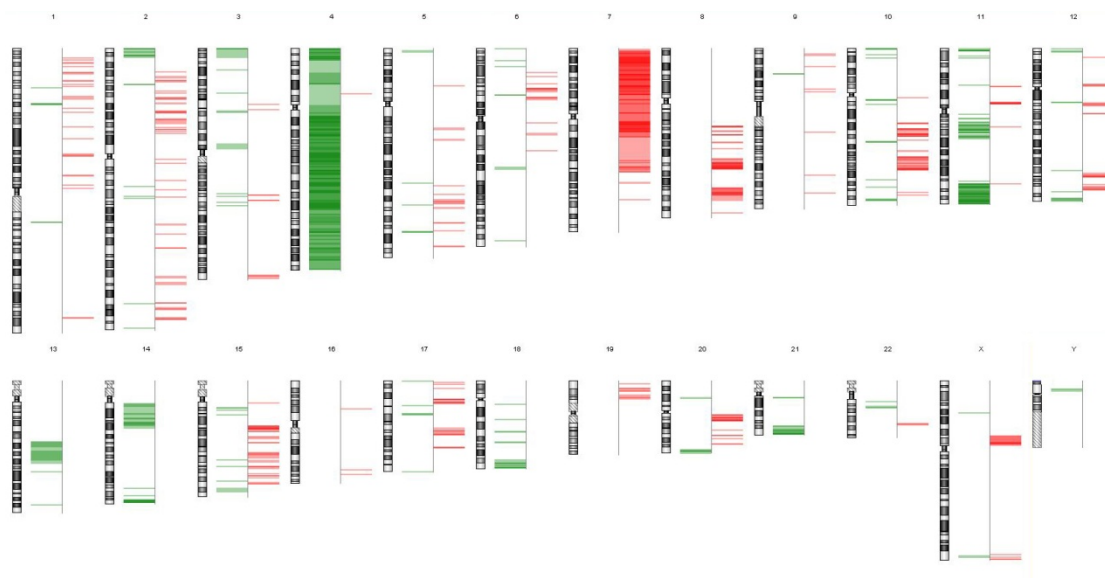
Figure 3.13. Ideogram display of common aberrations of A) all brain cancer, B) glioblastoma multiforme, C) radiosensitive and D) radioresistant cell lines. Dark green and light green signals indicate homozygous and heterozygous deletion respectively whereas red and pink indicate homozygous and heterozygous amplification respectively.

Figure 3.14. Aberration summary of chromosome 19 in brain cancer cell lines. Dark green and light green signals indicate homozygous and heterozygous deletion respectively whereas red and pink indicate homozygous and heterozygous amplification respectively.
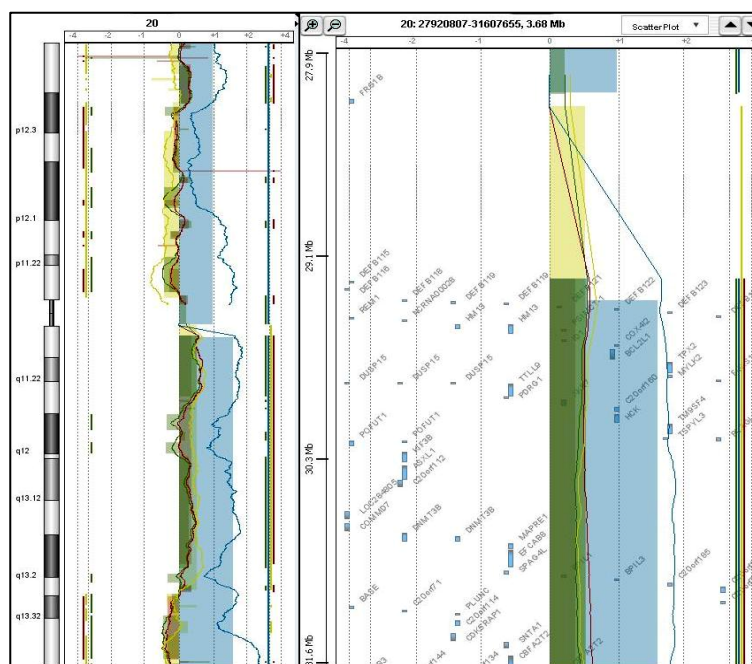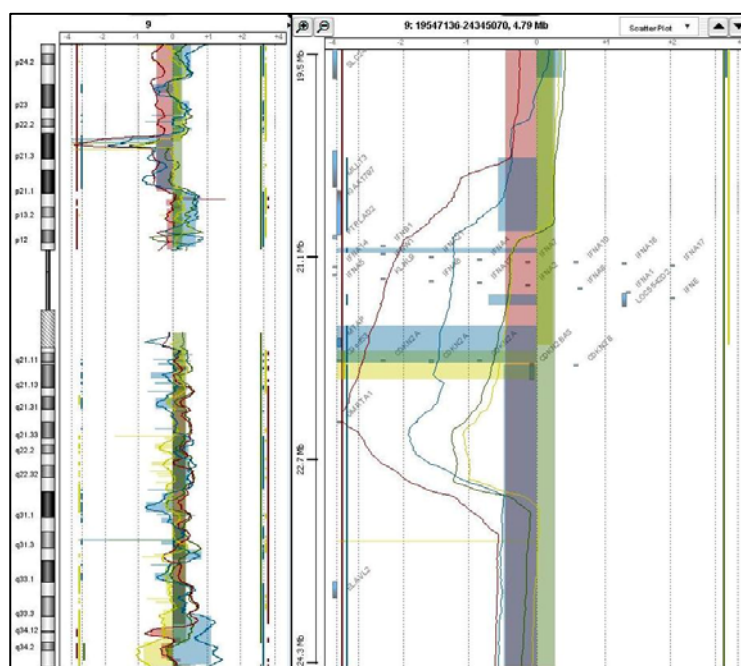
Figure 3.15. Copy number variation profile of A) chromosome 20 showing amplification of *BCL2L1* gene and B) chromosome 9 showing deletion of *CDKN2A* gene in all brain cancer cell lines.

3.3. Cell response to drug treatments.

The main focus of this section is to investigate the mechanisms or pathways triggered and regulated by three phytochemicals, i.e. plumbagin, genistein and curcumin. For this, phenotypical and molecular responses ranging from morphology to gene and protein expressions of each cell line will be discussed in detail.

3.3.1. Dimethyl sulfoxide (DMSO) at low concentration does not induce cell death and DNA damage.

To study the cell response to the drug alone, comparison with the drug solvent is necessary. As all three phytochemicals were dissolved in the solvent DMSO, it is important to validate that DMSO does not induce major changes in cell responses that might give rise to false positive results. Hence in this section, cell density, morphology and DNA damage analysis upon DMSO treatment were performed. DMSO at different concentrations ranging from 0.0 % [v/v] to 2.0 % [v/v] was used to study its toxicity in all brain cancer cell lines which are used in this investigation. As shown in Figure 3.16, cell density decreases in a dose-dependent manner. At DMSO 0.1 % [v/v], there was insignificant cell death observed using crystal violet cell density assay, indicating that this concentration of DMSO is non-cytotoxic. Thus, all phytochemicals used in this study were dissolved in DMSO to achieve a final concentration of 0.1 % [v/v] in the total cell culture media volume.

To further confirm that the 0.1 % [v/v] of DMSO is not cytotoxic, cell morphology was observed using a light microscope. Figure 3.17 shows the morphology of the normal untreated cells and cells treated with DMSO.

DMSO-treated cells show no changes in cell density and morphology compared to the untreated controls. This data shows that 0.1 % [v/v] of DMSO does not affect the density and morphology of brain cancer cell lines.

Subsequently, we investigated the DNA damage induced by DMSO treatment using the comet assay which was performed on brain cancer cells that are treated with 0.1 % [v/v] DMSO. As shown in Figure 3.18A, DMSO triggered very low levels of DNA damage with mean tail moments lower than 1 μm. DMSO-treated cells did not exhibit any significant increase in DNA damage when compared with untreated controls. Figure 3.18B shows the representation of the percentage of DNA content measured from the comet tails; none of the cell lines show significant increase in the DNA content in the comet tails post DMSO treatment suggesting that 0.1 % [v/v] DMSO does not induce any significant DNA damage and is hence appropriate to be used to dissolve the drugs of interest.

Altogether, these results have shown that a final concentration of 0.1 % [v/v] of DMSO does not induce significant increase in DNA damage and does not affect cell morphology and density.
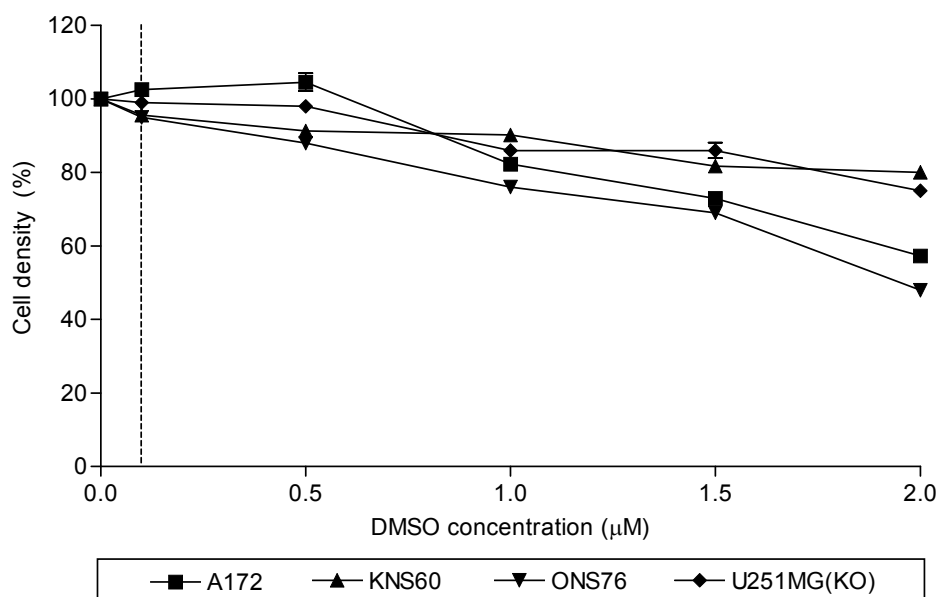
Figure 3.16. Cell density assay of brain cancer cell lines after 48 hours of DMSO treatment. All brain cancer cell lines showed a dose-dependent decrease in cell density after DMSO treatment. As seen in the graph, DMSO concentration at 0.1 % [v/v] (dotted line) does not lead to any significant decrease in cell density.
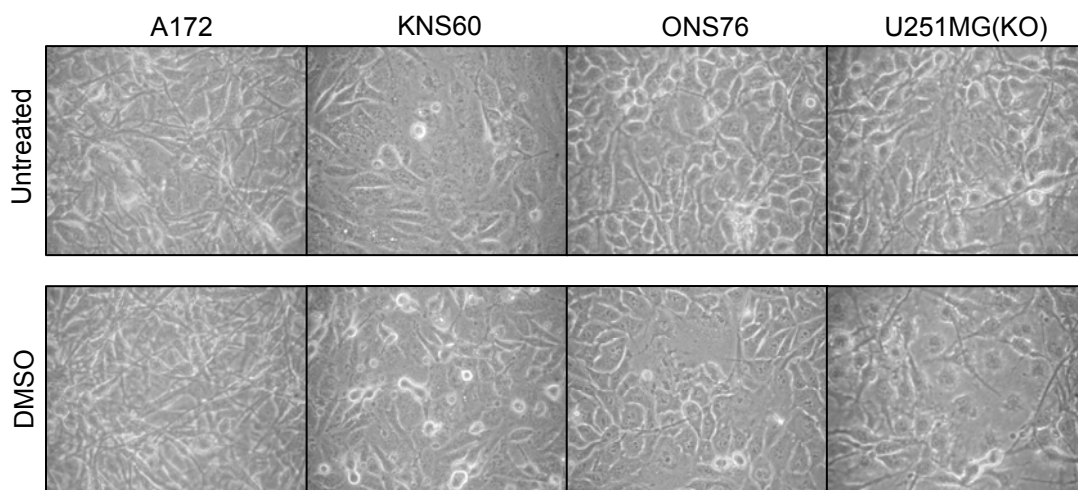
Figure 3.17. Morphological appearances of brain cancer cell lines treated with 0.1 % [v/v] of DMSO. No noticeable changes in cell morphology were observed after treatment in any of the cell lines used.

A)
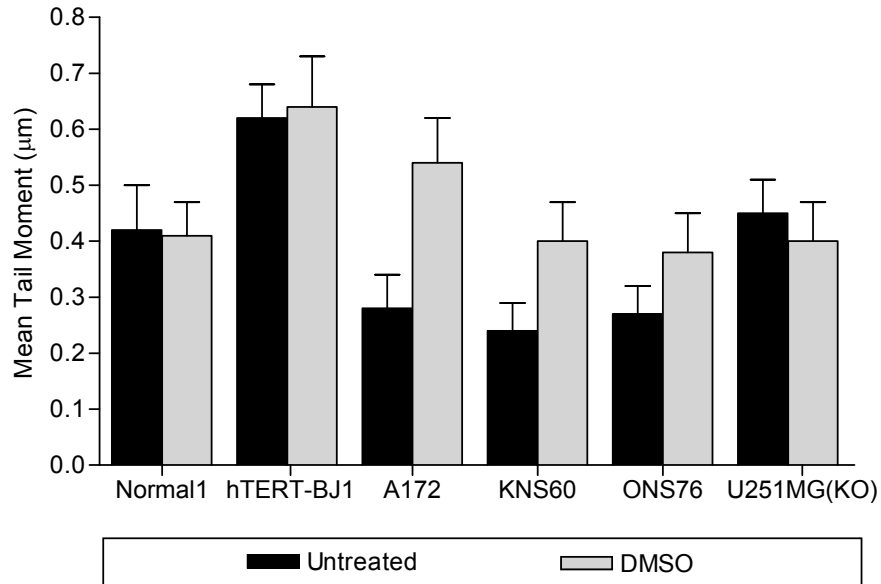
B)
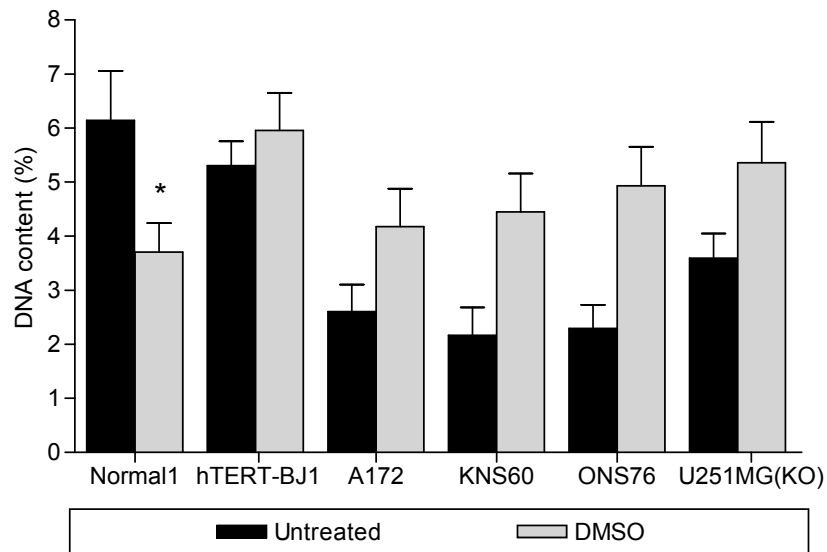
Figure 3.18. DNA damage analysis performed using single cell gel electrophoresis (Comet) assay. A) Degree of DNA damage induced by DMSO is measured in Mean Tail Moment. B) Percentage of DNA content measured from comet tails.

3.3.2. Plumbagin (5-hydroxy-2-methyl-1,4-naphthoquinone)

In this section, plumbagin was explored as a potential therapeutic for brain cancer cell lines whereby functional and molecular responses, such as cell cycle arrest, cell death, DNA damage and telomerase-telomere regulation were studied. Information obtained from this study will greatly improve our knowledge on cellular responses, particularly in the context of cancer treatment.

3.3.2.1. Plumbagin binds to cell surface membrane to enter cytoplasm and reduces cell density.

To investigate the effective concentration of plumbagin that causes 50 % reduction of cell population upon treatment, brain cancer cell lines and normal human lung fibroblasts were treated with increasing concentrations of plumbagin ranging from 0 to 7 µM for 48 hours. Difference in cell density was demonstrated by crystal violet assay and the effective inhibitory concentration resulting in 50 % reduction in cell density (half-maximal concentration, IC_{50}) was determined. As shown in Figure 3.19, exposure to plumbagin resulted in dose-dependent decrease in cell density in the following manner of reduction: with KNS60 being the most sensitive, followed by Normal1, ONS76, hTERT-BJ1, A172, then U251MG(KO). Specifically, the IC_{50} for plumbagin in the glioblastoma cell line, KNS60 cell line was 2.5 µM. A172 and U251MG(KO) cell lines showed the greatest resistance to plumbagin as indicated by the IC_{50} at 5.5 µM. Plumbagin led to a moderate decrease in cell density in the medulloblastoma cell line, ONS76, with IC_{50} at 4.5 µM. Generally, effective concentrations of plumbagin were found in the range between 2.5 µM to 5.5

µM. Established IC$_{50}$ concentrations of plumbagin for the individual cell lines were used to conduct subsequent experiments.

Reduction in the optical density (OD) readings of the crystal violet assay suggests cell death and/or growth arrest. To determine which process was involved, morphological changes were observed at 48-hours after cells were treated with plumbagin at the respective concentrations corresponding to the pre-determined IC$_{50}$. As shown in Figure 3.20A, while cells treated with DMSO continued to proliferate resulting in higher confluency, all cell lines exhibited different morphologies from that of DMSO controls, in that they were more sparse after plumbagin treatment. Flattened or enlarged cells were identified in plumbagin-treated KNS60 and ONS76 cells (Figure 3.20B), suggesting that some of these cells underwent growth arrest. Floating and rounded cells indicating dead or dying cells were also found in all plumbagin-treated samples. The appearance of dendritic spines in cellular morphology was increased notably particularly in KNS60 and ONS76 cells (Figure 3.20B), indicating that these cells are affected by plumbagin treatment. In addition, ONS76 and U251MG(KO) cells exhibited vacuolated morphology, an indicator of pre-apoptotic autophagy cell death. Preliminary morphological observation suggests that 48 hours of plumbagin treatment induces cell death leading to a reduction in live adherent cells. This data correlates with our observations in crystal violet assay.

In order to understand how plumbagin interacts with cells, we analysed the process of drug uptake via fluorescence microscopy. Excitation and emission wavelengths of plumbagin obtained from fluorescence spectrophotometry indicated that plumbagin emits a blue fluorescent signal at

a wavelength of 472 nm (Figure 3.2). Cells were stained with acridine orange which differentially stains the nucleus in green and cytoplasm in red. The route of drug trafficking was observed using fluorescence microscopy with DAPI, FITC and TRITC filters. As shown in Figure 3.21, KNS60 cell treated with plumbagin were compared with untreated and DMSO controls. Untreated and DMSO treated cells did not exhibit any blue fluorescence signal and cell nuclei remained intact. However upon plumbagin treatment, blue fluorescence was detected on the outer membrane of the cells. In some cells, blue signals in the cytoplasm and nucleus were observed, indicating a drug diffusion event. These observations suggest that plumbagin binds to the cell surface membrane and gradually permeates into the cytoplasm and nucleus of the cells. It is possible that plumbagin binds to death receptors present on the cell membrane and activates death signalling cascades subsequently. Plumbagin may also infiltrate into cells and inhibit or disrupt proteins and RNA, thus affecting normal cellular processes, eventually leading to cell death.

In summary, it is shown that 48 hours of treatment with plumbagin resulted in a decrease in cell density as compared to DMSO control cells. Morphological observations showed that plumbagin induces apoptotic cell death, as indicated by cell shrinking, nuclear fragmentation, membrane blebbing, possibly by binding and infiltrating into cells.
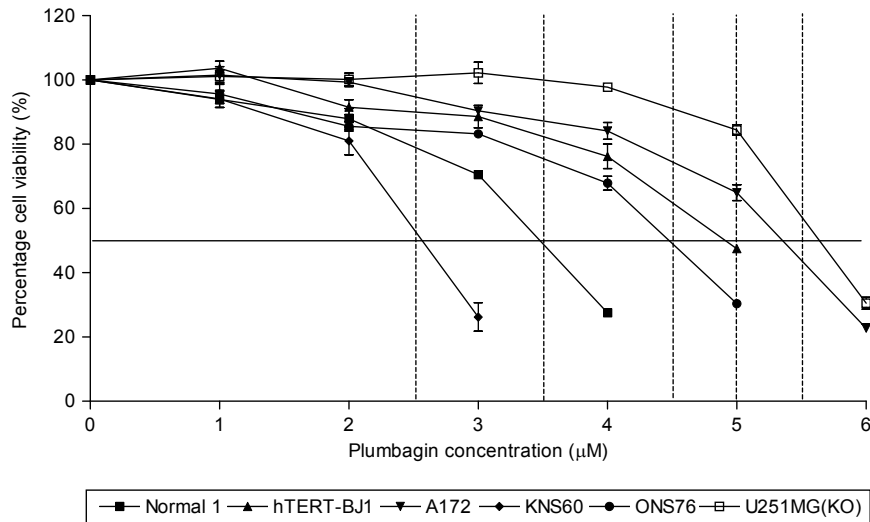
Figure 3.19. Crystal violet assay on 48-hour plumbagin treated cells. Cell density decreases in a dose-dependent manner; KNS60 cells showing highest sensitivity, whereas A172 and ONS76 cells exhibiting resistance to plumbagin.
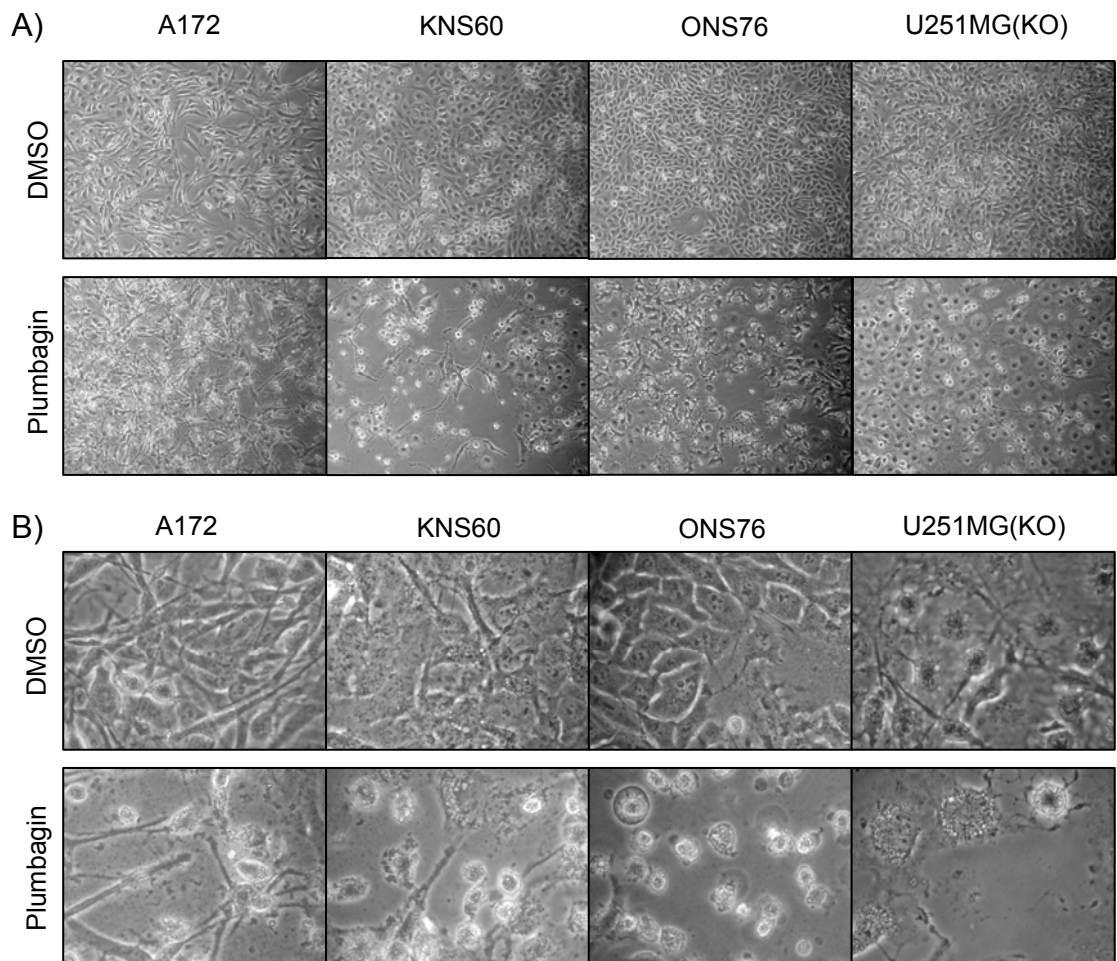
Figure 3.20. Morphology of cells after plumbagin treatment. A) Plumbagin exerts a cytotoxic effect on all cells resulting in cell death and lower cell density at 100 X magnification. B) Pictures of cell morphology captured at 200 X magnification.
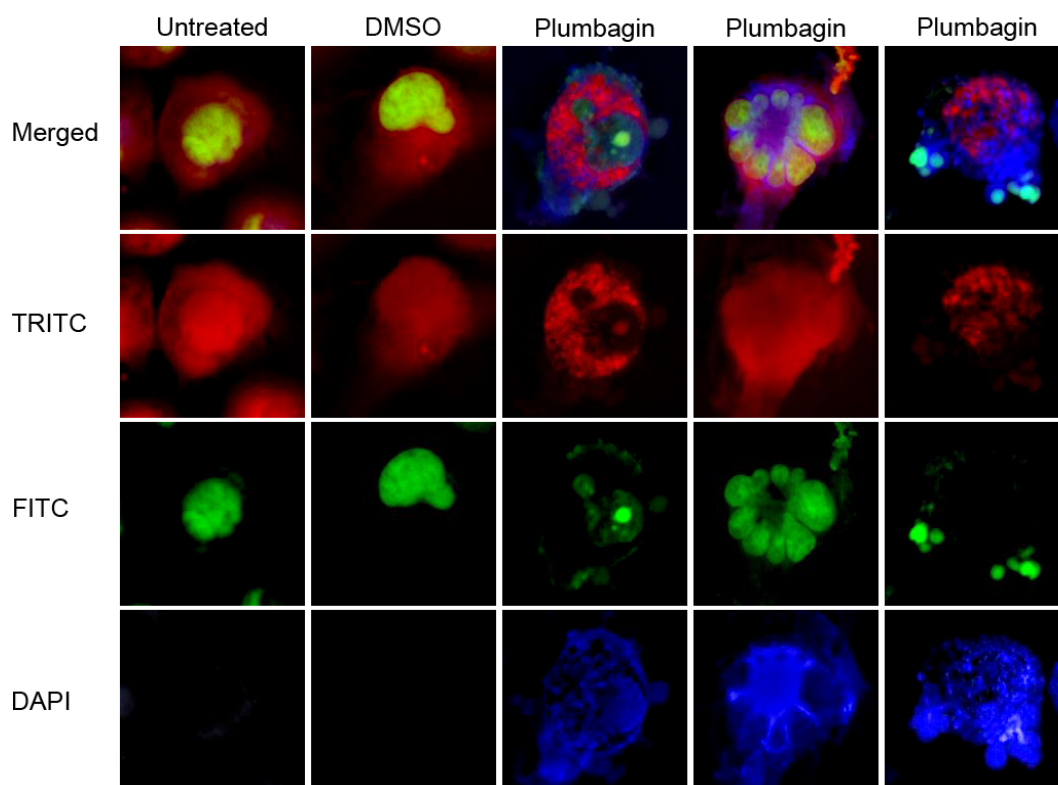
Figure 3.21. Plumbagin emits blue fluorescence signal that shows the route of drug trafficking into KNS60 cell. Cells were stained with acridine orange that differentially stain nucleus and cytoplasm. Plumbagin accumulates at cell surface membrane and permeates into the cytoplasm and trigger apoptotic cell death.

3.3.2.2. Plumbagin induces cell cycle arrest, cell death and suppresses the clonogenicity of cells.

To validate the cytotoxicity of plumbagin, cells were stained with propidium iodide (PI) and subjected to fluorescence-activated cell sorting (FACS) analysis. Increase in the sub-G1 population was observed in all the cell lines except A172 (Figure 3.22), indicating DNA fragmentation and hence cell death. Consistent with the crystal violet assay result on cell survival, KNS60 cells seemed very sensitive to plumbagin treatment as indicated by the increase in sub-G1 population that made up of 50 % of the entire population. However, A172 and U251MG(KO) cells were more resistant to plumbagin-induced cell death as low levels of sub-G1 population were detected. From the cell cycle profiles, it can be seen that plumbagin treatment also induces an increase in the G2/M population in KNS60, ONS76 and U251MG(KO) cells, suggestive of cell cycle arrest accompanied by a corresponding decrease in the G1 population. A172 cells on the other hand displayed a slight decrease in G2/M population with a corresponding increase in G1 population. This observation shows that plumbagin not only triggers cell death, but also induces cell cycle arrest predominantly at the G2/M phase of the cell cycle.

As a continuation of the cell cycle arrest investigation, brain cancer cells treated with plumbagin for 48 hours were harvested and 2×10^3 cells were reseeded in drug-free media for 10 days to study colony forming ability after drug treatment. As shown in Figure 3.23, the numbers of colonies formed by all the brain cancer cells were reduced in plumbagin treated samples. Taken together with the cell cycle data discussed earlier, the data

suggests that cell cycle arrest prevents further proliferation. Interestingly, the results obtained from this clonogenic assay showed A172 to be most affected in terms of colony forming ability after drug treatment.

The ability of cells to form colonies following drug treatments is believed to be influenced mostly by population doubling rate and cell viability. Population doubling may be influenced by cell cycle arrest after drug treatment and the inherent rate of cell division; cells that are arrested are unable to proliferate and form colony, while cells that are naturally slow growing such as A172 may have the even lesser colonies if cells were arrested (Figure 3.3). Hence, A172 may exhibit a lack of ability to form colonies following plumbagin treatment not only due to cell cycle arrest but also its inherently slow rate of growth compared to the other cell lines. Thus although the same number of different brain cancer cells (2×10^3 cells) was seeded onto the culture dish for the colony formation assay, not all A172 seeded cells formed colonies that were sufficiently large enough for detection. With respect to the cell sustainability after plumbagin treatment, a high IC_{50} for A172 may indicate the resistance of the cell line at the 48-hour time point to drug treatment. There is a possibility that A172 cells that exhibited resistance to plumbagin might be sensitized to cytotoxic effects at a later time point such that if these treated cells continued to grow in a drug-free media, they may undergo apoptosis gradually and also lead to less colony formation. These explain why plumbagin treatment can lead to a drastic decrease in colony numbers on slow growing A172 cells.

To summarise this section, the crystal violet assay has shown that all cell lines responded to plumbagin treatment in a dose-dependent manner.

Plumbagin treatment led cells to undergo morphological changes and eventually apoptosis. FACS analysis also showed that most cell lines underwent cell death and cell cycle arrest. In the colony formation assay, not all 2×10^3 plumbagin-treated cells were able to proliferate and form colonies. Some of these cells remained arrested while some apoptosised gradually over the period of 10 days in culture, leaving only those plumbagin-resistant cells that maintained clonogenic ability.
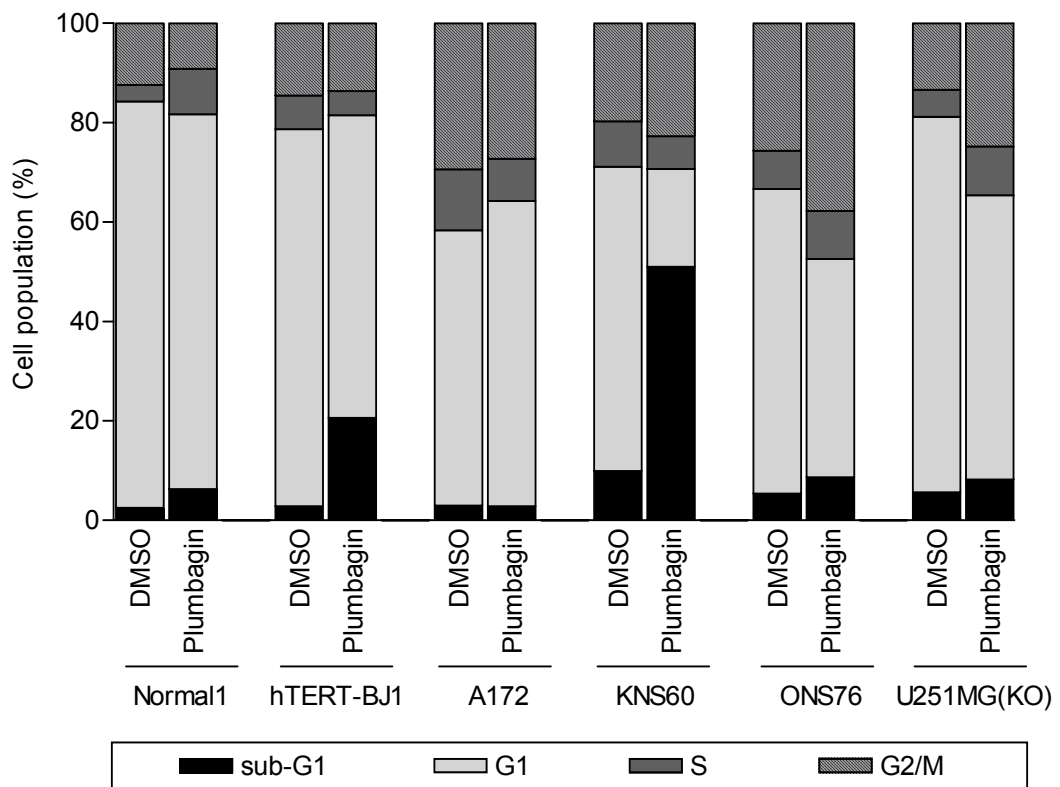
Figure 3.22. Cell cycle profile of plumbagin treated cells analysed using flow cytometry. Most cell lines exhibited higher sub-G1 population and cell cycle arrest at G2/M phase.
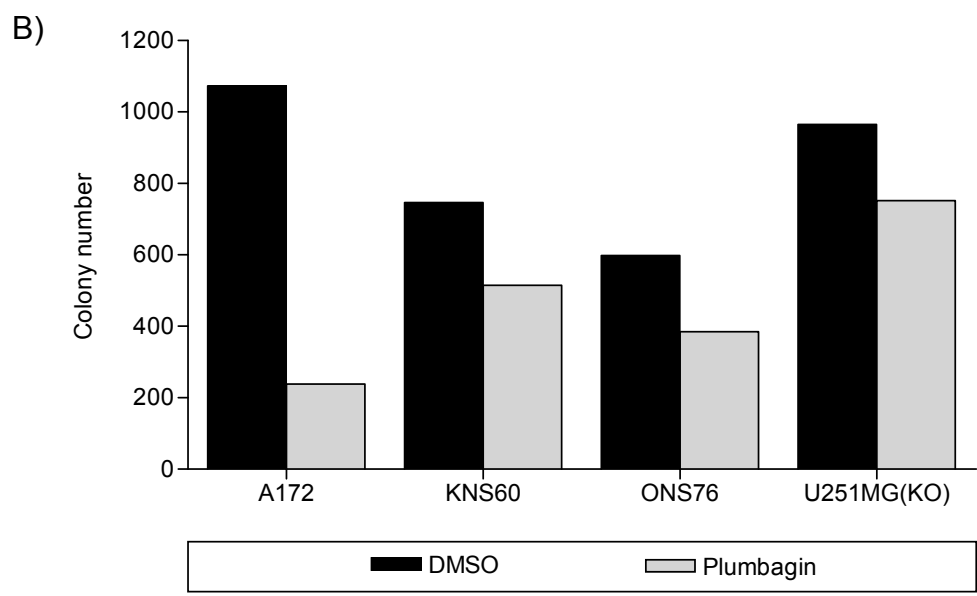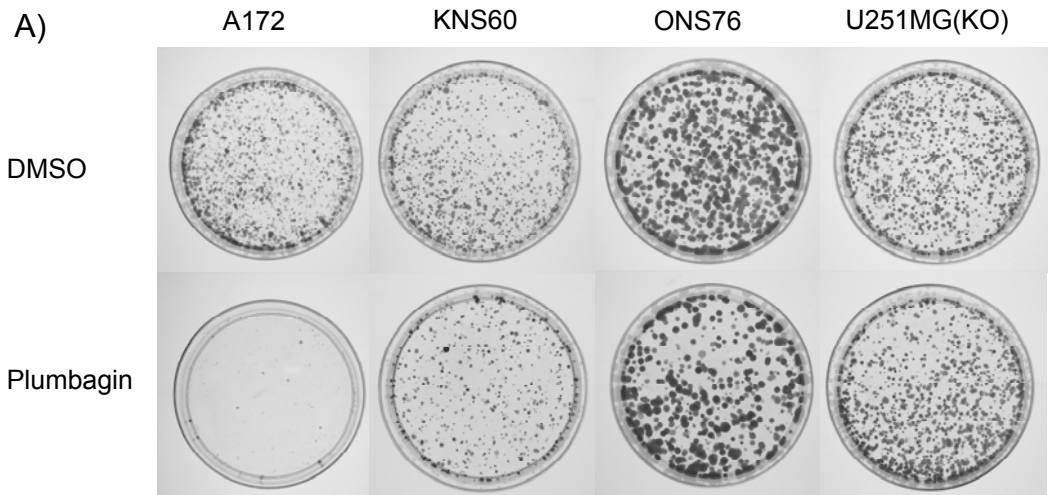
Figure 3.23. Colony formation assay was performed to study the clonogenic property of cell lines after plumbagin treatment. A) Pictures of colony formation assay done on 100 mm culture dish. B) Graphical representation of colony numbers obtained after 10 days of growth in culture.

3.3.2.3. Plumbagin-induced cell cycle arrest and apoptosis are associated with increased DNA damage.

To investigate whether the cell cycle arrest and cell death are associated with DNA damage, single cell gel electrophoresis assay, also known as the comet assay, was performed following 48-hour treatment with plumbagin. This assay allows the detection of both single and double strand DNA breaks. As shown in Figure 3.24, all the cell lines showed various degrees of increase in the mean tail moment after plumbagin treatment. Although the KNS60 cells were most sensitive to plumbagin treatment as indicated by crystal violet assay, the extent of DNA damage induced in it was not as significant as that in the ONS76 cells. The phenomenon of the ONS76 cells exhibiting the highest DNA damage without a major decrease in cell density as projected by crystal violet assay may be due to its high proliferation rate that is able to compensate for the loss of cells as a result of DNA damage and cell death. On the other hand, A172 and U251MG(KO) cells did not show any significant increase in DNA damage, indicating that these cell lines are resistant to the DNA damaging effects of plumbagin. Here, it is shown that the KNS60 is relatively sensitive to plumbagin treatment as demonstrated by the low but significant degree of damage and highest susceptibility to cell death.

To validate that plumbagin triggers cell death in these brain cancer cell lines, annexin V-FITC and PI staining were carried out using FACS analysis. As shown in Figure 3.25A and 3.25B, while all the brain cancer cells exhibited cell death at early and late apoptosis, minimal necrotic cells were detected. Among the viable cells, the KNS60 cells showed the smallest population after treatment while the A172 cells had the highest viable population. KNS60 and

ONS76 cells exhibited as high as 40 % cell population in the late apoptosis region indicating that these cells responded to plumbagin in the early hours upon treatment. A172 and KNS60 cells showed 45 % of cell population in the early apoptosis region which suggests that they underwent apoptotic cell death at a later time point after plumbagin treatment while ONS76 and U251MG(KO) cells had around 30 % of the population in the early apoptosis region. In conclusion, most cell lines responded to plumbagin treatment at an early time point except for the A172 cells that only showed significant apoptotic cell death at 48-hour after plumbagin treatment. Marginal necrosis was detected in all cells tested, indicating that plumbagin does not kill the cells randomly but specifically through programmed cell death.

Altogether, the cell death and cell cycle arrest reported above were associated with plumbagin-induced DNA damage. It is plausible that the significant DNA damage present in both the KNS60 and ONS76 cells led to a high population of apoptotic cells in early and late apoptosis. A172 and U251MG(KO) cells which showed lesser DNA damage corroborate with the observations in the annexin V staining and crystal violet assay in that these cell lines are relatively resistant to plumbagin treatment.

A)

B)
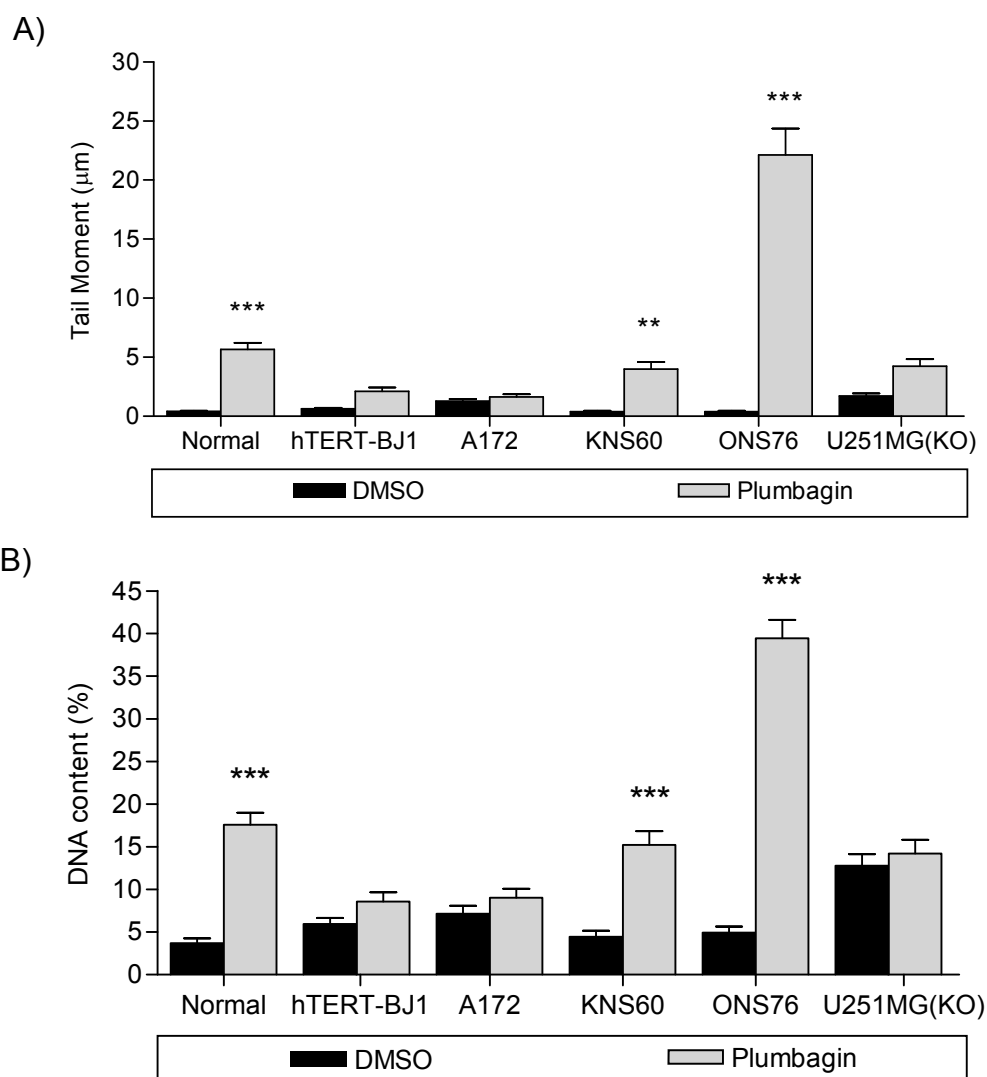
Figure 3.24. Degree of DNA damage detected in cells treated with plumbagin. A) Most cells showed an increase in the mean tail moment, an indicator of DNA damage, after plumbagin treatment. ONS76 cells exhibited the highest degree of damage. B) Representation of comet tail moment in percentage of DNA content. *** indicates P < 0.001.
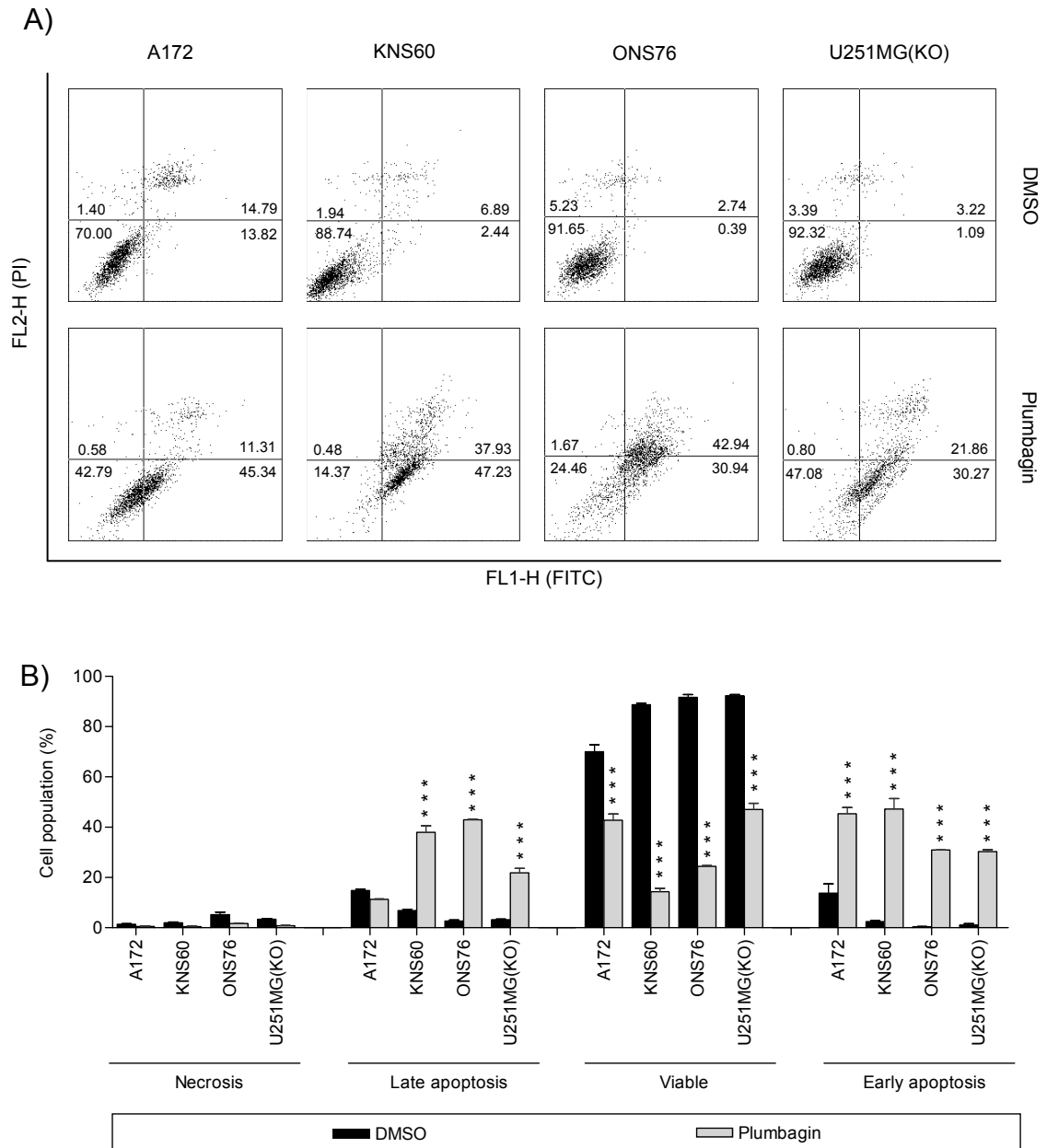
Figure 3.25. Annexin V staining of plumbagin treated cells. A) Dot-plot data of FITC and PI staining, indicating populations of viable, apoptotic and necrotic cells. B) Graphical representation of dot-plot data projecting apoptosis, not necrosis, as the main pathway of cell death. *** indicates P < 0.001.

3.3.2.4. Plumbagin may induce cell cycle arrest by downregulating *E2F1*, *CCNE1* genes and Cyclin B1 protein.

In order to understand the underlying mechanisms leading to cell cycle arrest, the gene and protein expressions after plumbagin treatment were studied using Oligo GEArray® Cancer PathwayFinder and western blot analysis. As shown in Figure 3.26, selected genes that may affect cell cycle progression and cell proliferation such as *CCNE1*, *CDK2*, *E2F* and *PTEN* were investigated. It is interesting to note that *E2F* was downregulated in all brain cancer cells upon plumbagin treatment, suggesting that transcription of cyclins, cdks, and checkpoint regulators were disrupted. After 48 hours of plumbagin treatment, expression of the *CCNE1* gene was decreased in most cell lines even though *CDK2* expression was upregulated in some cells. Downregulation of *CCNE1* suggests that cells may arrest at G1 phase of the cell cycle. *PTEN* which serves as an important negative regulator of the AKT cell proliferation and survival pathway was upregulated following plumbagin treatment, indicating that cell proliferation may have been inhibited. In conclusion, changes in the expression of *E2F* and *CCNE1* genes may account for the cell cycle arrest at the G2/M phase in most cell lines. This is strongly supported by the over expression of *PTEN* gene.

Western blotting was performed to validate the observations of the cell cycle arrest as reported earlier. Particularly of interest were proteins involved in cell cycle regulation, such as MDM2, p53, p21 and Cyclin B1. Figure 3.27 shows that MDM2, p53, p21 and Cyclin B1 exhibited different degrees of expression in plumbagin-treated brain cancer cells. Unlike the other cell lines, ONS76 cells exhibited an opposite trend where there is an increase in MDM2

and a slight decrease in p53. MDM2 functions as a negative regulator of p53 by exporting p53 from the nucleus to the cytoplasm and promoting the ubiquitination of p53, leading to its degradation by the proteasome. The A172 and ONS76 cells showed an increase in p21 protein expression suggesting cell cycle arrest, but p21 could not be detected in KNS60 and U251MG(KO) cells even at the basal level. As discussed earlier in section 3.2.2, cell lines with different *TP53* mutation and radioresponses have been used in the study. Cell lines harbouring mutations at the DNA binding domain (KNS60 and U251) were found to express high basal levels of the p53 protein. These cell lines also showed a higher basal expression of the MDM2 protein, suggesting an enhanced feedback loop whereby MDM2 is upregulated so as to reduce p53 levels. In contrast, absence of p21 protein suggesting abrogated p53-dependent p21 transcription, which is probably due to the mutation of *TP53* gene which render the ability of p53 to bind DNA and activate transcription of p21. On the other hand, cell lines with non-functional p53 (A172 and ONS76) expressed low levels of p53 and MDM2 but high levels of p21, suggesting p53-independent p21 transcription in these cells; p21 functions as a cdk inhibitor (CDKI) to suppress cyclin/cdk complexes, thereby preventing RB phosphorylation and cell cycle progression. Cyclin B1 was also found to be downregulated in all brain cancer cells studied, indicating that cells were unable to progress through the G2/M phase and thus arrested at that phase. These results suggest that most cells treated with plumbagin underwent G2/M phase arrest as established by the downregulation of Cyclin B1 and upregulation of p53 and p21, the data consistent with cell cycle results.

Overall, the gene and protein expression analyses have validated earlier observations of growth arrest at the G2/M phase as indicated by downregulation of the *CCNE1* and *E2F* genes. In addition, *PTEN* that inhibits AKT cell proliferation pathway was also upregulated. Furthermore, western blot data exhibited a decrease in the expression of Cyclin B1 upon plumbagin treatment, suggesting cell cycle arrest at G2/M phase.

In the next section, genes and proteins involved in cell death will be analysed to confirm the findings of plumbagin-induced cell death as discussed in section 3.3.2.3.

Figure 3.26. Expression analysis of cell cycle related genes using Oligo GEArray® on plumbagin treated brain cancer cells. Expression data showed trends of gene expression that support cell cycle arrest. Red-dotted lines indicate threshold level at ± 0.2.
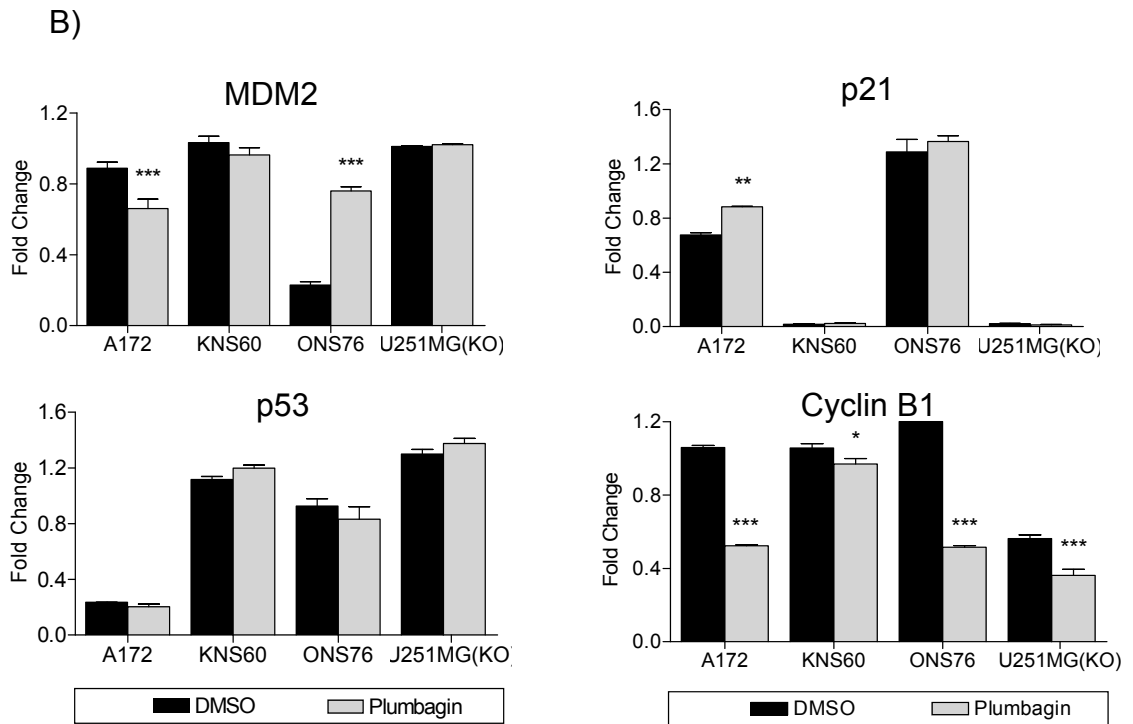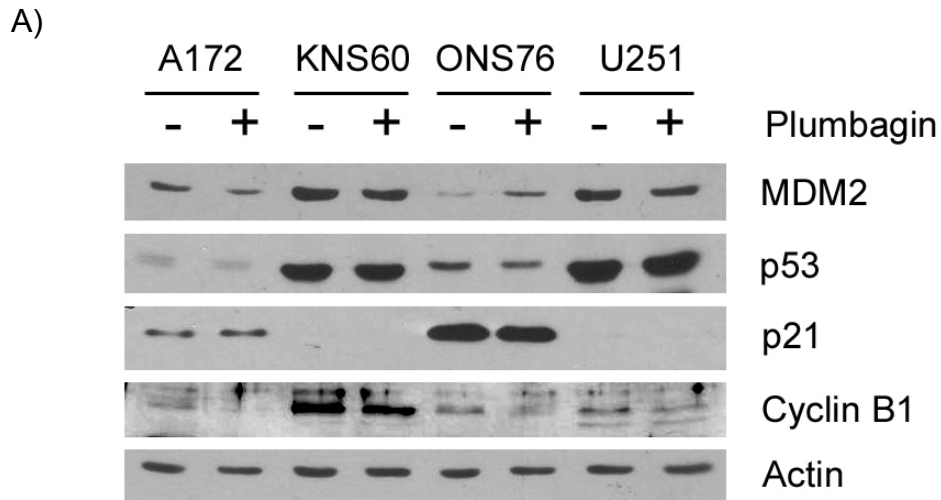
Figure 3.27. Western blot analysis of cell cycle related proteins after plumbagin treatment. A) Protein expressions of MDM2, p53, p21 and Cyclin B1 in brain cancer cell lines. Blots were probed with the indicated antibodies. Actin was used as a loading control. B) Fold change of protein expressions against β-actin was calculated using densitometer. ∗ indicates p < 0.05, ∗∗ indicates p < 0.01, ∗∗∗ indicatesp < 0.001.

3.3.2.5. Plumbagin may induce cell death via the decreased expression of Bcl2 and Survivin proteins.

As discussed earlier in section 3.3.2.3, plumbagin induces DNA damage in all cells possibly resulting in apoptosis, but not necrosis. In this section, we investigated which genes or proteins may be responsible for plumbagin-induced apoptosis in the brain cancer cells. As shown in Figure 3.28, expression analysis was carried out to study cell death related genes such as *BCL2L1*, *BIRC5*, *TNFRSF1A* and *TNFRSF25*. The protein encoded by the pro-apoptotic gene, *BCL2L1* is responsible for regulating outer mitochondrial membrane channel (VDAC) and hence for the release of reactive oxygen species (ROS) and cytochrome c. All brain cancer cell lines showed upregulation of *BCL2L1* gene upon plumbagin treatment. *BIRC5*, a gene encoding the anti-apoptotic Survivin protein, was detected to be at very low levels. *TNFRSF1A* and *TNFRSF25* encode for tumour necrosis factor receptors that play a role in triggering death signalling cascades via the stimulation of NF$_\kappa$B activity and regulation of apoptosis. These two genes show different degrees of upregulation; *TNFRSF1A* exhibits a marginal upregulation upon plumbagin treatment and *TNFRSF25* shows a drastic increase in most cell lines. Altogether, these gene expression results suggest that the intrinsic and extrinsic pathways of apoptotic cell death in all brain cancer cell lines may be activated after plumbagin treatment.

Western blot was carried out to investigate the expression of several proteins, including that of Caspase-9, Caspase-8, Bcl2 and Survivin (Figure 3.29A and 3.29B). Caspase-9 and Caspase-8, the initiator caspases of the intrinsic and extrinsic pathways respectively, could not be detected in any of

the cells. Only the uncleaved form of the caspases, procaspases, were detected, suggesting that activation of Caspase-8 and Caspase-9 may occur early and not after 48-hours of treatment. Interestingly, the anti-apoptotic proteins Bcl2 and Survivin were found to be downregulated in most cells after 48 hours of plumbagin treatment.

To further investigate the caspase activation upon plumbagin treatment, the activity of caspase was measured at different time points using Caspase-Glo$^®$ Assay Kit. Figure 3.30 represents the activity of caspase-3/7 in Relative Luminescence Units (RLU). As shown in Figure 3.30, a gradual increase in caspase-3/7 activity, an effector caspase, was detected early in all plumbagin treated samples indicating the fact that plumbagin triggers caspase-3/7 activity throughout the treatment duration. A distinct increase in caspase-3/7 activity was detected at 12 hours for plumbagin-treated A172 cell, 24 hours for plumbagin-treated KNS60 and U251MG(KO) cells and 48 hours for plumbagin-treated ONS76 cells. Although DMSO also induces caspase-3/7 activity, the extent of caspase activation was lesser than that induced by plumbagin.

The gene and protein expression analyses taken together with the caspase activity assay support the induction of apoptotic cell death in plumbagin treated samples.
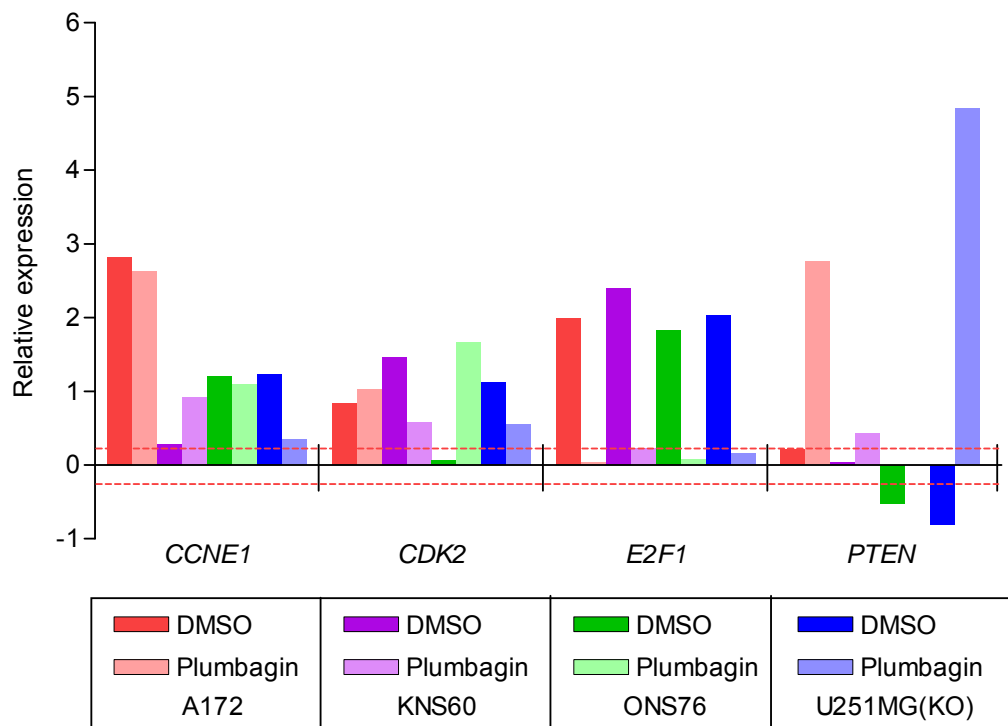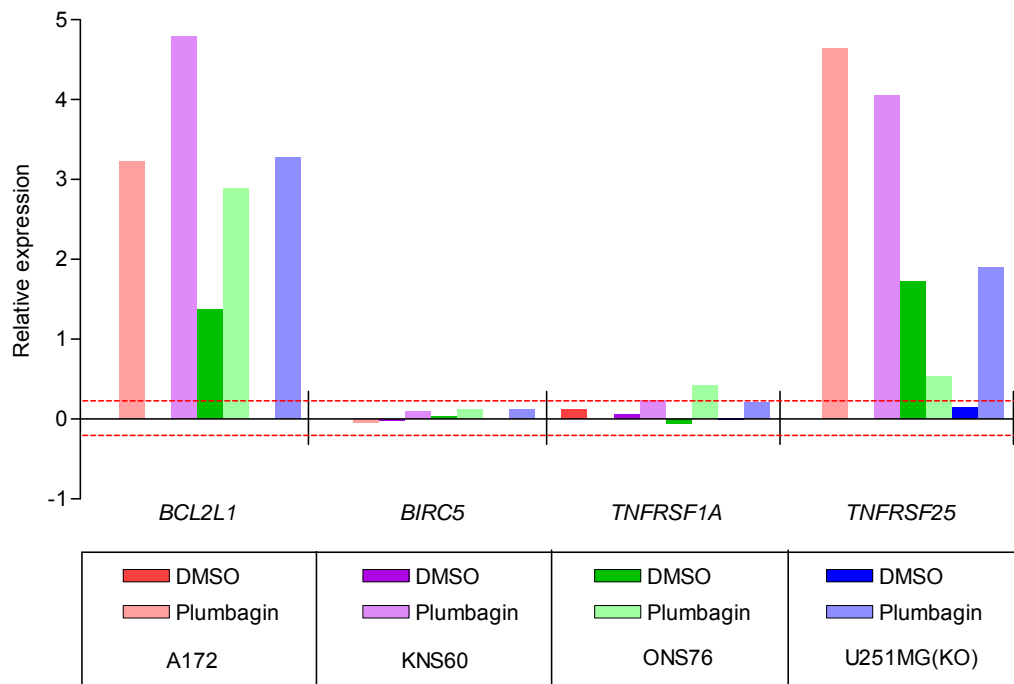
Figure 3.28. Expression analysis of cell death related genes using Oligo GEArray® on plumbagin treated brain cancer cells. Expression data showed promising trends of gene expression that support cell death. Red-dotted lines indicate threshold level at ±0.2.
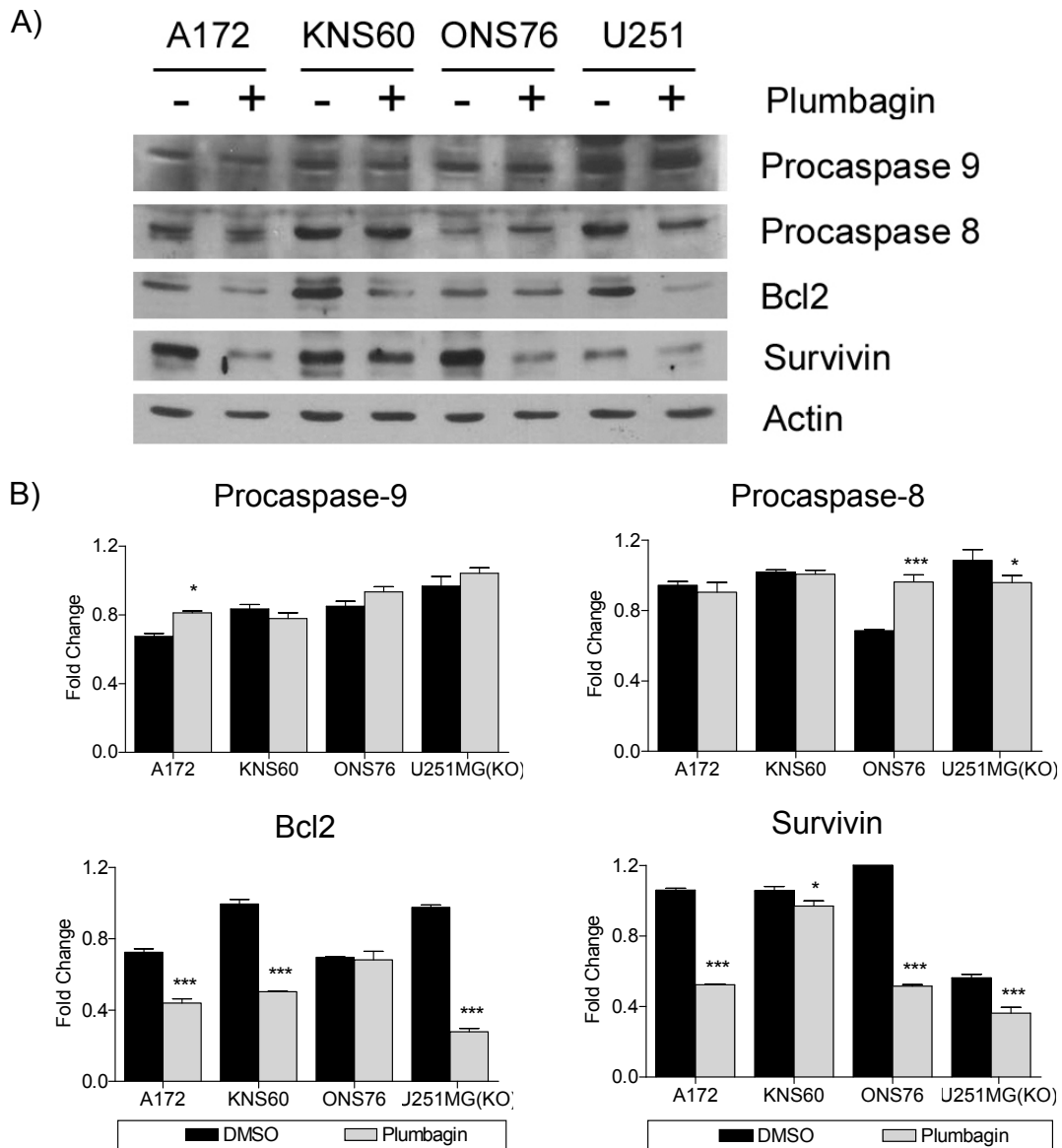
Figure 3.29. Western blot analysis of cell death related proteins upon plumbagin treatment. A) Protein expressions of Procaspase-9, Procaspase-8, Bcl2 and Survivin in brain cancer cells. Blots were probed with the indicated antibodies. Actin was used as a loading control. B) Fold changes of protein expressions against β-actin measured was calculated using a densitometer. $*$ indicates $p < 0.05$, $**$ indicates $p < 0.01$, $***$ indicates $p < 0.001$.
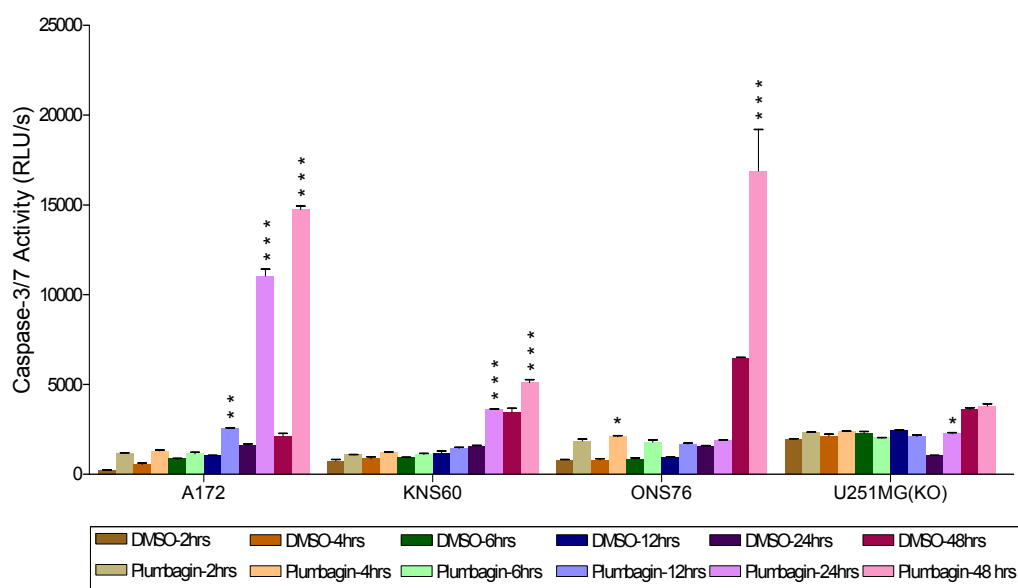
Figure 3.30. Activity of caspase-3/7 at different time points. Plumbagin-treated brain cancer cells exhibited high caspase-3/7 activity at 24 to 48 hours. * indicates $p < 0.05$, ** indicates $p < 0.01$, *** indicates $p < 0.001$.

3.3.2.6. Plumbagin inhibits telomerase activity leading to telomere shortening.

Besides directly triggering cell cycle arrest and cell death to control cancer cell proliferation, plumbagin may exert its anti-tumourigenic effects on other signalling pathways and protein expressions. Specifically, plumbagin may inhibit telomerase activity. In this section, effects of plumbagin on telomerase activity and telomere length are examined. The main factors that affect telomerase activity such as *hTERT* and *hTR* expressions are also investigated. Telomeric Repeat Amplification Protocol (TRAP) was employed to measure the telomerase activity of each cell line. Figure 3.31A shows the value of the Total Product Generated (TPG), a representation of telomerase activity, upon plumbagin treatment. KNS60 and ONS76 cells exhibited drastic decrease in telomerase activity compared to other cells and as indicated in Figure 3.31B, the decrease was more than 50 % compared to basal telomerase activities. On the other hand, A172 and U251MG(KO) did not display any significant changes in the TPG values. Results from TRAP assay correlates with the sensitivity and resistance of the cells against plumbagin treatment as reported earlier where A172 and U251MG(KO) cells were shown to be resistant, whereas KNS60 and ONS76 cells were shown to be sensitive to plumbagin.

To further investigate whether the changes of telomerase activity is a direct result of changes in expression levels of telomerase mRNA, levels of *hTERT* and *hTR* mRNA upon plumbagin treatment were analysed using real-time reverse transcription PCR. As shown in Figure 3.32, plumbagin treatment induced different levels of *hTERT* and *hTR* mRNA expression in each cell line.

117

Figure 3.32A shows that upon treatment, suppression of *hTERT* mRNA was detected in ONS76 and U251MG(KO) cells. However, A172 and KNS60 cells exhibited increased levels compared to DMSO controls. As for *hTR* mRNA (Figure 3.32B), there were no significant changes in expression in any of the cells except for the U251MG(KO). Downregulation of *hTERT* expression in ONS76 and U251MG(KO) cells maybe responsible for the decreased in percentage changes of the telomerase activity (Figure 3.32B), while KNS60 cells exhibited reduction in telomerase activity despite increased *hTERT* expression following plumbagin treatment, which suggests that plumbagin may also inhibit telomerase activity independent of *hTERT* expression changes.

Subsequently, telomere length, dictated by telomerase activity, was studied. Cells were cultured in half the concentration of the respective IC_{50} continuously for 15 days with a change of fresh media and drug every two days. On day-15, DNA was extracted to perform Terminal Restriction Fragment (TRF) analysis to examine telomere length. After 15 days of treatment with plumbagin (Figure 3.33A and 3.33B), brain cancer cells showed a significant decrease in telomere length. Consistent with reduced TPG, KNS60 and ONS76 cells exhibited a remarkable decrease in telomere length. Despite a reduction of TPG that was insignificant, A172 and KNS60 cells also exhibited telomere length decrease albeit not as significant as that of other two cell lines. This data correlates well with that obtained from the TRAP assay whereby a greater decrease in telomerase activity leads to greater telomere shortening.

Taken together, 48 hours of plumbagin treatment led to a reduction in the telomerase activity in all cell lines and the continued repression of telomerase activity in a 15-day treatment resulted in telomere shortening. However, there was no correlation between telomerase activity and *hTERT* or *hTR* mRNA expression levels. This suggests that the decrease in telomerase activity maybe attributed to other factors such as *hTERT* nuclear translocation, *hTERT* ubiquitination or inactivation of telomerase enzyme.
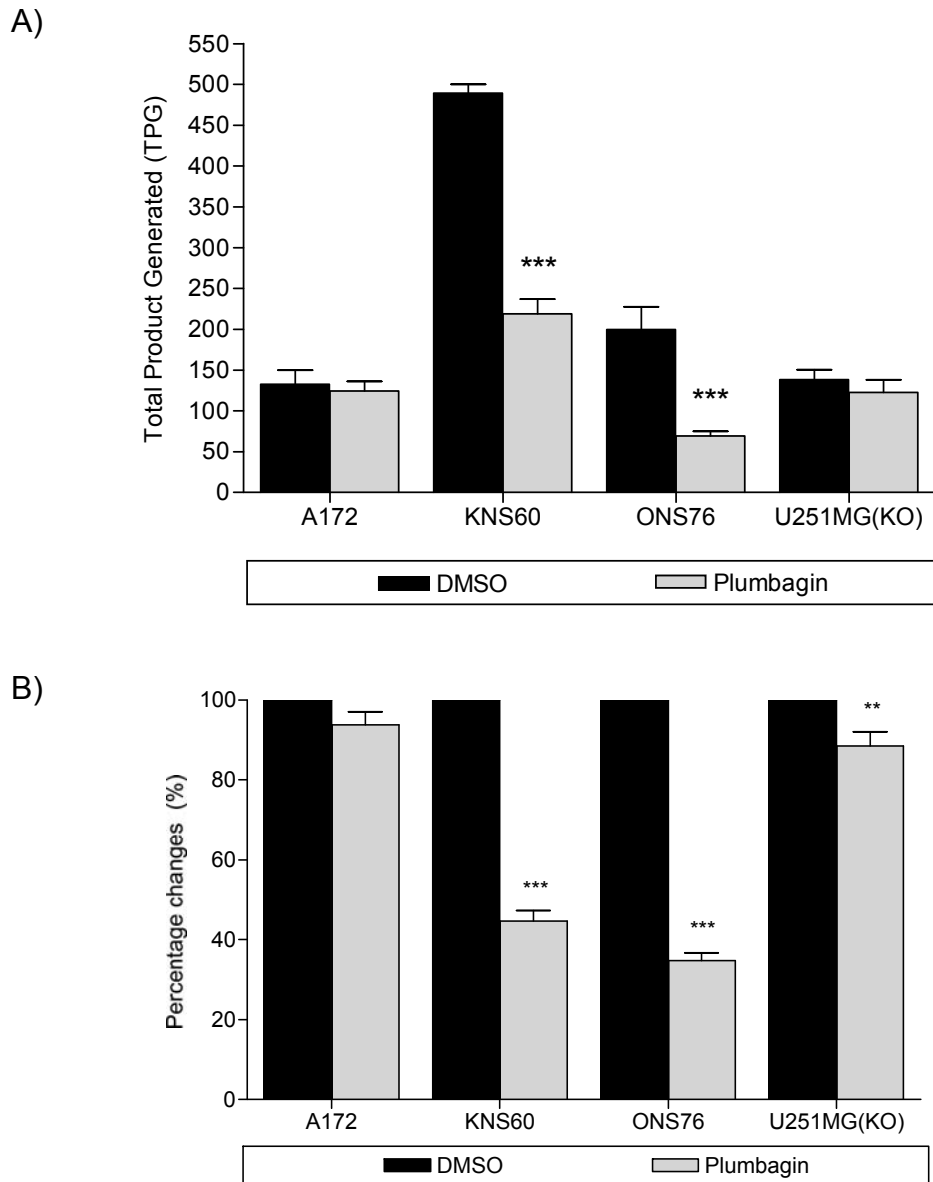
Figure 3.31. Telomerase activity of cells investigated using the TRAP assay. A) KNS60 and ONS76 cells showed significant reduction of telomerase activity as represented by Total Product Generated (TPG). B) Percentage changes of telomerase activity relative to DMSO vehicle control. *** indicates $p < 0.001$.
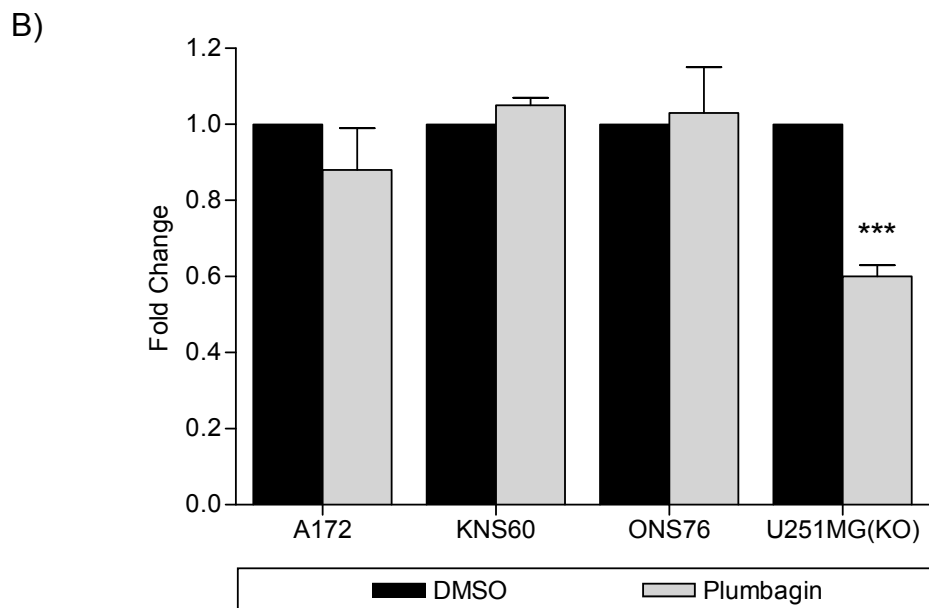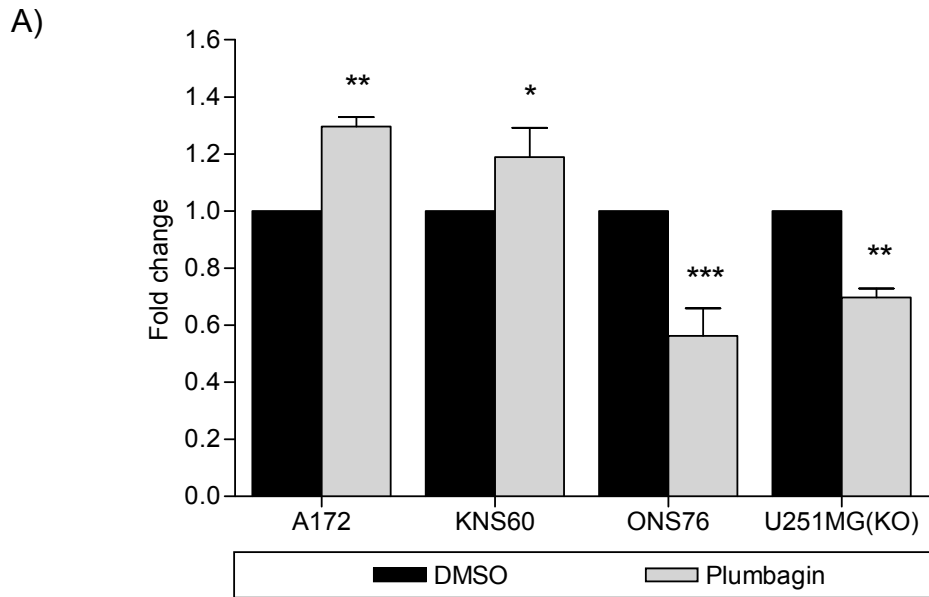
Figure 3.32. Expression analysis of *hTERT* and *hTR* mRNA levels of plumbagin-treated cells using real-time RT-PCR. A) Fold change of *hTERT* mRNA expression relative to that of DMSO treated controls. B) Fold change of *hTR* mRNA expression of all brain cancer cells relative to DMSO treated controls. * indicates $p < 0.05$, ** indicates $p < 0.01$, *** indicates $p < 0.001$.
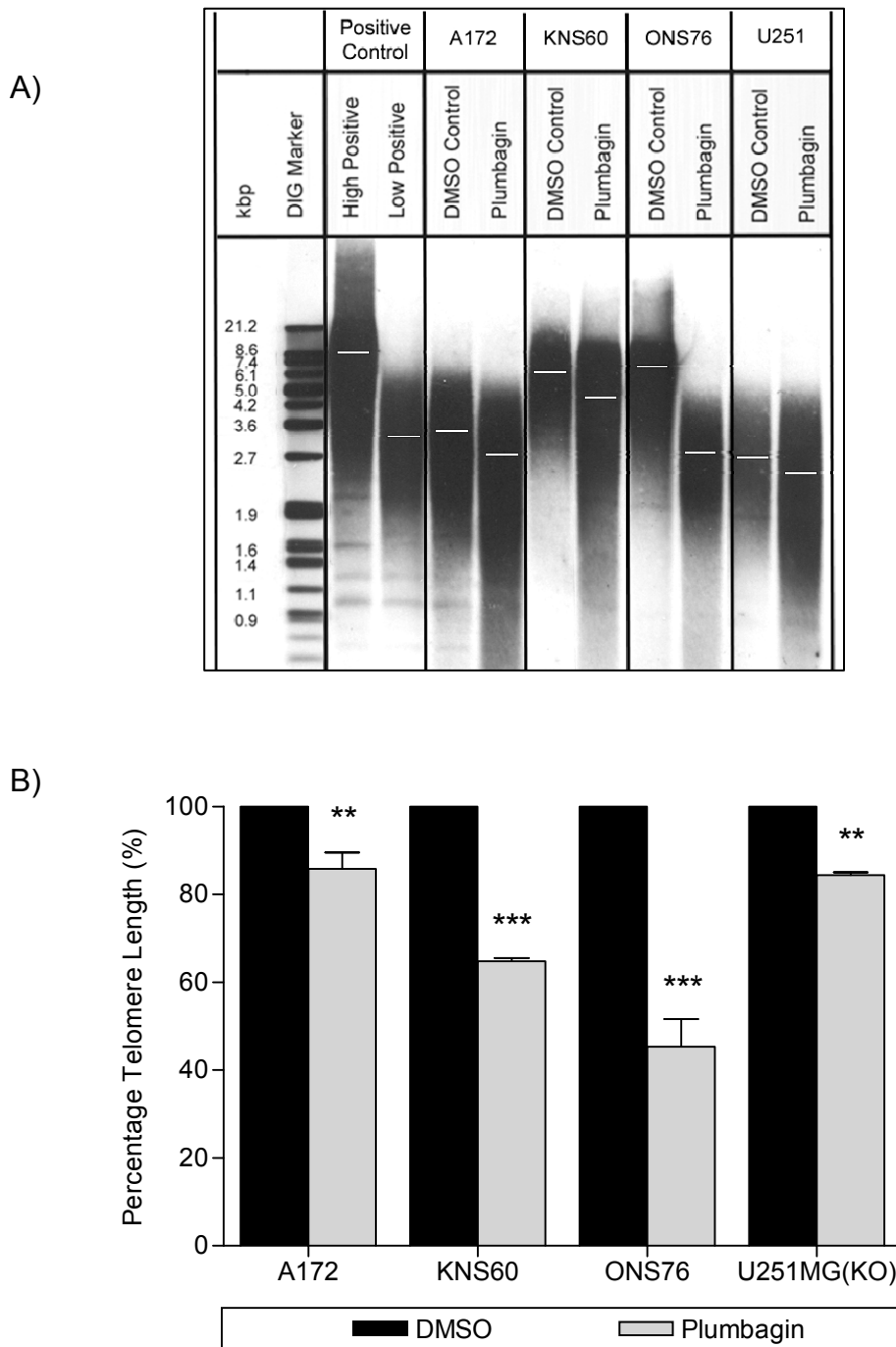
Figure 3.33. Telomere length analysis of plumbagin-treated cells using TRF assay. A) Southern blot analysis of telomeric regions in brain cancer cells. High and low positive samples were included as positive controls. Analysis was done using Kodak imaging software. B) Graphical representation of telomere length in percentage value relative to DMSO treated controls.

3.3.2.7. Discussion

In view that the therapeutic potential of plumbagin, not much anticancer research pertaining to this phytochemical has been carried out. Previous studies on the anticancer effects of plumbagin were performed on lung, liver, breast, prostate and cervical cancer cells (Srinivas *et al.*, 2004; Zhao and Lu, 2006; Ahmad *et al.*, 2008; Aziz *et al.*, 2008; Shih *et al.*, 2009). This is the first study to investigate the anticancer effect of plumbagin in human brain cancer cells, in particular glioblastoma multiforme and medulloblastoma cells.

Compared to previous reports, the concentrations of plumbagin used in this study for cancer cells treatment were within acceptable range and duration. The concentrations of plumbagin used in each study are determined based on the responsiveness of cells studied, some cancer cells may appear to be resistant to plumbagin and therefore require higher doses to show significant responses. The concentration of plumbagin at 2.5 µM and 3.0 µM, both for 48 hours, were used for breast cancer cells, MCF-7 and MDA-MB-231 and lung cancer cell line, A549 (Kuo *et al.*, 2006; Shieh *et al.*, 2009). However, for the same duration of treatment, prostate cancer cell lines, PC-3, LNCaP and C4-2 and skin carcinoma cells, A-431 showed IC$_{50}$ at 7.5 µM and 25 µM respectively (Powolny and Singh, 2008; Nazeem *et al.*, 2009).

An earlier study described that administration of plumbagin in mice that have undergone ectopic implantation of prostate cancer cells delayed the tumour growth by 3 weeks and reduced the tumour weight and volume by 90 %. In addition, discontinuation of plumbagin administration for 4 weeks in the same mouse model showed that there was no increase of tumour growth (Aziz *et al.*, 2008). These observations are corroborated by the colony

formation assay (Figure 3.23) in this study which showed that brain cancer cells treated with plumbagin for 48 hours exhibited reduced ability to form colonies as compared to control cells on continual culture for 10 days in drug-free culture conditions. Plumbagin-induced growth inhibition was mainly attributed to cell cycle arrest at the S-G2/M phase accompanied by the downregulation of cell cycle regulatory proteins such as Cyclin B1, Cyclin A, Cdc2, Cdc25C and upregulation of p21 protein (Kuo *et al.*, 2006; Zhao and Lu, 2006; Hsu *et al.*, 2006; Gomathinayagam *et al.*, 2008; Wang *et al.*, 2008). Similar findings were also obtained in the present study particularly in the radiosensitive A172 and ONS76 cells (Figure 3.22), suggesting that plumbagin indeed has cancer therapeutic potentials by exerting cell cycle arrest in brain cancer cells.

Besides the induction of growth arrest, plumbagin treatment was also reported to trigger apoptotic cell death as validated by translocation of phosphatidyl serine from the inner to the outer cellular membrane in the Annexin V assay (Figure 3.25). Plumbagin was shown to produce reactive oxygen species (ROS) production that induced apoptotic cell death (Srinivas *et al.*, 2004; Powolny and Singh, 2008; Wang *et al.*, 2008; Nazeem *et al.*, 2009). Furthermore, induction of ROS may lead to DNA damage (Srinivas *et al.*, 2004; Demma *et al.*, 2009; Nazeem *et al.*, 2009). In line with this, this study also showed that plumbagin treatment induces DNA damage (Figure 3.24). Subsequently, an orchestra of molecular events associated with cell death such as i) the downregulation of Bcl2 and NFκB, ii) upregulation of Bax, iii) reduction in the expression of anti-apoptotic and proliferation genes such as Inhibitor of Apoptosis (*IAP)* and S*urvivin*, iv) induction of Caspase-3/7

activity were observed in the present (Figure 3.29 and 3.30) and past investigations (Gomathinayagam *et al.*, 2008; Kuo *et al.*, 2006; Sandur *et al.*, 2006; Zhao and Lu, 2006; Wang *et al.*, 2008; Ahmad *et al.*, 2008; Nazeem *et al.*, 2009). Supporting the evidence that plumbagin induces cell death while the AKT pathway was found to be inhibited after plumbagin treatment (Kuo *et al.*, 2006; Gomathinayagam *et al.*, 2008). This study has shown upregulation of *PTEN* gene (Figure 3.26), a negative regulator of AKT cell survival pathway.

We report here for the first time that plumbagin can inhibit telomerase activity in human brain cancer cells. Plumbagin was found to suppress the activity of telomerase enzyme particularly in fast dividing cancer cells (Figure 3.31) resulting in greater telomere attrition in a 15-day treatment with half-dose of IC_{50} (Figure 3.32). This is a novel observation.

Overall, plumbagin has great potential in controlling the growth of brain cancer cells, especially those that are sensitive to radiation. A schematic diagram representing the plausible events or pathways involved in the induction of cell cycle arrest and apoptosis upon plumbagin treatment in this study is illustrated in Figure 3.34.
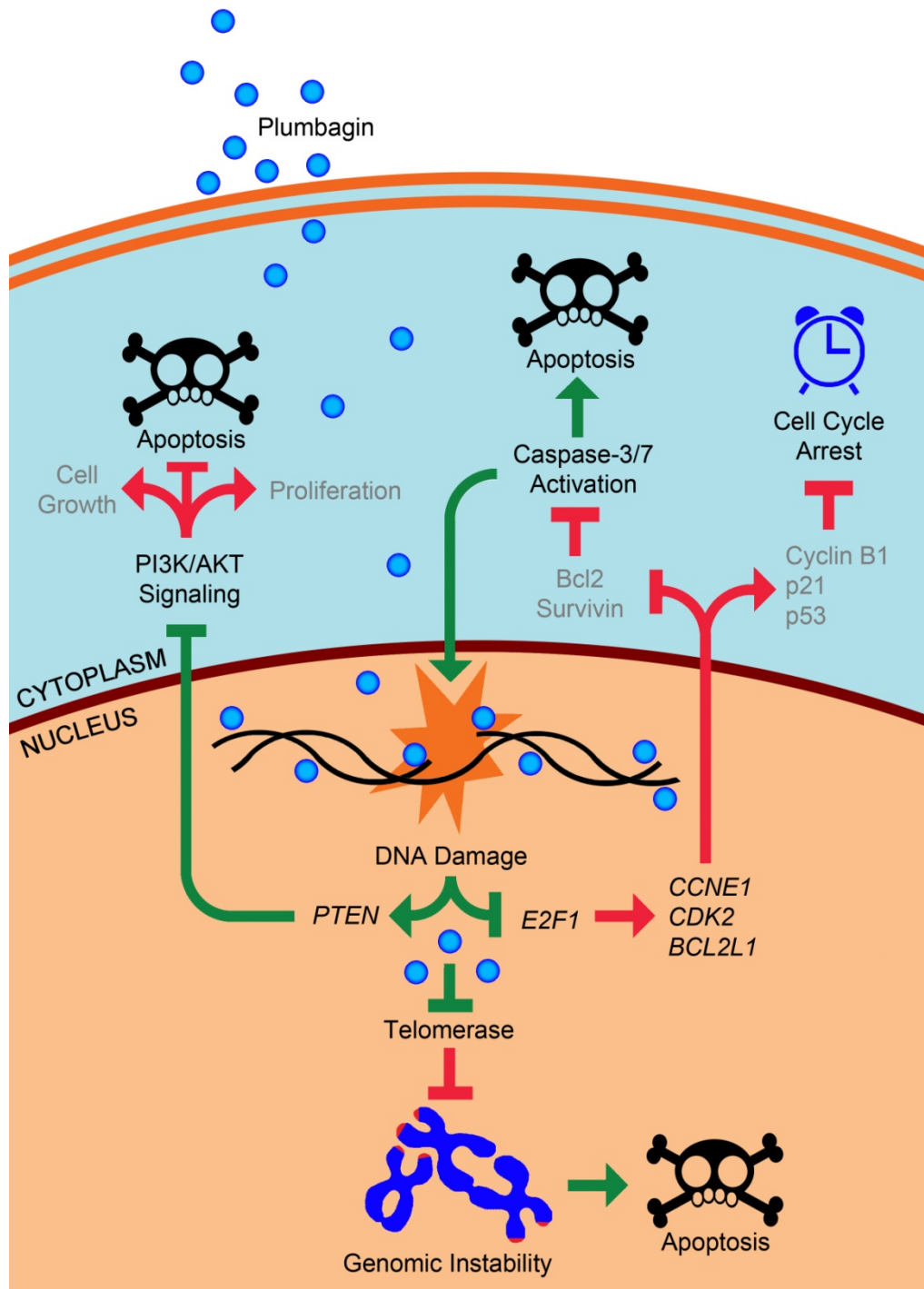
Figure 3.34. Schematic representation of cellular pathways possibly triggered upon plumbagin treatment. Plumbagin induces DNA damage that leads to downregulation of *E2F1* and upregulation of *PTEN* genes. Regulations of these genes inhibit cell proliferation and activate caspase-3/7 that eventually triggers cell death mechanisms. Suppression of telomerase enzyme by plumbagin results in the reduction of telomere length in long-term plumbagin treatment. Green arrows represent possible events whereas red arrows indicate inhibited pathways.

3.3.3. Genistein (5,7-dihydroxy-3-(4-hydroxyphenyl)chromen-4-one)

In this segment, genistein was used as the treatment drug for brain cancer cell lines. Functional and molecular studies were performed to examine the responses and sensitivity of each cell line to drug treatment.

3.3.3.1. Genistein decreases cell density by inducing cell cycle arrest.

To assess the growth inhibitory effects of genistein, brain cancer cells were treated with genistein (0 to 50 µM) for 48 hours. For experimental controls, normal human lung fibroblasts (Normal1) and hTERT-transfected BJ1 human foreskin fibroblast (hTERT-BJ1) cells were used. Exposure to genistein resulted in a decrease in cell density as shown in Figure 3.35. Cell lines more sensitive to genistein showed a greater decrease in cell density as seen in the crystal violet assay. Normal1 cells were the most sensitive cell line to genistein-induced reduction in cell density at 50 µM. This is followed by ONS76, A172, KNS60, U251MG(KO) and finally hTERT-BJ1. The marked reduction in the density of Normal1 could be attributed to its slower proliferation rate of 43.63 Hr/PD compared to the cancer cell lines as mentioned in figure 3.3 (Kimura *et al.*, 2005). All brain cancer cell lines exhibited enlarged and flattened morphology with little sign of apoptosis as observed under bright field microscope after genistein treatment (Figure 3.36A and 3.36B), this suggests that 50 µM genistein inhibits cell growth but does not induce cell death. Due to the fact that IC_{50} was not able to be determined at high dose of genistein, the optimal concentration of genistein to be used was fixed at 50 µM for the subsequent experiments.

To investigate whether the reduction of cell density following genistein treatment is indeed associated with growth arrest, cell cycle analysis was performed by staining genistein-treated cells with propidium iodide and analysed by fluorescent-activated cell sorting (FACS). As shown in Figure 3.37, all the cell lines except A172 exhibited an increase in the G2/M population following genistein treatment, suggestive of G2/M arrest. A172 on the other hand, displayed an increase in G1 population indicating G1 phase arrest. While genistein induced a G2/M arrest in the majority of the cell lines, the extent of G2/M arrest in Normal1 and hTERT-BJ1 were marginal compared to that of brain cancer cell lines KNS60, ONS76 and U251MG(KO). Our results suggest that genistein works more effectively in fast proliferating cancer cells than in slow growing cancer and control cells in inducing extensive cell cycle arrest at G2/M phase and hence growth arrest.

To study the long-term effects of genistein, cells were treated for 48 hours before harvesting and 2×10^3 cells were reseeded in drug-free medium and allowed to grow for 10 additional days to explore their colony forming ability. As shown in Figure 3.38A and 3.38B, 10-day maintenance of all 48-hour genistein-treated brain cancer cell lines exhibited decreased colony forming abilities as compared to DMSO treated controls. Most brain cancer cell lines showed more than 50 % reduction in colony numbers except for ONS76 cell line, which showed a 30 % reduction. This observation suggests that growth arrest triggered by genistein can be sustained for at least 10 days after drug removal. Taken together, our results show that genistein exhibited its cytostatic effect by inducing cell cycle arrest and not cell death, and such effect is maintained even after withdrawal of the drug.
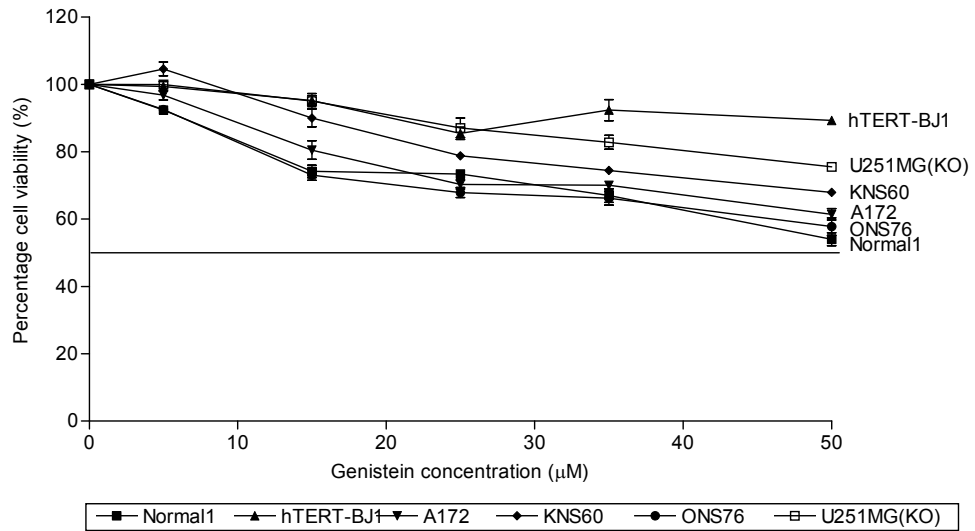
Figure 3.35. Growth inhibitory effects of genistein on all cell lines were determined using crystal violet assay after 48 hours of genistein treatment. Fifty micro Molar (μM) of genistein was established to be the working concentration for subsequent studies.
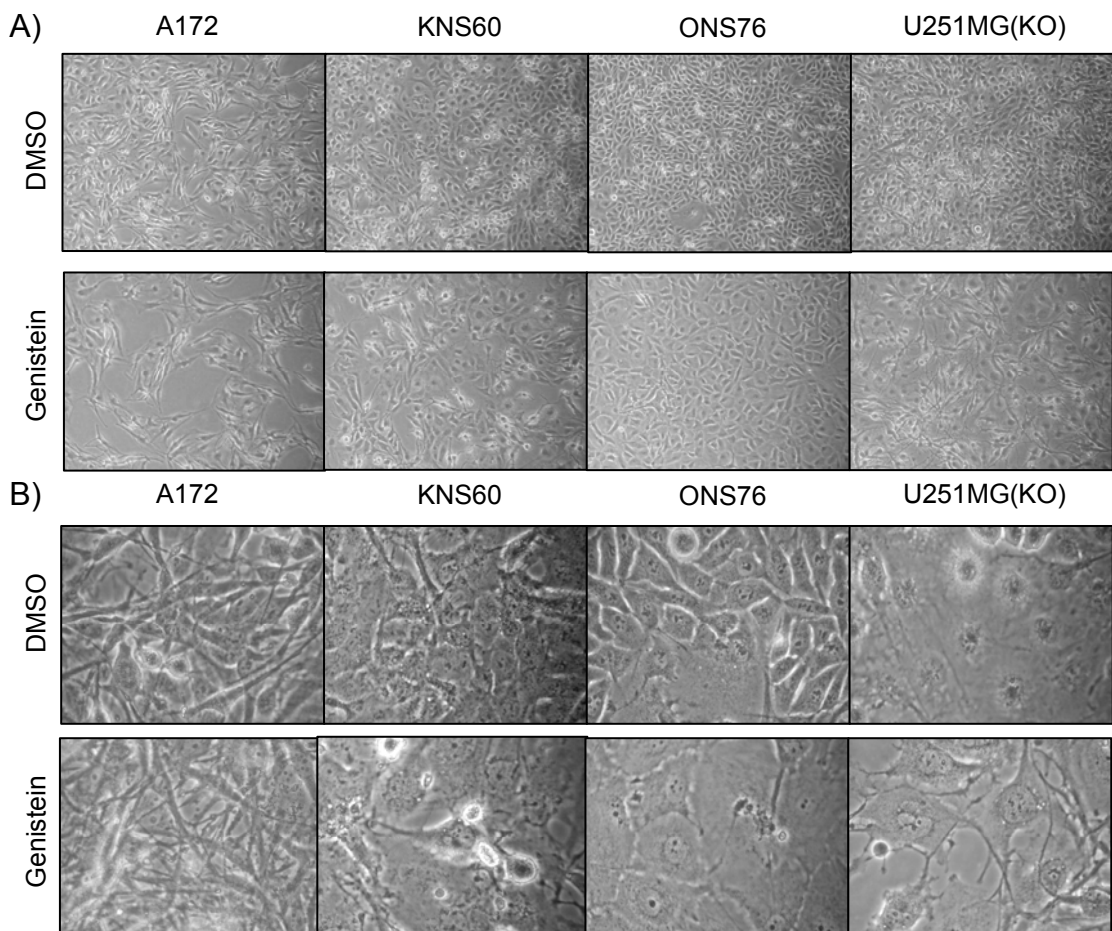
Figure 3.36. Morphology of cells after genistein treatment. A) Genistein exerts cytostatic effect without inducing of cell death in all cells resulting in lower cell density as shown in 100 X magnification. B) Pictures of genistein-treated cells captured at 200 X magnification.
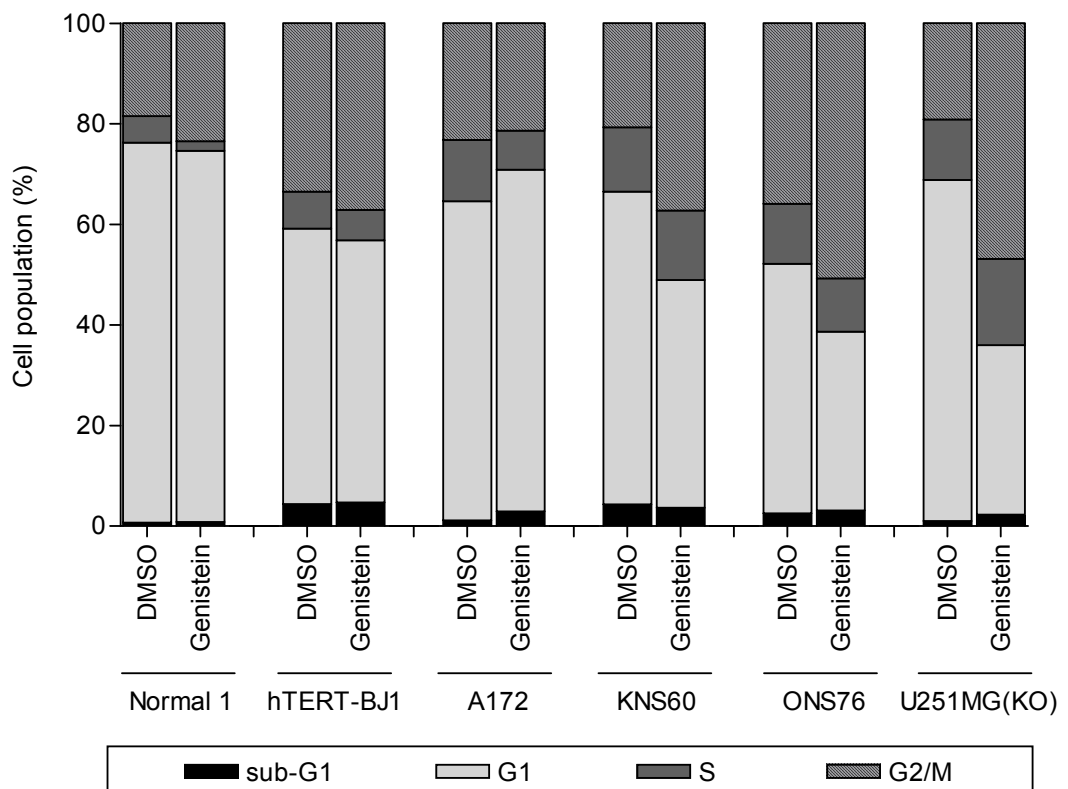
Figure 3.37. Cell cycle profiles of genistein treated cell lines detected using flow cytometry. Most cell lines exhibit G2/M arrest without showing significant changes in sub-G1 population.
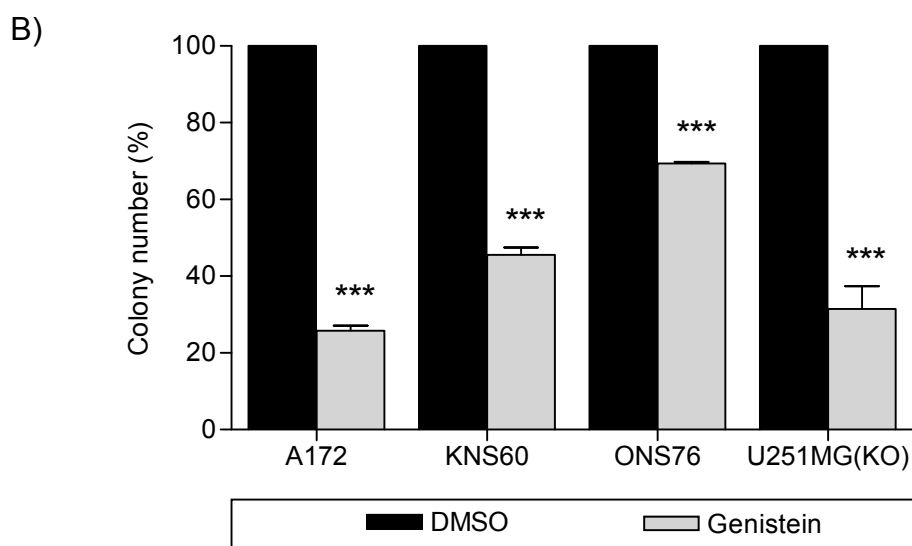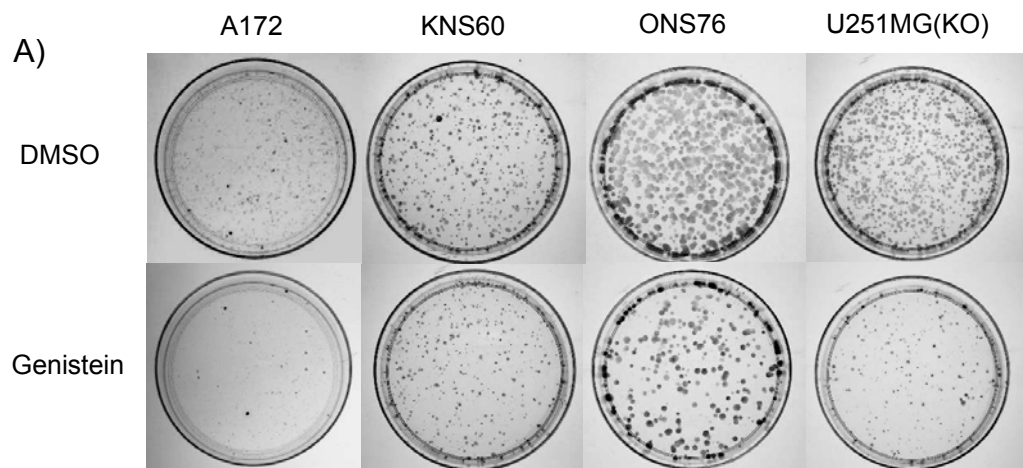
Figure 3.38. Colony formation assay was performed to study the clonogenic property of cell lines after genistein treatment. A) Pictures of colony formation done on 100 mm culture dish. B) Graphical representation of colony numbers.

3.3.3.2. Genistein does not induce DNA damage and cell death.

As the data above suggests, genistein induces growth arrest. We therefore, proceeded to investigate whether genistein induces cell death and DNA damage. According to the cell cycle analysis shown in Figure 3.37, minimal sub-G1 populations were detected in all DMSO and genistein treated cell lines. Sub-G1 population is an indicator of apoptotic cells with degraded DNA, which manifests as events with hypodiploid DNA content. None of the cell lines treated with genistein shows any considerable increase in the sub-G1 population when compared to the corresponding DMSO control, suggesting that 48-hour treatment with genistein does not induce cell death at 50 μM.

To confirm the observation that genistein does not induce cell death, annexin V-FITC staining was carried out to detect apoptotic and necrotic cells. As shown in Figure 3.39, all brain cancer cell lines showed a negligible increase in their necrotic and apoptotic populations, indicating that minimal cells underwent necrosis and apoptosis respectively. In view of this finding, it should be noted that there is a corresponding marked reduction of cells in the viable population. This confirms that genistein does not cause cell death either by necrosis or apoptosis. Generally, the low cytotoxic effect of genistein is associated with little DNA damage whereby there are minuscule changes in the apoptotic and necrotic populations of cells.

Comet assay was carried out to examine the extent of DNA damage, if any, triggered by genistein treatment. Detection of DNA damage by Comet analysis (Figure 3.40) is represented by tail moments. All the cell lines treated with both DMSO and genistein showed low and insignificant levels of DNA

damage. This indicates that genistein does not induce significant damage on DNA and also explains the unsubstantial sub-G1 population observed in cell cycle analysis.
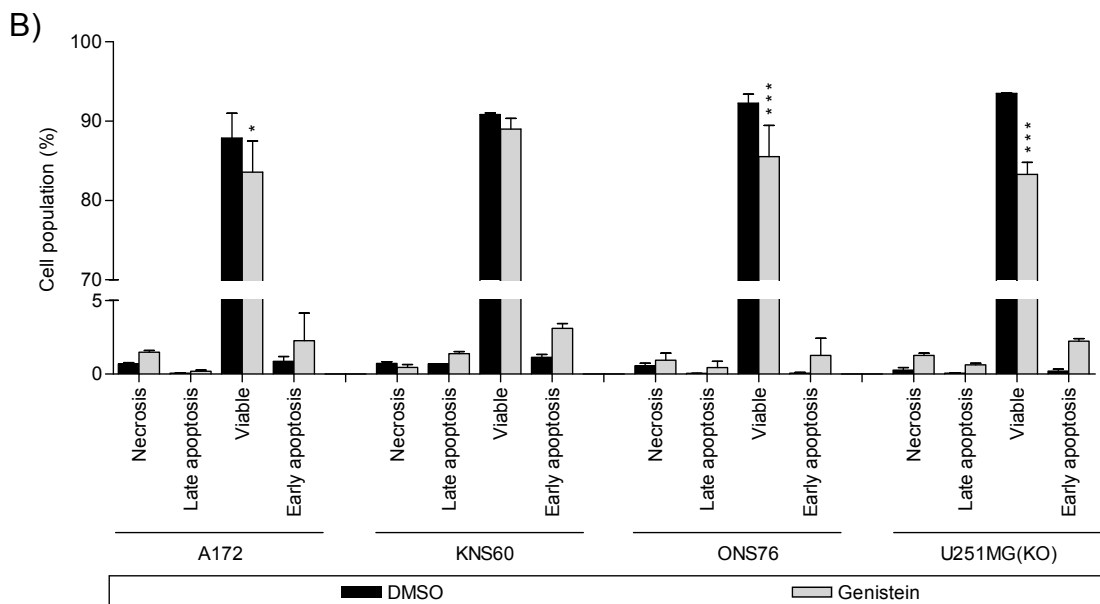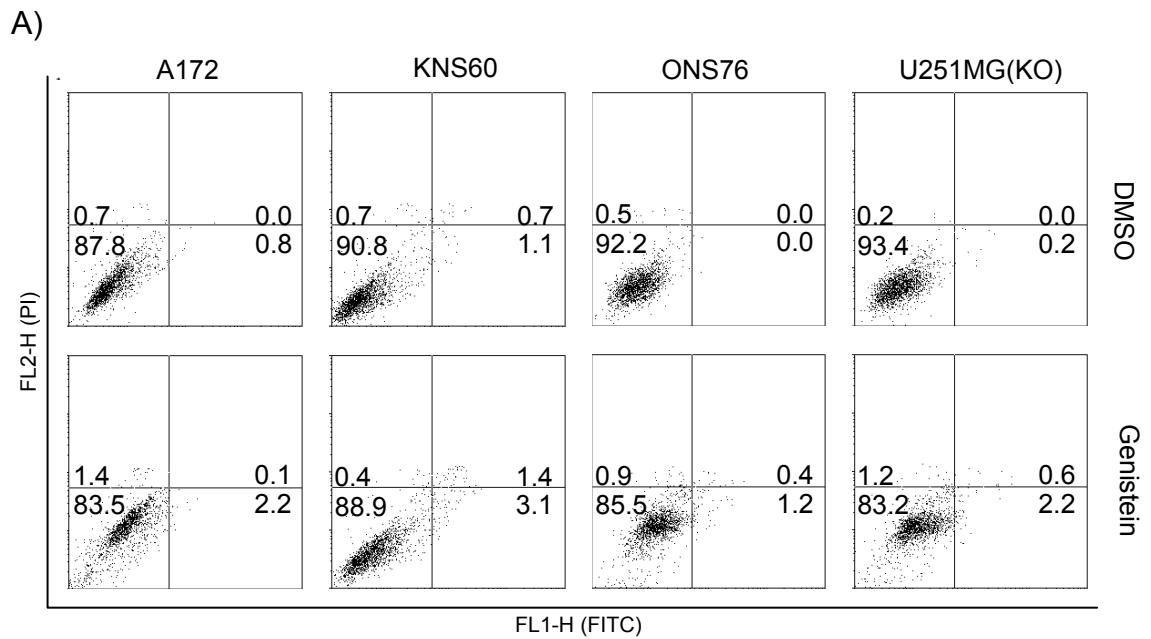
Figure 3.39. Genistein does not induce cell death. Annexin V-FITC staining assay was performed to determine the viability of cells. A) Genistein-treated cells remained viable with insignificant populations in necrosis, early and late apoptosis. B) Graphical representation of cell population according to results in Figure 3.25A. * indicates p < 0.05, *** indicates p < 0.001.
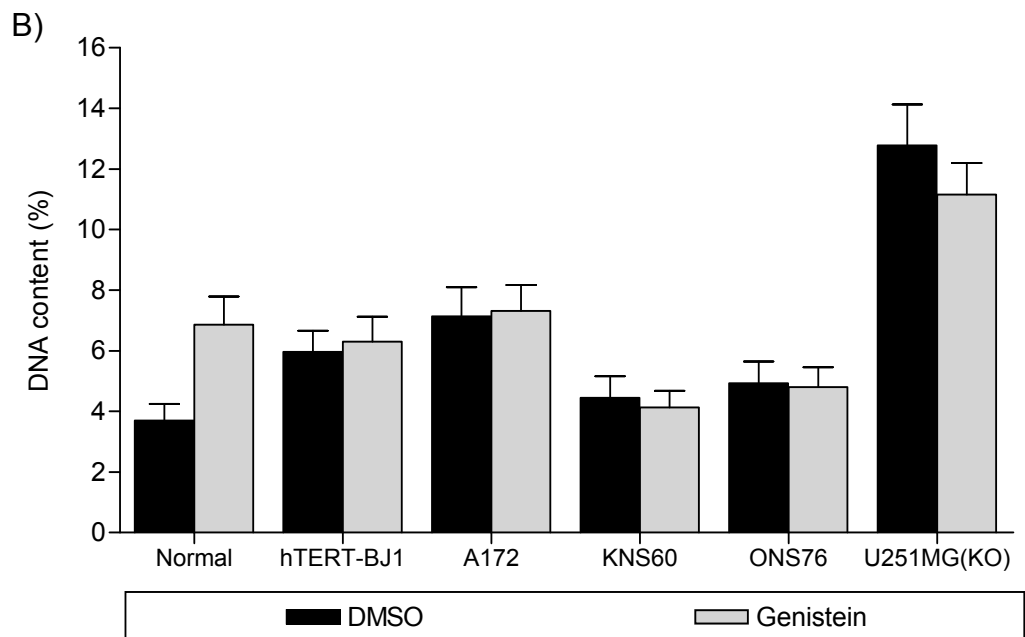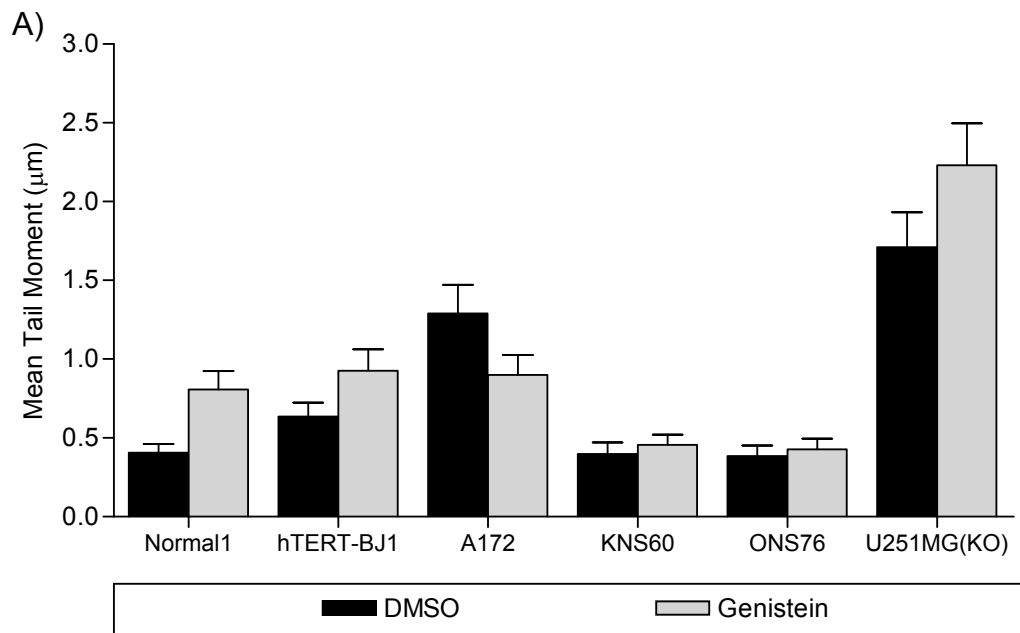
Figure 3.40. Genistein does not induce significant DNA damage. A) Single Cell Gel Electrophoresis (Comet) assay showed a low degree of DNA damage on each cell line following a 48-hour genistein treatment. The tail moment measured correlates to the extent of DNA damage. B) Graphical representation of DNA content measured from comet tail.

3.3.3.3. Cell cycle arrest in radiosensitive brain cancer cells correlated with downregulation of Cyclin B1 and Cdk1.

Present study shows that cells treated with genistein underwent growth arrest independent of DNA damage, with no cell death involved. While the mechanism by which genistein induces cell cycle arrest is as yet unclear, previous studies have reported that genistein induces cell cycle arrest by upregulating CDK inhibitors and downregulating cyclin/cdk complexes (Casagrande and Darbon, 2000; Choi *et al.*, 2000).

In this study, brain cancer cells with different *TP53* mutations and radioresponses were used to investigate if these parameters affect their responses to genistein treatment. According to Ishikawa *et al.* (2006), the four brain cancer cell lines which are used in this study harbour *TP53* mutations at different codons. A172 and ONS76 cell lines harbour a mutation at codon 72 that is located in the proline-rich region of *TP53*. Cell lines with mutation at this region have been reported to show higher growth arrest and capacity to repair DNA damage. In addition, these two cell lines were reported to be radiosensitive. For KNS60 and U251MG(KO) cell lines, the *TP53* mutations are at codon 193 and 273 respectively, both of which are in the DNA-binding domain. Mutations that occur within this domain have been reported to affect the DNA binding affinity of p53, consequently disrupting its transcriptional activities. In the same report, KNS60 and U251MG(KO) were reported to be radioresistant.

As shown in Figure 3.41, A172 and ONS76 have less endogenous p53 protein as compared to KNS60 and U251MG(KO) cell lines. The expressions of the p53 protein after genistein treatment did not show

significant change in any of the brain cancer cell lines. A similar observation was also made in the levels of phosphorylated p53. Despite the lack of increase in p53 and phosphorylated p53, p21 as a cell cycle regulatory protein downstream of p53, increased in expression in most of the brain cancer cell lines following genistein treatment. The upregulated expressions were more apparent in A172 and ONS76 and this is consistent with the knowledge that these two cell lines probably have higher DNA repair capacity (Hu *et al.*, 2005; Siddique and Sabapathy, 2006). Interestingly, there was decreased expression of Cyclin B1 and Cdk1 corresponding with the increased expression of p21 in A172 and ONS76 cell lines, suggesting that these proteins are working in concert to bring about cell cycle arrest to allow for repair.

KNS60 and U251MG(KO) harbour *TP53* mutations within the DNA binding domain (Ishikawa *et al.*, 2006). Incidentally, there are barely detectable levels of endogenous p21, possibly due to the mutations present in the DNA binding domain of p53 that may have affected the transcription of p21. The low levels of the p21 protein, even after genistein treatment, may be insufficient to exert an overt cell cycle arrest, leading to continued cycling as indicated by the increased expressions of Cyclin B1 and Cdk1 proteins. This is consistent with the increased ability of these cells to form colonies compared to A172 and ONS76 following genistein treatment.

Unlike that of western blotting, using Oligo GEArray® Cancer PathwayFinder, we did not notice a specific trend between radiosensitive and radioresistant cell lines. Expression of *CCNE1* and *CDK2* genes were lower as compared to the DMSO controls (Figure 3.42). Thus suggesting that either

there was inhibition of G1/S transition or that the cells were progressing towards S phase. Downregulation of *E2F1* gene may suggest the reduction of its transcriptional activity resulting in cell cycle arrest. Overall, this gene expression analysis indicated that brain cancer cells were undergoing cell cycle arrest upon genistein treatment.

Taken together, gene expression analysis has shown that genistein treatment induces suppression of cell cycle regulatory genes such as *CCNE1*, *CDK2* and *E2F1*. However, protein expressions exhibited two different patterns where radiosensitive cells exhibited stronger signals of cell cycle arrest as compared to radioresistant cells, the fact which is consistent with the cancer aggressiveness.
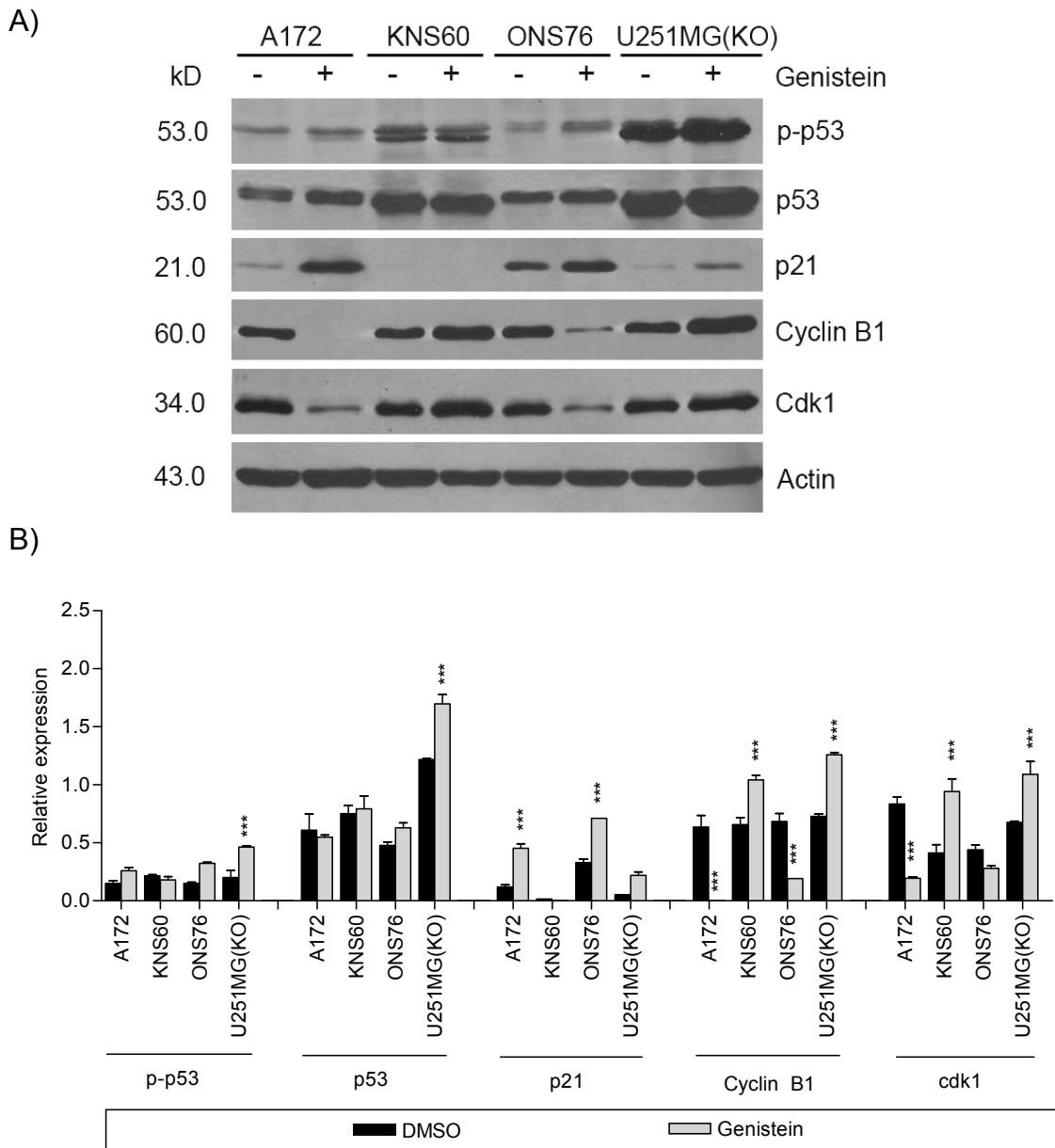
Figure 3.41. Cyclin B and Cdk1 are downregulated during G2/M cell cycle arrest in radiosensitive brain cancer cells but upregulated in radioresistant cancer cells. A) Radiosensitive brain cancer cells that harbour functional p53 show activation of downstream p21. B) Graphical representation of the band intensities on the western blots were measured using Kodak Molecular Imaging Software. *** indicates p < 0.001.
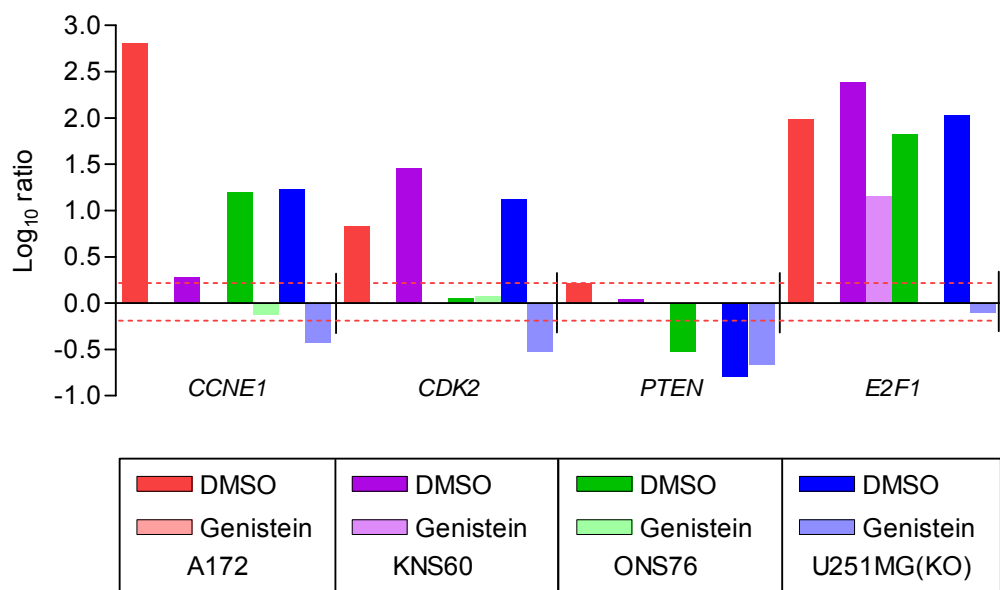
Figure 3.42. Expression analysis of cell cycle related genes performed using Oligo GEArray® on genistein-treated brain cancer cell lines. Expression data showed trends of gene expression that support cell cycle arrest observation. Red-dotted lines indicate cut-off threshold level at ± 0.2.

3.3.3.4. Radiosensitive brain cancer cell lines exhibited downregulation of cell survival associated genes, Bcl2 and Survivin.

In radiosensitive cell lines, A172 and ONS76, there was a distinct reduction in Cyclin B1 and Cdk1 protein levels after genistein treatment (Figure 3.41). This observation corresponded with lower expressions of Bcl2 and Survivin proteins (Figure 3.43). In contrast, there was increased expression levels of Bcl2 and Survivin proteins upon genistein treatment in the radioresistant cell lines, KNS60 and U251MG(KO). These results suggest that the A172 and ONS76 cell lines are more sensitive to genistein-induced growth arrest than their radioresistant counterparts.

This interesting observation prompted the investigation of the expression of other cell death related proteins such as Caspase-8 and Caspase-9, especially in A172 and ONS76 cell lines. Surprisingly, although cell survival related proteins such as Bcl2 and Survivin of radiosensitive cell lines showed decreased expression after genistein treatment, pro-caspases involved in apoptosis remained intact and no caspases were found to be cleaved (Figure 3.43). This suggests that either genistein does not cause apoptosis or no death signalling pathway was triggered at 50 µM genistein for 48 hours. To note, the decreased levels of Bcl2 and Survivin following genistein treatment deviated from earlier observations that genistein does not promote cell death.

Based on the data presented above, we speculate that cell death may impend following 48-hour of genistein treatment. KNS60 and U251MG(KO) cell lines may activate certain signalling pathways to improve chances of survival following genistein treatment. This pathway may include the activation

of Cyclin B1 and Cdk1 leading to a G2/M arrest and the upregulation of survival proteins, Bcl2 and Survivin. However, in the radiosensitive cell lines, A172 and ONS76, there appears to be no activation of these survival proteins to promote cell viability, thus rendering these two cell lines more sensitive to genistein treatment.

To investigate this observation at the level of genes, Oligo GEArray$^®$ was carried out on brain cancer cell lines upon genistein treatment. However, there was no supportive evidence of cell death in favour of radiosensitive cells (Figure 3.44). All cell lines showed decrease in expression of TNF receptor superfamily genes, suggesting potential cell survival. However, expression of *TERT* gene was also abrogated in genistein-treated A172 and ONS76 cell lines. This result correlated with earlier observation that genistein treatment does not induce cell death.

Altogether, decreased expression of death receptor genes has given a clue that supports the non-cytotoxicity of genistein. On the other hand, protein expression analysis has revealed more information on responses of radiosensitive cells to genistein treatment.
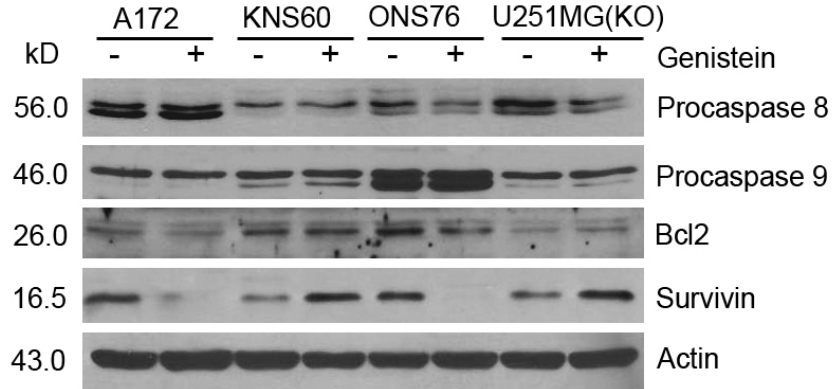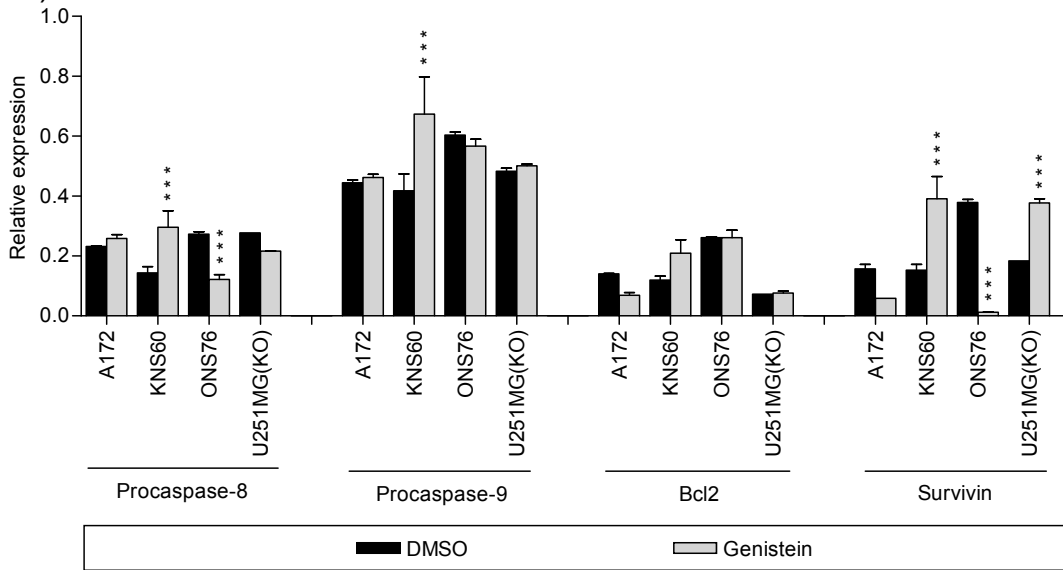
Figure 3.43. Radiosensitivity status affects molecular cell death responses in genistein-treated cells. Protein expression profile of cell death related proteins after genistein treatment. A) Western blots showed that there is no initiation of caspase-dependent cell death. B) Graphical representation of the band intensities on the western blots were measured using Kodak Molecular Imaging Software. *** indicates p < 0.001.
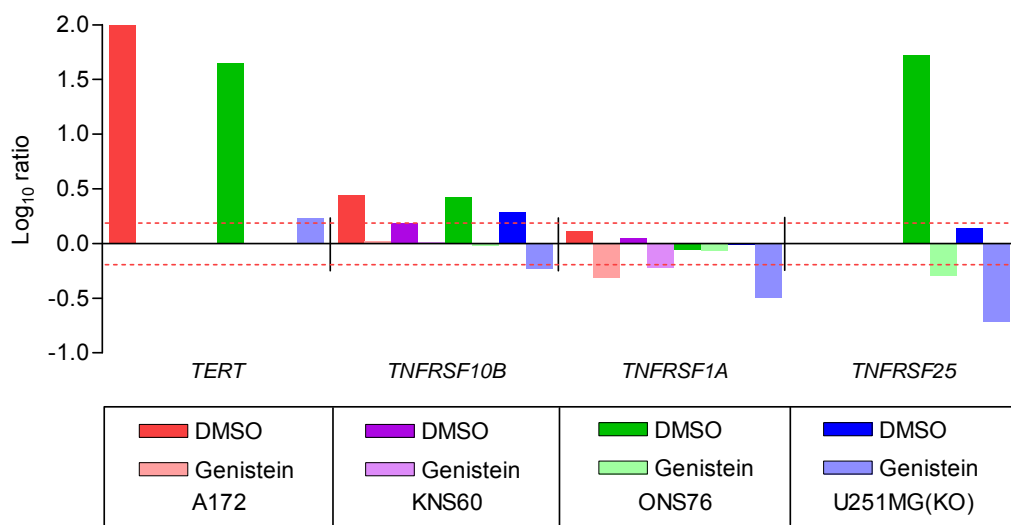
Figure 3.44. Gene expression analysis of selected cell death related genes in genistein-treated cell lines. Gene expression was performed using Oligo GEArray® Cancer PathwayFinder. TNF receptor superfamily genes showed downregulation upon genistein treatment. Red-dotted lines indicate cut-off threshold at ± 0.2.

3.3.3.5. Low telomerase activity was associated with downregulation of *hTERT* and *hTR* mRNA expressions, leading to telomere shortening.

It is well documented that inhibition of telomerase may synergise cancer therapy (Keith *et al.*, 2004). By inhibiting the telomerase enzyme, telomere length progressively shorten with every round of DNA replication, resulting in critically short telomere that elicits apoptosis and senescence. Inhibiting the telomerase enzyme thus limits the proliferation capability of cancer cells and thereby conferring mortality on cancer cells (Shay and Wright, 2006).

In this study, various aspects of telomerase expression and functions were examined. Real-time PCR was carried out to investigate the expression of *hTERT* and *hTR* genes (Figure 3.45A and 3.45B). Expression of *hTERT* and *hTR* were reduced in all brain cancer cells after genistein treatment except for insignificant increase in *hTR* expression in A172 cell line. Overall, the decrease in the expression of *hTERT* and *hTR* suggests that genistein can regulate expression of *hTERT* and *hTR* at the mRNA level.

The TRAP assay shows that all brain cancer cell lines except KNS60 exhibited a significant decrease in telomerase activity as represented by the TPG (Figure 3.46A) and percentage changes of telomerase activity (Figure 3.46B). In addition, the basal telomerase activities of ONS76 and U251MG(KO) were higher as compared to that in A172 and KNS60 cell lines. Possibly only in situations where high basal levels of telomerase activity are present, or when the activity levels exceed a certain threshold, genistein exhibits its anti-telomerase effect.

As a measure of the effectiveness of genistein in inhibiting telomerase function for long term, telomere length of the brain cancer cells was measured after 15-day treatment with genistein.

Figure 3.47 shows that in spite of treatment with genistein for 15 days, there is no drastic shortening of telomere length in any of the brain cell lines. It should be noted that the 15-day DMSO controls for each cell type showed a greater decrease in telomere length compared to the genistein treated cells. This suggests that although genistein is able to suppress telomerase activity, such suppression does not lead to drastic telomere attrition. It is known that telomeres undergo shortening with each successive round of cellular replication. In this study, genistein has been shown to induce cell cycle arrest, and thus cells undergo limited proliferation. As such, the effect of genistein on telomerase and consequently on telomere length is not apparent in an environment that is not permissive to cell cycling.

Overall, results indicate that genistein downregulates the expression of *hTERT* and *hTR* mRNA leading to the decrease in telomerase activity as evident in TRAP experiment. However, decrease in telomerase activity did not result in drastic shortening of telomere length, possibly due to the fact that genistein has triggered cell cycle arrest that thus slows down the proliferation rate.
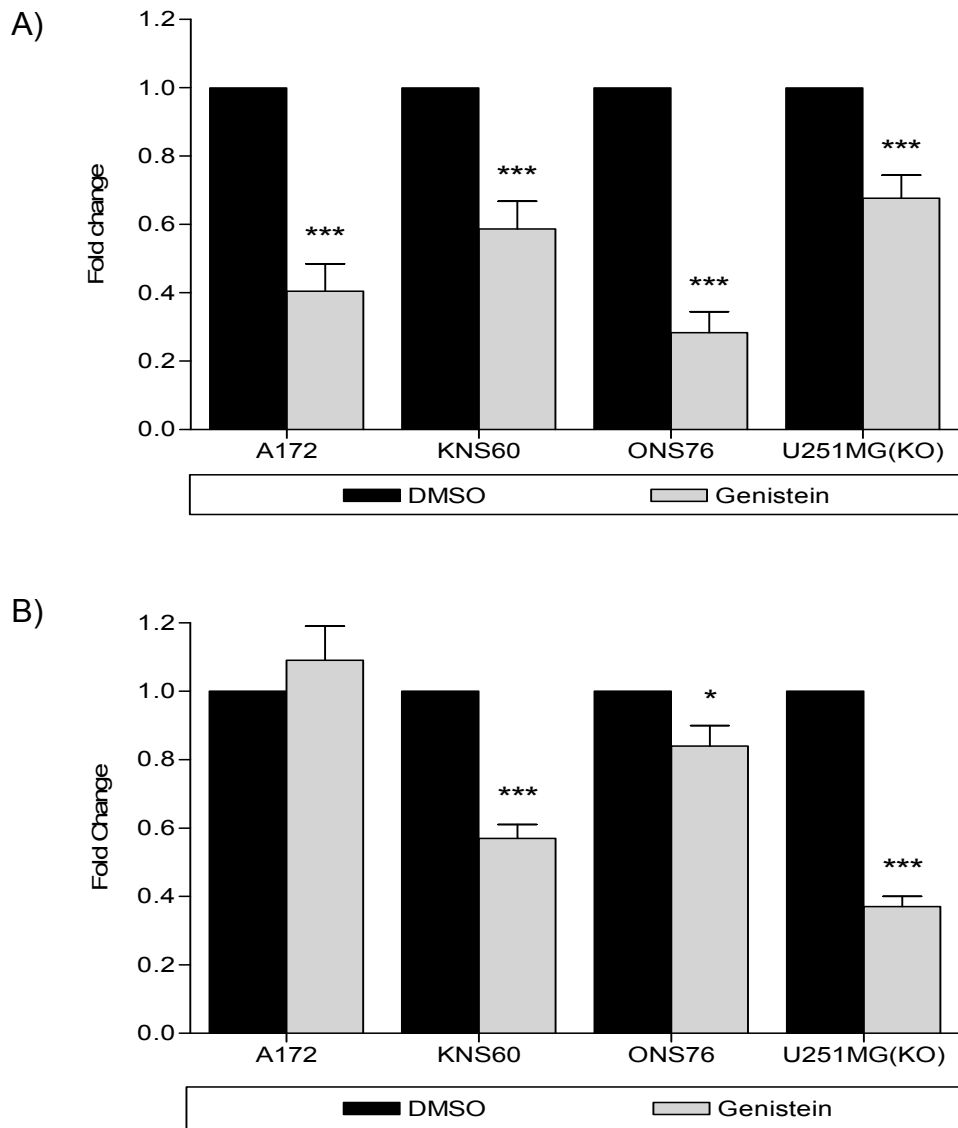
Figure 3.45. Genistein led to reduced mRNA levels of *hTERT* and *hTR* in brain cancer cells. A) Levels of *hTERT* mRNA were considerably reduced as observed via real-time PCR analysis. B) Genistein led to a similar reduction in mRNA levels of *hTR* in most brain cancer cells. * indicates p < 0.05, *** indicates p < 0.001.
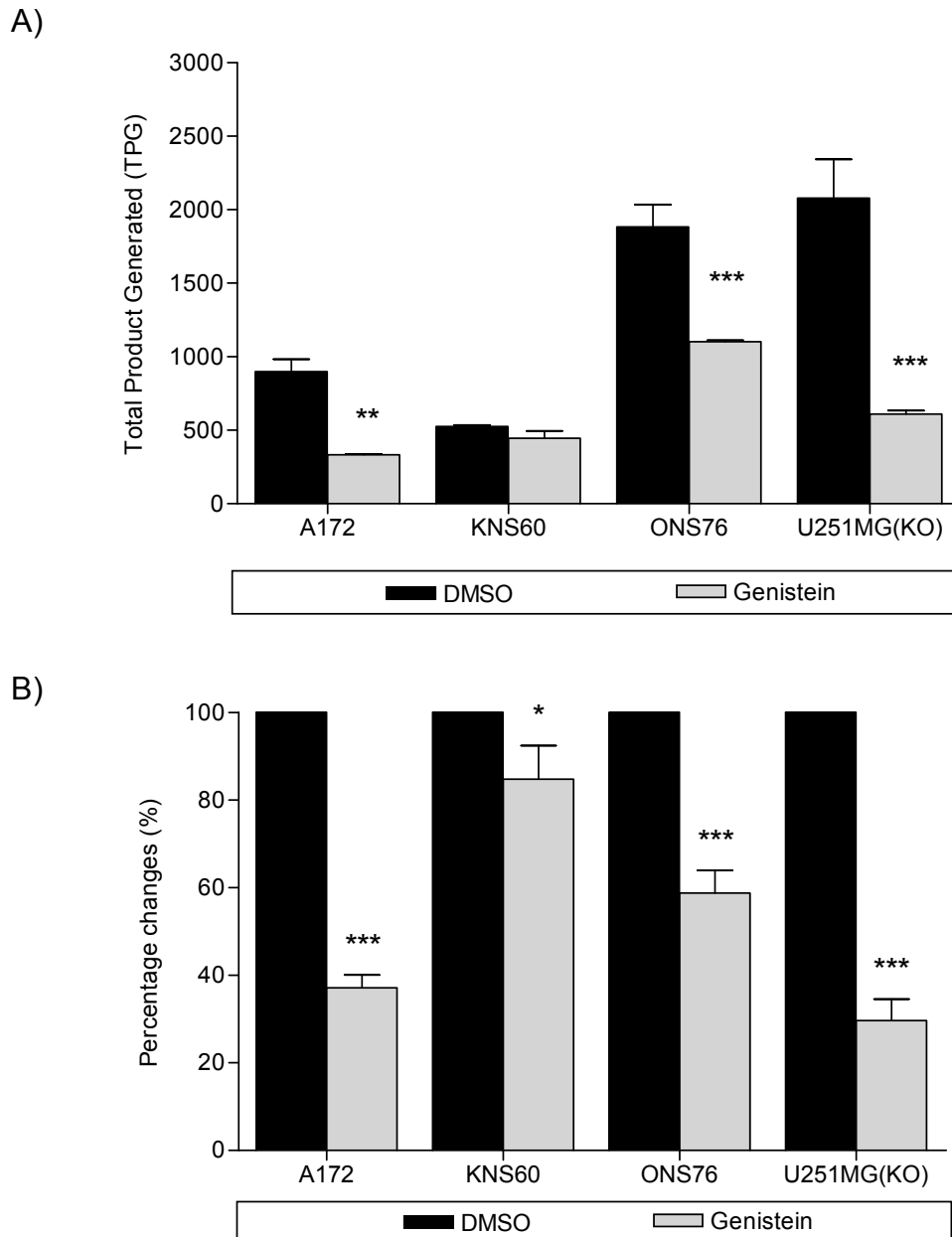
Figure 3.46. Telomerase activity of genistein-treated cells performed using TRAP assay. A) Decrease in telomerase activity as represented by Total Product Generated (TPG). B) Percentage changes of telomerase activity relative to DMSO vehicle control. ** indicates p < 0.01, *** indicates p < 0.001.
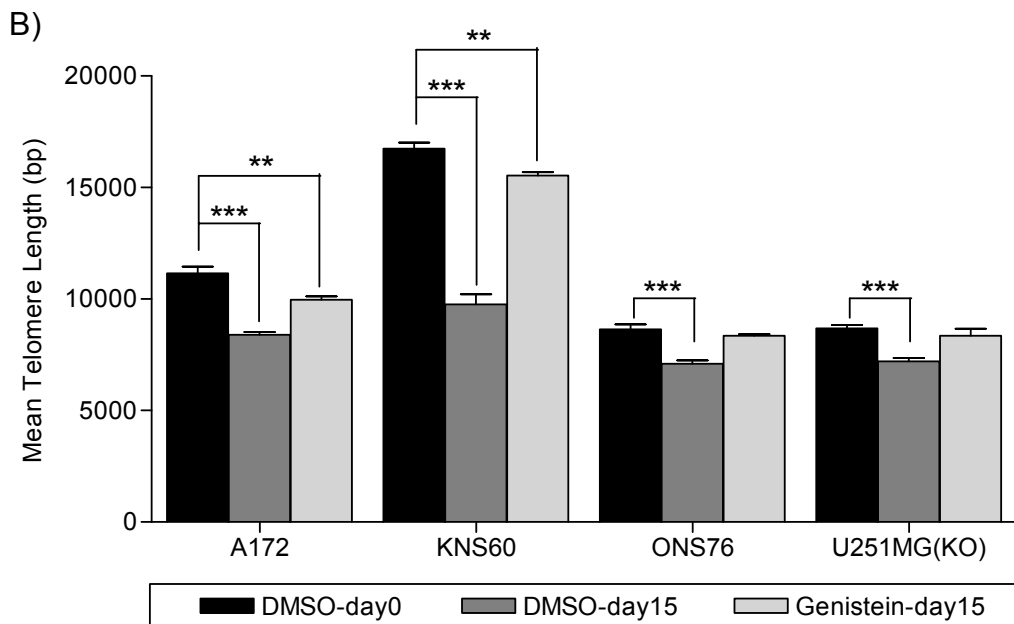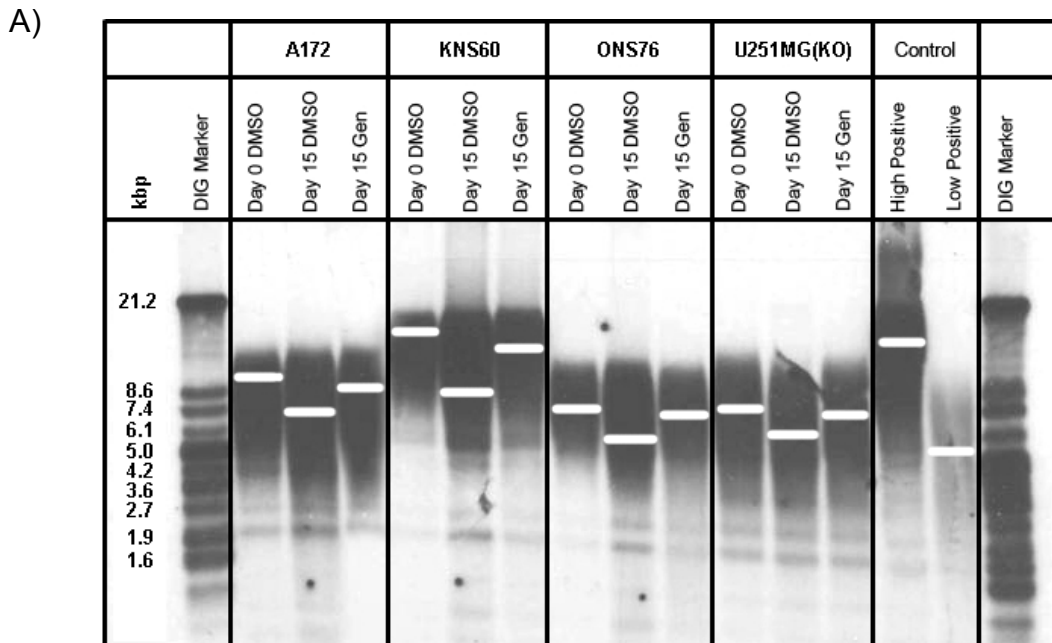
Figure 3.47. Telomere length measurement of genistein-treated cells using TRF assay. A) Detection of telomeric regions using southern blot transfer and telomere specific DIG-labelled probe. B) Graphical representation of mean telomere length. ** indicates p < 0.01, *** indicates p < 0.001.

3.3.3.6. Discussion

In the present study, 50 µM of genistein was used for all experiments. At this concentration, no cell death was observed as shown in crystal violet assay (Figure 3.34) and cell cycle analysis (Figure 3.36). Consistent with our findings, a similar study also reported that genistein treatment ranging from 1 to 100 µM did not exhibit cytotoxic effects (Farina *et al.*, 2006). Further investigations on cell death using annexin V staining (Figure 3.38) and DNA damage using comet assay (Figure 3.39) also indicated that neither apoptosis nor DNA damage was detected after genistein treatment, corroborating with an earlier report that genistein concentration of up to 180 µM did not induce significant DNA damage (Darbon *et al.,* 2000). However, these findings contradict with some other studies that show DNA damage and apoptotic cell death with the observations of cytochrome c release, ROS induction, caspase-3/7, 8, 9 activations and decreased Bcl2/Bax ratio following genistein treatment (Rucinska *et al.*, 2007; Thasni *et al.*, 2008b; Li *et al.*, 2008; Jin *et al.*, 2009; Rucinska and Gabryelak, 2009).

Genistein has been shown in this study to induce cell cycle arrest at the G1 and G2/M phases. The cell cycle arrest was associated with the downregulation of *CCNE1*, *CDK2* and *E2F1* genes (Figure 3.41). Interestingly, western blotting showed that brain cancer cells with differing radiosensitivity displayed opposite trends in the cell cycle protein expressions (Figure 3.40 and 3.42). Radiosensitive cells, A172 and ONS76, exhibited an increase in the p21 protein with reductions in Cyclin B1 and Cdk1 protein expressions, suggesting that radiosensitive cells underwent growth arrest upon genistein treatment. Observations of cell cycle arrest elicited by genistein were also

reported in numerous previous studies, where downregulation of Cyclin B and cyclin dependent kinases (CDKs), upregulation of CDK inhibitors (CDKIs) such as p21, p27 and p16 were among the commonly reported molecular responses (Raffoul *et al.*, 2006; Yu *et al.*, 2008; Majid *et al.*, 2008; Li *et al.*, 2008). In the case of radioresistant cells, KNS60 and U251MG(KO), increased expression of Cyclin B1 and Cdk1 proteins together with overexpression of Survivin and Bcl2 proteins suggest that these cells are relatively resistant to the cytostatic effect of genistein.

Besides the cell cycle arrest and cell death events, this study has shown that genistein suppresses the expression of *hTERT* and *hTR* (Figure 3.44), leading to lower activity of telomerase enzyme (Figure 3.45) and shorter telomere length compared to DMSO controls (Figure 3.46). Other studies also corroborate with our data as they have reported that genistein decreases expression and transcriptional activity of *hTERT*, the catalytic component of telomerase, via the downregulation of *c-Myc* expression in different cancer cells (Ouchi *et al.*, 2005; Jagadeesh *et al.*, 2006; Li *et al.*, 2009).

Many studies have independently reported that genistein elicits cell cycle arrest, cell death and telomerase inhibition concurrently (Alhasan *et al.,* 2001; Chinni *et al.,* 2003). However, the data from the current work reveals that genistein does not cause cell death despite the presence of cell cycle arrest and telomerase inhibition. Since telomere shortening happens only during physiological DNA replication and thus cannot be initiated in an arrested cell, it seems redundant for telomerase to be inhibited in cells that are arrested. However, it is reasonable to conclude that genistein exerts its

telomerase inhibition effect as a secondary strategy selectively targeting cancer cells that have escaped cell cycle arrest and continued to proliferate. Inhibition of the telomerase enzyme may lead to shortening of telomere length in replicating cells. When the telomere length becomes critically short, more genomic instability ensues, eventually resulting in cell death.

In summary, genistein treatment has been shown to initiate growth arrest and telomerase inhibition in all brain cancer cell lines. However, based on the molecular observations, observations of growth arrest were more prominent in radiosensitive cells compared to radioresistant cells, suggesting that genistein may be more effective in cancer therapy only in radiosensitive tumours. Figure 3.48 shows a schematic illustration of potential molecular events triggered upon the treatment with genistein.
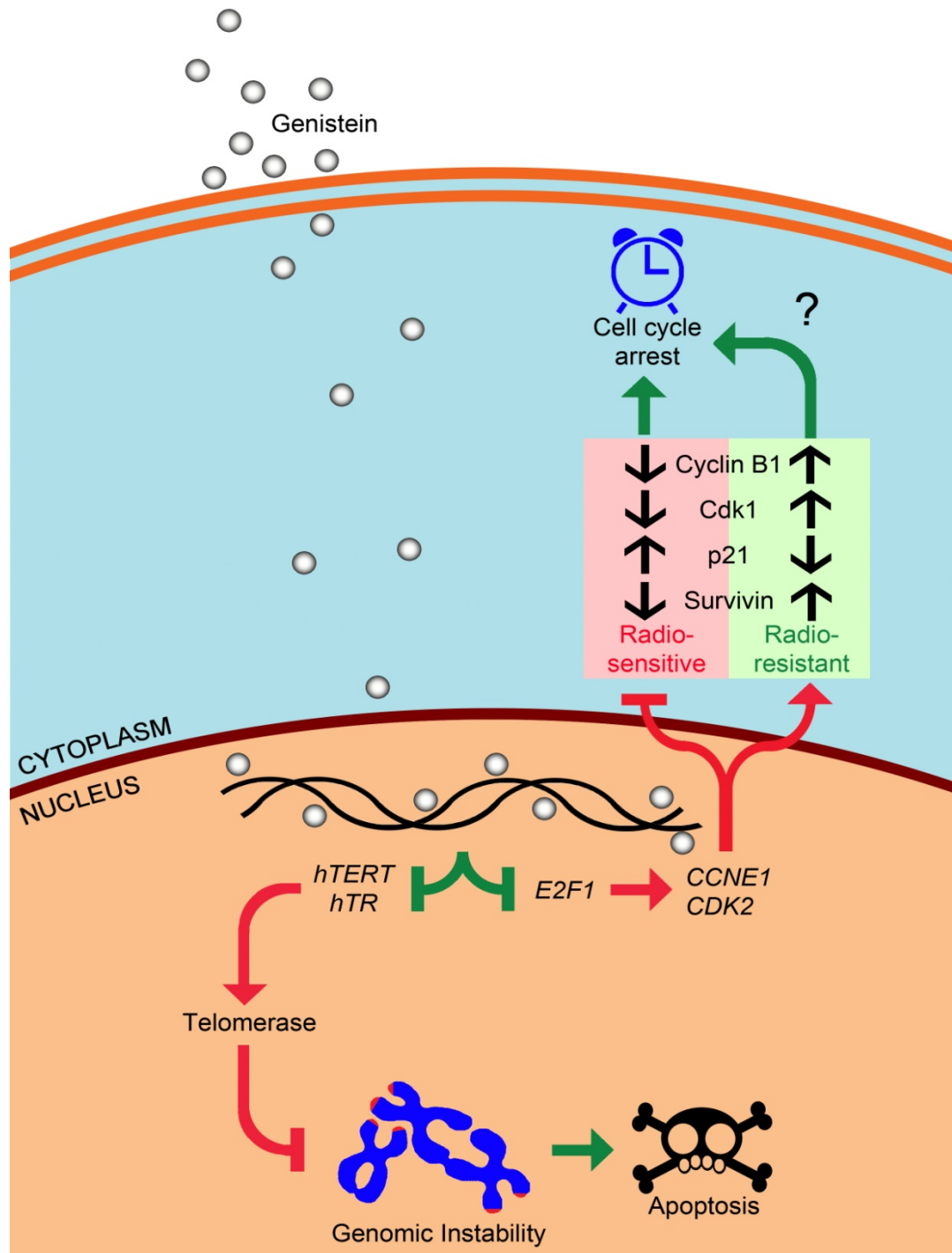
Figure 3.48. Schematic representation of cellular pathways potentially triggered upon genistein treatment. Genistein does not induce DNA damage and cell death; the cytostatic effect exhibited by genistein may be due to the downregulation of *E2F1* gene. However, cells with different radioresponses showed opposite regulation of protein expressions. Inhibition of telomerase activity may act as a second attack to cancer cells that escape cell cycle arrest. Green arrows represent possible events whereas red arrows indicate inhibited pathways.

153

3.3.4. Curcumin ((1E,6E)-1,7-bis(4-hydroxy-3-methoxyphenyl)-1,6-hepta -diene-3,5-dione)

In this section, we explored curcumin as a potential treatment drug for brain cancer cell lines. Functional and molecular aspects of cell cycle, cell death and telomere-telomerase regulations were investigated to understand the response and sensitivity of each cell line toward curcumin.

3.3.4.1. Curcumin binds to cell surface membrane and infiltrates into cells to induce cell death.

To investigate the inhibitory concentration of curcumin that leads to 50 % reduction of cell density (IC_{50}), crystal violet assay was performed. Cells were treated with curcumin at different concentrations ranging from 0 to 100 µM for 48 hours. The crystal violet assay (Figure 3.49) showed that curcumin treatment results in dose-dependent decrease in cell density. The responses of the cell lines are presented in the following order of decreasing sensitivity: hTERT-BJ1, KNS60, A172, U251MG(KO), ONS76 and finally Normal1. Among the brain cancer cells, the KNS60 cell line appears to be the most sensitive to curcumin whereas the ONS76 cell line shows a greater resistance towards any cytotoxic effects of curcumin. As for the two control cell lines, telomerase negative Normal1 reached 50 % cell density at a high dose of 90 µM while the IC_{50} of hTERT-BJ1 cell was at 20 µM. This is interesting as curcumin may sensitise cells that express the telomerase enzyme, thus resulting in a lower IC_{50} range of less than 50 µM for all brain cancer cells and the hTERT-BJ1 cells. This observation suggests that cells with activated telomerase, such as cancer cells, may be a promising target for curcumin.

Concentrations of curcumin at each determined IC_{50} were used for subsequent experiments.

In order to examine the effects of curcumin on cell density and morphology, DMSO and curcumin-treated cells were observed under normal light microscope at 100 X and 200 X magnifications. As shown in Figure 3.50A, treatment of curcumin for 48 hours led to significant changes in cell density and morphology in all cell lines treated. Upon curcumin treatment, all brain cancer cell lines showed a reduced density compared to their corresponding DMSO control. As low dose of DMSO does not induce cell death or cell cycle arrest, DMSO-treated cells continue to proliferate and increase in cell density. However, curcumin-treated cells may have undergone a certain degree of cell death and cell cycle arrest, causing the cells to detach from the culture dish, resulting in a lower cell density. As shown in Figure 3.50B, the 200 X magnification of cell morphology of most curcumin-treated cells exhibited granulated and condensed cytoplasm, indicating that cells were undergoing apoptotic cell death. The ONS76 cell line showed a vacuole-associated phenotype resembling autophagy (Tanaka *et al.*, 2000). Enlarged or flattened cell morphology was also seen in U251MG(KO) curcumin-treated cells. All these phenotypical observations suggest that the brain cancer cell lines in this study react to curcumin treatment strongly, resulting in more cell death and hence lower cell density.

By using the excitation and emission wavelengths of curcumin obtained from fluorescence spectrophotometer (section 3.1.2), the route of drug trafficking into the cells was investigated using fluorescence microscopy at different time-points. The FITC filter was used to detect green fluorescence

emitted by curcumin at 531 nm while the DAPI filter was used to detect blue fluorescence emitted by the auto-fluorescence of the U251MG(KO) cells. Figure 3.51 depicts a series of pictures of cell death observed throughout the duration of curcumin treatment. Curcumin bound to the cell surface membrane at an early time point after treatment and was later taken up into the cells, or infiltrated into the cell cytoplasm, leading to the induction of apoptotic events such as the disruption of cell membrane, nuclear fragmentation and cell disintegration. This observation clearly demonstrates the cytotoxicity of curcumin over a period of 48 hours of treatment. These observations were only presented as a series of cell death events. The possibility that some cells were still alive or in a late stage of apoptosis, at any point in time during curcumin treatment cannot be ruled out.
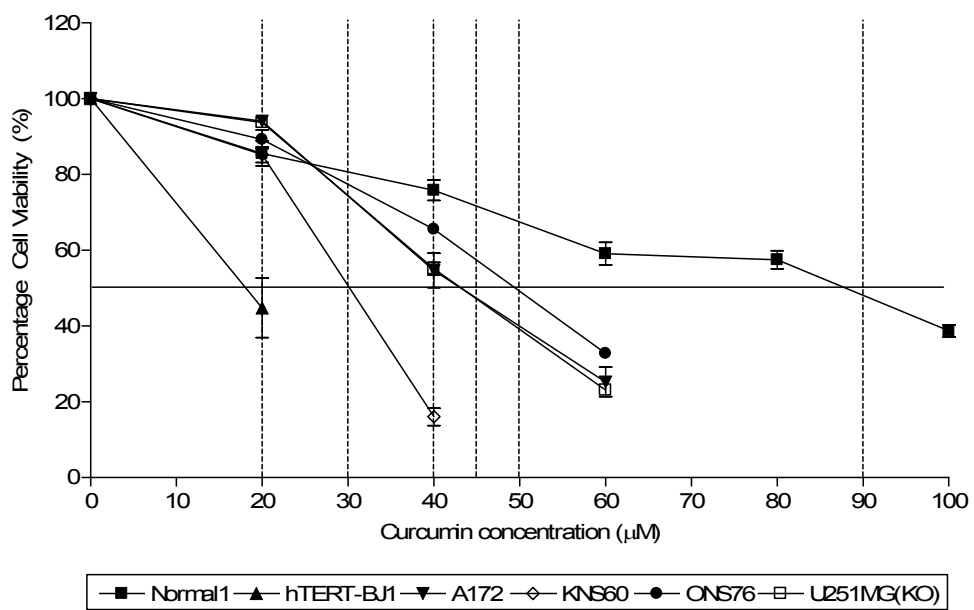
Figure 3.49. Crystal violet cell density assay on 48-hour curcumin-treated cells. Telomerase negative Normal1 cells appear to be resistant to curcumin treatment, whereas all telomerase positive cells showed lower IC_{50} values, indicating sensitivity to curcumin.
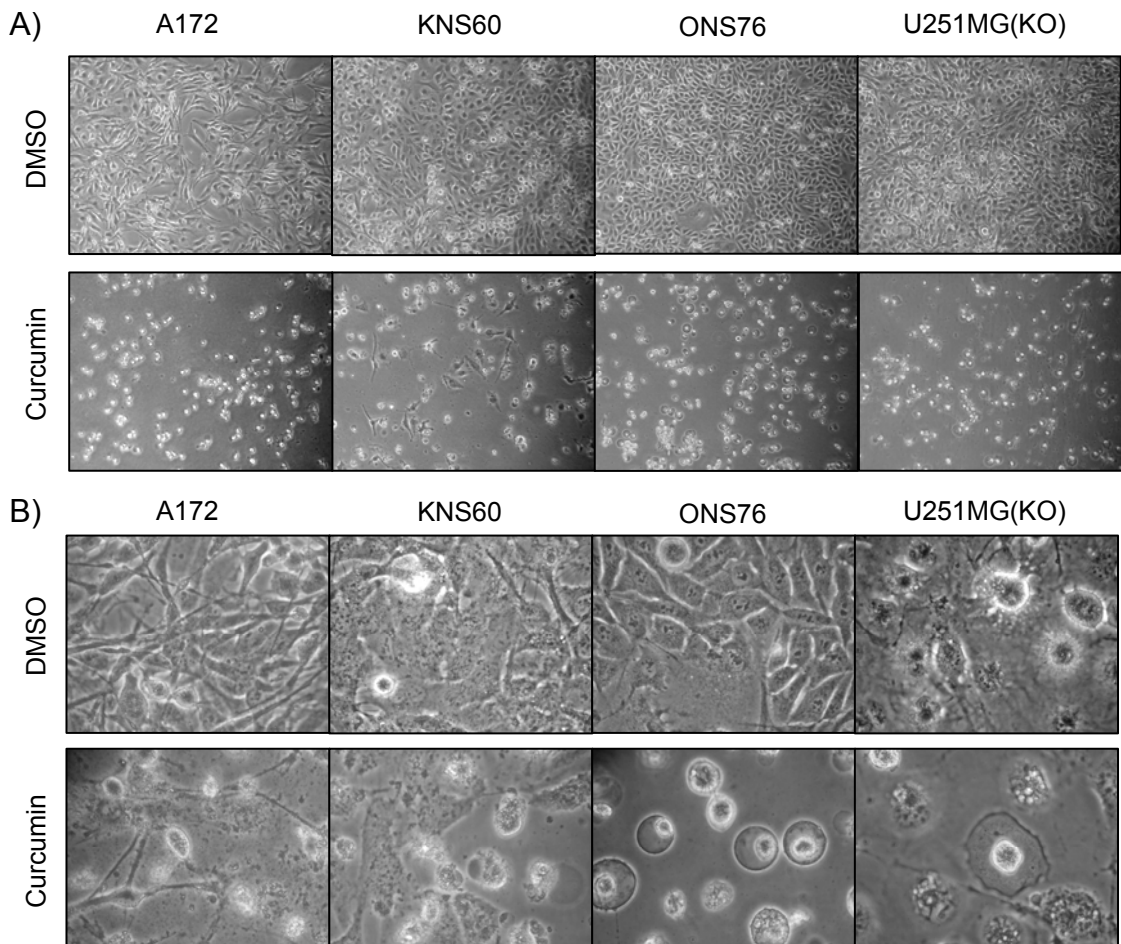
Figure 3.50. Cell morphology after curcumin treatment. A) Curcumin exerts a cytotoxic effect on all cells resulting in lower cell density through the induction of cell death as shown in 100 X magnification. Pictures of cell morphology captured at 200 X magnification.
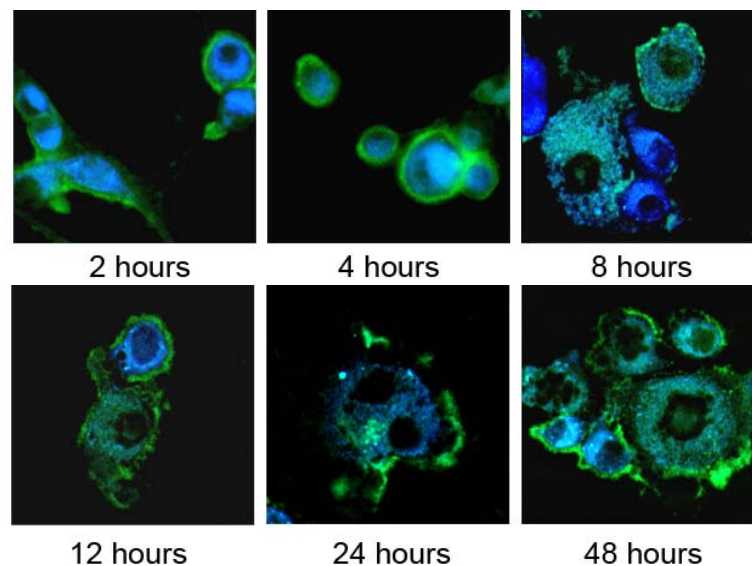
Figure 3.51. Green fluorescence of curcumin showing the route of drug trafficking into U251MG(KO) cell line. Auto-fluorescence of cells is indicated by blue signals. Curcumin accumulates at cell surface membrane and permeates into the cytoplasm and trigger apoptotic cell death.

3.3.4.2. Curcumin induces cell cycle arrest at G2/M phase and suppresses the clonogenic property of cells.

To investigate the two related aspects of cell viability that may result in decrease in cell density, cell cycle arrest and cell death were examined. In this section, cell cycle analysis was carried out by staining drug-treated cells with propidium iodide, followed by FACS analysis. Figure 3.52 shows the cell cycle profiles of all cell lines after 48 hours of DMSO and curcumin treatment. While some cell lines such as hTERT-BJ1, KNS60 and ONS76 underwent growth arrest at G2/M phase upon curcumin treatment, the other cell lines such as Normal1, A172 and U251MG(KO) did not show significant changes in their cell cycle profile. In addition, KNS60 and ONS76 had an increase in the sub-G1 population, with ONS76 showing more cell death as indicated by the high sub-G1 region.

In order to study the long-term effects of cell cycle arrest triggered by curcumin, clonogenicity of cells after treatment was explored. Colony formation assay was performed by treating the cells for 48 hours, after which 2×10^3 cells were reseeded and maintained in culture with drug-free medium for 10 days. As shown in Figure 3.53, all curcumin-treated cell lines showed decreased colony numbers compared to DMSO controls. Even though the KNS60 cell line was most sensitive to curcumin as shown in the crystal violet assay, this cell line showed resistance to the clonogenic inhibitory effect of curcumin. The same observation was also found in the ONS76 cell line. These observations suggest that in the case of fast growing cells, although cell death was triggered, removal of curcumin from the culture media allows the cells to continue to proliferate and form colonies. In contrast, A172 and

159

U251MG(KO) cells exhibited different responses where the colony numbers decreased drastically in the drug-free medium after 10 days of incubation, suggesting that 48 hours of curcumin treatment resulted in cell death and/or cytostasis in A172 and U251MG(KO) cells to bring about reduced colony numbers. Put together, these findings propose that cells that are sensitive to curcumin such as hTERT-BJ1, KNS60 and ONS76, responded by acutely exhibiting more cell death and/or cell cycle arrest, whereas A172, U251MG(KO) and Normal1 cells are less sensitive to cell death induced by curcumin at 48-hour. It is only in the event that when cells continue to grow in drug-free media after 48 hours of curcumin treatment, these cells began to manifest the cytotoxic and/or cytostatic effects of curcumin resulting in decreased clonogenicity.
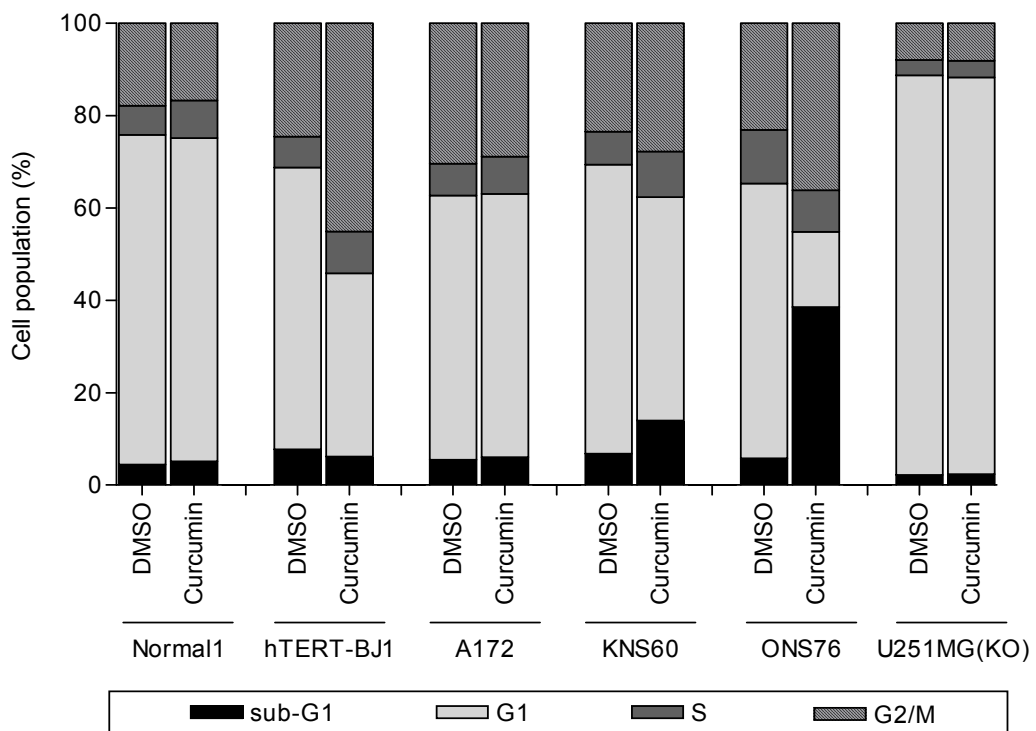
Figure 3.52. Cell cycle profiles of curcumin-treated cell lines stained with propidium iodide and subjected to flow cytometry analysis. Normal1, A172 and U251MG(KO) cells did not show any significant changes in their cell cycle profiles, indicating resistance to curcumin. Contrastingly, ONS76 cell showed a higher population in G2/M and sub-G1 region suggesting enhanced sensitivity to curcumin.
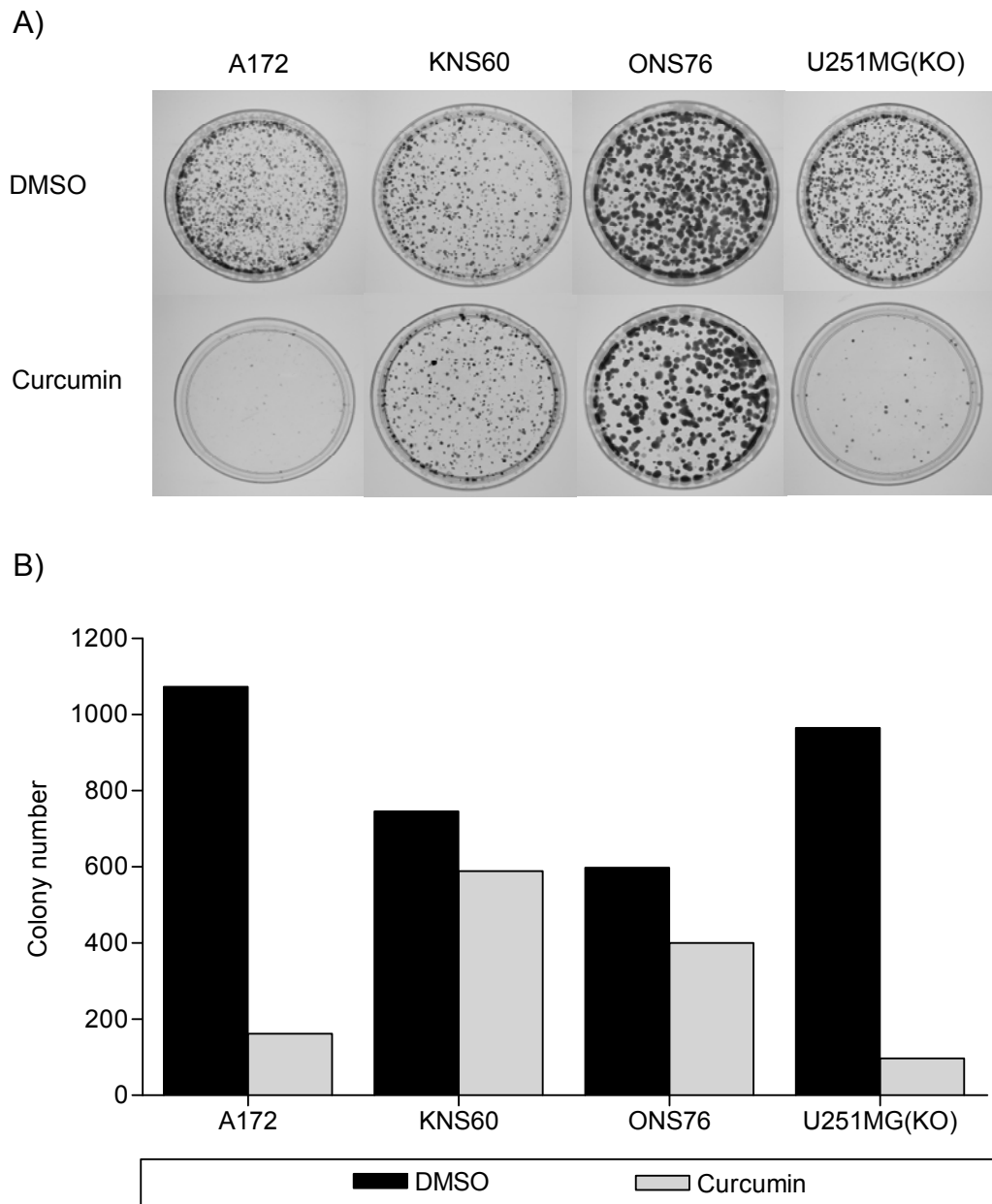
Figure 3.53. Colony formation assay of curcumin-treated brain cancer cells. A) Colonies were stained with crystal violet for visualization. B) Graphical representation of numbers of colonies counted in 100 mm culture dishes.

3.3.4.3. Cell death is associated with curcumin-induced DNA damage.

Apart from inducing cell cycle arrest, curcumin treatment has also led to significant levels of cell death in some cell lines as depicted by the sub-G1 region of the cell cycle profile. In this section, cell death analysis was validated by the use of caspase assay and annexin V staining. In addition, the degree of DNA damage induced by curcumin treatment was also examined using the comet assay.

As shown in Figure 3.54, DMSO and curcumin treatments induced various degrees of caspase-3/7 activity. Specifically, caspase-3/7 activity increased significantly after treatment with curcumin in A172, KNS60 and U251MG(KO) cell lines. A172 cell line exhibited highest caspase-3/7 activity at 24 and 48 hours after treatment. Overall, the caspase assay clearly indicates that the apoptotic cell death induced by curcumin was a result of caspase-3/7 activity. The reduction of caspase-3/7 levels in ONS76 may be a result of the massive cell death observed in the cell cycle, leading naturally to decreased expression of all genes.

To validate that apoptotic cell death was triggered by curcumin treatment, annexin V staining was performed using FACS analysis. Consistent with earlier observation, all cell lines underwent apoptosis upon curcumin treatment (Figure 3.55A). There is minimal population of necrotic cells detected in all cell lines, suggesting that the cell death encountered with curcumin treatment is largely due to apoptosis. Populations of early and late apoptosis were relatively balanced in most cell lines except for A172 and ONS76 cell lines that had more cells at the late apoptotic region (Figure

3.55B). This suggests that A172 and ONS76 cells may have been triggered to apoptosis in the early hours of curcumin treatment.

Comet assay was carried out to determine if curcumin induces DNA damage. Figure 3.56A shows that curcumin induced various degrees of DNA damage in different cell lines and these damages were relatively higher than that triggered by plumbagin (Figure 3.24) and genistein (Figure 3.40). Surprisingly, although curcumin treatment induced extensive DNA damage in Normal1 and A172 cell lines, their cell cycle profiles did not reflect the extent of damage incurred as seen by low levels of sub-G1 and lack of cell cycle arrest. It is possible that the Normal1 cell line has a highly efficient DNA repair mechanism that allows them to continue growing while the damages were being repaired, whereas the A172 cell line may have a rather inefficient repair system that render the cells prone to massive cell death that may occur only after 48-hour of curcumin treatment, especially when caspase activity increases preceding cell death. As for the other brain cancer cell lines, although the tail moments indicating DNA damage were not as high as that seen in Normal1 and A172, considerable DNA were present in tail moments suggest that they contain more damaged DNA than that of DMSO-treated controls (Figure 3.56B). In conclusion, comet assay has shown that all cell lines underwent various degrees of DNA damages upon curcumin treatment; the DNA content in comet tails of brain cancer cell lines was considerably higher than that in non-cancerous cell lines, suggesting that brain cancer cells suffered more damages in curcumin treatment.

Overall, these results have validated that 48 hours of curcumin treatment induces DNA damage and cell death. Annexin V staining confirms

that curcumin does not trigger necrotic cell death but apoptosis. Caspase assay shows that curcumin treatment leads to caspase-3/7 induction at 24 to 48 hours. All these cell death events are believed to be associated with DNA damage induced by curcumin.
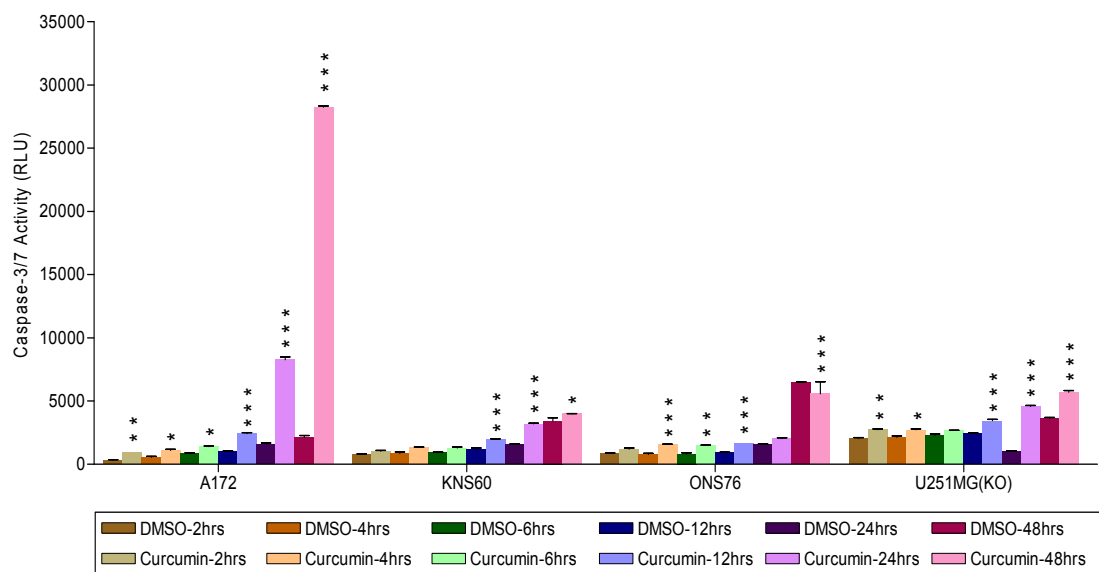
Figure 3.54. Activities of caspase-3/7 at different time points after curcumin treatment. Casapase-3/7 activity is mainly contributed by curcumin treated samples. * indicates p < 0.05, ** indicates p < 0.01, *** indicates p < 0.001.
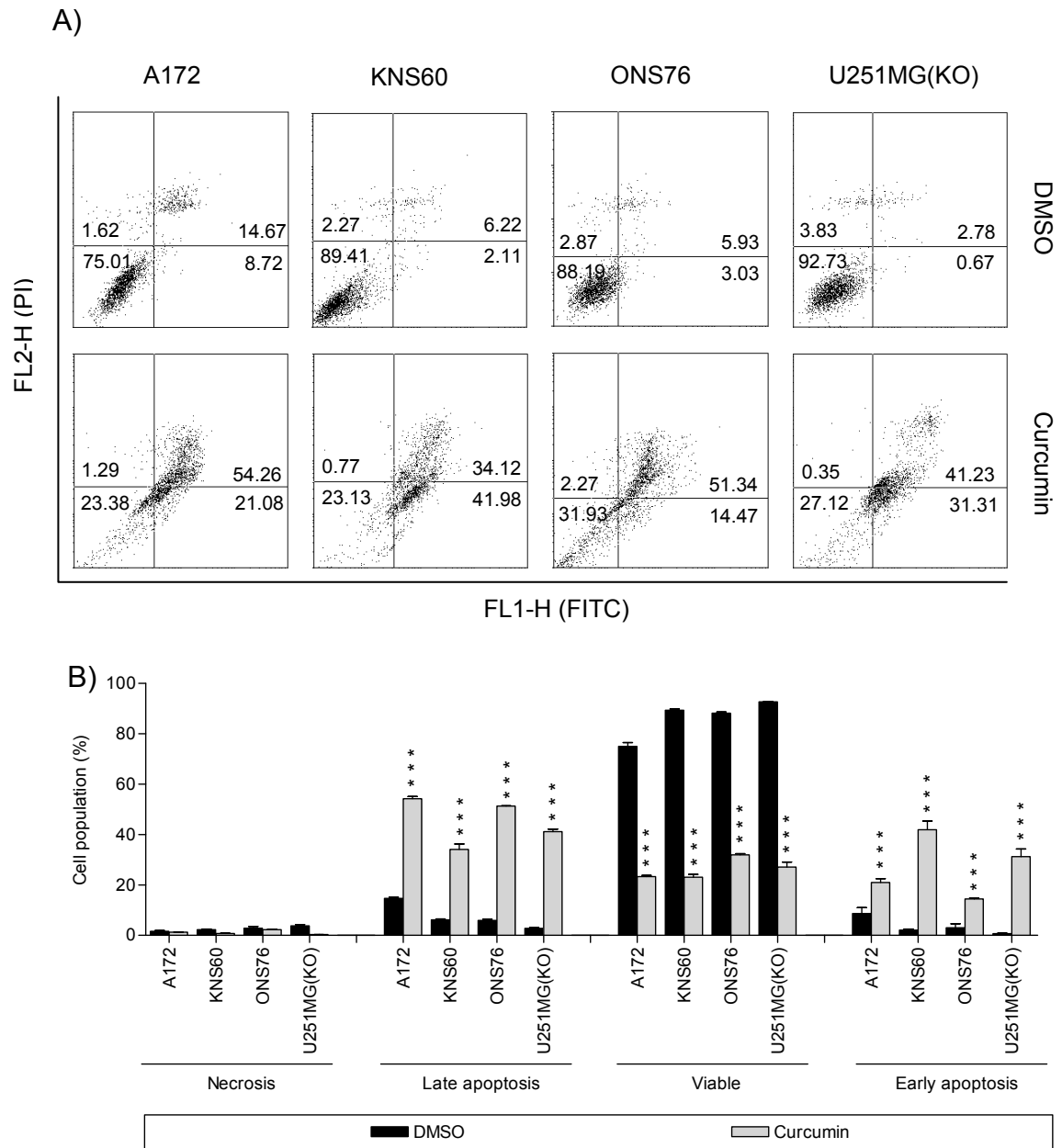
Figure 3.55. Annexin V staining of curcumin treated cell lines. A) Dot-plot data of FITC and PI staining measured by FACS analysis. B) Graphical chart representation of viable, necrosis, and apoptosis populations. *** indicates p < 0.001.
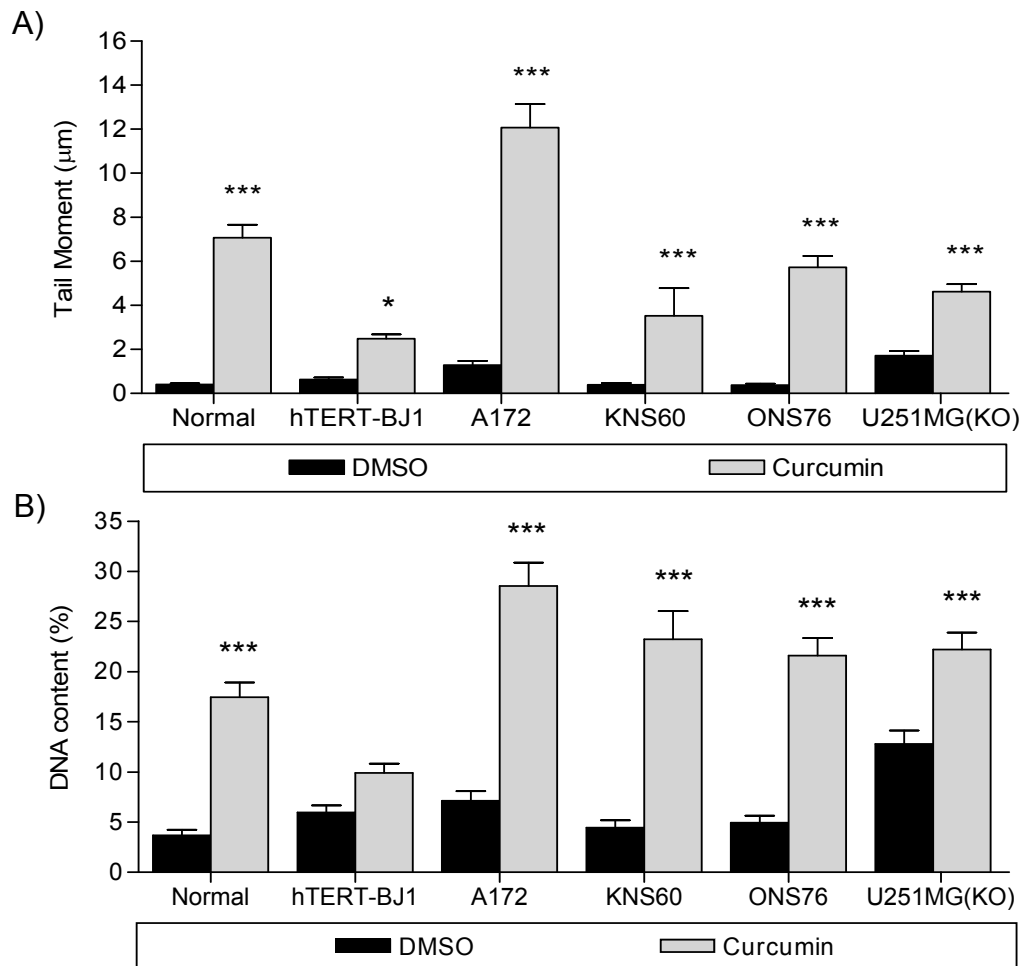
Figure 3.56. Degree of DNA damage in cell lines treated with curcumin. A) All cell lines showed significant increases in DNA damage after treatment with curcumin. A172 harboured the highest degree of damages. B) Graphical representation of DNA content in comet tails. * indicates $p < 0.05$, *** indicates $p < 0.001$.

3.3.4.4. Downregulation of *CCNE1* and *E2F1* genes together with upregulation of p21 protein resulting in growth arrest at G2/M phase.

In order to further elucidate the cell cycle arrest event, gene and protein expression analyses were carried out using Oligo GEArray® Cancer PathwayFinder and western blotting respectively. Genes involved in cell cycle regulation such as *CCNE1*, *CDK2*, *E2F1* and *PTEN* were also studied. As shown in Figure 3.57, all genes studied exhibited decreasing expressions except for the *PTEN* gene that was upregulated upon curcumin treatment. PTEN is a negative regulator of AKT cell survival and proliferation pathway. Upregulation of the *PTEN* gene indicates an inhibition in cell proliferation. Reduced expressions of *CCNE1* and *CDK2* genes, which encode for cyclin E and cdk2 proteins respectively, suggest that cells may arrest at G1 phase of cell cycle. In addition, *E2F* was downregulated in all brain cancer cell lines upon curcumin treatment, suggesting that the transcription of cyclins, cdks and checkpoint regulators were interrupted. Overall, the differential expressions of these selected genes suggest that cells underwent growth arrest that prevented them from continuing proliferation following curcumin treatment.

Western blot was then performed to validate the findings of cell cycle gene expressions. Figure 3.58 shows the cell cycle regulatory proteins including p53, p21, Cyclin B1 and Cdk1 which were analysed following curcumin treatment. All the cell lines exhibited a minimal difference in the expression of the Cdk1 protein except for ONS76 cells which showed a significant decrease. Moreover, ONS76 cells also exhibited an increase in the

expression of p21. Decrease in Cdk1 together with Cyclin B1 proteins coupled with an increased p21 expression very likely to have contributed to ONS76 cell cycle arrest at G2/M phase at the 48-hour time point. However, both the radioresistant cell lines, KNS60 and U251MG(KO), showed an enhanced expression of Cyclin B1 and low expression level for p21. These findings propose that KNS60 and U251MG(KO) cells did not undergo cell cycle arrest as observed in the ONS76 cell line. Additionally, radiosensitive cells have a low expression of p53 in both control and treated cells, but radioresistant cells have a high basal level of p53 that decreased upon curcumin treatment. This verifies that KNS60 and U251MG(KO) cell lines were indeed not arrested upon curcumin treatment. Protein expression analysis indicates that cell cycle arrest occurred in ONS76 cell but not in other cell lines. All together, these evidences of cell cycle gene and protein expressions correlate well with the cell cycle profiles demonstrating that curcumin treatment induces G2/M cell cycle arrest in the ONS76 cell line but not in KNS60 and U251MG(KO) cells.
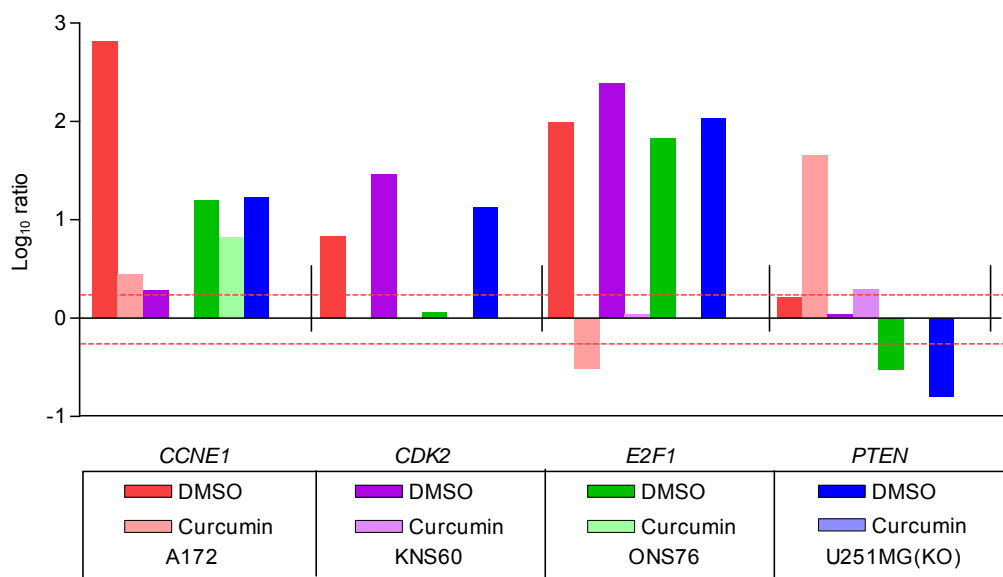
Figure 3.57. Gene expression analysis performed using Oligo GEArray® Cancer PathwayFinder. Cell cycle regulation genes include *CCNE1*, *CDK2*, *E2F1* and *PTEN* were analysed. Red-dotted lines indicate cut-off threshold at ± 0.2.
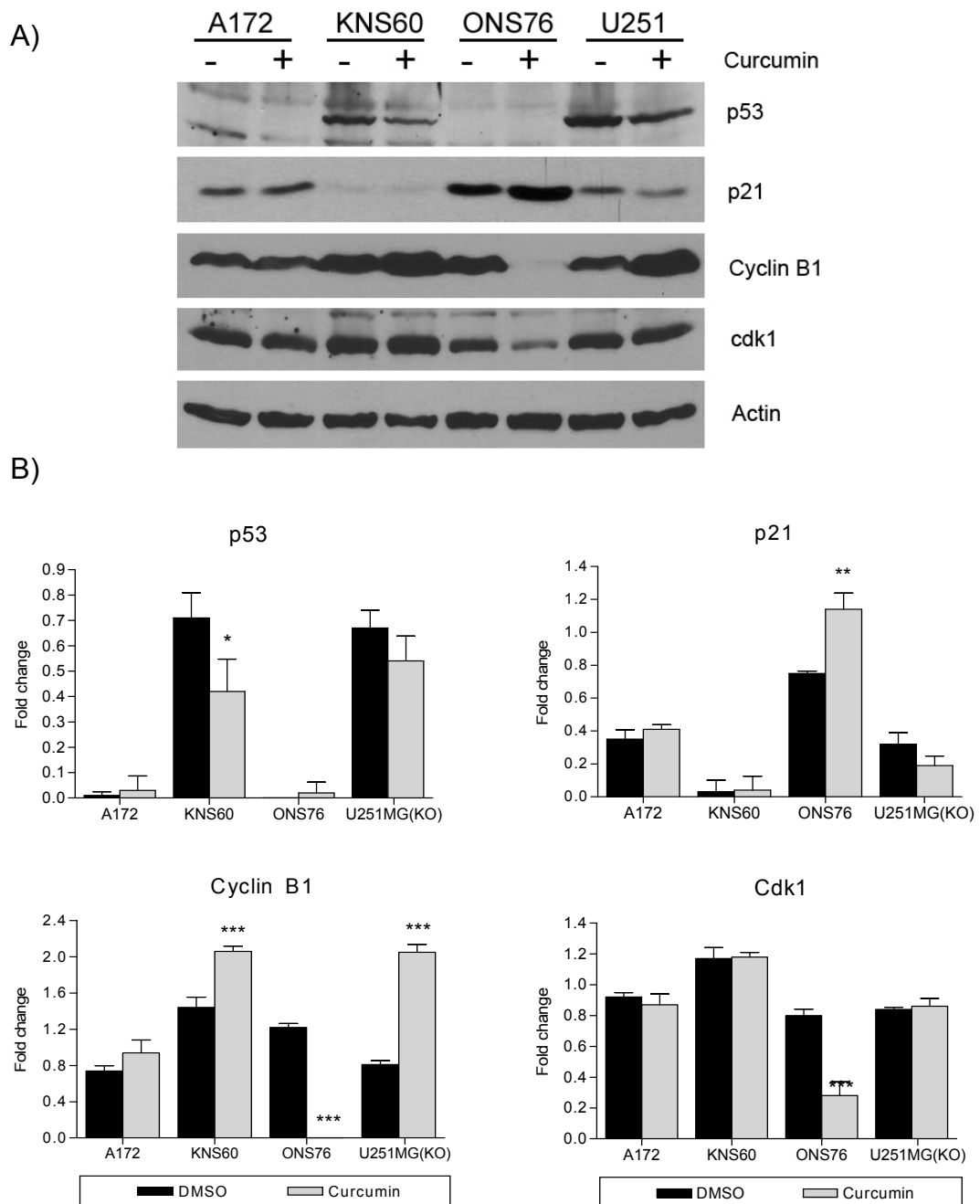
Figure 3.58. Western blot analysis of brain cancer cell lines treated with curcumin. A) Western blot of cell cycle regulatory proteins. Blots were probed with indicated antibodies. B) Fold change analysis of protein expressions obtained using densitometer. * indicates $p < 0.05$, ** indicates $p < 0.01$, *** indicates $p < 0.001$.

3.3.4.5. Curcumin triggers apoptotic cell death by over expressing Bax and downregulating Bcl2 and Survivin.

To elucidate the cell death events triggered by curcumin, gene and protein expression analyses were carried out by employing the same methods as discussed in section 3.1.1.4. Figure 3.59 shows the selected gene expression analysis of *BIRC5*, *TNFRSF10B* and *TNFRSF1A*. *BIRC5* that encodes for the Survivin protein is upregulated upon curcumin treatment in all the brain cancer cell lines except for the A172 cells. Similarly, *TNFRSF1A* displayed the same trend as observed in *BIRC5*. It is important to note that all the overexpressing trends of *BIRC5* and *TNFRSF1A* were actually below or marginally above the detection threshold of the experiment as indicated by the red dotted lines, suggesting that the regulations may not be significant. *TNFRSF10B* encodes for a tumour necrosis factor receptor that plays a role in triggering death signalling cascades. Most cells showed a decrease in *TNFRSF10B* expression upon curcumin treatment; downregulation of this gene may imply that cells are less responsive to the cell death induction by tumour necrosis factor. Hence, this result suggests that all cells, except for KNS60, are more resistant to curcumin treatment.

In another attempt to verify the cell death events induced by curcumin treatment, western blot analysis was performed on selected cell death related proteins. As shown in Figure 3.60, protein expressions of Bcl2, Bax, PARP1 and Survivin were examined. Contrary to mRNA levels, Survivin protein level was decreased in all brain cancer cells. In addition, protein level of Bcl2 was also decreased, indicating that these anti-apoptotic proteins were downregulated and cells were susceptible to apoptosis. In addition, most cells

except for KNS60 cells exhibited an increase in the expression of Bax, a pro-apoptotic protein, confirming the cell death events discussed earlier. It is interesting to note that PARP-1 did not show any significant change in its expression, and no cleaved-PARP-1 was detected in the western blot. This finding shows that PARP-1-independent cell death was activated and all proteins studied have verified the apoptotic cell death event triggered by curcumin. Overall, the protein expression analysis, but not gene expression analysis, has shown the correlation while confirming the findings of apoptotic cell death triggered by curcumin. Gene expression analysis failed to show conclusive results due to the low quality and quantity mRNA of the treated cells.
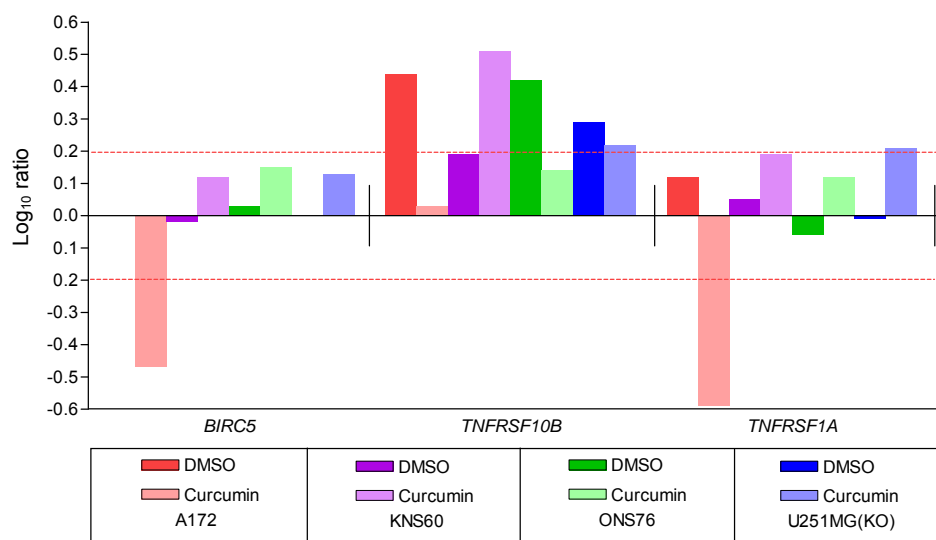
Figure 3.59. Gene expression analysis of selected cell death related genes in curcumin-treated cell lines. Gene expression analyses of *BIRC5*, *TNFRSF10B* and *TNFRSF1A* were performed using Oligo GEArray® Cancer PathwayFinder. Red-dotted lines indicate cut-off threshold at ± 0.2.
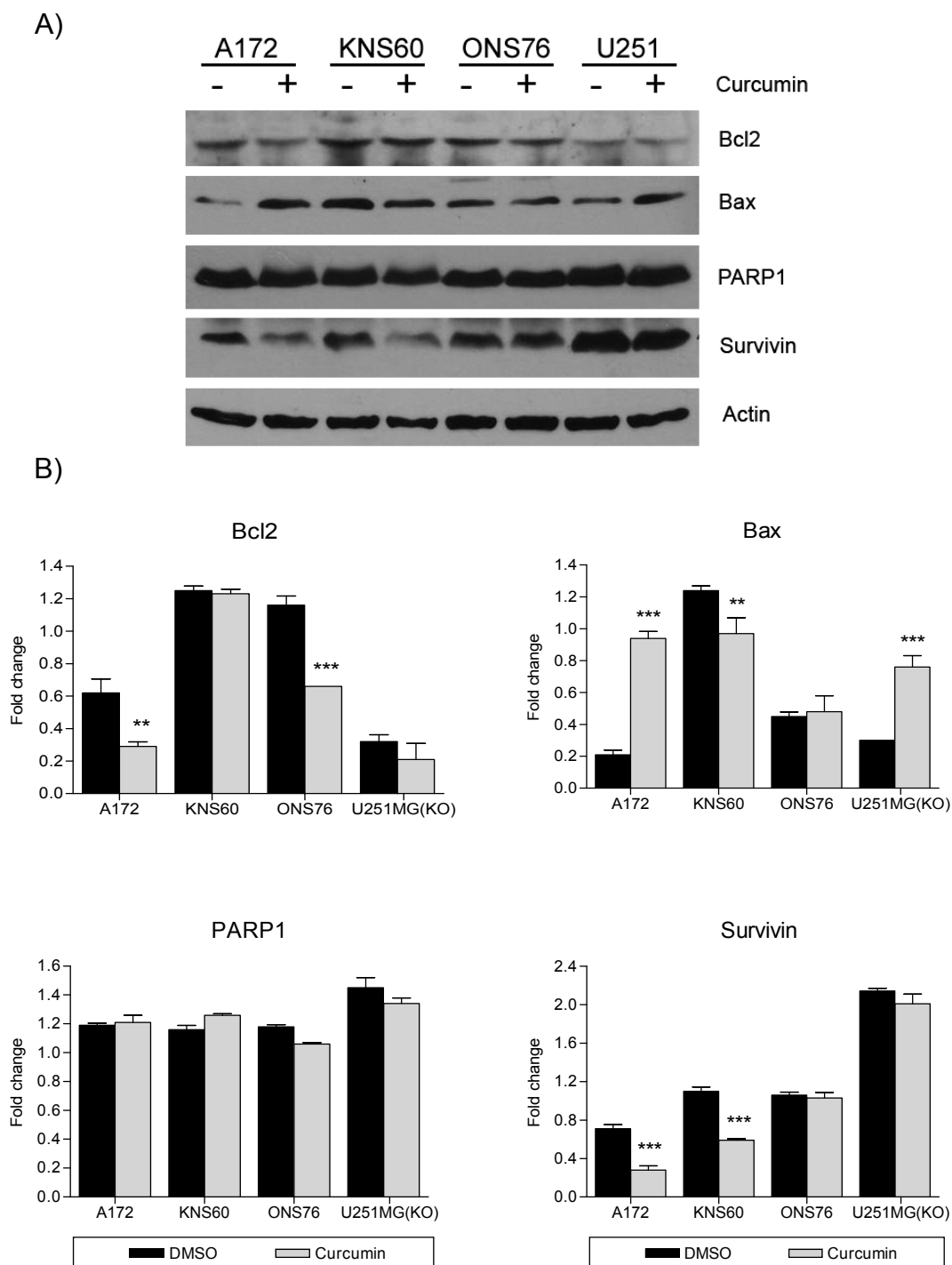
Figure 3.60. Western blot analysis of brain cancer cell lines treated with curcumin. A) Western blot data on cell death-related proteins. Blots were probed with the indicated antibodies. B) Fold changes analysis of protein expressions obtained using densitometer. ** indicates $p < 0.01$, *** indicates $p < 0.001$.

3.3.4.6. Curcumin inhibits telomerase activity by downregulating *hTERT* mRNA expression, leading to telomere shortening.

Besides the study of the growth arresting and cytotoxic properties of curcumin, another potential anticancer property such as the inhibition of telomerase activity was also investigated. This section mainly focuses on the telomerase inhibitory effect of curcumin that was demonstrated by the TRAP assay as well as real-time RT-PCR analysis on *hTERT* and *hTR* mRNA expression levels. The telomere length of cells that had undergone long-term treatment with curcumin was measured using the TRF assay. As shown in Figure 3.61A, telomerase activities, represented by the Total Product Generated (TPG), were downregulated after 48 hours of curcumin treatment. Although KNS60 and ONS76 cell lines exhibited exceptionally high basal telomerase activity, curcumin treatment significantly suppressed telomerase activity as demonstrated in Figure 3.61B. Although in A172 and U251MG(KO) cells, where the basal telomerase activity was not as high, the percentage decrease in activity after curcumin treatment was as dramatic as that seen in KNS60 and ONS76 cells. This suggests that curcumin may have effective inhibitory effect on telomerase in all these cell lines. In conclusion, curcumin has been shown to produce a significant decrease in the TPG values in cell lines with high basal telomerase activities; All cell lines exhibited a significant decrease in the percentage change in telomerase activity.

In order to examine factors affecting the reduction in telomerase activity, expression analyses of *hTERT* and *hTR* mRNA were performed using real-time RT-PCR. Figure 3.62A and 3.62B show the fold change in the expression of *hTERT* and *hTR* mRNA respectively. Upon curcumin treatment,

all cell lines exhibited a lower fold change in the value of *hTERT* mRNA expression as compared to DMSO controls. The DMSO controls were normalized across all samples to obtain a comparative fold change among the cell lines. Similar to the trend reported in the TRAP assay, KNS60 and ONS76 cell lines showed more than 50 % decrease in the expression of *hTERT* mRNA. Even though A172 and U251MG(KO) cells exhibited significant decreases in *hTERT* expression, these decreases were relatively low compared to the other two cell lines. On the other hand, the *hTR* mRNA expression did not project a conclusive trend as that seen in the *hTERT* expression. Surprisingly, ONS76 and U251MG(KO) cells exhibited an increase in the expression of *hTR* mRNA upon curcumin treatment compared to A172 and KNS60 cell lines. These results suggest that the expression of *hTERT* but not *hTR* mRNA, may be associated with curcumin-induced inhibition of telomerase activity.

To demonstrate the effectiveness of curcumin-induced telomerase inhibition, cells were treated with half the concentration of their respective IC_{50} for 15 continuous days with fresh medium and drug replenished every two days. As presented in Figure 3.63A, the southern blot analysis shows that all cell lines displayed a reduction in the mean telomere length following long-term treatment with curcumin. Interestingly, the decrease in telomere length projected a similar trend as shown in TRAP assay (Figure 3.61B). KNS60 and ONS76 cell lines, which had long basal telomere lengths, exhibited drastically shortened telomeres at the end of the long-term treatment. A172 and U251MG(KO) cells, which had shorter basal telomere lengths, showed a less extensive but significant shortening of telomere. These results directly

correlate the shortening of telomeres with a decrease in the telomerase activity that is probably directly a result of the reduction in the *hTERT* mRNA expression upon curcumin treatment.
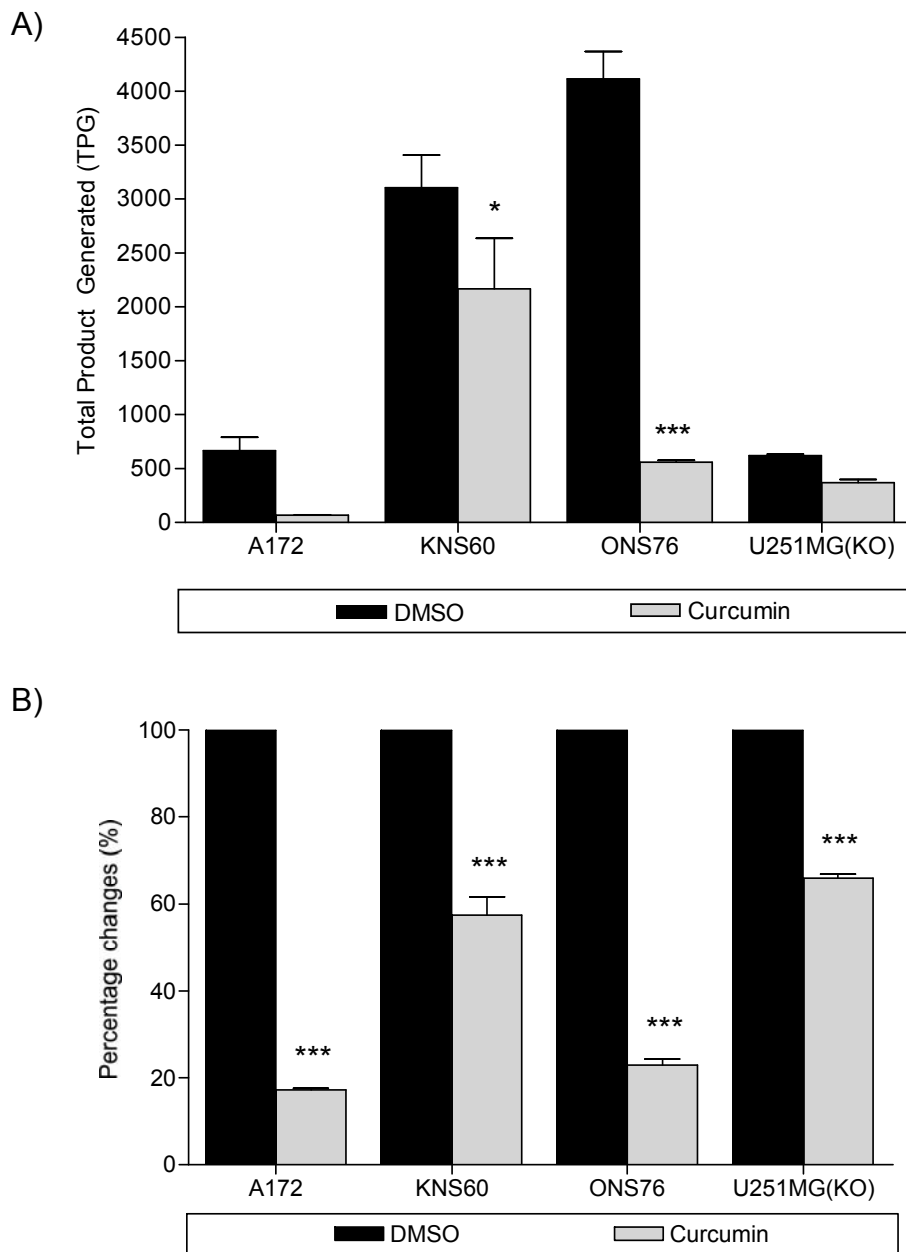
Figure 3.61. Telomerase activity of curcumin-treated cells as detected by the Telomeric Repeat Amplification Protocol (TRAP) assay. A) Decrease in telomerase activity is represented by a reduction in the Total Product Generated (TPG). B) Representation of telomerase activity in percentage changes compared to telomerase positive control of the experiment. * indicates $p < 0.05$, ** indicates $p < 0.01$, *** indicates $p < 0.001$.
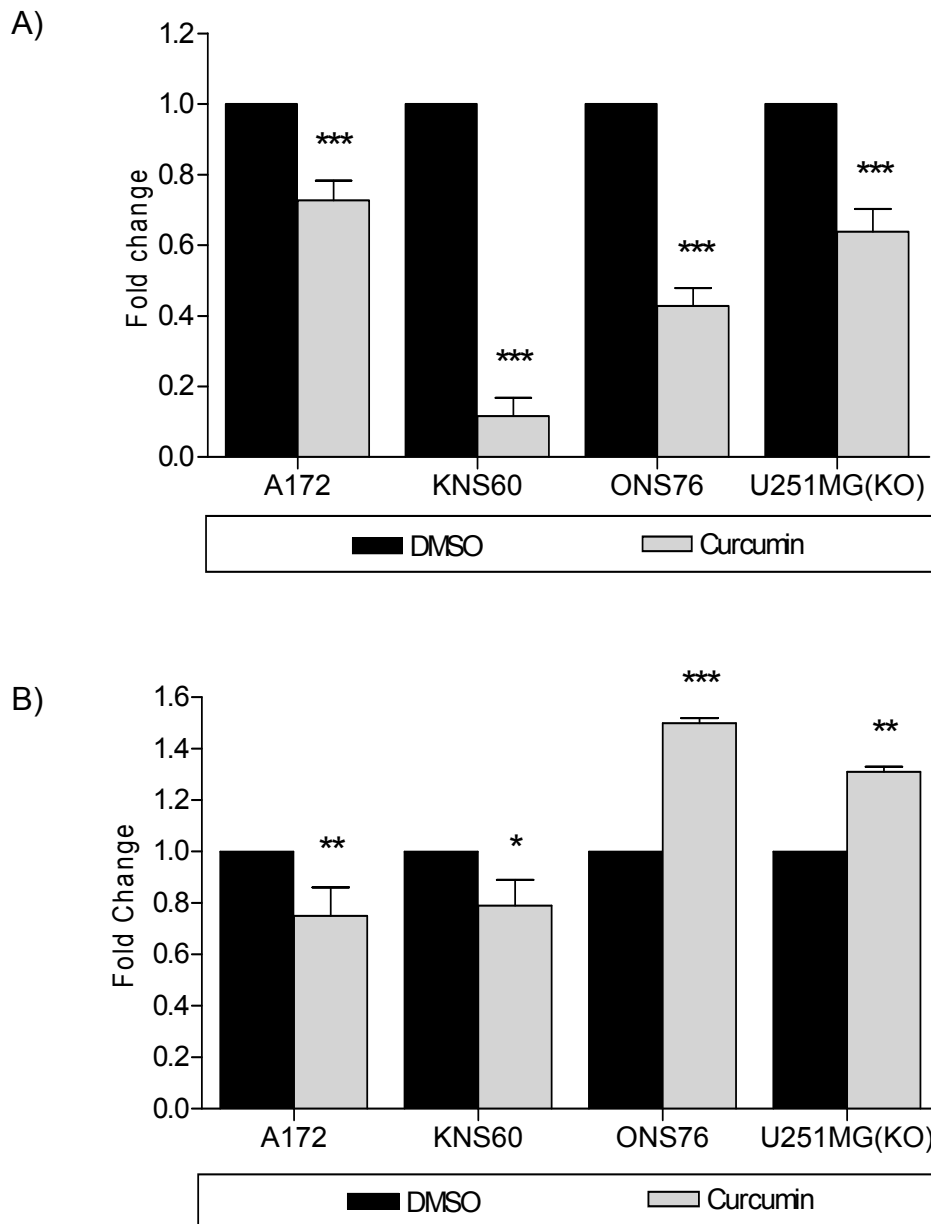
Figure 3.62. Real-time RT-PCR results of *hTERT* and *hTR* mRNA expression of curcumin-treated cell lines. A) Fold change of *hTERT* mRNA expression as compared to DMSO controls. B) Fold change of *hTR* mRNA expression as compared to DMSO controls. * indicates p < 0.05, ** indicates p < 0.01, *** indicates p < 0.001.

A)
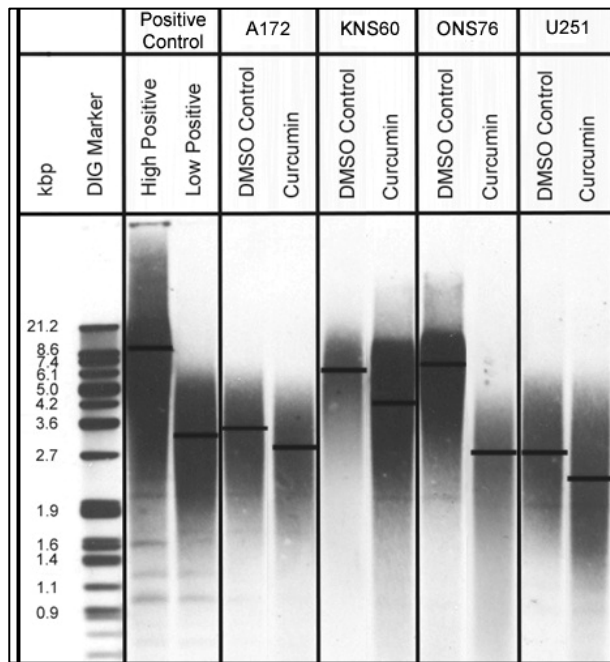
B)
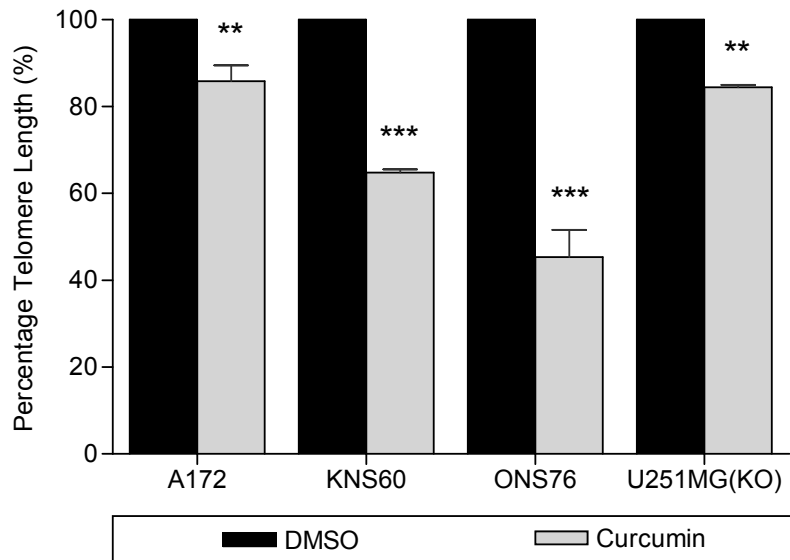
Figure 3.63. Analysis of telomere length of curcumin-treated cells using Terminal Restriction Fragment (TRF) assay. A) Telomeric probes were used to detect telomeric regions via southern blot. Black lines indicate the mean telomere length. B) Graphical representation of percentage changes in telomere length from southern blot data. ** indicates $p < 0.01$, *** indicates $p < 0.001$.

3.3.4.7. Discussion

The growth inhibitory effects of curcumin are multifactorial and telomerase inhibition may merely be one of the ways it affects tumour cell growth (Ramachandran *et al.,* 2002). Various aspects of cellular and molecular responses upon curcumin treatment have been investigated in this study; Curcumin was found to induce cell cycle arrest (Figure 3.50) and cell death (Figure 3.47) associated with DNA damage induction (Figure 3.54) in all brain cancer cell lines. Similar findings have reported the cytotoxic effects of curcumin in different cancer cells such as pancreatic cancer, ovarian cancer and lung carcinoma (Zheng *et al.,* 2006; Lin *et al.,* 2008; Sahu *et al.,* 2009). Interestingly, our data shows that telomerase negative human lung fibroblast exhibited higher IC_{50} and no cell cycle arrest, suggesting that non-cancerous cells may have better tolerance to the cytotoxic effects of curcumin.

Data from annexin V staining (Figure 3.53) and the Capase-3/7 activity assay (Figure 3.52) supported the notion of apoptotic cell death triggered by curcumin. In addition, most cell lines exhibited decreased expression of Bcl2, Survivin and increased expression of Bax following treatment with curcumin (Figure 3.58). In line with this, previous studies have associated curcumin-related cell death events with the inhibition of NFκB (Zheng *et al.,* 2004; Samuhasaneeto *et al.,* 2009), activation of death receptors (Bush *et al.,* 2001; Lu *et al.,* 2009), induction of ROS (Su *et al.,* 2006; Thayyullathil *et al.,* 2008) and induction of mitochondrial hyperpolarisation (Cao *et al.,* 2006; Cao *et al.,* 2007).

Gene expression analysis in this study showed that curcumin downregulates *CCNE1*, *CDK2*, *E2F1* and upregulates *PTEN* genes (Figure

3.55), suggesting that cancer cells treated with curcumin may undergo cell cycle arrest and cease proliferation. Meanwhile, western blotting showed that curcumin treatment resulted in increased expression of p21 and Cyclin B1 proteins in radiosensitive cells, indicating cell cycle arrest, whereas radioresistant cells projected an opposite trend where p53 was downregulated and Cyclin B1 was upregulated, suggesting resistance to cell cycle arrest (Figure 3.56). To date, there is no study reporting the differential responses of cell lines with different radioresponses following curcumin treatment, leading this study to be the first report to compare the molecular responses of radiosensitive and radioresistant cells with the same drug treatment.

While the telomerase inhibition effects of curcumin have only been reported on a few cancer cell types such as breast cancer (Ramachandran *et al.*, 2002), leukaemia (Chakraborty *et al.,* 2006; Mukherjee Nee *et al.,* 2007) and pancreatic cancer (Teng and Fahey, III, 2002), no such study has yet been carried out on brain cancer cells. In this study, curcumin has proved to be promising in the suppression of telomerase activity in brain cancer cells (Figure 3.59). This inhibition of telomerase activity was associated with the reduction of *hTERT* expression (Figure 3.60). Previous studies have reported the association of decreased telomerase activity with *hTERT* downregulation (Ramachandran *et al.,* 2002; Cui *et al.,* 2006; Mukherjee Nee *et al.,* 2007) and suppression of the translocation of hTERT to the nucleus (Chakraborty *et al.*, 2006) in a *hTR-* or *c-Myc*-independent manner (Ramachandran *et al.*, 2002). In support, this study has shown that long-term curcumin treatment on brain cancer cell lines resulted in significant telomere shortening (Figure 3.61),

suggesting that curcumin has great potential to be used as a telomerase inhibitor clinically.

This study hypothesizes that curcumin may selectively target cells that express telomerase enzyme; by inhibiting the telomerase enzyme, cells may become more sensitive to the cytotoxic effects of curcumin. Although many studies have sought to investigate the mechanisms of curcumin, more work must be done in order to understand the correlation between its effects on cell death, growth inhibition and telomerase inhibition. A schematic diagram representing the cellular events upon curcumin treatment is shown in Figure 3.64.
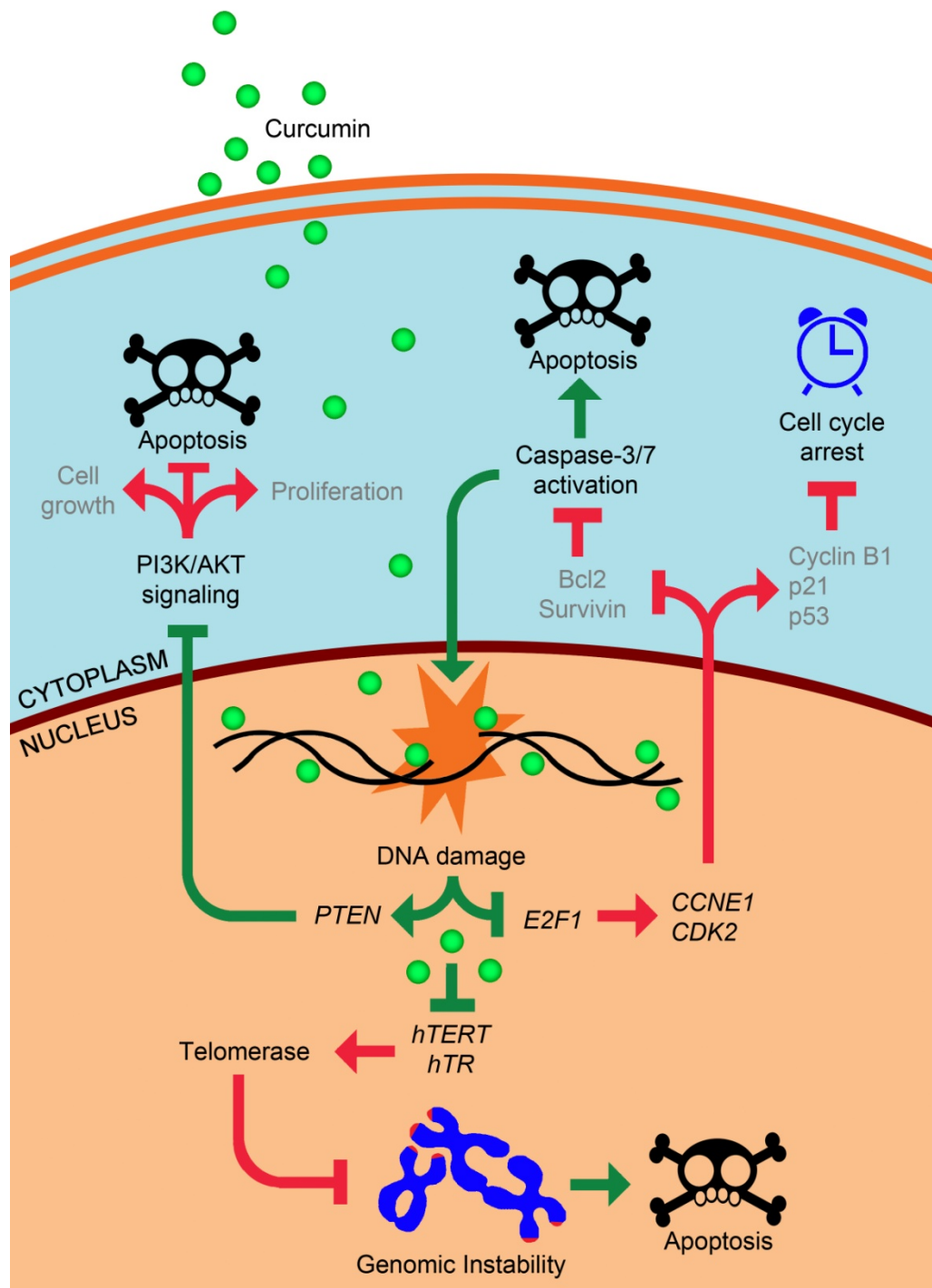
Figure 3.64. Schematic representation of cellular events triggered upon curcumin treatment in brain cancer cell lines. Treatment with curcumin has shown downregulation of *E2F1*, *CCNE1* and *CDK2* genes together with overexpression of *PTEN* rendering the cells towards growth inhibition and apoptosis. Suppression of telomerase activity through the downregulation of *hTERT* and *hTR* expressions has resulted in telomere shortening. Green arrows represent possible events whereas red arrows indicate inhibited pathways.

Chapter 4   CONCLUSIONS AND FUTURE DIRECTIONS

4.1   Reviews and justifications of the objectives in this study.

The objectives of this study are reviewed and justified in this section. The strengths and shortcomings of this study as well as future directions are proposed in each objective.

4.1.1 Objective 1: To determine the basal characteristics of the glioblastoma and medulloblastoma cell lines used in this study.

The basal characteristics of brain cancer cells were investigated in the first section. Several cytogenetic markers and common aberrations were identified from the integrated analysis of mFISH, microarray and array-CGH experiments. However, these genomic signatures may only have the potential to serve as additional validation of histological observation in determining brain cancer types. These markers are not suitable to be used solely for the prediction of brain cancer due to two main reasons. Firstly, the markers identified here were generated from a small sample size. To accurately identify promising markers, a larger sample set of the same brain cancer types, different cancer grades and different cancer types should be compared and analysed. Secondly, the cytogenetic markers and common aberration profiles developed from the *in vitro* cell culture may not fully represent the *in vivo* condition in brain cancer tissue; cell lines maintained in culture over a period of time may accumulate further mutations overtime.

4.1.2 Objective 2: To investigate the growth inhibitory mechanisms of plant products on glioblastoma and medulloblastoma cell lines.

This study has successfully analysed various aspects of cellular responses triggered upon phytochemicals treatment including that of cell viability, cell cycle, cell death, clonogenicity, DNA damage and caspase activity. Plumbagin and curcumin displayed similar effects on growth inhibition wherein cell cycle arrest was associated with DNA damage. Cells that acquire severe DNA damage often initiate caspase-3/7 activation and apoptotic cell death whereas cells that can better sustain damage usually undergo cell cycle arrest rather than cell death.

The growth rate of cells may be an important factor that decides tumour growth; fast growing cells can compensate for cell loss by having faster cell division even if there is significant cell death, while slow growing cells hardly tip the balance of live cells over dead cells. As an example, both radiosensitive cells (A172 and ONS76) are susceptible to curcumin treatment as indicated by the comet assay (DNA damage) and annexin V staining (Cell death). However, the ONS76 cell line, which has higher population doubling rate, compensated the loss of cells during treatment. On the other hand, A172 cells with its slower doubling rate was unable to regain the equilibrium and thus exhibited greater cell death upon treatment.

For genistein treatment, all cells underwent cell cycle arrest without showing significant cell death and DNA damage. This brings about the possibility of using genistein in combination with either plumbagin or curcumin for cancer treatment. Pre-treatment with genistein can inhibit the proliferation of cancer cells and treatment with a secondary cytotoxic drug such as plumbagin, curcumin or other known cytotoxic drugs with a lower IC_{50} concentration can boost apoptosis synergistically in arrested or sensitized

cells. Recent studies have also reported the use of genistein in combinatorial approaches to treat cancers (Zhao *et al.,* 2009; Mohan *et al.,* 2009; Karmakar *et al.,* 2009; Shiau *et al.,* 2009; Harper *et al.,* 2009).

4.1.3 Objective 3: To study the inhibitory potential of plant products on telomerase activity and on telomere length in glioblastoma and medulloblastoma cell lines.

In this study, it is of particular importance, to show that the phytochemicals can be used as effective anticancer drugs through the inhibition of telomerase activity and shortening of telomere length.

For the first time, this study has demonstrated the telomerase inhibitory effects of plumbagin in brain tumour cells which eventually led to the decrease of telomere length following long-term treatment. For genistein and curcumin, even though they have been reported to inhibit telomerase function (Ramachandran *et al.*, 2002; Ouchi *et al.*, 2005; Jagadeesh *et al.*, 2006; Cui *et al.*, 2006; Li *et al.*, 2009), not many studies have tested their potential effects telomere status after long term treatment. In this study, investigation on telomere length has been successfully carried out to validate the significance and outcome of telomerase inhibition.

It is known that telomere shortening occurs only in dividing cells, while arrested cells would not exhibit any decrease in telomere length (Holt *et al.*, 1996). As genistein exerts its cytostatic effect by inhibiting cell proliferation, any decrease in telomere length was not expected in this study. However, the TRAP and TRF assays showed that genistein suppressed telomerase activity resulting in shortening of telomere length. This suggests that the additional

telomerase inhibition property exerted by genistein has strengthened its effect by affecting cancer cells that have escaped from cell cycle arrest.

In agreement with a previous study by Ramachandran *et al.* (2002), the present investigation showed that curcumin may selectively target telomerase positive cells and spare telomerase negative cells as suggested in crystal violet assay. However, more work needs to be done to relate the cytotoxic effect of curcumin to the telomerase activity of more cell lines in order to investigate whether its cytotoxic effects are telomerase-dependent.

In summary, the findings reported in this thesis suggest that the phytochemicals may have a great potential to be used as effective anticancer drugs. Nevertheless, more work need to be carried out to establish an effective drug combination so that a lower IC_{50} of each drug can be used to minimize non-specific killing of neighbouring healthy normal cells.

4.2   Conclusion

As mentioned in the introduction chapter, the intention of this study is to explore alternative options such as natural plant products that may enhance the efficiency of cancer treatment or to compliment the current therapy to improve the quality of life of cancer patients. Regular consumption or incorporation of natural plant products into the daily diet can then be recommended to healthy individuals as a chemopreventive measure as well.

Reference List

Ahmad,A., Banerjee,S., Wang,Z., Kong,D., and Sarkar,F.H. (2008). Plumbagin-induced apoptosis of human breast cancer cells is mediated by inactivation of NF-kappaB and Bcl-2. J. Cell Biochem. *105*, 1461-1471.

Alhasan,S.A., Aranha,O., and Sarkar,F.H. (2001). Genistein elicits pleiotropic molecular effects on head and neck cancer cells. Clin. Cancer Res. *7*, 4174-4181.

Artandi,S.E. and Attardi,L.D. (2005). Pathways connecting telomeres and p53 in senescence, apoptosis, and cancer. Biochem. Biophys. Res. Commun. *331*, 881-890.

Aziz,M.H., Dreckschmidt,N.E., and Verma,A.K. (2008). Plumbagin, a medicinal plant-derived naphthoquinone, is a novel inhibitor of the growth and invasion of hormone-refractory prostate cancer. Cancer Res. *68*, 9024-9032.

Barnes, P. M, Bloom, B, and Nahin, R. Complementary and Alternative Medicine Use Among Adults and Children: United States, 2007. 12, 1-24. 12-10-2008. National Health Statistics Report. Ref Type: Report

Black,P. (2006). Living with a Brain Tumor: Dr. Peter Black's Guide to Taking Control of Your Treatment. Holt Paperback.

Blackburn,E.H. (1991). Structure and function of telomeres. Nature *350*, 569-573.

Bouker,K.B. and Hilakivi-Clarke,L. (2000). Genistein: does it prevent or promote breast cancer? Environ. Health Perspect. *108*, 701-708.

Bower,J.E., Woolery,A., Sternlieb,B., and Garet,D. (2005). Yoga for cancer patients and survivors. Cancer Control *12*, 165-171.

Boyer,J. and Liu,R.H. (2004). Apple phytochemicals and their health benefits. Nutr. J. *3*, 5.

Bryan,T.M. and Cech,T.R. (1999). Telomerase and the maintenance of chromosome ends. Curr. Opin. Cell Biol. *11*, 318-324.

Bryan,T.M., Englezou,A., Gupta,J., Bacchetti,S., and Reddel,R.R. (1995). Telomere elongation in immortal human cells without detectable telomerase activity. EMBO J. *14*, 4240-4248.

Bryan,T.M., Marusic,L., Bacchetti,S., Namba,M., and Reddel,R.R. (1997). The telomere lengthening mechanism in telomerase-negative immortal human cells does not involve the telomerase RNA subunit. Hum. Mol. Genet. *6*, 921-926.

Bush,J.A., Cheung,K.J., Jr., and Li,G. (2001). Curcumin induces apoptosis in human melanoma cells through a Fas receptor/caspase-8 pathway independent of p53. Exp. Cell Res. *271*, 305-314.

Cao,J., Jia,L., Zhou,H.M., Liu,Y., and Zhong,L.F. (2006). Mitochondrial and nuclear DNA damage induced by curcumin in human hepatoma G2 cells. Toxicol. Sci. *91*, 476-483.

Cao,J., Liu,Y., Jia,L., Zhou,H.M., Kong,Y., Yang,G., Jiang,L.P., Li,Q.J., and Zhong,L.F. (2007). Curcumin induces apoptosis through mitochondrial hyperpolarization and mtDNA damage in human hepatoma G2 cells. Free Radic. Biol. Med. *43*, 968-975.

Casagrande,F. and Darbon,J.M. (2000). p21CIP1 is dispensable for the G2 arrest caused by genistein in human melanoma cells. Exp. Cell Res. *258*, 101-108.

Chakraborty,S., Ghosh,U., Bhattacharyya,N.P., Bhattacharya,R.K., and Roy,M. (2006). Inhibition of telomerase activity and induction of apoptosis by curcumin in K-562 cells. Mutat. Res. *596*, 81-90.

Chen,H., Li,Y., and Tollefsbol,T.O. (2009). Strategies targeting telomerase inhibition. Mol. Biotechnol. *41*, 194-199.

Chen,J.W., Sun,C.M., Sheng,W.L., Wang,Y.C., and Syu,W.J. (2006). Expression Analysis of Up-Regulated Genes Responding to Plumbagin in Escherichia coli. J. Bacteriol. *188*, 456-463.

Chen,K. and Yeung,R. (2002). Exploratory studies of Qigong therapy for cancer in China. Integr. Cancer Ther. *1*, 345-370.

Chen,W.F., Huang,M.H., Tzang,C.H., Yang,M., and Wong,M.S. (2003). Inhibitory actions of genistein in human breast cancer (MCF-7) cells. Biochim. Biophys. Acta *1638*, 187-196.

Chinni,S.R., Alhasan,S.A., Multani,A.S., Pathak,S., and Sarkar,F.H. (2003). Pleotropic effects of genistein on MCF-7 breast cancer cells. Int. J. Mol. Med. *12*, 29-34.

Choi,Y.H., Lee,W.H., Park,K.Y., and Zhang,L. (2000). p53-independent induction of p21 (WAF1/CIP1), reduction of cyclin B1 and G2/M arrest by the isoflavone genistein in human prostate carcinoma cells. Jpn. J. Cancer Res. *91*, 164-173.

Cui,S.X., Qu,X.J., Xie,Y.Y., Zhou,L., Nakata,M., Makuuchi,M., and Tang,W. (2006). Curcumin inhibits telomerase activity in human cancer cell lines. Int. J. Mol. Med. *18*, 227-231.

Cunningham,A.P., Love,W.K., Zhang,R.W., Andrews,L.G., and Tollefsbol,T.O. (2006). Telomerase inhibition in cancer therapeutics: molecular-based approaches. Curr. Med. Chem. *13*, 2875-2888.

Darbon,J.M., Penary,M., Escalas,N., Casagrande,F., Goubin-Gramatica,F., Baudouin,C., and Ducommun,B. (2000). Distinct Chk2 activation pathways are triggered by genistein and DNA-damaging agents in human melanoma cells. J. Biol. Chem. *275*, 15363-15369.

de Lange,T. (2002). Protection of mammalian telomeres. Oncogene *21*, 532-540.

de Paiva,Sr., Figueiredo,M.R., Aragao,T.V., and Kaplan,M.A. (2003). Antimicrobial activity in vitro of plumbagin isolated from Plumbago species. Mem. Inst. Oswaldo Cruz *98*, 959-961.

Deeb,D.D., Jiang,H., Gao,X., Divine,G., Dulchavsky,S.A., and Gautam,S.C. (2005). Chemosensitization of hormone-refractory prostate cancer cells by curcumin to TRAIL-induced apoptosis. J. Exp. Ther. Oncol. *5*, 81-91.

Demma,J., Hallberg,K., and Hellman,B. (2009). Genotoxicity of plumbagin and its effects on catechol and NQNO-induced DNA damage in mouse lymphoma cells. Toxicol. In Vitro *23*, 266-271.

Dhawan,V. and Jain,S. (2005). Garlic supplementation prevents oxidative DNA damage in essential hypertension. Mol. Cell Biochem. *275*, 85-94.

Dhillon,N., Aggarwal,B.B., Newman,R.A., Wolff,R.A., Kunnumakkara,A.B., Abbruzzese,J.L., Ng,C.S., Badmaev,V., and Kurzrock,R. (2008). Phase II trial of curcumin in patients with advanced pancreatic cancer. Clin. Cancer Res. *14*, 4491-4499.

DiStasio,S.A. (2008). Integrating yoga into cancer care. Clin. J. Oncol. Nurs. *12*, 125-130.

Divisi,D., Di,T.S., Salvemini,S., Garramone,M., and Crisci,R. (2006). Diet and cancer. Acta Biomed. *77*, 118-123.

Durga,R., Sridhar,P., and Polasa,H. (1990). Effects of plumbagin on antibiotic resistance in bacteria. Indian J. Med. Res. *91*, 18-20.

Duthie,S.J., Jenkinson,A.M., Crozier,A., Mullen,W., Pirie,L., Kyle,J., Yap,L.S., Christen,P., and Duthie,G.G. (2006). The effects of cranberry juice consumption on antioxidant status and biomarkers relating to heart disease and cancer in healthy human volunteers. Eur. J. Nutr. *45*, 113-122.

Dyson,N., Howley,P.M., Munger,K., and Harlow,E. (1989). The human papilloma virus-16 E7 oncoprotein is able to bind to the retinoblastoma gene product. Science *243*, 934-937.

Faqi,A.S., Johnson,W.D., Morrissey,R.L., and McCormick,D.L. (2004). Reproductive toxicity assessment of chronic dietary exposure to soy isoflavones in male rats. Reprod. Toxicol. *18*, 605-611.

Farina,H.G., Pomies,M., Alonso,D.F., and Gomez,D.E. (2006). Antitumor and antiangiogenic activity of soy isoflavone genistein in mouse models of melanoma and breast cancer. Oncol. Rep. *16*, 885-891.

Feng,J., Funk,W.D., Wang,S.S., Weinrich,S.L., Avilion,A.A., Chiu,C.P., Adams,R.R., Chang,E., Allsopp,R.C., Yu,J. (1995). The RNA component of human telomerase. Science *269*, 1236-1241.

Gao,X., Deeb,D., Jiang,H., Liu,Y.B., Dulchavsky,S.A., and Gautam,S.C. (2005). Curcumin differentially sensitizes malignant glioma cells to TRAIL/Apo2L-mediated apoptosis through activation of procaspases and release of cytochrome c from mitochondria. J. Exp. Ther. Oncol. *5*, 39-48.

Gomathinayagam,R., Sowmyalakshmi,S., Mardhatillah,F., Kumar,R., Akbarsha,M.A., and Damodaran,C. (2008). Anticancer mechanism of plumbagin, a natural compound, on non-small cell lung cancer cells. Anticancer Res. *28*, 785-792.

Greider,C.W. (1990). Telomeres, telomerase and senescence. Bioessays *12*, 363-369.

Greider,C.W. (1991). Telomeres. Curr. Opin. Cell Biol. *3*, 444-451.

Greider,C.W. and Blackburn,E.H. (1985). Identification of a specific telomere terminal transferase activity in Tetrahymena extracts. Cell *43*, 405-413.

Greider,C.W. and Blackburn,E.H. (1987). The telomere terminal transferase of Tetrahymena is a ribonucleoprotein enzyme with two kinds of primer specificity. Cell *51*, 887-898.

Greider,C.W. and Blackburn,E.H. (1989). A telomeric sequence in the RNA of Tetrahymena telomerase required for telomere repeat synthesis. Nature *337*, 331-337.

Griffith,J.D., Comeau,L., Rosenfield,S., Stansel,R.M., Bianchi,A., Moss,H., and de,L.T. (1999). Mammalian telomeres end in a large duplex loop. Cell *97*, 503-514.

Hanahan,D. and Weinberg,R.A. (2000). The hallmarks of cancer. Cell *100*, 57-70.

Hande,M.P., Azizova,T.V., Burak,L.E., Khokhryakov,V.F., Geard,C.R., and Brenner,D.J. (2005). Complex chromosome aberrations persist in individuals many years after occupational exposure to densely ionizing radiation: an mFISH study. Genes Chromosomes. Cancer *44*, 1-9.

Harle-Bachor,C. and Boukamp,P. (1996). Telomerase activity in the regenerative basal layer of the epidermis inhuman skin and in immortal and carcinoma-derived skin keratinocytes. Proc. Natl. Acad. Sci. U. S. A *93*, 6476-6481.

Harley,C.B., Futcher,A.B., and Greider,C.W. (1990). Telomeres shorten during ageing of human fibroblasts. Nature *345*, 458-460.

Harper,C.E., Cook,L.M., Patel,B.B., Wang,J., Eltoum,I.A., Arabshahi,A., Shirai,T., and Lamartiniere,C.A. (2009). Genistein and resveratrol, alone and in combination, suppress prostate cancer in SV-40 tag rats. Prostate. *69*, 1668-1682.

Hastie,N.D., Dempster,M., Dunlop,M.G., Thompson,A.M., Green,D.K., and Allshire,R.C. (1990). Telomere reduction in human colorectal carcinoma and with ageing. Nature *346*, 866-868.

Herbert,B.S., Wright,W.E., and Shay,J.W. (2001). Telomerase and breast cancer. Breast Cancer Res. *3*, 146-149.

Hiyama,K., Hirai,Y., Kyoizumi,S., Akiyama,M., Hiyama,E., Piatyszek,M.A., Shay,J.W., Ishioka,S., and Yamakido,M. (1995). Activation of telomerase in human lymphocytes and hematopoietic progenitor cells. J. Immunol. *155*, 3711-3715.

Holt,S.E., Shay,J.W., and Wright,W.E. (1996). Refining the telomere-telomerase hypothesis of aging and cancer. Nat. Biotechnol. *14*, 836-839.

Hsu,Y.L., Cho,C.Y., Kuo,P.L., Huang,Y.T., and Lin,C.C. (2006). Plumbagin (5-hydroxy-2-methyl-1,4-naphthoquinone) induces apoptosis and cell cycle arrest in A549 cells through p53 accumulation via c-Jun NH2-terminal kinase-mediated phosphorylation at serine 15 in vitro and in vivo. J. Pharmacol. Exp. Ther. *318*, 484-494.

Hu,Y., McDermott,M.P., and Ahrendt,S.A. (2005). The p53 codon 72 proline allele is associated with p53 gene mutations in non-small cell lung cancer. Clin. Cancer Res. *11*, 2502-2509.

Ishikawa,K., Koyama-Saegusa,K., Otsuka,Y., Ishikawa,A., Kawai,S., Yasuda,K., Suga,T., Michikawa,Y., Suzuki,M., Iwakawa,M., and Imai,T. (2006). Gene expression profile changes correlating with radioresistance in human cell lines. Int. J. Radiat. Oncol. Biol. Phys. *65*, 234-245.

Jagadeesh,S., Kyo,S., and Banerjee,P.P. (2006). Genistein represses telomerase activity via both transcriptional and posttranslational mechanisms in human prostate cancer cells. Cancer Res. *66*, 2107-2115.

Jefferson,W.N., Padilla-Banks,E., and Newbold,R.R. (2007). Disruption of the developing female reproductive system by phytoestrogens: genistein as an example. Mol. Nutr. Food Res. *51*, 832-844.

Jemal,A., Murray,T., Ward,E., Samuels,A., Tiwari,R.C., Ghafoor,A., Feuer,E.J., and Thun,M.J. (2005). Cancer statistics, 2005. CA Cancer J. Clin. *55*, 10-30.

Jian,L. (2008). Soy, isoflavones, and prostate cancer. Mol. Nutr. Food Res.

Jin,C.Y., Park,C., Kim,G.Y., Lee,S.J., Kim,W.J., and Choi,Y.H. (2009). Genistein enhances TRAIL-induced apoptosis through inhibition of p38 MAPK signaling in human hepatocellular carcinoma Hep3B cells. Chem. Biol. Interact. *180*, 143-150.

Jung,E.M., Lim,J.H., Lee,T.J., Park,J.W., Choi,K.S., and Kwon,T.K. (2005). Curcumin sensitizes tumor necrosis factor-related apoptosis-inducing ligand (TRAIL)-induced apoptosis through reactive oxygen species-mediated upregulation of death receptor 5 (DR5). Carcinogenesis *26*, 1905-1913.

Jung,E.M., Park,J.W., Choi,K.S., Park,J.W., Lee,H.I., Lee,K.S., and Kwon,T.K. (2006). Curcumin sensitizes tumor necrosis factor-related apoptosis-inducing ligand (TRAIL)-mediated apoptosis through CHOP-independent DR5 upregulation. Carcinogenesis *27*, 2008-2017.

Karmakar,S., Choudhury,S.R., Banik,N.L., and Ray,S.K. (2009). Combination of N-(4-hydroxyphenyl) retinamide and genistein increased apoptosis in neuroblastoma SK-N-BE2 and SH-SY5Y xenografts. Neuroscience *163*, 286-295.

Kawiak,A., Piosik,J., Stasilojc,G., Gwizdek-Wisniewska,A., Marczak,L., Stobiecki,M., Bigda,J., and Lojkowska,E. (2007). Induction of apoptosis by plumbagin through reactive oxygen species-mediated inhibition of topoisomerase II. Toxicol. Appl. Pharmacol. *223*, 267-276.

Keith,W.N., Bilsland,A., Hardie,M., and Evans,T.R. (2004). Drug insight: Cancer cell immortality-telomerase as a target for novel cancer gene therapies. Nat. Clin. Pract. Oncol. *1*, 88-96.

Kim,E.J., Shin,H.K., and Park,J.H. (2005). Genistein inhibits insulin-like growth factor-I receptor signaling in HT-29 human colon cancer cells: a possible mechanism of the growth inhibitory effect of Genistein. J. Med. Food *8*, 431-438.

Kim,N.W., Piatyszek,M.A., Prowse,K.R., Harley,C.B., West,M.D., Ho,P.L., Coviello,G.M., Wright,W.E., Weinrich,S.L., and Shay,J.W. (1994). Specific association of human telomerase activity with immortal cells and cancer. Science *266*, 2011-2015.

Kimura,M., Cao,X., Skurnick,J., Cody,M., Soteropoulos,P., and Aviv,A. (2005). Proliferation dynamics in cultured skin fibroblasts from Down syndrome subjects. Free Radic. Biol. Med. *39*, 374-380.

Kroll,R.A. and Neuwelt,E.A. (1998). Outwitting the blood-brain barrier for therapeutic purposes: osmotic opening and other means. Neurosurgery *42*, 1083-1099.

Kuo,P.L., Hsu,Y.L., and Cho,C.Y. (2006). Plumbagin induces G2-M arrest and autophagy by inhibiting the AKT/mammalian target of rapamycin pathway in breast cancer cells. Mol. Cancer Ther. *5*, 3209-3221.

Kurd,S.K., Smith,N., VanVoorhees,A., Troxel,A.B., Badmaev,V., Seykora,J.T., and Gelfand,J.M. (2008). Oral curcumin in the treatment of moderate to severe psoriasis vulgaris: A prospective clinical trial. J. Am. Acad. Dermatol. *58*, 625-631.

Lamartiniere,C.A. (2000). Protection against breast cancer with genistein: a component of soy. Am. J. Clin. Nutr. *71*, 1705S-1707S.

Lansdorp,P.M. (2000). Repair of telomeric DNA prior to replicative senescence. Mech. Ageing Dev. *118*, 23-34.

Lanzilli,G., Fuggetta,M.P., Tricarico,M., Cottarelli,A., Serafino,A., Falchetti,R., Ravagnan,G., Turriziani,M., Adamo,R., Franzese,O., and Bonmassar,E. (2006). Resveratrol down-regulates the growth and telomerase activity of breast cancer cells in vitro. Int. J. Oncol. *28*, 641-648.

Lee,H., Schmidt,K., and Ernst,E. (2005). Acupuncture for the relief of cancer-related pain--a systematic review. Eur. J. Pain *9*, 437-444.

Lee,M.S., Chen,K.W., Sancier,K.M., and Ernst,E. (2007). Qigong for cancer treatment: a systematic review of controlled clinical trials. Acta Oncol. *46*, 717-722.

Levy,M.Z., Allsopp,R.C., Futcher,A.B., Greider,C.W., and Harley,C.B. (1992). Telomere end-replication problem and cell aging. J. Mol. Biol. *225*, 951-960.

Li,Y., Liu,L., Andrews,L.G., and Tollefsbol,T.O. (2009). Genistein depletes telomerase activity through cross-talk between genetic and epigenetic mechanisms. Int. J. Cancer *125*, 286-296.

Li,Z., Li,J., Mo,B., Hu,C., Liu,H., Qi,H., Wang,X., and Xu,J. (2008). Genistein induces G2/M cell cycle arrest via stable activation of ERK1/2 pathway in MDA-MB-231 breast cancer cells. Cell Biol. Toxicol. *24*, 401-409.

Lin,S.S., Huang,H.P., Yang,J.S., Wu,J.Y., Hsia,T.C., Lin,C.C., Lin,C.W., Kuo,C.L., Gibson,W.W., and Chung,J.G. (2008). DNA damage and endoplasmic reticulum stress mediated curcumin-induced cell cycle arrest and apoptosis in human lung carcinoma A-549 cells through the activation caspases cascade- and mitochondrial-dependent pathway. Cancer Lett. *272*, 77-90.

Liu,R.H. (2004). Potential synergy of phytochemicals in cancer prevention: mechanism of action. J. Nutr. *134*, 3479S-3485S.

Lu,H.F., Lai,K.C., Hsu,S.C., Lin,H.J., Yang,M.D., Chen,Y.L., Fan,M.J., Yang,J.S., Cheng,P.Y., Kuo,C.L., and Chung,J.G. (2009). Curcumin induces apoptosis through FAS and FADD, in caspase-3-dependent and -independent pathways in the N18 mouse-rat hybrid retina ganglion cells. Oncol. Rep. *22*, 97-104.

Lu,Q., Tan,Y.H., and Luo,R. (2007). Molecular dynamics simulations of p53 DNA-binding domain. J. Phys. Chem. B *111*, 11538-11545.

Lu,W., an-Clower,E., Doherty-Gilman,A., and Rosenthal,D.S. (2008). The value of acupuncture in cancer care. Hematol. Oncol. Clin. North Am. *22*, 631-48, viii.

Luo,H., Jiang,B.H., King,S.M., and Chen,Y.C. (2008). Inhibition of cell growth and VEGF expression in ovarian cancer cells by flavonoids. Nutr. Cancer *60*, 800-809.

Ma,B., Pan,Y., Gunasekaran,K., Venkataraghavan,R.B., Levine,A.J., and Nussinov,R. (2005). Comparison of the protein-protein interfaces in the p53-DNA crystal structures: towards elucidation of the biological interface. Proc. Natl. Acad. Sci. U. S. A *102*, 3988-3993.

Majid,S., Kikuno,N., Nelles,J., Noonan,E., Tanaka,Y., Kawamoto,K., Hirata,H., Li,L.C., Zhao,H., Okino,S.T., Place,R.F., Pookot,D., and Dahiya,R. (2008). Genistein induces the p21WAF1/CIP1 and p16INK4a tumor suppressor genes in prostate cancer cells by epigenetic mechanisms involving active chromatin modification. Cancer Res. *68*, 2736-2744.

McClintock,B. (1941). The Stability of Broken Ends of Chromosomes in Zea Mays. Genetics *26*, 234-282.

McClintock,B. (1938). The Production of Homozygous Deficient Tissues with Mutant Characteristics by Means of the Aberrant Mitotic Behavior of Ring-Shaped Chromosomes. Genetics *23*, 315-376.

Mitchell, J and Rook, A. Droseraceae. Richard J.Schmidt. Botanical Dermatology Database (http://bodd.cf.ac.uk/BotDermFolder/DROS.html) . 1984.
Ref Type: Electronic Citation

Mitchell, J and Rook, A. Plumbaginaceae. Richard J.Schmidt. Botanical Dermatology Database (http://bodd.cf.ac.uk/BotDermFolder/PLUM.html) . 2004.
Ref Type: Electronic Citation

Mitchell,J.R., Wood,E., and Collins,K. (1999). A telomerase component is defective in the human disease dyskeratosis congenita. Nature *402*, 551-555.

Mohan,N., Karmakar,S., Choudhury,S.R., Banik,N.L., and Ray,S.K. (2009). Bcl-2 inhibitor HA14-1 and genistein together adeptly down regulated survival factors and activated cysteine proteases for apoptosis in human malignant neuroblastoma SK-N-BE2 and SH-SY5Y cells. Brain Res. *1283*, 155-166.

Mukherjee Nee,C.S., Ghosh,U., Bhattacharyya,N.P., Bhattacharya,R.K., Dey,S., and Roy,M. (2007). Curcumin-induced apoptosis in human leukemia cell HL-60 is associated with inhibition of telomerase activity. Mol. Cell Biochem. *297*, 31-39.

Mukherjee,P.K., Kumar,V., Mal,M., and Houghton,P.J. (2007). Acetylcholinesterase inhibitors from plants. Phytomedicine. *14*, 289-300.

Müller,H. (1938). The remaking of chromosomes. Collecting Net *13*, 181-198.

Munday,R. and Munday,C.M. (2000). Induction of quinone reductase and glutathione transferase in rat tissues by juglone and plumbagin. Planta Med. *66*, 399-402.

Munshi,A., Ni,L.H., and Tiwana,M.S. (2008). Complementary and alternative medicine in present day oncology care: promises and pitfalls. Jpn. J. Clin. Oncol. *38*, 512-520.

Nair,S., Nair,R.R., Srinivas,P., Srinivas,G., and Pillai,M.R. (2008). Radiosensitizing effects of plumbagin in cervical cancer cells is through modulation of apoptotic pathway. Mol. Carcinog. *47*, 22-33.

Nakamura,T.M., Morin,G.B., Chapman,K.B., Weinrich,S.L., Andrews,W.H., Lingner,J., Harley,C.B., and Cech,T.R. (1997). Telomerase catalytic subunit homologs from fission yeast and human. Science *277*, 955-959.

Nazeem,S., Azmi,A.S., Hanif,S., Ahmad,A., Mohammad,R.M., Hadi,S.M., and Kumar,K.S. (2009). Plumbagin induces cell death through a copper-redox cycle mechanism in human cancer cells. Mutagenesis *24*, 413-418.

Newman,D.J. and Cragg,G.M. (2007). Natural products as sources of new drugs over the last 25 years. J. Nat. Prod. *70*, 461-477.

Olovnikov,A.M. (1973). A theory of marginotomy. The incomplete copying of template margin in enzymic synthesis of polynucleotides and biological significance of the phenomenon. J. Theor. Biol. *41*, 181-190.

Ouchi,H., Ishiguro,H., Ikeda,N., Hori,M., Kubota,Y., and Uemura,H. (2005). Genistein induces cell growth inhibition in prostate cancer through the suppression of telomerase activity. Int. J. Urol. *12*, 73-80.

Parkin,D.M., Bray,F., Ferlay,J., and Pisani,P. (2005). Global cancer statistics, 2002. CA Cancer J. Clin. *55*, 74-108.

Parkinson,E.K. and Minty,F. (2007). Anticancer therapy targeting telomeres and telomerase : current status. BioDrugs. *21*, 375-385.

Parodi,F.E., Mao,D., Ennis,T.L., Pagano,M.B., and Thompson,R.W. (2006). Oral administration of diferuloylmethane (curcumin) suppresses proinflammatory cytokines and destructive connective tissue remodeling in experimental abdominal aortic aneurysms. Ann. Vasc. Surg. *20*, 360-368.

Pop,E.A., Fischer,L.M., Coan,A.D., Gitzinger,M., Nakamura,J., and Zeisel,S.H. (2008). Effects of a high daily dose of soy isoflavones on DNA damage, apoptosis, and estrogenic outcomes in healthy postmenopausal women: a phase I clinical trial. Menopause. *15*, 684-692.

Powolny,A.A. and Singh,S.V. (2008). Plumbagin-induced apoptosis in human prostate cancer cells is associated with modulation of cellular redox status and generation of reactive oxygen species. Pharm. Res. *25*, 2171-2180.

Puli,S., Lai,J.C., and Bhushan,A. (2006). Inhibition of matrix degrading enzymes and invasion in human glioblastoma (U87MG) cells by isoflavones. J. Neurooncol. *79*, 135-142.

Raffoul,J.J., Wang,Y., Kucuk,O., Forman,J.D., Sarkar,F.H., and Hillman,G.G. (2006). Genistein inhibits radiation-induced activation of NF-kappaB in prostate cancer cells promoting apoptosis and G2/M cell cycle arrest. BMC. Cancer *6*, 107.

Ramachandran,C., Fonseca,H.B., Jhabvala,P., Escalon,E.A., and Melnick,S.J. (2002). Curcumin inhibits telomerase activity through human telomerase reverse transcritpase in MCF-7 breast cancer cell line. Cancer Lett. *184*, 1-6.

Reddel,R.R., Bryan,T.M., Colgin,L.M., Perrem,K.T., and Yeager,T.R. (2001). Alternative lengthening of telomeres in human cells. Radiat. Res. *155*, 194-200.

Ries LAG, Melbert D, Krapcho M, Stinchcomb DG, Howlader N, Horner MJ, Mariotto A, Miller BA, Feuer EJ, Altekruse SF, Lewis DR, Clegg L, Eisner MP, and Reichman M. SEER Cancer Statistics Review, 1975-2005. Edwards BK. 2009. National Cancer Institute. Bethesda, MD. Ref Type: Report

Rucinska,A. and Gabryelak,T. (2009). Effect of genistein-8-C-glucoside from Lupinus luteus on DNA damage assessed using the comet assay in vitro. Cell Biol. Int. *33*, 247-252.

Rucinska,A., Kirko,S., and Gabryelak,T. (2007). Effect of the phytoestrogen, genistein-8-C-glucoside, on Chinese hamster ovary cells in vitro. Cell Biol. Int. *31*, 1371-1378.

Sahu,R.P., Batra,S., and Srivastava,S.K. (2009). Activation of ATM/Chk1 by curcumin causes cell cycle arrest and apoptosis in human pancreatic cancer cells. Br. J. Cancer *100*, 1425-1433.

Samuhasaneeto,S., Thong-Ngam,D., Kulaputana,O., Suyasunanont,D., and Klaikeaw,N. (2009). Curcumin decreased oxidative stress, inhibited NF-kappaB activation, and improved liver pathology in ethanol-induced liver injury in rats. J. Biomed. Biotechnol. *2009*, 981963.

Sandur,S.K., Ichikawa,H., Sethi,G., Ahn,K.S., and Aggarwal,B.B. (2006). Plumbagin (5-hydroxy-2-methyl-1,4-naphthoquinone) suppresses NF-kappaB activation and NF-kappaB-regulated gene products through modulation of p65 and IkappaBalpha kinase activation, leading to potentiation of apoptosis induced by cytokine and chemotherapeutic agents. J. Biol. Chem. *281*, 17023-17033.

Schmidt,F., Knobbe,C.B., Frank,B., Wolburg,H., and Weller,M. (2008). The topoisomerase II inhibitor, genistein, induces G2/M arrest and apoptosis in human malignant glioma cell lines. Oncol. Rep. *19*, 1061-1066.

Seymour,E.M., Singer,A.A., Bennink,M.R., Parikh,R.V., Kirakosyan,A., Kaufman,P.B., and Bolling,S.F. (2008). Chronic intake of a phytochemical-enriched diet reduces cardiac fibrosis and diastolic dysfunction caused by prolonged salt-sensitive hypertension. J. Gerontol. A Biol. Sci. Med. Sci. *63*, 1034-1042.

Sha,G.H. and Lin,S.Q. (2008). Genistein inhibits proliferation of human endometrial endothelial cell in vitro. Chin Med. Sci. J. *23*, 49-53.

Shankar,S., Chen,Q., Sarva,K., Siddiqui,I., and Srivastava,R.K. (2007). Curcumin enhances the apoptosis-inducing potential of TRAIL in prostate cancer cells: molecular mechanisms of apoptosis, migration and angiogenesis. J. Mol. Signal. *2*, 10.

Shay,J.W. and Bacchetti,S. (1997). A survey of telomerase activity in human cancer. Eur. J. Cancer *33*, 787-791.

Shay,J.W. and Wright,W.E. (2002). Telomerase: a target for cancer therapeutics. Cancer Cell *2*, 257-265.

Shay,J.W. and Wright,W.E. (2005a). Senescence and immortalization: role of telomeres and telomerase. Carcinogenesis *26*, 867-874.

Shay,J.W. and Wright,W.E. (2005b). Mechanism-based combination telomerase inhibition therapy. Cancer Cell *7*, 1-2.

Shay,J.W. and Wright,W.E. (2000). Hayflick, his limit, and cellular ageing. Nat. Rev. Mol. Cell Biol. *1*, 72-76.

Shay,J.W. and Wright,W.E. (2006). Telomerase therapeutics for cancer: challenges and new directions. Nat. Rev. Drug Discov. *5*, 577-584.

Shiau,R.J., Chen,K.Y., Wen,Y.D., Chuang,C.H., and Yeh,S.L. (2009). Genistein and beta-carotene enhance the growth-inhibitory effect of trichostatin A in A549 cells. Eur. J. Nutr. *49*, 19-25.

Shieh,J.M., Chiang,T.A., Chang,W.T., Chao,C.H., Lee,Y.C., Huang,G.Y., Shih,Y.X., and Shih,Y.W. (2009). Plumbagin inhibits TPA-induced MMP-2 and u-PA expressions by reducing binding activities of NF-kappaB and AP-1 via ERK signaling pathway in A549 human lung cancer cells. Mol. Cell Biochem. *355*, 181-193.

Shih,Y.W., Lee,Y.C., Wu,P.F., Lee,Y.B., and Chiang,T.A. (2009). Plumbagin inhibits invasion and migration of liver cancer HepG2 cells by decreasing productions of matrix metalloproteinase-2 and urokinase- plasminogen activator. Hepatol. Res. *39*, 998-1009.

Shippen-Lentz,D. and Blackburn,E.H. (1990). Functional evidence for an RNA template in telomerase. Science *247*, 546-552.

Siddique,M. and Sabapathy,K. (2006). Trp53-dependent DNA-repair is affected by the codon 72 polymorphism. Oncogene *25*, 3489-3500.

Speicher,M.R., Gwyn,B.S., and Ward,D.C. (1996). Karyotyping human chromosomes by combinatorial multi-fluor FISH. Nat. Genet. *12*, 368-375.

Srinivas,P., Gopinath,G., Banerji,A., Dinakar,A., and Srinivas,G. (2004). Plumbagin induces reactive oxygen species, which mediate apoptosis in human cervical cancer cells. Mol. Carcinog. *40*, 201-211.

Su,C.C., Lin,J.G., Li,T.M., Chung,J.G., Yang,J.S., Ip,S.W., Lin,W.C., and Chen,G.W. (2006). Curcumin-induced apoptosis of human colon cancer colo 205 cells through the production of ROS, Ca2+ and the activation of caspase-3. Anticancer Res. *26*, 4379-4389.

Tahara,H., Yasui,W., Tahara,E., Fujimoto,J., Ito,K., Tamai,K., Nakayama,J., Ishikawa,F., Tahara,E., and Ide,T. (1999). Immuno-histochemical detection of human telomerase catalytic component, hTERT, in human colorectal tumor and non-tumor tissue sections. Oncogene *18*, 1561-1567.

Tanaka,Y., Guhde,G., Suter,A., Eskelinen,E.L., Hartmann,D., Lullmann-Rauch,R., Janssen,P.M., Blanz,J., von,F.K., and Saftig,P. (2000). Accumulation of autophagic vacuoles and cardiomyopathy in LAMP-2-deficient mice. Nature *406*, 902-906.

Taylor,R.S., Ramirez,R.D., Ogoshi,M., Chaffins,M., Piatyszek,M.A., and Shay,J.W. (1996). Detection of telomerase activity in malignant and nonmalignant skin conditions. J. Invest Dermatol. *106*, 759-765.

Teng,L.S. and Fahey,T.J., III (2002). Can inhibition of telomerase increase pancreatic cancer cell's susceptibility to chemotherapeutic reagents? Hepatobiliary. Pancreat. Dis. Int. *1*, 155-160.

Thasni,K.A., Rakesh,S., Rojini,G., Ratheeshkumar,T., Srinivas,G., and Priya,S. (2008a). Estrogen-dependent cell signaling and apoptosis in BRCA1-blocked BG1 ovarian cancer cells in response to plumbagin and other chemotherapeutic agents. Ann. Oncol. *19*, 696-705.

Thasni,K.A., Rojini,G., Rakesh,S.N., Ratheeshkumar,T., Babu,M.S., Srinivas,G., Banerji,A., and Srinivas,P. (2008b). Genistein induces apoptosis in ovarian cancer cells via different molecular pathways depending on Breast Cancer Susceptibility gene-1 (BRCA1) status. Eur. J. Pharmacol. *588*, 158-164.

Thayyullathil,F., Chathoth,S., Hago,A., Patel,M., and Galadari,S. (2008). Rapid reactive oxygen species (ROS) generation induced by curcumin leads to caspase-dependent and -independent apoptosis in L929 cells. Free Radic. Biol. Med. *45*, 1403-1412.

Virginia,S. and Dubay,M.L. (2003). 100 Questions & Answers About Brain Tumors. Jones and Bartlett Publishers, Inc.

Vulliamy,T.J., Knight,S.W., Mason,P.J., and Dokal,I. (2001). Very short telomeres in the peripheral blood of patients with X-linked and autosomal dyskeratosis congenita. Blood Cells Mol. Dis. *27*, 353-357.

Wahl,H., Tan,L., Griffith,K., Choi,M., and Liu,J.R. (2007). Curcumin enhances Apo2L/TRAIL-induced apoptosis in chemoresistant ovarian cancer cells. Gynecol. Oncol. *105*, 104-112.

Wang,C.C., Chiang,Y.M., Sung,S.C., Hsu,Y.L., Chang,J.K., and Kuo,P.L. (2008). Plumbagin induces cell cycle arrest and apoptosis through reactive oxygen species/c-Jun N-terminal kinase pathways in human melanoma A375.S2 cells. Cancer Lett. *259*, 82-98.

Watson,J.D. (1972). Origin of concatemeric T7 DNA. Nat. New Biol. *239*, 197-201.

Werness,B.A., Levine,A.J., and Howley,P.M. (1990). Association of human papillomavirus types 16 and 18 E6 proteins with p53. Science *248*, 76-79.

Wright,W.E., Piatyszek,M.A., Rainey,W.E., Byrd,W., and Shay,J.W. (1996). Telomerase activity in human germline and embryonic tissues and cells. Dev. Genet. *18*, 173-179.

Wright,W.E. and Shay,J.W. (1992). The two-stage mechanism controlling cellular senescence and immortalization. Exp. Gerontol. *27*, 383-389.

Yu,G.L., Bradley,J.D., Attardi,L.D., and Blackburn,E.H. (1990). In vivo alteration of telomere sequences and senescence caused by mutated Tetrahymena telomerase RNAs. Nature *344*, 126-132.

Yu,J.Y., Lee,J.J., Lim,Y., Kim,T.J., Jin,Y.R., Sheen,Y.Y., and Yun,Y.P. (2008). Genistein inhibits rat aortic smooth muscle cell proliferation through the induction of p27kip1. J. Pharmacol. Sci. *107*, 90-98.

Zhao,R., Xiang,N., Domann,F.E., and Zhong,W. (2009). Effects of selenite and genistein on G2/M cell cycle arrest and apoptosis in human prostate cancer cells. Nutr. Cancer *61*, 397-407.

Zhao,Y.L. and Lu,D.P. (2006). [Effects of plumbagin on the human acute promyelocytic leukemia cells in vitro]. Zhongguo Shi Yan. Xue. Ye. Xue. Za Zhi. *14*, 208-211.

Zheng,L.D., Tong,Q.S., and Wu,C.H. (2006). Growth inhibition and apoptosis inducing mechanisms of curcumin on human ovarian cancer cell line A2780. Chin J. Integr. Med. *12*, 126-131.

Zheng,M., Ekmekcioglu,S., Walch,E.T., Tang,C.H., and Grimm,E.A. (2004). Inhibition of nuclear factor-kappaB and nitric oxide by curcumin induces G2/M cell cycle arrest and apoptosis in human melanoma cells. Melanoma Res. *14*, 165-171.

Zhou,S., Hu,Y., Zhang,B., Teng,Z., Gan,H., Yang,Z., Wang,Q., Huan,M., and Mei,Q. (2008). Dose-dependent absorption, metabolism, and excretion of genistein in rats. J. Agric. Food Chem. *56*, 8354-8359.